UNIVERSIDADE ESTADUAL PAULISTA “JÚLIO DE MESQUITA FILHO”
FACULDADE DE ENGENHARIA
CÂMPUS DE ILHA SOLTEIRA

VÍCTOR HUGO RIBEIRO

MODELLING OF THE FATIGUE CRACK INITIATION AND PROPAGATION BEHAVIOUR IN METALS AND ALLOYS

Ilha Solteira
2021

PROGRAMA DE PÓS-GRADUAÇÃO EM ENGENHARIA MECÂNICA

VÍCTOR HUGO RIBEIRO

MODELLING OF THE FATIGUE CRACK INITIATION AND PROPAGATION BEHAVIOUR IN METALS AND ALLOYS

A thesis submitted to the Faculdade de Engenharia de Ilha Solteira - UNESP in partial fulfillment of the requirements for obtaining the Doctorate in Mechanical Engineering. Knowledge area: Solid Mechanics

Advisors: Aparecido Carlos Gonçalves
José António Fonseca de Oliveira Correia

Ilha Solteira
2021

FICHA CATALOGRÁFICA
Desenvolvido pelo Serviço Técnico de Biblioteca e Documentação

R484m

Ribeiro, Víctor Hugo.
Modelling of the fatigue crack initiation and propagation behaviour in metals and alloys / Víctor Hugo Ribeiro. -- Ilha Solteira: [s.n.], 2021
210 f. : il.

Tese (doutorado) - Universidade Estadual Paulista. Faculdade de Engenharia de Ilha Solteira. Área de conhecimento: Mecânica dos Sólidos, 2021

Orientador: Aparecido Carlos Gonçalves
Co-orientador: José António Fonseca de Oliveira Correia
Inclui bibliografia

1. Low-cycle fatigue. 2. Crack growth rates. 3. Crack closure effects. 4. Strain energy. 5. Dislocation density. 6. Residual stress effects.

Amanda Sertori dos Santos
Bibliotecária - CRB/8-9061
Seção Técnica de Referência, Atendimento ao Usuário e Documentação
Diretoria Técnica de Biblioteca e Documentação

UNIVERSIDADE ESTADUAL PAULISTA

Campus de Ilha Solteira

CERTIFICADO DE APROVAÇÃO

TÍTULO DA TESE: MODELLING OF THE FATIGUE CRACK INITIATION AND PROPAGATION BEHAVIOU R IN METALS AND ALLOYS.

AUTOR: VÍCTOR HUGO RIBEIRO

ORIENTADOR: APARECIDO CARLOS GONCALVES

COORIENTADOR: JOSÉ ANTÓNIO FONSECA DE OLIVEIRA CORREIA

Aprovado como parte das exigências para obtenção do Título de Doutor em ENGENHARIA MECÂNICA, área: Mecânica dos Sólidos pela Comissão Examinadora:

Dr. JOSÉ ANTÔNIO FONSECA DE OLIVEIRA CORREIA (Participaçao Virtual)
Universidade do Porto

Prof. Dr. MARCIO ANTONIO BAZANI (Participaçao Virtual)
Departamento de Engenharia Mecânica / Unesp - Ilha Solteira

Prof. Dr. RUBENS RIBEIRO (Participaçao Virtual)
Departamento de Engenharia de Produção / Universidade Federal de Mato Grosso do Sul -UFMS/CPTL

Prof. Dr. ABÎLIO MANUEL PINHO DE JESUS (Participaçao Virtual)
Departamento de Engenharia Mecânica / Faculdade de Engenharia, Universidade do Porto

Prof. Dr. ALFREDO DA SILVA RIBEIRO (Participaçao Virtual)
Engenharia Mecânica / Universidade de Trás-os-Montes e Alto Douro

Ilha Solteira, 17 de dezembro de 2021

This thesis is especially dedicated

to my family.

ACKNOWLEDGEMENTS

I thank God, for life, for the opportunities, overcomings, and wonders that I experience every day.

To my wife Elis, who was always by my side and willing to take care of our family.

To my father Raul, my example and guide, who along with my mother, Sonia, “in memorial”, made me a good person with character.

To my brother Ricardo and his wife Margarita, and my nephews Sheldon and Penny, for all their affection, adventures, emotions, and fun days.

To my mother-in-law Marina, my brother-in-law Rogério and my wife's entire family, for the moments of relaxation and support.

To all my family and friends who, even from a distance, have always been with me and supporting me in this project.

Thanks to São Paulo State University “Júlio de Mesquita Filho” (UNESP), Faculty of Engineering, University of Porto (FEUP), and Wroclaw University of Science and Technology for offering their space and infrastructure to carry out this work.

To my advisor Prof. Aparecido C. Gonçalves for his friendship and partnership, always present, patient, confident, and active, willing to collaborate with the progress and development of the work, as well as my personal and professional evolution.

To my co-advisor Prof. José Correia, I am immensely grateful for having believed in me since the first contact, without measuring efforts to help me. An excellent professional, extremely intelligent and dedicated, besides being a great person, and a good friend.

To co-advisor Prof. Gzegorz Lesiuk from Poland for all reviews, contributions, and experimental tests.

I thank God for having placed these advisors in my path, for knowing them, and for having lived with them, contributing a lot to my professional growth. They are, without a doubt, a great source of inspiration and a reference for me.

To the professors and the entire technical staff of the Mechanical Engineering Department at UNESP. Special thanks to Prof. Márcio, for the long conversations and discussions at the beginning of this project and his excellent contributions; and also, a special thanks to Carlos, responsible for all the technical support given in the experimental execution.

To Prof. Rubens, for all the companionship, words, conversations, concern, and help during this difficult journey.

To Prof. Eli and IFSP campus Votuporanga, for all the help in manufacturing the specimens.

A very special thanks to the Examination Board, for the availability and for the contributions that they will make to the final document.

To Ph.D. student António Mourão for all his contributions, and for all his support during my stay in Porto.

To Peter Huffman, from Successful Failure Consulting Corp, USA, for the support given in the application of the strain energy density model.

To Prof. Joelton and Prof. Hermes, for everything they did for me before and during my stay in Portugal, in addition to all contributions to the qualification exam.

To Prof. Aldemir and Prof. Guilherme, who referred me to Portugal, the former having the honor of being a colleague at Engineering, and the latter also having the honor of meeting him in Portugal, and we had good conversations, making my stay better.

To my roommates Aline, Thayanne, and Rafael, for all the conversations, events, dinners, the 2019 New Year's Eve, and every effort made to welcome and help us on this trip.

To all postgraduate colleagues at UNESP and also at FEUP.

To Coordenação de Aperfeiçoamento de Pessoal de Nível Superior - Brasil (CAPES) for the financial support.

Victor Hugo Ribeiro

02 December 2021

“*The ear that heareth the reproof of life abideth among the wise.*
He that refuseth instruction despiseth his own soul, but he that heareth reproof getteth understanding.”

Proverbs 15:31-32

RESUMO

A fadiga é uma das principais causas de falhas e também de fraturas mecânicas em detalhes estruturais sob carregamento cíclico. Existem vários modelos para descrever o comportamento de fadiga de baixo ciclo com base em critérios de dano por deformação, como Coffin-Manson-Morrow, utilizado na fase iniciação de trinca. A lei de Paris só é aplicável na região estável de crescimento de trinca (região II), e como consequência, surgiram diversos modelos dela derivados para contornar essa limitação, aumentando o número de variáveis e parâmetros necessários e, consequentemente, tornando a solução onerosa. Outros modelos como UniGrow, Huffman, Peeker, entre outros, descrevem as fases de iniciação e propagação de trincas de fadiga, adotando o conceito de reinicializações sucessivas de trincas (incrementos) com base em abordagens locais.

Nesta pesquisa, a modelagem de fadiga de baixo ciclo baseada na abordagem de Huffman usando a densidade de energia de deformação e considerando a densidade de discordâncias é investigada e discutida. Para isso, várias metodologias para avaliar a resistência à fadiga de baixo ciclo com base na abordagem de Huffman e explorar diferentes parâmetros de densidade de deslocamento são sugeridas: (i) densidade de discordâncias crítica associada a maior amplitude de deformação; (ii) valor médio da densidade de discordâncias dos dados experimentais de fadiga disponíveis e, (iii) predição estocástica de Monte Carlo(MC) considerando a variabilidade da densidade de discordâncias e o coeficiente de endurecimento por deformação cíclica. Dados experimentais de fadiga das ligas de Al1050, Al6061-T651 e AlMgSi0.8 da literatura são usados neste estudo. E ainda, é feita uma comparação entre os dados experimentais de fadiga e as curvas de tensão-vida com base nas várias metodologias sugeridas.

Adicionalmente, é apresentada uma comparação do efeito de vários modelos de fechamento/abertura de trinca no comportamento de crescimento de trinca por fadiga da liga de Al6061-T651. Os modelos de fechamento de trinca em consideração são: Elber; Katcher-Kaplan; Clerivet-Bathias; Schijve; Zhang; Newman; Savaidis; Codrington-Kotousov; Correia. Uma comparação entre esses modelos é feita.

Além disso, foi sugerida modelagem do comportamento de crescimento de trinca por fadiga para a liga 6061-T651 através do modelo Huffman com base na densidade de

energia de deformação das discordâncias considerando os efeitos das tensões residuais à frente da ponta da trinca(x), onde essas tensões estão relacionadas ao dano por fadiga de um incremento de fissura Δa, como parâmetro do calibrador. Duas abordagens sugeridas por Noroozi e Huffman são estudadas e discutidas. Na modelagem do comportamento de crescimento de trinca por fadiga, a influência da densidade de energia de deformação calculada para os valores de densidade de discordâncias crítica associada a maior amplitude de deformação e o valor médio da densidade de discordâncias para os resultados de fadiga experimentais disponíveis também foram considerados nesta investigação. Os valores de densidade de discordâncias estudados não influenciam significativamente o comportamento de propagação de trincas por fadiga. Conclui-se também que o procedimento de consideração dos efeitos das tensões residuais influencia o calibrador, Δa, não sendo possível concluir qual é o melhor método para descrever os efeitos das tensões residuais.

Palavras-chave: ligas de alumínio; fadiga de baixo ciclo; taxa de crescimento de trincas; efeitos do fechamento de trincas; energia de deformação; densidade de discordâncias; efeitos de tensões residuais.

ABSTRACT

Fatigue is the main causes of mechanical fractures in structural details under cyclic loading. There are several models to describe low-cycle fatigue behavior based on strain damage criteria, such as Coffin-Manson-Morrow, which is used in the crack initiation phase. The Paris law is only applicable in the stable region of crack growth (region II), and, as a consequence of this, several models have emerged derived from it emerged to overcome this limitation, increasing the number of variables and parameters required and, consequently, making the solution costly. Other models such as UniGrow, Huffman, Peeker, among others, describe the initiation and propagation phases of fatigue cracks, adopting the concept of successive crack restarts (increments) based on local approaches.

In this research, low-cycle fatigue modeling based on the Huffman approach using strain energy density and considering dislocation density is investigated and discussed. To this end, several methodologies to evaluate low-cycle fatigue resistance based on the Huffman approach and exploring different dislocation density parameters are suggested: (i) critical dislocation density associated with greater strain amplitude; (ii) average value of dislocation density from available experimental fatigue data and, (iii) stochastic Monte Carlo (MC) prediction considering the variability of dislocation density and the cyclic strain hardening coefficient. Experimental fatigue data of Al1050, Al6061-T651 and AlMgSi0.8 alloys from the literature are used in this study. Furthermore, a comparison is made between the experimental fatigue data and the stress-life curves based on the various suggested methodologies.

Additionally, a comparison of the effect of various crack closure/opening models on the fatigue crack growth behavior of Al6061-T651 alloy is presented. The crack closure models under consideration are: Elber; Katcher-Kaplan; Clerivet-Bathias; Schijve; Zhang; Newman; Savaidis; Codrington-Kotosov; and Correia. A comparison between these models is done.

Furthermore, modeling of the fatigue crack growth behavior for the Al6061-T651 alloy was suggested using the Huffman model based on the strain energy density of the dislocations considering the effects of residual stresses ahead of the crack tip(x), where these stresses are related to the fatigue damage of a crack increment Δa, as a calibrator parameter. Two approaches suggested by Noroozi and Huffman are studied and discussed. In modeling fatigue crack growth behavior, the influence of the calculated strain energy density for the critical dislocation density values associated with the largest strain amplitude and the average dislocation density value for available experimental fatigue results were also considered in this investigation. The dislocation density values studied do not significantly influenced the fatigue crack propagation behavior. It is also concluded that the procedure for considering the effects of residual stresses influences the calibrator, Δa, and it is not possible to conclude which is the best method to describe the effects of residual stresses.

Keywords: aluminium alloys; low-cycle fatigue; crack growth rates; crack closure effects; strain energy; dislocation density; residual stress effects.

LIST OF FIGURES

LIST OF TABLES

NOMENCLATURE

LATIN

$\boldsymbol{a}$	Crack length
$\boldsymbol{a}^*$	Normalized crack length
$\boldsymbol{a_1}, \boldsymbol{a_i}$	Initial crack size, crack size increment
$\boldsymbol{a_n}$	Distance of load-line to notch tip
$\boldsymbol{a_0}$	Notch size
$\boldsymbol{\Delta a}$	Calibration parameter
$\boldsymbol{\Delta a_i}$	Crack range increment
$\boldsymbol{A}$	Elongation at fracture, Codrington-Kotousov model parameter
$\boldsymbol{A_0}, \boldsymbol{A_1}, \boldsymbol{A_2}, \boldsymbol{A_3}$	Newman's or Savaidis model parameters
$\boldsymbol{b}$	Fatigue strength exponent
$\vec{\boldsymbol{b}}$	Burger's vector
$\boldsymbol{B}$	Thickness, Codrington-Kotousov model parameter
$\boldsymbol{c}$	Fatigue ductility exponent
$\boldsymbol{C}, \boldsymbol{C_1}, \boldsymbol{C_2}, \boldsymbol{C_C}, \boldsymbol{C_{el}}, \boldsymbol{C_{pl}}, \boldsymbol{C_F}, \boldsymbol{C_{HS}}, \boldsymbol{C_{MOD}}, \boldsymbol{C_P}, \boldsymbol{C_W}$	Material constant; parameter related to endurance limit in probabilistic fatigue model, Codrington-Kotousov model parameter
$\boldsymbol{COV}$	Coefficient of variation
$\boldsymbol{d}$	Distance of load-line from edge of the plate
$\boldsymbol{D}$	Huffman fatigue damage parameter
$\frac{da}{dN}, \frac{da^*}{dN^*}$	Fatigue crack growth rate
$\boldsymbol{e}$	Eccentricity of load-line, error
$\bar{\boldsymbol{e}}$	Mean error
$\boldsymbol{E}$	Modulus of elasticity or Young´s modulus
$\boldsymbol{E_{steel}}$	Elastic modulus of steel
$\boldsymbol{f}, \boldsymbol{f}()$	Function of the stress intensity factor range; frequency; yield function
$\boldsymbol{F}(), \boldsymbol{F^{-1}}()$	Cumulative distribution function
$\boldsymbol{f_y}$	Higher yield strength
$\boldsymbol{f_u}$	Ultimate tensile strength
$\boldsymbol{F_T}$	Geometric factor for tension
$\boldsymbol{F_B}$	Geometric factor for bending
$\boldsymbol{F_{max}}$	Maximum force
$\boldsymbol{F_{min}}$	Minimum force
$\boldsymbol{\Delta F}$	Force range
$\boldsymbol{H}$	Distance between the points of load application
$\boldsymbol{K}$	Stress intensity factor; Applied stress intensity factor; Strain hardening coefficient; Material constant

$\boldsymbol{K_0}$	Stress intensity factor for $R = 0$.
$\boldsymbol{K_L}$	Limiting $\boldsymbol{K_{max}}$ value for detectable closure
$\boldsymbol{K'}$	Cyclic strength coefficient
$\boldsymbol{K_C, K_{IC}}$	Fracture toughness
$\boldsymbol{K_{mat}}$	Material toughness measured by stress intensity factor
$\boldsymbol{K_{max}}$	Maximum stress intensity factor
$\boldsymbol{K_{max,applied}}$	Applied maximum stress intensity factor
$\boldsymbol{K_{max,tot}}$	Total maximum stress intensity factor
$\boldsymbol{K_{min}}$	Minimum stress intensity factor
$\boldsymbol{K_{op}}$	Opening Stress intensity factor
$\boldsymbol{K_r, K_{residual}}$	Residual stress concentration factor
$\boldsymbol{\Delta K}$	Stress intensity factor range
$\boldsymbol{\overline{\Delta K}}$	Walker equivalent stress intensity range
$\boldsymbol{\Delta K_I}$	Stress intensity factor range in mode I
$\boldsymbol{\Delta K_{I,Tension}}$	Tension component of stress intensity factor range in mode I
$\boldsymbol{\Delta K_{I,Bending}}$	Bending component of stress intensity factor range in mode I
$\boldsymbol{\Delta K_{app}, \Delta K_{applied}}$	Applied stress intensity factor range
$\boldsymbol{\Delta K_{cl}}$	Stress intensity factor range at closuring
$\boldsymbol{\Delta K_{eff}}$	Effective stress intensity factor range
$\boldsymbol{\Delta K_{eff,0}}$	Effective stress intensity factor range for $R = 0$
$\boldsymbol{\Delta K_{eff,max}}$	Maximum Effective stress intensity factor range
$\boldsymbol{\Delta K_{eff,min}}$	Minimum effective stress intensity factor range
$\Delta \boldsymbol{K_{op}}$	Stress intensity factor range at opening
$\boldsymbol{\Delta K_{tot}}$	Total stress concentration factor range
$\boldsymbol{\Delta K_{th,eff}}$	Effective threshold ΔK_{eff}
$\boldsymbol{\Delta K_{up,eff}}$	Effective limiting ΔK_{eff}
$\Delta \boldsymbol{K^*_{eff}}$	Normalized ΔK_{eff}
$\Delta \boldsymbol{K^*_{th,eff}}$	Normalized $\Delta K_{th,eff}$
$\Delta \boldsymbol{K^*_{up,eff}}$	Normalized $\Delta K_{up,eff}$
$\boldsymbol{\Delta K_{th}}$	Threshold of stress intensity factor range
$\boldsymbol{\Delta K_{th,0}}$	Threshold of stress intensity factor range for $R = 0$
$\boldsymbol{\Delta K_{th,steel}}$	Threshold of stress intensity factor range of steel
$\boldsymbol{\Delta K_{up}}$	Ultimate stress intensity factor range
$\Delta \boldsymbol{K^*}$	Normalized ΔK
$\Delta \boldsymbol{K^{*+}}$	Normalizing variable of ΔK
$\Delta \boldsymbol{K^*_{th}}$	Normalized ΔK_{th}
$\Delta \boldsymbol{K^*_{up}}$	Normalized ΔK_{up}
$\boldsymbol{J_{mat}}$	Material toughness measured by J-methods
$\boldsymbol{\Delta J}$	Strain energy release density
$\boldsymbol{\Delta J_{up}}$	Ultimate value of J-integral range
$\boldsymbol{\Delta J_{th}}$	Threshold value of the cyclic J-integral

$\Delta \mathbf{J}^{*+}$	Normalizing variable of ΔJ
$\Delta \mathbf{J}^{*}_{th}$	Normalized ΔJ_{th}
$\Delta \mathbf{J}^{*}_{up}$	Normalized ΔJ_{up}
L, L_1, L_2	Characteristic length
L_{0p}	Length at fracture
$m, m_1, m_2, m_C,$ $m_{el}, m_{pl}, m_F, m_{HS},$ m_{MOD}, m_P, m_W	Material constant
n	Strain hardening exponent, number of specimens
n'	Cyclic strain-hardening exponent
N	Number of cycles (fatigue life)
N^*	Normalized number of cycles
N_0	Reference number of cycles; Threshold value of lifetime
N_E	Experimental number of cycles
N_f	Number of cycles to failure
N_i	Number of cycles in crack initiation; Number of cycles of the specimen i
N_P	Predicted number of cycles
$2N_f$	Reversals to failure
$2N_{f,i}$	Reversals to failure of the specimen i
p	Material constant; Probabilistic to failure
$P1, P2 \ldots P5$	Transversal direction specimen identification
P_{max}	Maximum force
P_{min}	Minimum force
ΔP	Eccentric applied force range
r	Crack tip polar coordinate, radius
R, R_σ	Stress ratio, radius
R_{eff}	Effective stress R-ratio
$R_{eff,1}$	Deterministic effective stress R-ratio for first cycle measurement
$R_{eff,s}$	Deterministic effective stress R-ratio for stabilized measurement
R_ε	Strain ratio
$R_{p,0.2}$	Monotonic 0.2% proof stress
R_m	Ultimate tensile stress
R^2	Determination coefficient
S_{max}	Maximum stress
$S_{op,phen}$	Opening stress
T	Thickness
SWT	Smith, Watson and Topper fatigue damage parameter
U, U_{SIF}	Quantitative closure parameter; Effective stress intensity ratio
U_1	Quantitative closure parameter for the first cycle

U_d	Dislocation strain energy
$U_{d,1}$	Deterministic quantitative closure parameter for the first cycle measurement
$U_{d,s}$	Deterministic quantitative closure parameter for the stabilised measurement
U_e	Tensile elastic strain energy density
U_i	Quantitative closure parameter related to crack increment i
U_s	Quantitative closure parameter for stabilised measurement
U_{th}	Quantitative closure parameter for the first crack length
U_{up}	Quantitative closure parameter for the last crack length
U_p^*	Complimentary plastic strain energy density
W	Characteristic length, width
$W1, W2 \dots W5$	Longitudinal direction specimen identification
x	Distance from the crack tip, calibration parameter
$\overline{x}$	Mean value
X	Cartesian component
Y	Cartesian component, function depending on geometric and loading conditions
Z	Reduction in cross-section at failure

GREEK

α	Material constant; scale parameter of 2-parameter Weibull and Logistic distribution; relation of crack length and specimen width
β	Shape parameter of the 2-parameter Weibull and Logistic distribution
$\gamma, \gamma_{th}, \gamma_w$	Curve fitting parameter; Fatigue crack growth equation exponent, parameter of the statistical Gumbel distribution
δ	Scale parameter of Weibull model; Elementary material blocks of length
δ^*	Elementary material blocks of length in the process zone
ε	Strain
ε_a	Amplitude Strain; Principal in-plane strain (axial direction)
ε_f'	Fatigue ductility coefficient
ε_w	Walker strain
$\Delta\varepsilon$	Strain range
$\Delta\varepsilon^E$	Elastic strain range
$\Delta\varepsilon^P$	Plastic strain range
η	Material property, Codrington-Kotousov non-dimensional parameter
υ	Poisson ratio
ρ	Dislocation density
ρ^*	Notch tip radius; Elementary material block size

$\boldsymbol{\rho_c}$	Critical blunt tip radius, critical dislocation density
$\boldsymbol{\rho_i}$	Dislocation density for each tested specimen
$\boldsymbol{\rho_m}$	Mean dislocation density of available experimental fatigue results
$\boldsymbol{\sigma}$	Stress, standard deviation of Normal distribution
$\boldsymbol{\sigma_0}$	Cyclic yield stress; Stress fatigue limit
$\boldsymbol{\sigma_a}$	Stress amplitude
$\boldsymbol{\sigma_{a,i}}$	Stress amplitude obtained during low-cycle fatigue tests for the specimen i
$\boldsymbol{\sigma_f, \sigma_o}$	Flow stress
$\boldsymbol{\sigma'_f}$	Fatigue strength coefficient
$\boldsymbol{\sigma_M, \sigma_{max}}$	Maximum stress
$\boldsymbol{\sigma_{max,i}}$	Maximum stress amplitude obtained during low-cycle fatigue tests for the specimen i
$\boldsymbol{\sigma^*_M}$	Normalized maximum stress
$\boldsymbol{\sigma_m, \sigma_{min}}$	Minimum stress, mean stress
$\boldsymbol{\sigma^*_m}$	Normalized minimum stress
$\boldsymbol{\sigma_{med}}$	Mean stress
$\boldsymbol{\sigma_{op}}$	Opening stress
$\boldsymbol{\sigma_x}$	Elastic stress along the x direction
$\boldsymbol{\sigma_{xx}, \sigma_{yy}}$	Analytical elastoplastic stress distributions
$\boldsymbol{\sigma_y}$	Yield stress; Elastic stress along the y direction
$\boldsymbol{\sigma_r, \sigma_{residual}}$	Residual stress
$\boldsymbol{\Delta\sigma}$	Stress range
$\boldsymbol{\Delta\sigma^*}$	Normalized stress range
$\boldsymbol{\Delta\sigma_0}$	Endurance fatigue limit
$\boldsymbol{\Delta\sigma_T}$	Tensile stress range
$\boldsymbol{\Delta\sigma_B}$	Bending stress range
$\boldsymbol{\sigma_{\varepsilon_p=0.05}}$	Stress at 0.05 plastic strain
$\boldsymbol{\sigma_{\varepsilon_p=0.001}}$	Stress at 0.001 plastic strain
$\boldsymbol{\Delta\kappa}$	Fatigue crack growth driving force
$\boldsymbol{\mu}$	Mean value of Normal distribution

ACRONYMS

AA	Aluminum association
ASME	American Society of Mechanical Engineers
ASTM	American Society for Testing and Materials
BS	British standards
CAPES	Coordenação de Aperfeiçoamento de Pessoal de Nível Superior

CCS	Castillo-Canteli-Siegele model
COV	Coefficient of variation
CT	Compact tension specimen
CTOD	Crack tip opening displacement
DIC	Digital image correlation
DNVGL	Det Norske Veritas (Norway) and Germanischer Lloyd (Germany)
EC3	Eurocode 3: Design of steel structures
EDM	Electrical discharge machining
ESE(T)	Single-edge cracked geometry
FCG	Fatigue crack growth
FEA	Finite element analysis
FEUP	Faculdade de Engenharia da Universidade do Porto
IFSP	Instituto Federal de São Paulo
iLAPS	Improved LAPS
LAPS	Long and physically short crack model
LCF	Low cycle fatigue
LEFM	Linear elastic fracture mechanics
MC, M.C.	Monte Carlo
NASA/FLAGRO	NASGRO computer program for fracture control analysis
SENB	Single-edge notched bending specimen
STP	Special technical publication (ASTM)
SWT	Smith-Watson-Topper (damage parameter)
TEM	Transmission electron microscopy
UNESP	Universidade Estadual Paulista “Júlio de Mesquita Filho”

CONTENTS

CHAPTER I

1 INTRODUCTION

1.1 MOTIVATION

Fatigue is the main cause of mechanical failures and fractures in mechanical components when subjected to load fluctuations[1-3]. Its studies had begun in the early nineteenth century and today it is still much addressed by the scientific and technical community. Despite the many advances, the infinity of proposed models, and its huge application in design codes[4-6], fatigue modeling is always linked to experimental results due to the high complexity of the phenomenon. In view of the recent evolution of experimental techniques[7-9], what is seen most in fatigue is the development of models that depend less and less on experimental data, either because of the scarcity of data, high occupancy of available equipment, or its high testing cost.

In this context, this research started with the development of a low-cost workbench (methodology) combining an experimental-analytical analysis to characterize the fatigue crack growth behaviour for the ESE(T) specimens of small thickness. A comparison between the crack growth constants (e.g. slope *m*) obtained in the low-cost workbench combining an experimental-analytical analysis and application of the ASTM E647 standard is done. A low-cycle fatigue modelling supported by the Huffman approach based on strain energy density considering the variability of the density of dislocations was suggested. In addition, the crack closure effects on fatigue crack propagation behaviour is also studied and discussed. Finally, the modelling of the fatigue crack growth behaviour based on the strain energy density approach suggested by Huffman[10], taking into account residual stress effects, is presented. In this investigation, experimental data on low cycle fatigue and fatigue crack propagation of 1050/1100[11], 6061-T651[12,13], and AlMgSi0.8[11] aluminium alloys were used.

1.2 OBJECTIVES

The general objective of this research project thesis is to investigate and discuss the modelling of the fatigue crack initiation and propagation behaviour in metals and alloys. To achieve this goal the main objectives are the following:

- To create a simple low-cost useful workbench, to establish a measurement setup for studying the fatigue crack propagation; To use the conventional machines to describe the fatigue crack propagation, the tensile test, hardness and microstructure of the selected material; and finally, to discuss and compare the results obtained in the workbench and conventional system.
- To investigate and discuss the low-cycle fatigue modelling based on the Huffman approach using the strain energy by suggesting different approaches for the dislocation density parameter. To apply Monte Carlo stochastic simulations for obtaining the strain-life parameters, fatigue strength and ductility coefficients, and to generate probabilistic fields for the low-cycle fatigue behaviour of metals. To analyse the various suggested methodologies using available experimental data from the literature, and compare them with each other.
- To compare and discuss the effects of various crack closure/opening models on the fatigue crack growth behaviour of 6061-T651 aluminium alloy and additionally to compare the models to experimental results of crack closure available in the literature.
- To model the fatigue crack growth behaviour for the 6061-T651 aluminium alloy through the Huffman fatigue crack growth approach based on the strain energy density from dislocations considering the residual stress effects, where a comparison with the fatigue crack growth data is done.

1.3 ORGANIZATION OF THESIS

This thesis is organized by: an introduction (Chapter I); a review on fatigue crack growth modelling (Chapter II); an experimental program to characterize the fatigue crack growth of 1100 aluminium alloy (Chapter III); a low-cycle fatigue modelling supported by strain energy density-based Huffman model considering the variability of dislocation density to (Chapter IV); an application and discussion of various crack closure models to predict fatigue crack growth in 6061-T651 aluminium alloy (Chapter V); a fatigue crack growth modelling supported by strain energy density-based Huffman model considering the residual stress effects (Chapter VI); and, finally, the main conclusions and future works (Chapter VII).

The thesis begins with an Introduction (Chapter I), presenting the motivation, the objectives, thesis organization and research contribution. The scope of the introductory part of this thesis is to describe and integrate each piece of this project and give the reader a broad view of the organization of this research.

Then, in Chapter II, a review on fatigue crack growth modelling is presented, where the following topics were addressed – fatigue crack growth laws, fatigue crack growth laws including crack closure effects and fatigue crack propagation based on local damage criteria.

Next, Chapter III is presented, whose title is **an experimental program to characterize the fatigue crack growth of 1100 aluminium alloy**, containing a useful low-cost workbench to describe fatigue crack propagation of very thin aluminium alloy specimens using digital image correlation. The chemical composition, hardness measurements, tensile strength, fatigue crack propagation, and microscopy analysis for Al1100 and Al1050 are also assessed. Furthermore, a comparison between the crack growth constants obtained in the low-cost workbench combining an experimental-analytical analysis and application of the ASTM E647 standard, considering the thickness effects, was also done.

In Chapter IV, entitled **Low-cycle fatigue modelling supported by strain energy density-based Huffman model considering the variability of dislocation density**, it is suggested various methodologies to evaluating low-cycle fatigue strength based on Huffman approach and exploring different dislocation density parameters: the critical dislocation density, the mean value of dislocation density of available experimental fatigue data, and a Monte Carlo stochastic prediction considering the variability of dislocation density and the cyclic strain hardening coefficient. Monte Carlo stochastic simulations are also used to obtain the strain-life parameters, fatigue strength and ductility coefficient, and to generate probabilistic fields for the low-cycle fatigue behaviour. Experimental fatigue data of aluminium alloys were used to apply and compare the suggested methodologies.

Chapter V, proposes **an application and discussion of various crack closure models to predict fatigue crack growth in 6061-T651 aluminium alloy**. At first, a review of fatigue crack growth laws considering the regions of applicability, and laws including crack closure effects is presented. Then, a comparison of the effect of various crack closure/opening models on the fatigue crack growth behaviour is done. Experimental data obtained from literature is compared with these models using deterministic quadratic relation. It was possible to observe that few models presented good fit to experimental crack closure results for the first or stabilised cycles, and many models are inappropriate to do the same.

In Chapter VI, the **modelling of the fatigue crack growth behaviour for the 6061-T651 aluminium alloy through the Huffman fatigue crack growth approach based on the strain energy density** from dislocations considering the residual stress effects was suggested. The Huffman fatigue crack growth modelling is based on the cyclic stress-strain behaviour of the material as well as the local elastoplastic stresses and strains obtained for a distance ahead of the crack tip (x), where those stresses are related to the fatigue damage of a crack increment Δa, as calibrator parameter. The calculations of the elastoplastic stresses and strains are done using Neuber’s or Glinka’s approach. Two approaches supported by the Noroozi and Huffman's suggestions to consider the residual stress effects were studied and discussed. Besides, in the modelling of the fatigue crack growth behaviour, the influence of the strain energy density calculated for values of critical dislocation density driven by the highest strain amplitude specimen and the mean value of the dislocation density for the available experimental fatigue results was also considered in this investigation.

And finally, in Chapter VII, the main conclusions and future works are presented. It starts with a summary of the main results obtained in each section, and then, it lists the contributions that were made and future steps for the continuity of this research.

1.4 RESEARCH CONTRIBUTIONS

The research contributions presented in this research project thesis are the following:

- A low-cost useful workbench to characterize the fatigue crack propagation in thin specimens;
- Fatigue crack propagation behaviour, mechanical properties, microstructure of commercially pure aluminium were evaluated;
- A comparison of the effect of various crack closure/opening models on the fatigue crack growth behaviour of 6061-T651 aluminium alloy was presented.
- Various fatigue crack closure/opening models were explored.

- Deterministic quadratic relations between U vs. R and R_{eff} vs. R, for the 6061-T651 aluminium alloy, were suggested.
- Low-cycle fatigue behaviour based on the Huffman approach, 1050, 6061-T651 and AlMgSi0.8 aluminium alloys, was studied and discussed.
- Variability of dislocation density on the low-cycle fatigue behaviour was introduced.
- A Monte Carlo stochastic procedure for probabilistic low-cycle fatigue modelling was suggested.
- A comparison between the experimental fatigue data and strain-life curves, 1050, 6061-T651 and AlMgSi0.8 aluminium alloys, is done.
- Fatigue crack growth modelling based on the Huffman FCG approach based on strain energy density and residual stress effects, for the fatigue data of the 6061-T651 aluminium alloy, was done.
- Strain energy density for values of critical dislocation density driven by the highest strain amplitude specimen and the mean value of the dislocation density for the available experimental fatigue results was discussed.
- Residual stress effects based on Noroozi and Huffman's suggestions were studied.

REFERENCES

1 SURESH, S. **Fatigue of materials**. 2. ed. Cambridge: Cambridge university press, 1998.

2 GONCALVES, A.C.; EKWARO-OSIRE, S.; ALEMAYEHU, F.M. **Probabilistic prognostics and health management of energy systems.** 1. ed. Cham: Springer, 2017.

3 PARIS, P.C. A rational analytic theory of fatigue. **The trend in engineering**, Seattle, v. 13, n. 9, p. 9-14, 1961.

4 BRITISH STANDARDS INSTITUTION. **BS7910:2005**: Guidance on Methods for Assessing the Acceptability of Flaws in Metallic Structures. London: BSI, 2005.

5 EUROPEAN COMMITTEE FOR STANDARDIZATION. **CEN-TC 250. EN 1993-1-9: Eurocode 3**: Design of steel structures – Part 1-9: Fatigue. Brussels: European Committee for Standardization, 2003.

6 DET NORSKE VERITAS AND GERMANISCHER LLOYD GROUP - DNV GL

Group. **DNVGL-RP-C203:** fatigue design of offshore steel structures. Oslo: DNV GL AS, 2016.

7 AMERICAN SOCIETY FOR TESTING AND MATERIALS – ASTM. **ASTM E647-15e1**: Standard test method for measurement of fatigue crack growth rates. West Conshohocken: ASTM International, 2015.

8 AMERICAN SOCIETY FOR TESTING AND MATERIALS – ASTM. **ASTM E606M-19e1**: Standard Test Method for Strain-Controlled Fatigue Testing. West Conshohocken: ASTM International, 2019

9 AMERICAN SOCIETY FOR TESTING AND MATERIALS – ASTM. **ASTM E8/E8M-21**: Standard test methods for tension testing of metallic materials. West Conshohocken: ASTM International, 2021.

10 HUFFMAN, P.J. A strain energy based damage model for fatigue crack initiation and growth. **International Journal of Fatigue**, London, vol. 8, p. 197-204, 2016.

11 BOLLER C.; SEEGER T. **Materials data for cyclic loading**: part D: aluminium and titanium alloys. Amsterdam: Elsevier Science Publishers, 1987. (Materials Science Monographs, v. 42D).

12 CORREIA, J.A.F.O.; DE JESUS, A.M.P.; RIBEIRO, A.S.; FERNANDES, A.A.; Strain-based approach for fatigue crack propagation simulation of the 6061-T651 aluminium alloy, **International Journal of Materials and Structural Integrity**, Geneva, v. 11, n. 1-3, p. 1-15, 2017.

13 RIBEIRO, A.S.; JESUS, A.M.P.; FERNANDES, A.A. Fatigue crack propagation rates of the aluminium alloy 6061-T651. *In*: INTERNATIONAL CONGRESS OF MECHANICAL ENGINEERING, 18., 2005, Ouro Preto. **Proceedings** […]. Ouro Preto: COBEM, 2005.

CHAPTER II

2 REVIEW ON FATIGUE CRACK GROWTH MODELLING

2.1 INTRODUCTION

Over the years the scientific community has presented several models to describe the fatigue crack growth mechanisms in metals, taking into account different stages of the fatigue crack evolution. Fatigue crack growth models presented by many researchers can be based on stress intensity factor, K, or J-Integral formulations, energetic parameters as well as they can be formulated in terms of fatigue local approaches[1-23]. In several fatigue crack propagation laws, the crack opening and closure effects are taken into account. These effects are typically defined using the quantitative closure parameter, U, that can be evaluated using many theoretical assumptions, the plasticity-induced crack-closure theory being a most used one.

2.2 FATIGUE CRACK GROWTH LAWS

With the advancement of Fracture Mechanics, several fatigue crack propagation models emerged in the literature. The first crack growth law was obtained using experimental results from fatigue crack growth tests of the materials and was proposed by Paris[1] being denominated in the literature by Paris's law. This gives a good description of the fatigue crack propagation in fatigue regime II (see Figure 2.1), correlating the fatigue crack growth rate, da/dN, with the stress intensity factor range, ΔK, using a power relation:

$$\frac{da}{dN} = C_p \cdot \Delta K^{m_p} \tag{2.1}$$

where C_p and m_p are material constants. This crack propagation law was validated for a specific fatigue crack propagation regime II, which occurs in between the near threshold fatigue crack propagation regime (regime I) and the near unstable crack propagation regime (regime III), as displayed in Figure 2.1.

The differential equation to represent these three regimes takes the following configuration:

$$\frac{da}{dN} = f(\Delta K, R_\sigma) \tag{2.2}$$

where ΔK is the applied stress intensity factor range, R_σ is the stress R-ratio, and f() is the function defining the fatigue crack growth rates.

Given the Paris law limitations (e.g. does not consider the stress R-ratio effects), Walker[2] proposed an alternative law to overcome these limitations, resulting:

$$\frac{da}{dN} = C_w\left[\frac{\Delta K}{(1-R_\sigma)^{1-\gamma_w}}\right]^{m_w} = C_w[\overline{\Delta K}]^{m_w} \tag{2.3}$$

For R_σ=0, the Walker law takes the form of the Paris relation. The constants C_w and m_w are equivalent to the ones appearing in the Paris law and γ_w is an extra constant introduced to account for stress ratio effects.

Forman[3] proposed an improved version of the Walker law aiming at describing the crack propagation regime III and also to include the stress R-ratio effects. This law is given by the following expression:

$$\frac{da}{dN} = \frac{C_F(\Delta K)^{m_F}}{(1-R_\sigma)(K_c-K_{max})} \tag{2.4}$$

where K_{max} is the maximum stress intensity factor, K_c is the fracture toughness, C_f and m_f are constants that are equivalent to the Paris law constants. In further studies, Forman modified Equation (2.4) to represent the regimes I, II and III, with the inclusion of the threshold stress intensity factor range, ΔK_{th}. In this regard, Hartman and Schijve[4] proposed an expression that represents the continuity of the study by Forman:

$$\frac{da}{dN} = \frac{C_{HS}(\Delta K-\Delta K_{th})^{m_{HS}}}{(1-R_\sigma)K_c-\Delta K} \tag{2.5}$$

Other version of the Forman law is given by:

$$\frac{da}{dN} = \frac{C_{MOD}(\Delta K)^{m_{MOD}}(\Delta K-\Delta K_{th})^{0.5}}{(1-R_\sigma)K_c-\Delta K} \tag{2.6}$$

where C_{MOD} and m_{MOD} are material constants. Other expressions to describe the three fatigue crack propagation regimes have been proposed by other authors, such as Collipriest and Miller and Gallagher[5]. There were also various proposals to describe the regimes I and II by several authors, notably McEvily[5] and Alves *et al.*[6]. Many other fatigue crack propagation models have been proposed to represent the fatigue crack propagation regime II[5]. These models have been proposed by different authors, such as Frost and Pook, Lal and Weiss, Zheng, Wang, Miller and Gallagher[5].

Figure 2.1 - Fatigue crack propagation regimes.

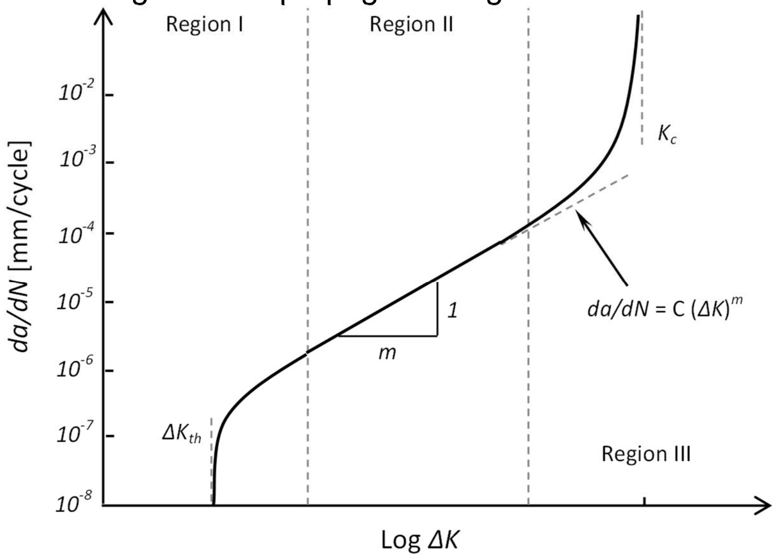

Source: Prepared by the author.

Recently, a new approach was developed to describe the fatigue crack propagation rates based on the cumulative distribution function – statistical Gumbel distribution. This new model for fatigue crack propagation was proposed by Castillo-Canteli-Siegele (so called CCS fatigue crack propagation model)[7,8]. This model makes an appropriate dimensional analysis of the influent variables in order to use non-dimensional normalized parameters. Thus, the crack growth rate curve is identified by a statistical cumulative distribution function of ΔK^{*+} (normalizing variable of ΔK) assuming values in the interval [0,1] and log (da/dN) is assumed as the random variable. The proposed CCS model is an explicit fatigue crack growth model supported by mathematical and physical assumptions, and is defined by[7,8]:

$$\Delta K^{*+} = \frac{log\ \Delta K^{*} - log\ \Delta K^{*}_{th}}{log\ \Delta K^{*}_{up} - log\ \Delta K^{*}_{th}}$$

$$\Delta K^{*+} = F\left(log \frac{da^{*}}{dN^{*}}\right) = exp\left[-exp\left(\frac{\alpha - log\ \frac{da^{*}}{dN^{*}}}{\gamma}\right)\right] \tag{2.7}$$

where, $F()$ is the cumulative distribution function, α and γ are parameters of the statistical Gumbel distribution.

This recent model depends on normalized variables suggested by the authors, namely[7,8]:

$$a^{*} = \frac{a}{W} \tag{2.8}$$

$$N^* = \frac{N}{N_0}$$

$$\Delta K^* = \frac{K_{max} - K_{min}}{K_c}$$

$$\Delta K_{th}^* = \frac{\Delta K_{th}}{K_c}$$

$$\Delta K_{up}^* = \frac{\Delta K_{up}}{K_c}$$

where, a is the crack length, W is a characteristic length (e.g. specimen width), N is the number of cycles, N_0 is a reference number of cycles (this parameter can take any value), K_{max} and K_{min} are the maximum and minimum stress intensity factors, respectively, ΔK_{th} is the threshold stress intensity factor range, ΔK_{up} is the ultimate stress intensity factor range, and finally, K_c is the material characteristic fracture toughness. The Equation (2.7) of the CCS model can be written in the following form:

$$\frac{da^*(N^*)}{dN^*} = exp\left[F^{-1}\left(\frac{log\ \Delta K^* - log\ \Delta K_{th}^*}{log\ \Delta K_{up}^* - log\ \Delta K_{th}^*}\right)\right] \tag{2.9}$$

This model does not take into account the stress R-ratio and crack closure effects, i.e.; it is not possible to generate da/dN vs. ΔK curves for other stress R-ratios from other already known propagation curves for a given material. The constants of this model may be determined from the least squares technique.

The fatigue crack growth models previously presented are all in the field of linear-elastic Fracture Mechanics (LEFM). For the generalized elastoplastic conditions, Dowling and Begley[9] proposed the J-Integral parameter (ΔJ) using elastoplastic Fracture Mechanics in order to evaluate the fatigue crack growth, which is very similar to the Paris expression. Moreover, an expression for the fatigue crack growth law using the J-integral parameter was proposed by Alves *et al.*[6,10] in order to account for the regime I fatigue crack propagation.

In a recent publication, Correia *et al.*[11] proposed an extension of CCS model to cover the cases of elastoplastic loading. This updated CCS model is based on the replacement of stress intensity factor range, ΔK, by the cyclic J-integral range, ΔJ, which results in a modification of the CSS crack growth model. This model also does not take into account the effects of the crack closure and stress R-ratio. The adjustments for each stress ratio were made independently.

Therefore, for generalized elastoplastic conditions, some authors have proposed the use of elastoplastic Fracture Mechanics parameters to correlate the fatigue crack growth, as is the case of the J-Integral, as proposed by Dowling and Begley[12]:

$$\frac{da}{dN} = C \cdot \Delta J^{m} \tag{2.10}$$

where da/dN is the fatigue crack growth rate, ΔJ is the range of the cyclic J-integral. This equation is similar to the Paris relation (fits data in region II), but can be advantageously applied in situations of large scale yielding.

Rice[13] introduced the initial concept of the J-integral, using the general definition of the range value of the cyclic J-integral, ΔJ. The ΔJ value is calculated using for the material behaviour based on the cyclic stress-strain curve taking into account an established hysteresis loop, which may be described by the Ramberg–Osgood relation[14]:

$$\frac{\Delta\varepsilon}{2} = \frac{\Delta\sigma}{2E} + \left(\frac{\Delta\sigma}{2K'}\right)^{1/n'} \tag{2.11}$$

where, n' and K' are the cyclic strain hardening coefficient and exponent, respectively.

Another extension of the Paris-type crack growth law was proposed by Alves *et al.*[6], to account for fatigue crack propagation regime I with the following expression:

$$\frac{da}{dN} = C(\Delta J - \Delta J_{th})^{m}, for\ \Delta J \geq \Delta J_{th} \tag{2.12}$$

where ΔJ_{th} is threshold value of the cyclic J-integral.

An extended CCS model was proposed by Correia *et al.*[11] to cover the cases of elastoplastic loading, replacing the stress intensity factors on Equations (2.7) to (2.9) by the cyclic J-integral counterparts. The modified CCS crack growth model is therefore given by the following expression:

$$\begin{gathered} \Delta J^{*+} = \frac{log\ \Delta J^{*} - log\ \Delta J^{*}_{th}}{log\ \Delta J^{*}_{up} - log\ \Delta J^{*}_{th}} \\ \Delta J^{*+} = F\left(log\frac{da^{*}}{dN^{*}}\right) = exp\left[-exp\left(\frac{\alpha - log\ \frac{da^{*}}{dN^{*}}}{\gamma}\right)\right] \end{gathered} \tag{2.13}$$

which depends on four parameters α, γ, ΔJ_{th} and ΔJ_{up}. The normalized variables suggested by authors, are then rewritten by the following relations:

$$a^* = \frac{a}{W};\ N^* = \frac{N}{N_0};\ \Delta J^* = \frac{J_{max} - J_{min}}{J_c};\ \Delta J^*_{th} = \frac{\Delta J_{th}}{J_c};\ \Delta J^*_{up} = \frac{\Delta J_{up}}{J_c} \tag{2.14}$$

where, a, W, N and N_0 have the same characteristics that the crack growth model proposed by Castillo-Canteli-Siegele[7,8], J_{max} and J_{min} is the maximum and minimum values of the cyclic J-integral, respectively, ΔJ_{th} is the threshold range value of the cyclic J-integral, ΔJ_{up} is the limit range value of the cyclic J-integral, and finally, J_c is the material characteristic fracture toughness in J-integral. More precisely, we can write of the following forms:

$$\begin{aligned} log\frac{da^*}{dN^*} &= F^{-1}(\Delta J^{*+}) = F^{-1}\left(\frac{log\ \Delta J^* - log\ \Delta J^*_{th}}{log\ \Delta J^*_{up} - log\ \Delta J^*_{th}}\right) \\ \frac{da^*}{dN^*} &= exp[F^{-1}(\Delta J^{*+})] = exp\left[F^{-1}\left(\frac{log\ \Delta J^* - log\ \Delta J^*_{th}}{log\ \Delta J^*_{up} - log\ \Delta J^*_{th}}\right)\right] \end{aligned} \tag{2.15}$$

where, F() is a cumulative distribution function.

According to Correia *et al.*[11], this modified CCS model was applied to the P355NL1 steel for various stress R-ratios, as shown in Figure 2.2. A good agreement can be found between the experimental results and the model application.

Figure 2.2 - Fatigue crack propagation regimes[11].

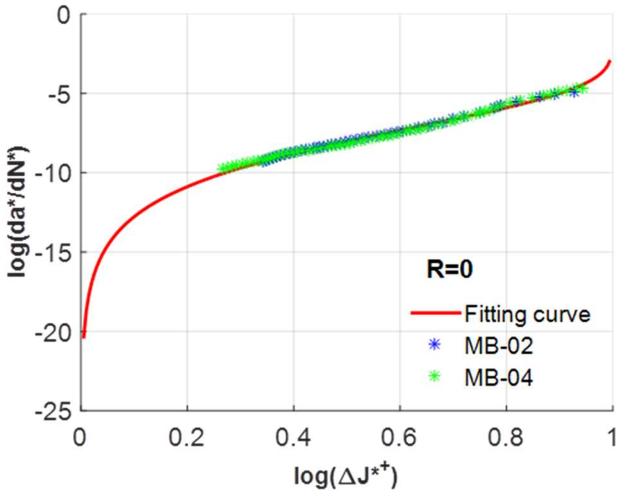

a)

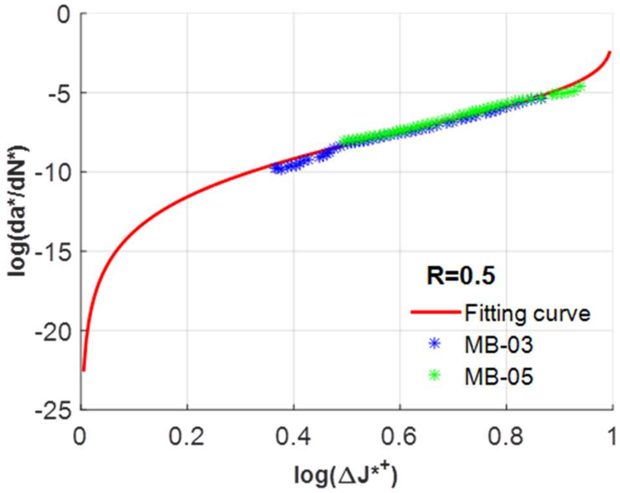

b)

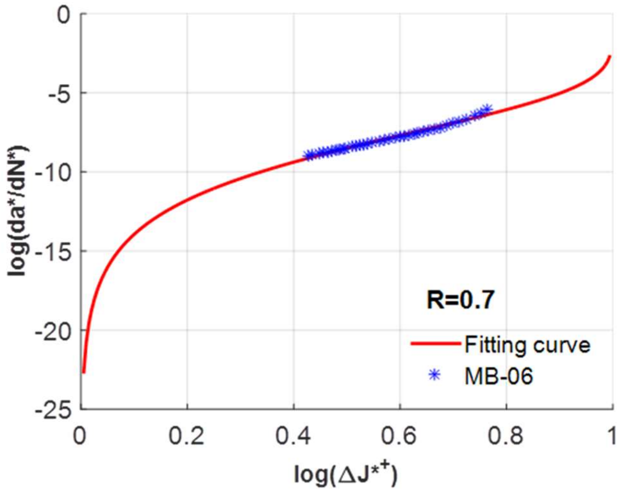

c)

Source: Correia *et al.*[11].

2.3 FATIGUE CRACK GROWTH LAWS INCLUDING CRACK CLOSURE EFFECTS

The fatigue crack growth laws including crack closure effects are based on the relationship between the fatigue crack growth rate, da/dN, and a function of the effective stress intensity factor range, ΔK_{eff}, in the following general form:

$$\frac{da}{dN} = f\left(\Delta K_{eff}\right) \tag{2.16}$$

The effective stress intensity factor will be defined using the closure parameter, U, as suggested by Elber, which presents the following form[15,16]:

$$U = \frac{\Delta K_{eff}}{\Delta K} = \frac{K_{max} - K_{op}}{K_{max} - K_{min}} \tag{2.17}$$

where, ΔK_{eff} is the effective stress intensity factor range, K_{max} is the maximum stress intensity factor, K_{op} is the crack opening stress intensity factor, ΔK is the applied stress intensity factor range and K_{min} is the minimum stress intensity factor. The definitions of each of these parameters are illustrated in Figure 2.3.

Figure 2.3 - Definitions of the effective stress intensity factor range and related parameters.

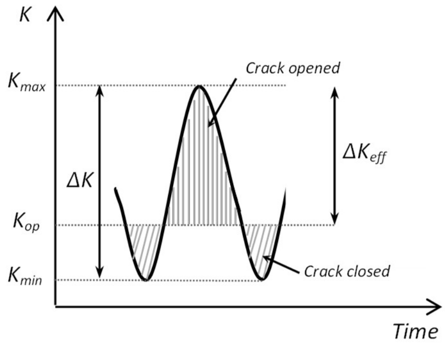

Source: Prepared by the author.

The quantitative closure parameter U takes different expressions depending on the studies carried out by different authors. Some expressions for the quantitative closure parameter U are the following:

$U = 0.5 + 0.4R, \quad -0.1 \leq R \leq 0.7$ Elber[15,16] (2.18)

$U = 0.55 + 0.33R + 0.12R^2, \quad -1 \leq R \leq 1$ Schijve[17] (2.19)

$U = 0.576 + 0.015R + 0.409R^2$

$\Delta K = K_{max} \; for \; R < 0$ ASTM[12,13] (2.20)

$\Delta K = K_{max} - K_{min} \; for \; R \geq 0$

Equation (2.19) proposed by Schijve[17] describes a more realistic behaviour of the crack closure and opening effects than the others equations.

Approaches based on experimental results from fatigue crack propagation tests and theoretical assumptions were proposed by Hudak and Davidson[18], Ellyin[19] and Correia *et al.*[14,20]. These approaches are given by the following expressions:

$U = \gamma\left(1 - \frac{K_o}{K_{max}}\right), \quad K_{max} \leq K_L$

$U = 1, \quad K_{max} \geq K_L$

Hudak and Davidson[18] (2.21)

$\Delta K_{eff,0} = (\Delta K^2 - \Delta K_{th}^2)^{1/2}$ Ellyin[19] (2.22)

$$\Delta K_{eff,0} \approx \Delta K \left[1 - \frac{1}{2}\left(\frac{\Delta K_{th}}{\Delta K}\right)^2\right]$$
$$> \Delta K - \Delta K_{th} \quad for\ R \approx 0$$
$$\Delta K_{eff} = \frac{\Delta K_{eff,0}}{\left[1 - \left(\sigma_m/\sigma_f'\right)\right]}$$
$$= \frac{\Delta K_{eff,0}}{\left[1 - \left((1+R)\,\sigma_{max}/2\sigma_f'\right)\right]} \quad for\ R \neq 0$$

$$U = \left(1 - \frac{\Delta K_{th,0}}{K_{max}}\right)(1-R)^{\gamma-1}\ for\ K_{max} \leq K_L$$
$$U = 1\ \ for\ K_{max} \geq K_L$$

Correia *et al.*[14,20] (2.23)

where, K_o is a constant related to the pure Mode I fatigue crack growth threshold, K_L is the limiting K_{max} value above which no detectable closure occurs, σ_m is the mean stress, σ_{max} is the maximum stress, and σ_f' is the fatigue strength coefficient.

Others approaches were proposed by Newman[21], Vormwald *et al.*[22] and Savaidis *et al.*[23] to estimate the fatigue crack closure and opening effects based on the plasticity-induced effects. The classic plasticity-induced model proposed by Newman[21] was suggested for constant amplitude loading, function of the stress R-ratio, stress level, σ, and four non-dimensional constants that are dependent on the uniaxial yield stress and uniaxial ultimate tensile strength of the material. The models proposed by Vormwald *et al.*[22] and Savaidis *et al.*[23] are based on classic plasticity-induced model proposed by Newman[21].

A proposed modification of the normalized CCS fatigue crack growth model was presented, taking into account the crack opening and closure effects based on plasticity-induced crack-closure of the material[3]. The proposal for modification of the normalized CCS fatigue crack growth model[3] is supported by replacing of the applied stress intensity factor range, ΔK, by the effective stress intensity factor range, ΔK_{eff}, in the original law[3,4]. That proposed modification results in the following normalized effective stress intensity factor parameter:

$$\Delta K_{eff}^{*+} = \frac{log\Delta K_{eff}^{*} - log\ \Delta K_{th,eff}^{*}}{log\ \Delta K_{up,eff}^{*} - log\ \Delta K_{th,eff}^{*}}$$
$$\Delta K_{eff}^{*+} = F\left(log\frac{da^{*}}{dN^{*}}\right) = exp\left[-exp\left(\frac{\alpha - log\ \frac{da^{*}}{dN^{*}}}{\gamma}\right)\right] \tag{2.24}$$

The authors suggest the new normalized variables[3], given by the following relations:

$$\Delta K_{eff}^{*} = \frac{\Delta K_{eff}}{K_c} = \frac{\Delta K \cdot U}{K_c}$$
$$\Delta K_{th,eff}^{*} = \frac{\Delta K_{th,eff}}{K_c} \tag{2.25}$$
$$\Delta K_{up,eff}^{*} = \frac{\Delta K_{up,eff}}{K_c}$$

where, a, W, N, N_0, ΔK and K_c have the same characteristics of the original CCS crack growth model, $\Delta K_{th,eff}$ is the effective stress threshold and $\Delta K_{up,eff}$ is the effective limit stress intensity factor range.

The quantitative parameter U can be obtained for the experimental results using a crack closure model and it takes the following form:

$$U = \frac{\Delta K_{eff}}{\Delta K}$$
$$U = U_i\left[K_{op}(a_i), K_{max}(a_i), a_i, R\right], where\ i = 1\ to\ n \tag{2.26}$$

or

$$U = U_i\left\{R_{eff,i}\left[K_{op}(a_i), K_{max}(a_i)\right], a_i, R\right\}, where\ i = 1\ to\ n$$

where, K_{op} is the crack opening stress intensity factor, K_{max} is the maximum stress intensity factor, R is the stress R-ratio, a_i is the crack length and R_{eff} $(= K_{op}/K_{max})$ is the effective stress R-ratio that accounts for higher minimum stress intensity factor range due to crack closure. Index i stands for the crack increment with i=1 and i=n corresponding to the first crack length and last crack length of the propagation phase, respectively.

The $\Delta K_{th,eff}$ parameter can be evaluated taking into account the quantitative parameter U and stress intensity range threshold, ΔK_{th}, function of the stress R-ratio, R, that is based on the relation proposed by Klesnil and Lukáš[24,25]:

$$\Delta K_{th} = \Delta K_{th,0} \cdot (1 - R)^{\gamma_{th}} \tag{2.27}$$

$$\Delta K_{th,eff} = \Delta K_{th} \cdot U_{th}$$
$$U_{th} = U_1\left[K_{op}(a_1), K_{max}(a_1), a_1, R\right]$$

where, $\Delta K_{th,0}$ is the pure Mode I stress intensity factor range threshold for null stress ratio, γ_{th} is material constant, R is the stress R-ratio, U_{th} is the quantitative parameter U for the first crack length that corresponds to the crack closure effects for the threshold stress intensity factor range, ΔK_{th}, regime I of the propagation phase, and it is linked to roughness-induced crack-closure.

The $\Delta K_{up,eff}$ parameter can be estimated taking into account the material characteristic fracture toughness, K_c, and the U_{up} that is the quantitative closure parameter U for the last crack length corresponding to the ΔK_{up}. This parameter is given by the following equation:

$$\begin{aligned} &\Delta K_{up} = K_c(1-R)^{\gamma_{up}} \\ &\Delta K_{up,eff} = \Delta K_{up} \cdot U_{up} \\ &U_{up} = U_n\left[K_{op}(a_n), K_{max}(a_n), a_n, R\right] \end{aligned} \tag{2.28}$$

where, γ_{up} is a material constant, R is the stress R-ratio, U_{up} is the quantitative closure parameter U for the last crack length that corresponds to the crack closure effects for the limit stress intensity factor range, ΔK_{up}, in the regime III of the propagation phase, and it can be determined using the plasticity-induced crack-closure model based on experimental results.

The U quantitative parameter can be obtained with experimental fatigue tests using experimental techniques[17-19] or estimated using analytical[21-23] and numerical[26,27] methods. These methods are presented in the literature. In the modified CCS fatigue crack growth model, the U quantitative closure parameter is calculated based on plasticity-induced crack-closure model that was proposed by Huffman[28].

Thus, the modified CSS model for the fatigue crack growth rates can be written in the following explicit form:

$$\begin{aligned} &log\,\frac{da^*}{dN^*} = F^{-1}\left(\Delta K_{eff}^{*+}\right) = F^{-1}\left(\frac{log\,\Delta K_{eff}^* - log\,\Delta K_{th,eff}^*}{log\,\Delta K_{up,eff}^* - log\,\Delta K_{th,eff}^*}\right) \\ &\frac{da^*}{dN^*} = exp\left[F^{-1}\left(\Delta K_{eff}^{*+}\right)\right] = exp\left[F^{-1}\left(\frac{log\,\Delta K_{eff}^* - log\,\Delta K_{th,eff}^*}{log\,\Delta K_{up,eff}^* - log\,\Delta K_{th,eff}^*}\right)\right] \end{aligned} \tag{2.29}$$

where $F()$ is a cumulative distribution function which was selected as the minimal Gumbel function.

According to Correia *et al.*[29], this CCS model considering the crack closure effects using the Huffman model conducted to a good agreement when compared with the experimental results. In Figure 2.4, an application of this model proposed by Correia *et al.*[29] was made for the experimental fatigue crack growth data of the 2219-T851 aluminium alloy.

Figure 2.4 - Fatigue crack growth data correlated with the updated CCS crack growth model taking into account the crack closure effects for all stress R-ratios[29].

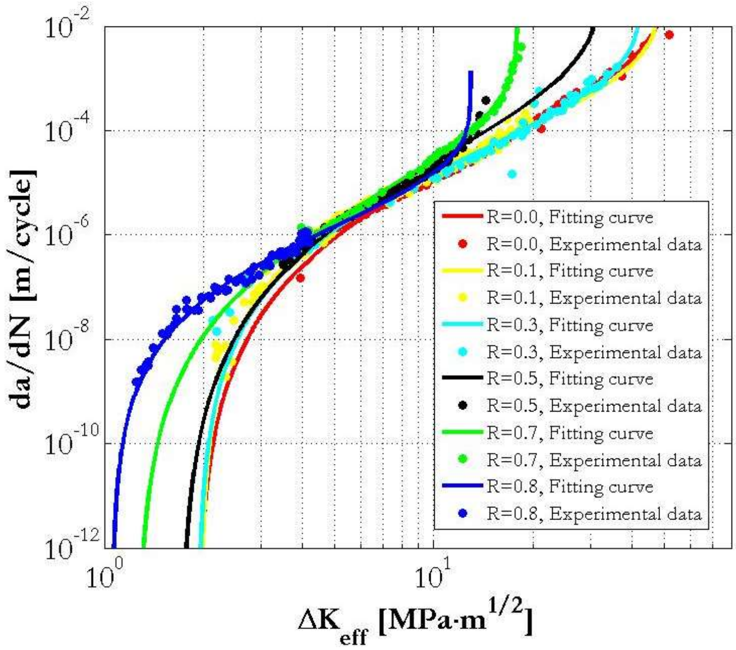

Source: Correia *et al.*[29].

2.4 FATIGUE CRACK PROPAGATION MODELLING BASED ON LOCAL DAMAGE CRITERIA

The research about the fatigue behaviour of materials and structures has been engaged by both academia and industry. Fatigue has been investigated since the industrial revolution and still is a hot topic in research due to the lack of trustful predictive models and due to new materials and applications being continuously explored[30]. The investigation on fatigue crack propagation is not fully accomplished, despite the great achievements of the last decades, in particular probabilistic approached are still lacking.

Paris *et al.*[31] were the first to establish a correlation between the fatigue crack propagation rates and the stress intensity factor, suggesting the well-known and widely accepted Paris's law. Since this contribution, the pioneer Paris's law has been used extensively to model fatigue crack growth under constant amplitude loading and also random loading. However, Paris' law shows several limitations, namely it only models the stable crack propagation, excluding near threshold and near unstable fatigue crack propagation regimes. It is a deterministic approach for fatigue crack propagation. Also, the stress ratio effects are not accounted for by the Paris' law. Many other fatigue crack propagation laws have been proposed to overcome the limitations of the Paris' law and also to deal with variable amplitude loading[5]. The assorted of fatigue models available in the literature differ on the number of variables and parameters involved and application domains. However their use requires the evaluation of expensive time consuming fatigue crack propagation tests in order to identify their constants.

Local fatigue strain-based approaches[32-35] could represent an alternative to the Fracture Mechanics fatigue crack propagation approaches. These local strain-based approaches to fatigue are very often applied to model the fatigue crack initiation on notched components[36]. Also, many times they are complemented with fracture mechanics to allow full fatigue life assessments.

Some authors, such as Glinka[37], Peeker and Niemi[38], Noroozi *et al.*[39,41,42], Hurley and Evans[40] have been applied the local-strain based fatigue models to model fatigue crack propagation. Glinka was one of the first researchers to model fatigue crack propagation using a strain-based fatigue relation[37]. The crack was assumed to have a notch with a tip radius, ρ* and the material ahead of the crack tip was assumed to be divided into elemental blocks of finite linear dimension, ρ* (see Figure 2.5). The crack growth was assumed as the failure of the successive elemental blocks, the fatigue crack growth rate being defined by the following relation:

$$\frac{da}{dN} = \frac{\rho^*}{N_f} \tag{2.30}$$

where N_f represents the number of cycles to fail the elemental block of dimension, ρ*. This approach allowed expressing directly the fatigue crack growth rate with the strain-life relation constants.

Similarly, the model proposed by Peeker and Niemi[39] allowed the description of the near threshold fatigue crack propagation data and the stable crack growth (see Figure 2.6). For the near threshold fatigue crack propagation, the authors derived the following analytical relations function of the strain-life constants:

$$\frac{da}{dN} = C_{el} \Delta K^{m_{el}} \tag{2.31}$$

$$C_{el} = 2\delta\left[\left(\sigma'_f - \sigma_m\right)\sqrt{2\pi\delta}\right]^{\frac{1}{b'}}$$

$$m_{el} = -\frac{1}{b'}$$

For the stable crack growth, the above authors derived the following alternative relations, that besides the elastoplastic strain-life constants it uses the cyclic stress-strain constants:

$$\frac{da}{dN} = C_{pl}\Delta K^{m_{pl}}$$

$$C_{pl} = 2\delta\left[\varepsilon'_f\left(\frac{4\pi\delta K'E}{n'+1}\right)^{\frac{1}{n'+1}}\right]^{\frac{1}{c'}} \quad (2.32)$$

$$m_{pl} = -\frac{2}{c'(n'+1)}$$

Superposition the previous two relations, led the following analytical expression for the fatigue crack propagation law covering both fatigue propagation regimes I and II:

$$\frac{da}{dN} = \frac{1}{\frac{1}{C_{pl}\Delta K^{m_{pl}}} + \frac{1}{C_{el}\Delta K^{m_{el}}}} \quad (2.33)$$

The application of the local approaches to fatigue on fatigue crack growth simulation requires the definition of a crack path discretization. The size of the elements used to discretize the crack path should account for two criteria: a) the size must be large enough to represent the local material properties by their mean values using continuous variables, and b) its size should be related to material micro-structural parameters, such as the material grain-size. For structural steels, and according reference[10], the criteria result in an average element size of 0.1mm.

Figure 2.5 - Crack discretization according to the UniGrow model: a) crack and the discrete elementary material blocks; b) crack shape at the tensile maximum and compressive minimum loads[37].

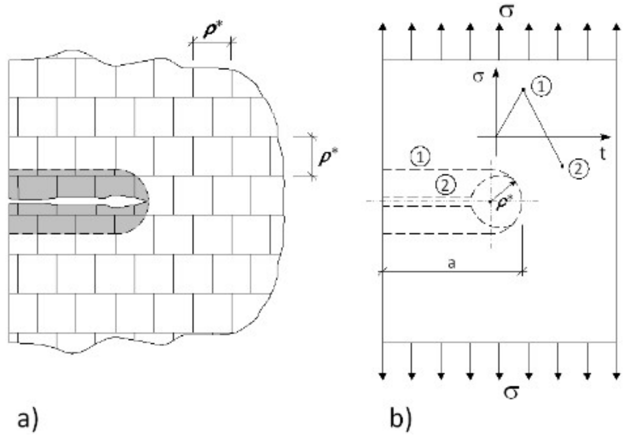

Source: Glinka[37].

Figure 2.6 - Crack discretization with elements according to the model proposed by Peeker and Niemi[38].

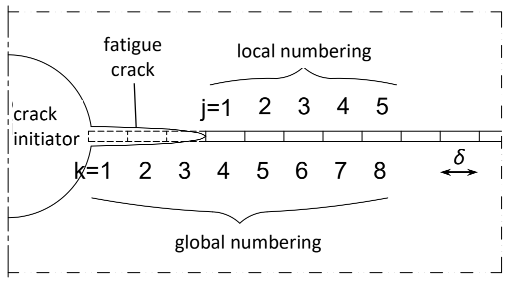

Source: Peeker and Niemi[38].

In general, elastoplastic stress analysis at the crack vicinity is required and very often analytical approaches are followed. Nonetheless Hurley and Evans[40] proposed the use of elastoplastic finite element analysis. The fatigue life of the process zone was computed using the Walker strain that was correlated directly with the fatigue life, from the experimental data using a power relation. This Walker strain is defined according to the following relation:

$$\varepsilon_w = \frac{\sigma_{max}}{E}\left(\frac{\Delta\varepsilon E}{\sigma_{max}}\right)^w \tag{2.34}$$

where σ_{max} is the maximum stress, E is the Young modulus, $\Delta\varepsilon$ is the strain range and w is a constant varying between 0 and 1. These authors applied the following definition of the cyclic plastic zone, which is assumed equal to the fatigue process damage zone under plane strain conditions:

$$\Delta a_i = \frac{1}{3\pi}\left(\frac{\Delta K}{2\sigma_0}\right)^2 \tag{2.35}$$

where σ_0 is the cyclic yield stress and ΔK the stress intensity factor range computed from the numerical model. The approach proposed by these authors was much simpler than those proposed by previous authors. It was supported by numerical models disregarding analytical aspects that allowed previous authors to verify the relation between these local approaches to fatigue and the Fracture Mechanics approaches for fatigue crack propagation.

In all previous studies, the fatigue crack propagation is assumed as a process of continuous crack re-initializations (failure of consecutive representative materials elements). The resulting crack propagation models have demonstrated to correlate fatigue crack propagation data from several sources, including the stress ratio effects, as shown in Figure 2.7 for the Glinka studies. The crack tip stress-strain fields are computed using elastoplastic analysis, which are applied together with a fatigue damage law to predict the failure of the representative material elements. The simplified method of Neuber[43] or Moftakhar *et al.*[44] may be used to compute the elastoplastic stress field at the crack tip vicinity using the elastic stress distribution given by the Linear Elastic Fracture Mechanics[39,44,45].

Figure 2.7 - Fatigue crack growth data for Al 2024 T351 aluminium alloy according to UniGrow model[39].

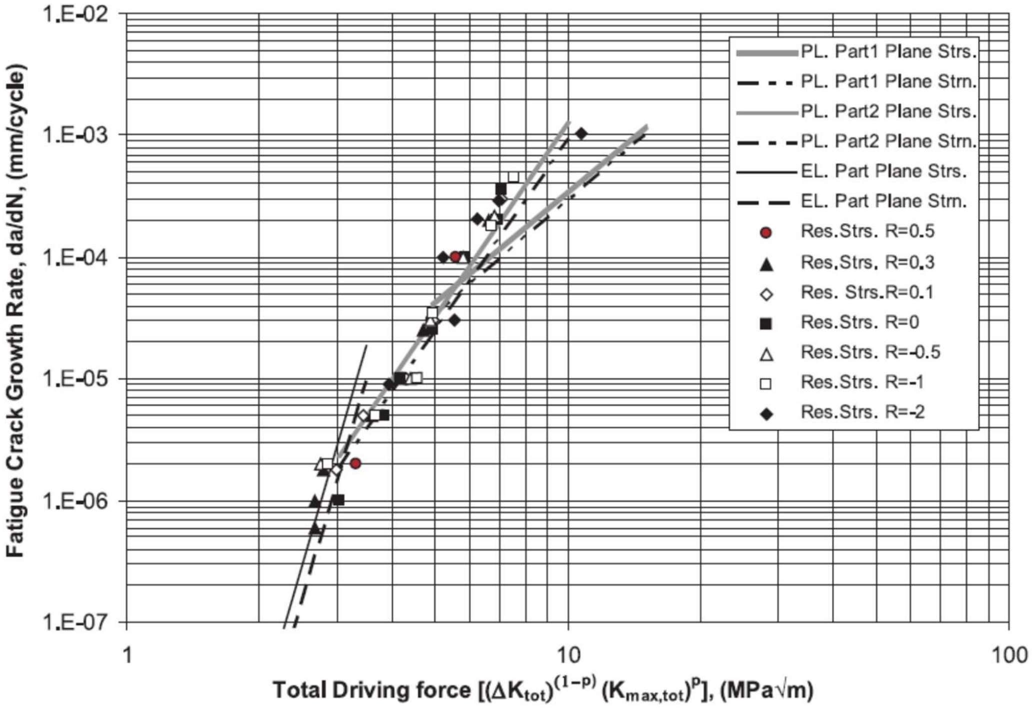

Source: Noroozi *et al.*[39].

Correia adapted the Unigrow model in order to use the residual stress distributions obtained numerically. In addition, this author used various damage parameters such as strain, SWT, etc. Additionally, probabilistic fields from these local damage parameters were used to model the probabilistic fatigue crack propagation behaviour. These studies were conducted for several materials from the old steel bridges and current mild steel, as shown in Figure 2.8 to Figure 2.10, respectively. A good agreement was found in this analysis.

Figure 2.8 - Fatigue crack growth data for Eiffel bridge steel (R=0.1) according to updated UniGrow model proposed by Correia[45].

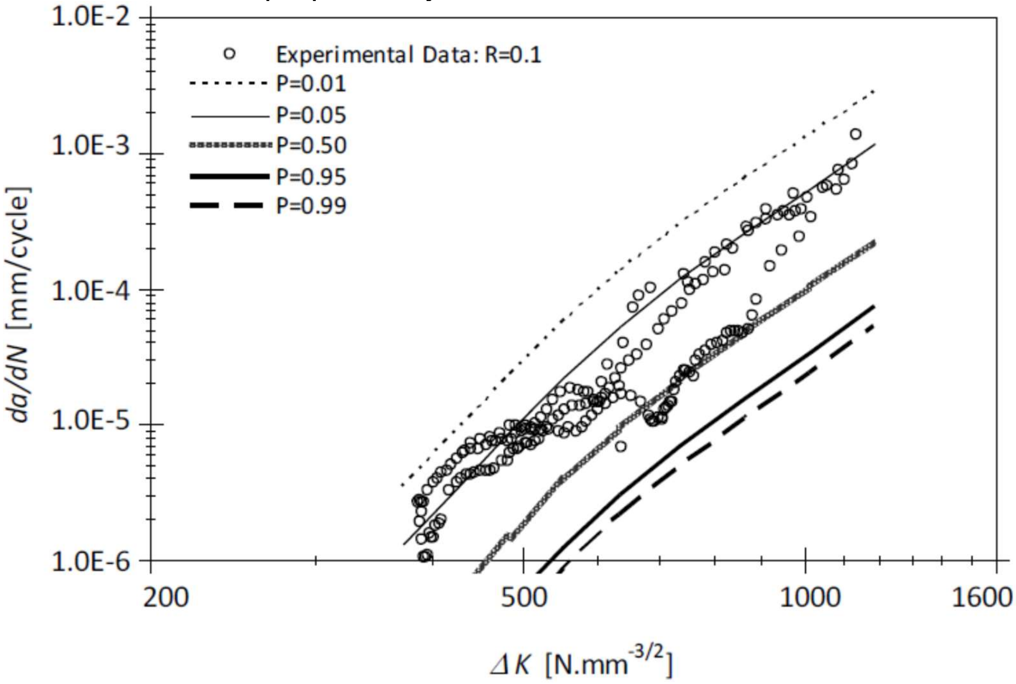

Source: Correia[45].

Figure 2.9 - Fatigue crack growth data for Fão bridge steel (R=0.0) according to updated UniGrow model proposed by Correia[45].

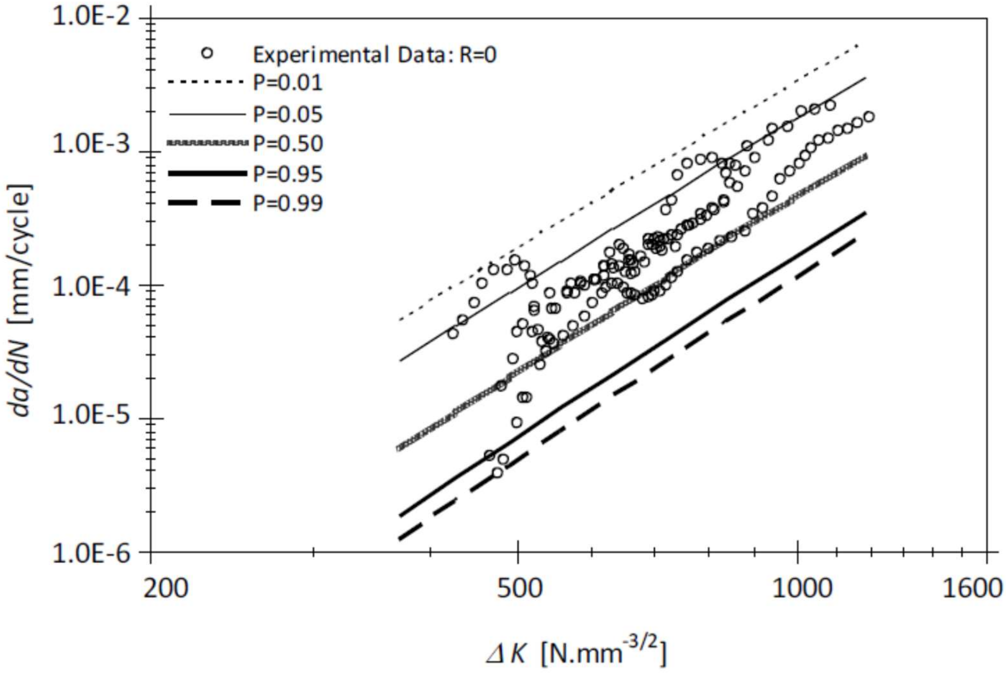

Source: Correia[45].

Figure 2.10 - Fatigue crack growth data for S355 steel (R=0.0) according to updated UniGrow model proposed by Correia[45].

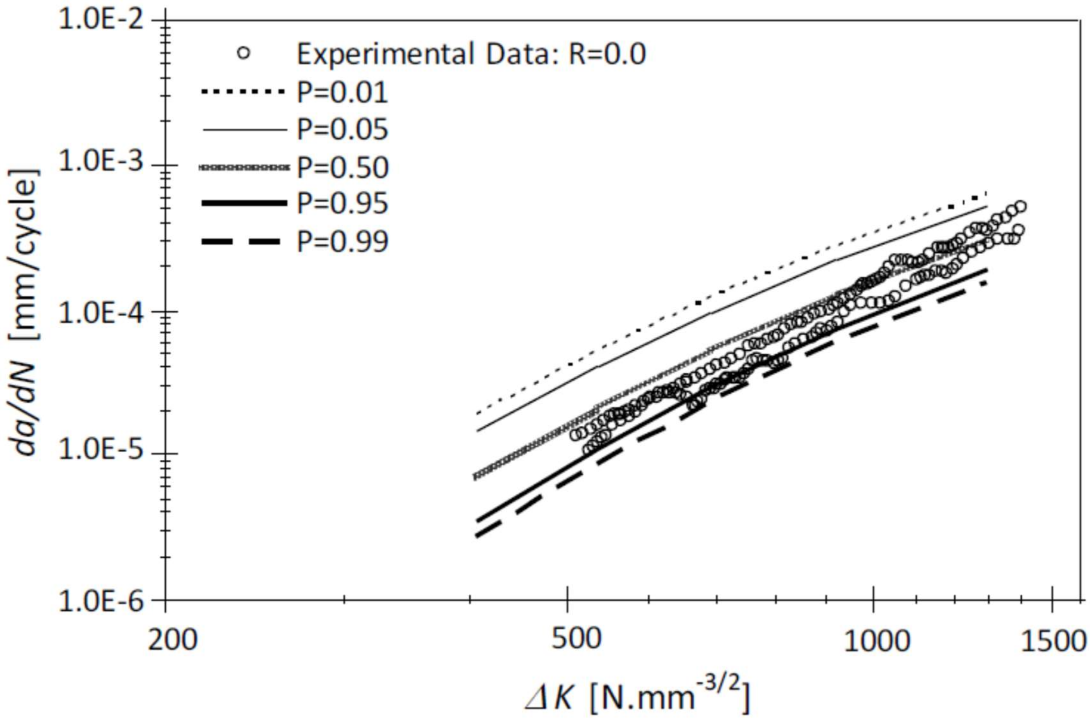

Source: Correia[45].

Recently, Huffman[28] proposed a fatigue damage parameter, D, based on strain energy density concepts and calculated it from cyclic stress-strain properties as given by:

$$\left(\frac{U_e}{U_d\rho_c}\right)\left(\frac{U_p^*}{U_d\rho_c}\right) = D = \frac{2N}{2N_f} \tag{2.36}$$

where U_e is the elastic strain energy density, U_p^* is the complementary plastic strain energy density, ρ_c is the critical dislocation density, and U_d is the dislocation strain energy density that can be estimated by

$$U_d = \left(\frac{E}{2(1+\upsilon)}\right)\cdot\left|\vec{b}\right|^2 \tag{2.37}$$

where υ is the Poisson's ratio and $\vec{b}$ is the Burger's vector. The value of $|\vec{b}\,|$ is equal to 2.52×10^{-10}m for iron, steel or similar metals as can be found in reference[28]. Finding the strain energy density by integrating the Ramberg-Osgood stress-strain relationship, results the damage equation in terms of materials parameters:

$$\left(\frac{2}{U_d^2\rho_c^2}\right)\left(\frac{n'}{1+n'}\right)\left(\frac{1}{K'}\right)(\sigma_{max}{}^2)(\sigma_a)^{\frac{1+n\prime}{n\prime}} = D = \frac{1}{2N_f} \tag{2.38}$$

where σ_{max} is the maximum stress and σ_a is the stress amplitude. This equation can be used to generate the stress-life, strain-life, and fatigue crack growth curves from cyclic stress-strain properties.

In the studies developed by Huffman[28] for the A588C steel, a good agreement is found between the strain energy density model and the experimental results, as shown in Figure 2.11.

Figure 2.11 - Huffman fatigue crack growth model applied to A588C steel[28].

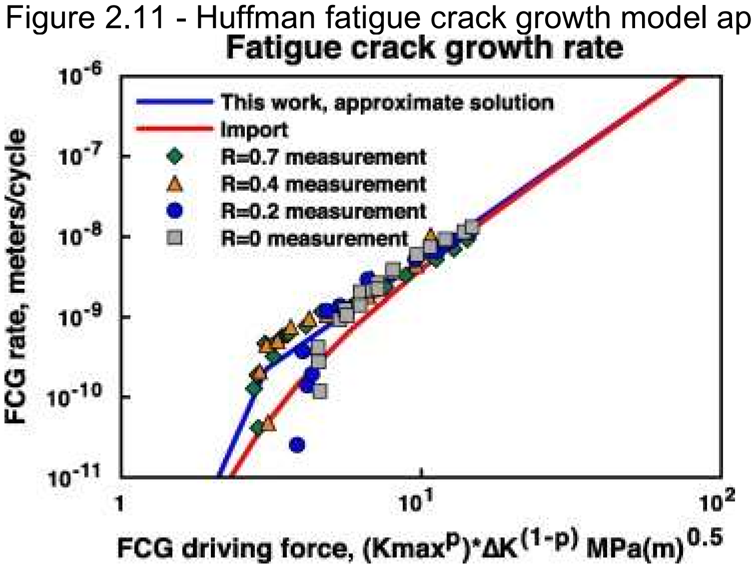

Source: Huffman[28].

REFERENCES

1 PARIS, P.; ERDOGAN, F. A critical analysis of crack propagation laws. **Journal of Fluids Engineering**, New York, v. 85, n. 4, p. 528-533, 1963.

2 DOWLING, N.E. **Mechanical Behaviour of Materials**. Engineering Methods for Deformation, Fracture and Fatigue. 3 ed. London: Pearson Prentice Hall, 2007.

3 FORMAN, R.G. Study of fatigue crack initiation from flaws using fracture mechanics theory. **Engineering Fracture Mechanics**, Oxford, v. 4, n. 2, p. 333-345, 1972.

4 HARTMAN, A.; SCHIJVE, J. The effects of environment and load frequency on the crack propagation law for macro fatigue crack growth in aluminium alloys. **Engineering Fracture Mechanics**, Oxford, v. 1, n. 4, p. 615-631, 1970.

5 BEDEN, S.M.; ABDULLAH, S.; ARIFFIN, A.K. Review of fatigue crack propagation models for metallic components. **European Journal of Scientific Research**, Victoria, v. 28, n. 3, p. 364-397, 2009.

6 ALVES, A.S.F.; SAMPAYO, L.M.C.M.V.; CORREIA, J.A.F.O.; DE JESUS, A.M.P.; MOREIRA, P.M.G.P.; TAVARES, P.J.S. Fatigue Life Prediction Based on Crack Growth Analysis Using an Equivalent Initial Flaw Size Model: Application to a Notched Geometry. **Procedia Engineering**, Amsterdam p. 730, 2015

7 CASTILLO, E.; FERNÁNDEZ-CANTELI, A.; SIEGELE, D. Obtaining S-N curves from crack growth curves: An alternative to self-similarity. **International Journal of Fracture**, Dordrecht, v. 187, n. 1, p. 159-172, 2014.

8 BLASÓN, S.; RODRÍGUEZ, C.; FERNÁNDEZ-CANTELI, A. Fatigue characterization of a crankshaft steel: use and interaction of new models. **Frattura ed Integrità Strutturale**, v. 10, n. 35, p. 187-195. DOI: 10.3221/IGF-ESIS.35.22.

9 DOWLING, N.E.; BEGLEY, J.A. Fatigue crack growth during gross plasticity and the Jintegral, Mechanics of Crack Growth. **American Society for Testing and Materials Special Technical Publication,** Philadelphia, v. 590, p. 82–105, 1976.

10 CORREIA, J.A.F.O.; DE JESUS, A.M.P.; FERNÁNDEZ-CANTELI, A.; BRIGHENTI, R.; MOREIRA, P.M.G.P.; CALÇADA, R.A.B. A procedure to obtain the probabilistic kitagawa-takahashi diagram, **UPB Scientific Bulletin, Series D: Mechanical Engineering**, Bucharest, v. 78, n. 1, p. 3-12, 2016.

11 CORREIA, J.A.F.O.; BLASÓN, S.; DE JESUS, A.M.P.; CANTELI, A.F.; MOREIRA, P.M.G.P.; TAVARES, P.J. Fatigue life prediction based on an equivalent initial flaw size approach and a new normalized fatigue crack growth model. **Engineering Failure Analysis**, Oxford, v. 69, p. 15-28, 2016.

12 AMERICAN SOCIETY FOR TESTING AND MATERIALS – ASTM. **ASTM E647**: standard test method for measurement of fatigue crack growth rates. ASTM, West

Conshohocken, p. 591–630, 1999.

13 GEERLOFS, N.; ZUIDEMA, J.; SIETSMA, J. On the Paris exponent and crack closure effects of alporas aluminum foam. *In*: EUROPEAN CONFERENCE OF FRACTURE, ECF15, ADVANCED FRACTURE MECHANICS FOR LIFE AND SAFETY ASSESSMENTS, 15, 2004, Stockholm. **Proceedings of the** […]. Stockholm: [s.n.], 2004.

14 BLASÓN, S.; CORREIA, J.A.F.O.; DE JESUS, A.M.P.; APETRE, N.; ARCARI, A.; MOREIRA, P.M.G.P.; FERNÁNDEZ-CANTELI, A. Proposal of a fatigue crack propagation model taking into account crack closure effects using a modified CCS crack growth model, **Procedia Structural Integrity**, Amsterdam, v. 1C, p. 110–117, 2016.

15 ELBER. W. Fatigue crack closure under cyclic tension, **Engineering Fracture Mechanics**, Oxford, v. 2, n. 1, p. 37-44, 1970.

16 ELBER, W. The significance of fatigue crack closure. **American Society for Testing and Materials Special Technical Publication**, Philadelphia, v. 486, p. 230–242, 1971.

17 SCHIJVE, J. **Fatigue of structures and materials**. 1. ed. Dordrecht: Kluwer Academic Publishers, 2004.

18 HUDAK, S. J.; DAVIDSON, D. L. The dependence of crack closure on fatigue loading variables. **American Society for Testing and Materials Special Technical Publication**, Philadelphia, v. 982, p. 121-138, 1988.

19 ELLYIN, F. **Fatigue Damage, Crack Growth and Life Prediction**. 1. ed. London: Chapman; Hall, 1997

20 CORREIA, J.A.F.O.; DE JESUS, A.M.P.; MOREIRA, P.M.G.P.; TAVARES, P.J.S. Crack Closure Effects on Fatigue Crack Propagation Rates: Application of a Proposed Theoretical Model. **Advances in Materials Science and Engineering**, London, v. 2016, 2016.

21 NEWMAN JR.; J.C. A crack opening stress equation for fatigue crack growth. **International Journal of Fracture**, Dordrecht, v. 24, n. 4, p. R131-R135, 1984.

22 VORMWALD, M.; SEEGER, T. The consequences of short crack closure on fatigue crack growth under variable amplitude loading. **Fatigue; Fracture of Engineering Materials; Structures**, Chichester, v. 14, n. 2-3, p. 205-225, 1991.

23 SAVAIDIS, G.; DANKERT, M.; SEEGER, T. An analytical procedure for predicting opening loads of cracks at notches. **Fatigue; Fracture of Engineering Materials; Structures**, Chichester, v. 18, n. 4, p. 425-442, 1995.

24 KLESNIL, M.; LUKÁŠ, P. Fatigue of Metallic Materials. 2. ed.; Amsterdam: Elsevier Science Publisher, 1992.

25 SZATA, M.; LESIUK, G. Algorithms for the estimation of fatigue crack growth using energy method. **Archives of Civil and Mechanical Engineering**, Heidelberg, v. IX, n. 1, p. 119–134, 2009.

26 MCCLUNG, R.C.; SEHITOGLU, H. Characterization of fatigue crack growth in intermediate and large scale yielding. **Journal of Engineering Materials and Technology**, New York, v. 113, p. 15–22, 1991.

27 NAKAGAKI, M.; ATLURI, S.N. Fatigue crack closure and delay effects under mode I spectrum loading: an efficient elastic-plastic analysis procedure. **Fatigue; Fracture of Engineering Materials; Structures**, Chichester, v. 1, n. 4, p. 421–429, 1979.

28 HUFFMAN, P.J. A strain energy based damage model for fatigue crack initiation and growth. **International Journal of Fatigue**, London, v. 88, p. 197-204, 2016.

29 CORREIA, J.A.F.O.; BLASÓN, S.; ARCARI, A.; CALVENTE, M.; APETRE, N.; MOREIRA, P.M.G.P.; DE JESUS, A.M.P.; CANTELI, A.F. Modified CCS fatigue crack growth model for the AA2019-T851 based on plasticity-induced crack-closure. **Theoretical and Applied Fracture Mechanics**, Amsterdam, v. 85, p. 26-36, 2016.

30 SCHÜTZ, W. A History of Fatigue. **Engineering Fracture Mechanics**, Oxford, v. 54, p. 263–300, 1996.

31 PARIS, P.C. A rational analytic theory of fatigue. **The trend in engineering**, Seattle, v. 13, n. 9, p. 9-14, 1961.

32 COFFIN, L.F. A study of the effects of the cyclic thermal stresses on a ductile metal. **Transactions of The American Society of Mechanical Engineers**, New York, v. 76, n. 6, p. 931–950, 1954.

33 MANSON, S.S. Behaviour of materials under conditions of thermal stress. **National Advisory Committee for Aeronautics - NACA TN-2933**, Washington DC, p.1-105, 1954.

34 MORROW, J.D. Cyclic plastic strain energy and fatigue of metals. **American Society for Testing and Materials Special Technical Publication**, West Conshohocken, v. 378, p. 45-87, 1965.

35 SMITH, K.N.; WATSON, P.; TOPPER, T.H. Stress-strain function for the fatigue of metals. **Journal of Materials**, West Conshohocken, v. 5, n. 4, p. 767-778, 1970.

36 SHANG D-G, WANG D-K, LI M, YAO W-X. Local stress–strain field intensity approach to fatigue life prediction under random cyclic loading. **International Journal of Fatigue**, London, v. 23, p. 903–910, 2001.

37 GLINKA, G.; A notch stress-strain analysis approach to fatigue crack growth. **Engineering Fracture Mechanics**, Oxford, v. 21, n. 2, p. 245-261, 1985.

38 PEEKER, E.; NIEMI, E.; Fatigue crack propagation model based on a local strain approach. **Journal of Constructional Steel Research**, London, v. 49, n. 2, p. 139-155,1999.

39 NOROOZI, A.H.; GLINKA, G.; LAMBERT, S.; A two parameter driving force for fatigue crack growth analysis. **International Journal of Fatigue**, London, v. 27, n. 10-12, p. 1277-1296, 2005.

40 HURLEY, P.J.; EVANS, W.J.; A methodology for predicting fatigue crack propagation rates in titanium based on damage accumulation. **Scripta Materialia**, Oxford, v. 56, n. 8, p. 681-684, 2007.

41 NOROOZI, A.H.; GLINKA, G.; LAMBERT, S.; A study of the stress ratio effects on fatigue crack growth using the unified two-parameter fatigue crack growth driving force. **International Journal of Fatigue**, London, v. 29, n. 9-11, p. 1616-1633, 2007.

42 NOROOZI, A.H.; GLINKA, G.; LAMBERT, S.; Prediction of fatigue crack growth under constant amplitude loading and a single overload based on elasto-plastic crack tip stresses and strains. **Engineering Fracture Mechanics**, Oxford, v. 75, n. 2, p. 188-206, 2008.

43 NEUBER, H. Theory of stress concentration for shear-strained prismatical bodies with arbitrary nonlinear stress–strain law. **Journal of Applied Mechanics**, New York; v. 28, n. 4, p. 544–551, 1961.

44 MOFTAKHAR, A.; BUCZYNSKI, A.; GLINKA, G. Calculation of elasto-plastic strains and stresses in notches under multiaxial loading. **International Journal of Fracture**, Dordrecht, v. 70, p. 357-373, 1995.

45 REINHARD, W.; MOFTAKHAR, A.; GLINKA, G. An Efficient Method for Calculating Multiaxial Elasto-Plastic Notch Tip Strains and Stresses under Proportional Loading. **Fatigue and Fracture Mechanics**, West Conshohocken, v. 27, p. 613-629, 1997.

46 CORREIA, J. A. F. O.; **An Integral Probabilistic Approach for Fatigue Lifetime Prediction of Mechanical and Structural Components**. 2014. Ph.D. Thesis. University of Porto, Porto, 2015.

CHAPTER III

3 AN EXPERIMENTAL PROGRAM TO CHARACTERIZE THE FATIGUE CRACK GROWTH OF 1100 ALUMINIUM ALLOY

3.1 INTRODUCTION

Fatigue crack growth (FCG) is the main cause of failures and mechanical fracture in systems subjected to cyclic loading. Its evolution is related to material chemical and mechanical properties, surface and environmental characteristics, as well as loading types, amplitudes, frequencies and stress R-ratios[1,2].

So, many efforts have been made to establish fatigue crack propagation models. In this sense, we can highlight the milestone contributions of Paris[3], correlating FCG rates and the stress intensity factor, a fracture mechanics parameter. It is known that the Paris law is only applicable in region II, so many derived models emerged to overcome this limitation[4], increasing the number of variables and required parameters, and consequently made the solution costly[5,6].

Just as models have to be improved, testing methods must also be enhanced. Hereupon and understanding the current political and scientific scenario in which future researchers are inserted in and knowing the difficulty in obtaining financial support, studies involving less-time-consuming experiments and low-cost workbenches are always welcome. Therefore, this investigation aims to assess data from proposed workbench/methodology combining an experimental-analytical analysis for the 1100 aluminium alloy specimens under consideration. Additionally, the chemical composition, hardness measurements, tensile strength, fatigue crack propagation, and microscopy analysis for Al1100 and Al1050 are also assessed. Therefore, in this investigation, a comparison between the crack growth constants (slope *m*) obtained in the low-cost workbench by combining an experimental-analytical analysis and obtained results by application of the ASTM E647 standard, considering the thickness effects, is also done.

3.2 WORKBENCH PROPOSAL

3.2.1 Suggested workbench and required equipment

The first idea of this chapter is to suggest a workbench where it is possible measure the fatigue crack growth of very thin specimens made of commercially pure aluminium alloy (AL 1100). The schematic representation of the suggested workbench is illustrated in figure 3.1.

Figure 3.1 - Schematic representation of proposed workbench.

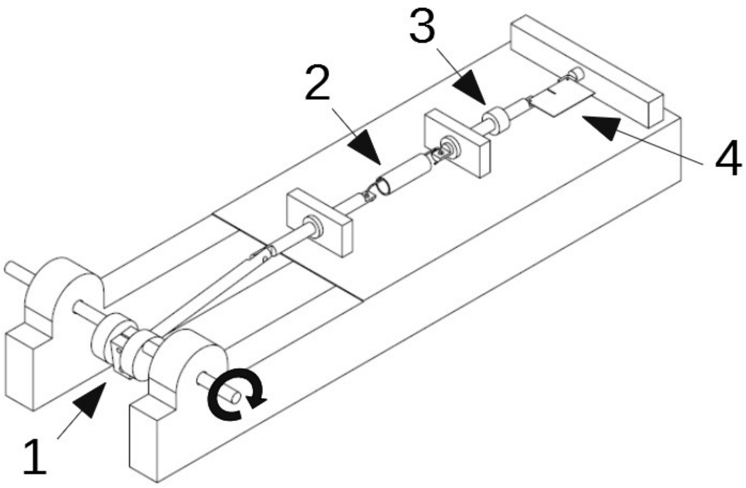

Source: Prepared by the author.

In Figure 3.1, the workbench is presented, where the number 1 represents the eccentricity that converts rotation provided by the induction motor to displacement; 2, is an elastic element (a spring), in this specific application it was used a A-75 steel spring; 3 consists in a load cell to measure the cyclic sinusoidal force applied at that side of specimen, and number 4 is the test piece. A picture of the real workbench is shown in the following Figure 3.2.

Figure 3.2 - Overview of the first proposed workbench.

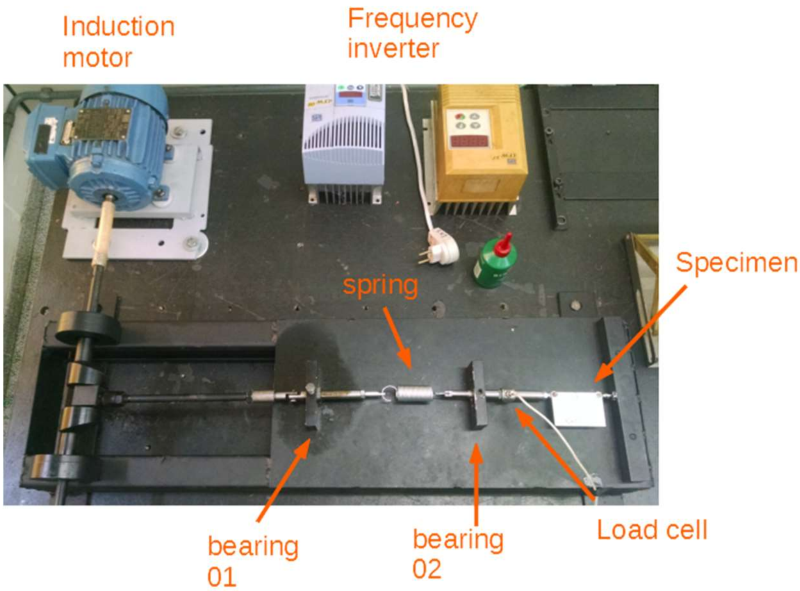

Source: Prepared by the author.

In order to improve this setup, some modifications were done in the first workbench. The bearing 02 and the load cell, exposed in Figure 3.2, have been changed for enhance the setup performance. The original bearing 02, in its configuration did not prevent possible rotations that could affect the crack growth, so, that device was replaced by a linear guide (rail and car) with unidirectional movement, which restricts the force only in the direction to excite the specimen in mode I. In addition, some troubles were found the load cell presented in Figure 3.2, so it was replaced by the one listed on Table 3.1. The actual configuration, containing these modifications, that was used on the experiments is shown in Figure 3.3.

Figure 3.3 - Proposed workbench after some modifications, identifying the load cell, the linear guide (rail and car) and test specimen.

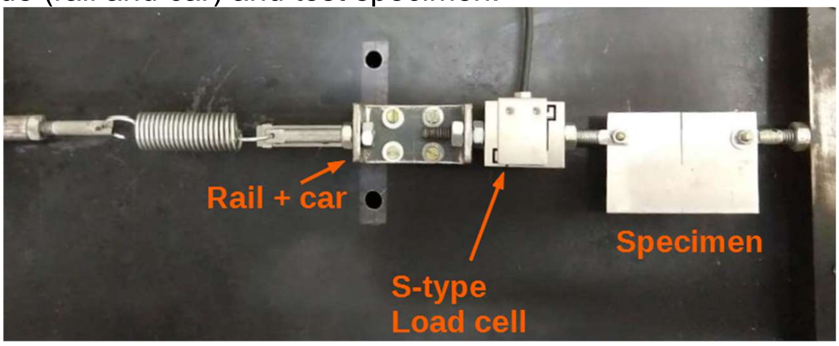

Source: Prepared by the author.

For measuring the crack propagation, a digital microscope is positioned externally to this apparatus and focusing on the notch detail. Details about the equipment used in this research are shown in Table 3.1.

Table 3.1 - Equipment used in this research.

	Induction motor	**Load cell**	**Digital Microscope**	**Digital Microscope**
Brand	WEG	XIN NUO QI	ANDONSTAR	Carl Zeiss
Model	~3 63 FI17075	DYLY-106	AD-106	Stereo Discovery.v8
Capacity	0.12kW(0.16HP)	0-10 Kg	Mag 10x-220x	1μm resolution
Additional information	Nominal rpm 3380	S type	Remote and usb image output	8x manual zoom

Source: Prepared by the author.

3.2.2 Specimen material and geometry

Aluminium is the second most used metals in the world, being only behind the steels. It is estimated that 8% of the Earth crust is composed of aluminium, being the most abundant structural metal. It is notable for its lightness, electrical conductivity, excellent corrosion resistance, high thermal conductivity, high mechanical strength when alloyed and good appearance[7,8]. Additionally, it is sustainable, non-toxic and recyclable without losing its properties[8]. The 1100 aluminium, termed unalloyed and commercially pure with at least 99% purity, is highly resistant to chemical attack and weathering, and still has low cost, good weldability and good ductility for stamping[7,8]. It has been used in the aeronautical, automotive, chemical and packaging industries, as well as in general structures[9].

The material used in this investigation was 1100 aluminium alloy, also designated as commercially pure aluminium, obtained in sheet form from the local market as a cold rolled plate, whose chemical composition and mechanical properties (provided by seller), are given in Table 3.2 and Table 3.3, respectively.

Table 3.2 - Chemical composition provided by the seller (mass fraction,%) of Al 1100.

Al	Fe	Si	Cu	Mn	Zn	Ti
99	0.40	0.25	0.05	0,05	0.05	0,03

Source: Prepared by the author.

Table 3.3 - Mechanical properties of Al 1100 provided by the seller.

Ultimate Strength [MPa]	Yield Strength [MPa]	Brinell Hardness [Brinell]	Modulus Elasticity [GPa]	Volumetric Density [g/cm^3]
108-142	93-115	32	64-68	2.71

Source: Prepared by the author.

The specimens and the notch were manufactured by wire electrical discharge machining (EDM) in the as-received condition. The manufactured eccentrically loaded single edge cracked geometry ESE(T) is shown in Figure 3.4 and its parameters are expressed in Table 3.4.

Figure 3.4 - Eccentrically loaded single edge cracked geometry ESE(T) specimen geometry.

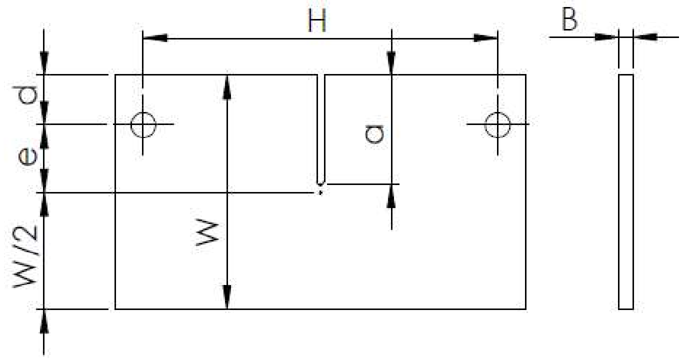

Source: Prepared by the author.

In the Figure above, W is the width of plate, H is distance between the points of load application, B is specimen thickness, a is crack length, d is distance of load-line from edge of plate, e is eccentricity of load-line and ∅ is the hole diameter.

Table 3.4 - Specimen nominal parameters in [mm].

W	H	B	a	d	e	∅
33.0	50.0	0.3	15.0	7.0	9.5	3.0

Source: Prepared by the author.

3.2.3 Test conditions and procedures - suggested methodology

This experimental procedure consists in testing crack propagation (mode I) in the geometry previously related (see Figure 3.4), using the proposed workbench. The test was conducted in laboratory environment at 25°C. The specimen is fixed at one side and excited by a sinusoidal force at its other end, whose amplitude flows from around 11 to 50N, with stress ratio about R = 0.22, in a frequency of 11Hz. The load cell is connected to an acquisition system and the signals are processed using the software DasyLab11.

The proposed methodology suggests to use the following procedures to establish crack propagation measurements for each sample:

- At first, specimen and microscope is positioned, fixed and angles are checked to prevent other exciting modes; The microscope is positioned in a way to have the notch and crack always near the image centre to prevent image distortion due to lens curvature; So, an initial picture is taken.
- A pre-crack is obtained using periodic inspection and set as initial crack propagation condition; Pre-crack picture is registered. The nucleation or crack

initiation is difficult to be identified using this actual microscope, but in future updates this capacity can be enhanced.

- Tests starts and periodically it is stopped for registering a crack size steps picture, until crack reaches a critical behaviour (crack length and vibration);
- The test is conducted until the specimen shows behavioral changes that may affect the test, such as vibration due to reduced thickness and remaining section of the specimen (crack size near 2.5mm).
- When test ends, the specimen is taken to another digital microscope, with 1 *μm* resolution, to calibrate the measurement, establishing a mm/pixel relation;
- Collected pictures are cut in the crack region and the image are processed (contrast, bright, gray scale adjustments); Digital image correlation (DIC) is applied to identify crack tip position in each collected image (see Figure 3.5); the notch centre is considered as a reference to reproduce all crack tips positions in a mm x mm diagram, presenting the data collected during test.
- da/dN is derived using the obtained mm/pixel relation, crack tip increments and step cycles.

Figure 3.5 - Details about crack tip position identification and measurement results.

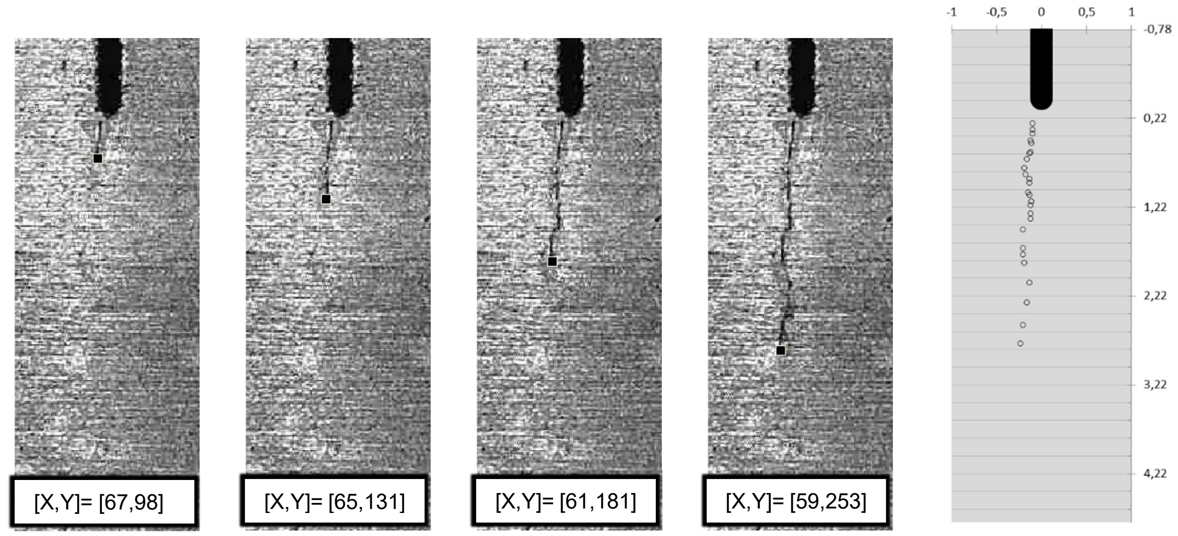

Source: Prepared by the author.

3.2.4 Analytical solutions – stress intensity factor calculation

Crack propagation rates with stable growth, in region II, could be well described using Paris law:

$$\frac{da}{dN} = C\Delta K^m \quad (3.1)$$

where C and m are material constants, that could be obtained fitting experimental data, and ΔK is the stress intensity factor range. According to John[10], the stress intensity factor range for ESE(T) for mode I could be calculated using the superposition of tension and bending effects, with the following equation:

$$\Delta K_I = \Delta K_{I,Tension} + \Delta K_{I,Bending} = F_T \Delta\sigma_T \sqrt{\pi a} + F_B \Delta\sigma_B \sqrt{\pi a} \quad (3.2)$$

where, F_T and F_B are the geometry factor for tension and bending, respectively; $\Delta\sigma_T$ is tensile stress range and $\Delta\sigma_B$ is bending stress range; and a is crack length. The geometry factor for tensile stress F_T and geometry factor for bending stress, F_B, could be obtained as:

$$F_T = \sqrt{\frac{2W}{\pi a}\tan\frac{\pi a}{2W}}\left(\frac{0.752 + 2.02\frac{a}{W} + 0.37\left(1 - \sin\frac{\pi a}{2W}\right)^3}{\cos\frac{\pi a}{2W}}\right) \quad (3.3)$$

$$F_B = \sqrt{\frac{2W}{\pi a}\tan\frac{\pi a}{2W}}\left(\frac{0.923 + 0.199\left(1 - \sin\frac{\pi a}{2W}\right)^4}{\cos\frac{\pi a}{2W}}\right) \quad (3.4)$$

The tensile and bending stress could be calculated using:

$$\Delta\sigma_T = \frac{\Delta P}{BW} \quad (3.5)$$

$$\Delta\sigma_B = \frac{6\Delta Pe}{BW^2} \quad (3.6)$$

where ΔP is the eccentric force range applied and $\Delta P = P_{max} - P_{min}$.

3.3 RESULTS AND DISCUSSION

3.3.1 Workbench results

In order to determine fatigue crack propagation curves for 1100 aluminium alloy, eccentrically loaded single edge cracked specimen ESE(T) were used. Specimens with thickness B=0.3mm, width W=33mm, H=50mm, eccentricity e =9.5mm and initial crack length a=15mm were manufactured by wire EDM. A total of six specimens were tested under load control, R-ratio equal to 0.22. Figure 3.6 illustrates crack length data derived for the 1100 aluminium alloy.

As we can see in Figure 3.6, data obtained using the proposed workbench seems to follow a pattern, which was represented by the “calculated” line.

Using obtained data for 1100 aluminium alloy with the equations suggested by Jonh[10], exposed in section 3.2.4, it was possible to calculate the stress intensity factor range for the specimens. Thereby, Paris’s law could be satisfactory correlated applying a curve fitting program to calculate the material properties C and m. The material properties obtained could be seen in Table 3.5.

Figure 3.6 - Crack length vs. number of cycles diagram.

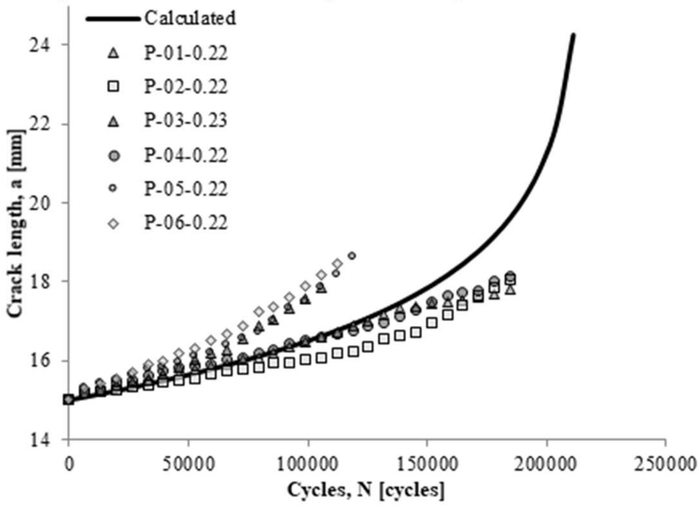

Source: Prepared by the author.

Table 3.5 - Material constants calculated fitting experimental data.

Specimens	**C_1**	**m**	**R^2**	**C_2**
P-01-0.22	1.35E-13	3.6848	0.710	4.53E-11
P-02-0.22	1.30E-13	3.6994	0.973	4.61E-11
P-03-0.23	1.18E-13	3.7439	0.913	4.86E-11
P-04-0.22	3.05E-13	3.5014	0.827	5.46E-11
P-05-0.22	1.24E-13	3.7818	0.955	5.83E-11
P-06-0.22	3.12E-13	3.6089	0.755	8.09E-11
All Pieces	1.14E-13	3.7498	0.688	4.81E-11
Omer and Metin[11]	-	1.8200	-	6.38E-07

In Table 3.5, C_1 is the material constant for *da/dN* in *mm/cycles* and ΔK in $N.mm^{-3/2}$ and C_2 is the material constant when *da/dN* in *m/cycles* and ΔK in $MN.m^{-3/2}$.

Source: Prepared by the author.

The FCG curves for each specimen, Omer and Metin[11] and obtained curve for all specimens are presented in Figure 3.7, below. It is important to note that the thicknesses of the tested specimens are 0.3*mm*, while the thicknesses of Omer and Metin's works[11] are 3mm. In this way, in the fatigue crack growth results, a scale effect can be observed.

Figure 3.7 - FCG rates vs. stress intensity factor range curves.

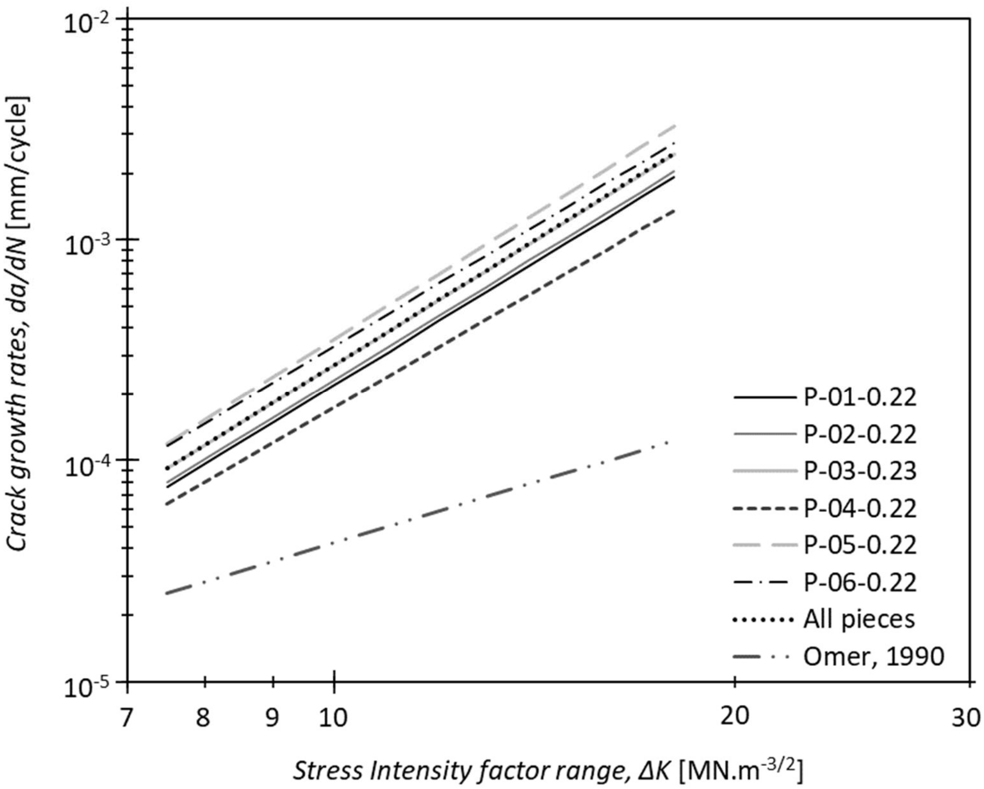

Source: Prepared by the author.

3.3.2 Standardized experimental program to characterize commercially pure aluminium alloys.

In this section, the main objectives are to characterize the chemical composition, execute the hardness, tensile, fatigue crack propagation tests, and assess the failure surface structures using microscopy for Al1100 and Al1050 aluminium alloys.

3.3.2.1 Chemical composition

The chemical composition was assessed using the Energy Dispersive X-Ray Spectroscopy (EDS technique), which detects x-rays emitted from the analysed volume during bombardment by an electron beam to characterize the elemental composition of the sample – see Figure 3.8. Table 3.6 summarizes the chemical composition of some material samples under investigation. The samples A and B correspond to the Al1100 and Al1050, respectively.

Figure 3.8 - EDS of the aluminium alloys under investigation.

Sample A - Al 1100

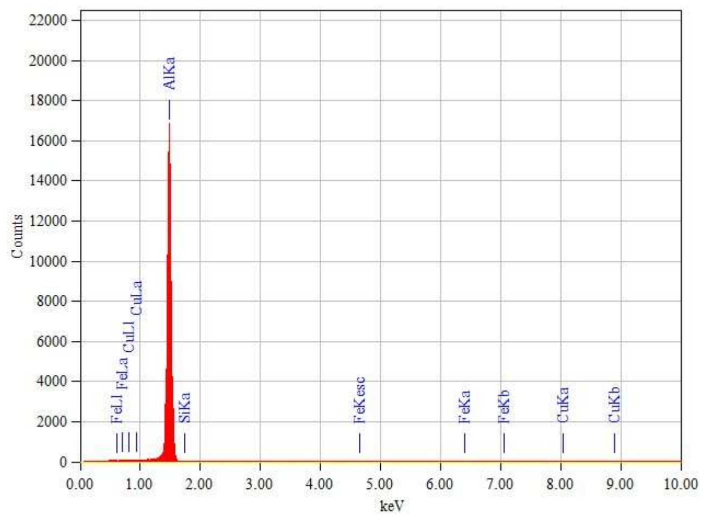

Sample B - Al 1050

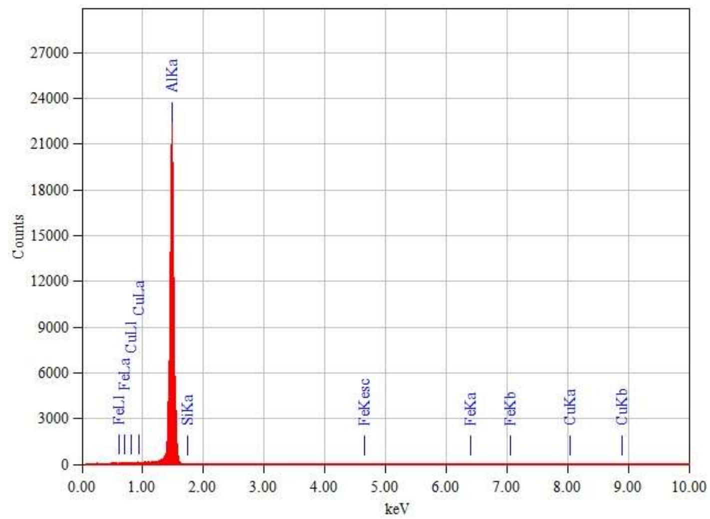

Source: Prepared by the author.

Table 3.6 - Chemical composition of the aluminium alloys detected by the EDS technique.

Mass fraction	% Al	% Fe	% Cu
A - Al1100	99.46	0.28	0.26
B - Al1050	99.60	0.18	0.23

Atomic fraction	% Al	% Fe	% Cu
A - Al1100	99.75	0.14	0.11
B - Al1050	99.82	0.09	0.10

Source: Prepared by the author.

According to the results, the analysed samples had a very similar chemical composition, indicating high purity aluminium materials. Given the similarity found, it is possible that both materials could be characterized in the same category of commercially pure aluminium.

3.3.2.2 Hardness measurements

In Figure 3.9, Vickers hardness tester is presented. Test conditions for the micro-hardness scale HV0.2 are: load force 9.81 N; and, dwell time 10s. Measurements were taken for the CT specimens made in Al1100 and Al1050 aluminiums. It was collected 5 measurements per sample and per side. In sample Al1100, hardness measurements were collected for the following sides: Face A; Face B; Thickness C; and, Thickness D. For the sample Al1100, hardness measurements were collected for the Face and Thickness. In Figure 3.10, it is identified the locations where the Vicker hardness measurements were taken. Mean values for both samples under consideration were obtained – Table 3.7.

Figure 3.9 - Vickers hardness tester.

Source: Prepared by the author.

Figure 3.10 - Identification of locations in the samples Al1100 and Al1050 for Vicker hardness measurements.

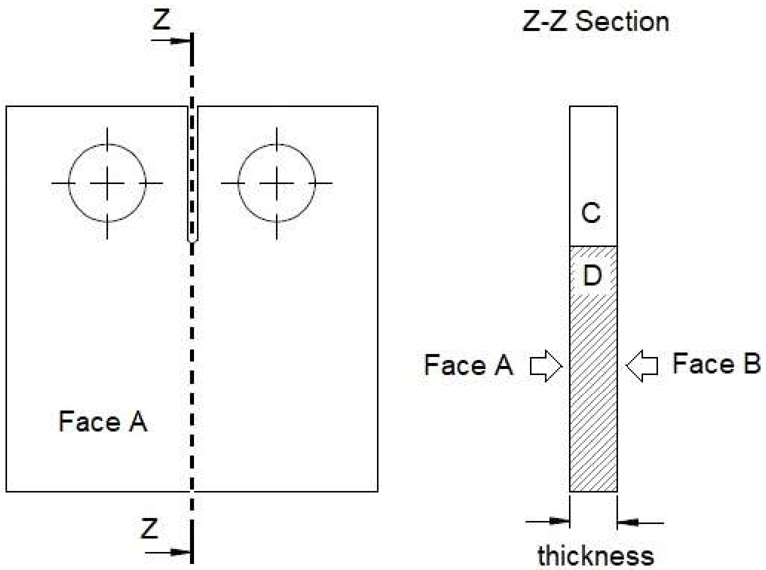

Source: Prepared by the author.

Table 3.7 - Vickers hardness of the aluminium alloys.

	Location	1	2	3	4	5	$\bar{x}$
Al 1100	Face A	35.1	41.3	32.3	40.6	39.8	37.82
	Face B	39.8	40.2	37.3	35.1	33.4	37.16
	Thickness C	48.6	39.0	42.9	44.0	42.0	43.30
	Thickness D	46.2	45.6	44.8	42.9	43.4	44.58
Al 1050	Face	34.2	35.3	34.8	32.2	33.0	33.90
	Thickness	38.3	39.3	40.1	39.0	39.5	39.24

Source: Prepared by the author.

Considering the results presented in Table 3.7, the Al 1050 alloy (of 99.5% Al) had a slightly lower Vickers hardness than the Al 1100 alloy (of 99% Al), as expected because it is a higher purity aluminium alloy. It is also observed that the Vickers hardness measured is higher in thickness than in the faces, this is certainly related to specimen manufacturing process and plastic deformation due to crack propagation.

3.3.2.3 Tensile test

The test material, aluminium 1100, was purchased from the local market in the form of 3mm thick plates. According to the ASTM E8/E8M-21 standard[13], the specimens were machined from the aluminium plate and two directions were considered in the tensile tests – longitudinal and transversal, recognized by the letters “W” and “P”, respectively. For each direction, 5 specimens were tested. Specimen geometry is presented in Figure 3.11. The geometry, cross-section, and elongation are detailed in Table 3.8, where H is the specimen width, T is the specimen thickness, L_1 is the initial specimen length, L_{po} is the final specimen length (after breaking), and A is the elongation at fracture.

As recommended by ASTM E8/E8M-21 standard[13], the tensile tests were conducted with 200 N/s resulting in the experimental curves presented in Figures 3.12 and 3.13. Using the results obtained and shown in Figures 3.12 and 3.13, it was possible to estimate the material properties related to the tensile strength, as shown in Tables 3.9 and 3.10. Furthermore, with the estimated data, it was possible to calculate the mean value, the standard deviation, and the coefficient of variation (COV) for each of the manufacturing directions and considering all the specimens. These results are summarized in Table 3.11.

Figure 3.11 - Specimen geometry used in monotonic tensile test.

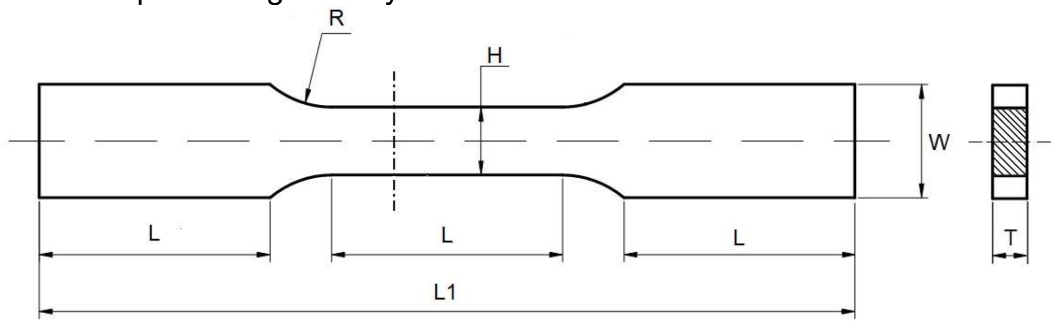

Source: Prepared by the author.

Table 3.8 - Specimen geometry for the considered 1100 aluminium alloy.

Specimen	H [mm]	T [mm]	Cross Section [mm^2]	L_1 [mm]	L_{po} [mm]	A [mm/mm]
W1	11.95	2.92	34.8940	50.09	57.16	0.141145937
W2	11.97	2.93	35.0721	49.84	57.20	0.147672552
W3	12.00	2.94	35.2800	50.23	56.38	0.122436791
W4	11.90	2.93	34.8670	49.88	57.79	0.158580593
W5	11.98	2.91	34.8618	50.37	57.16	0.134802462
P1	11.91	2.97	35.3727	50.42	55.22	0.095200317
P2	11.96	2.95	35.2820	50.72	55.30	0.090299685
P3	11.92	2.96	35.2832	50.56	55.48	0.097310127
P4	11.96	2.93	35.0428	50.51	55.14	0.091665017
P5	11.93	2.96	35.3128	50.52	55.41	0.096793349

Source: Prepared by the author.

Figure 3.12 - Tensile strength curves for the specimens manufactured in longitudinal direction.

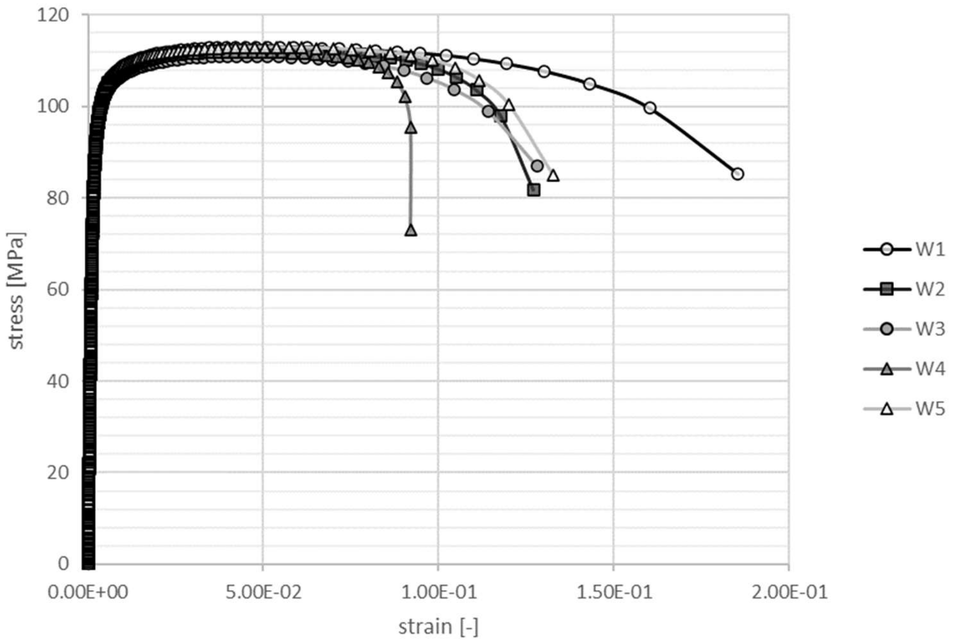

Source: Prepared by the author.

Figure 3.13 - Tensile strength curves for the specimens manufactured in transversal direction.

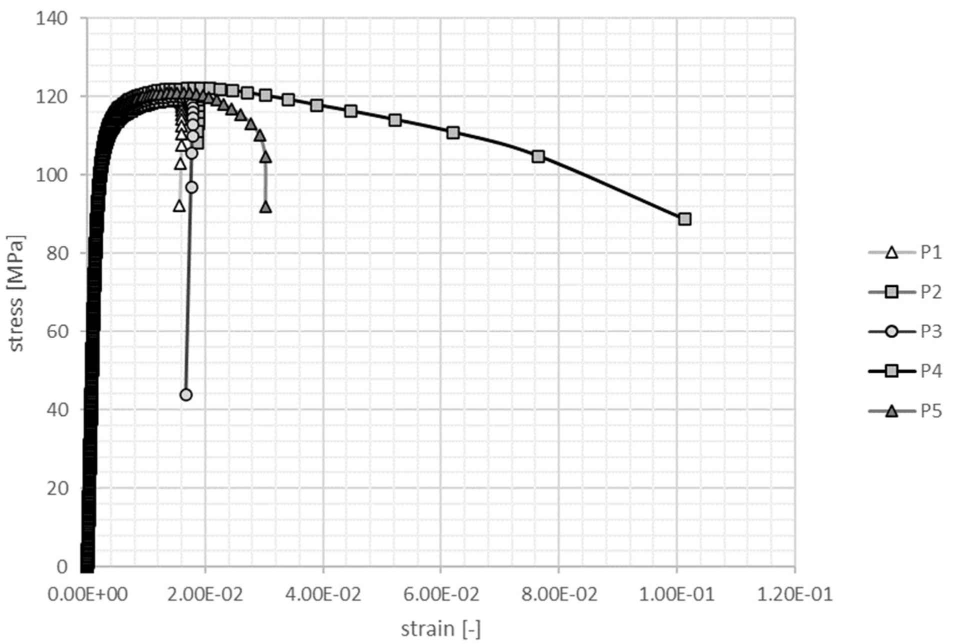

Source: Prepared by the author.

Table 3.9 - Al 1050 properties from tensile test for the longitudinal direction specimen.

	Young's Modulus [GPa]	Ultimate Tensile Strength [MPa]	Fracture stress [MPa]	0.2% yield strength [MPa]	elongation failure [mm/mm]	Ep_max [mm/mm]
W1	67.02	112.99	85.26	100.52	0.185440	0.184168
W2	66.80	112.11	81.84	99.74	0.127115	0.125890
W3	67.70	110.93	86.99	98.85	0.128115	0.126830
W4	66.07	111.95	72.96	99.43	0.091999	0.090895
W5	67.42	112.88	85.09	101.22	0.132657	0.131395

Source: Prepared by the author.

Table 3.10 - Al 1050 properties from tensile test for the transversal direction specimens.

	Young's Modulus [GPa]	Ultimate Tensile Strength [MPa]	Fracture stress [MPa]	0.2% yield strength [MPa]	elongation failure [mm/mm]	Ep_max [mm/mm]
P1	66.97	119.41	92.14	111.60	0.015626	0.014250
P2	67.30	119.50	91.99	110.84	0.018577	0.017211
P3	67.12	120.06	43.94	110.92	0.016776	0.016121
P4	68.12	122.16	88.73	112.50	0.101305	0.100002
P5	66.89	121.08	91.93	112.96	0.030311	0.028937

Source: Prepared by the author.

Table 3.11 - Mean, standard deviation and COV properties obtained using the longitudinal, transversal, and all direction specimens.

	Young's Modulus [GPa]	Ultimate Tensile Strength [MPa]	Fracture stress [MPa]	0.2% yield strength [MPa]	elongation failure [mm/mm]	Ep_max [mm/mm]
W_mean	67.00	112.17	82.43	99.95	0.133065	0.131835
Std dev	0.63	0.83	5.61	0.93	0.033502	0.033449
COV [%]	0.94	0.74	6.81	0.93	25.18	25.37
P_mean	67.28	120.44	81.75	111.76	0.036519	0.035304
Std dev	0.49	1.17	21.18	0.94	0.036688	0.036623
COV [%]	0.73	0.97	25.91	0.84	100.46	103.74
W+P_mean	67.14	116.31	82.09	105.86	0.084792	0.083570
Std dev	0.55	4.46	14.61	6.29	0.060715	0.060678
COV [%]	0.82	3.84	17.80	5.94	71.60	72.61

Source: Prepared by the author.

3.3.2.4 Fatigue crack growth tests

Fatigue crack growth tests were conducted on aluminium materials Al 1050 and Al 1100, according to the ASTM E647-15 standard[12], in order to assess the fatigue crack propagation rates for these materials. Compact tension specimens (CT specimens) with thickness B=3.0mm were prepared with the aluminium materials – Al 1050 and Al 1100, see Figure 3.14. Table 3.12 shows the dimensions for the compact tension specimens and the total number of specimens tested for each material. All tests were performed in air, at room temperature, under a sinusoidal waveform with a frequency of 10 Hz for all materials. The crack length size was determined by compliance procedures[14]. The tests were performed in load control conditions in the MTS 810 machine rated to 50 KN.

Figure 3.14 - Compact tension specimen geometry used in fatigue crack growth tests.

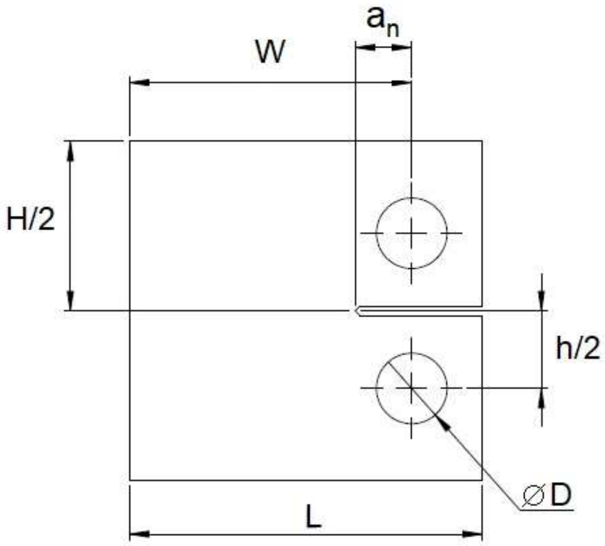

Source: Prepared by the author.

Table 3.12 – Compact Tension specimen nominal parameters in milimeters.

W	L	H/2	B	a_n	h/2	D
48.0	60.0	28.8	3.0	9.6	13.2	12.0

Source: Prepared by the author.

The following Table 3.13, shows the number of specimens for each stress ratios that were investigated for each material.

Table 3.13 – Number of tested specimens for each stress ratios for each alloy.

Material	Specimens	Specimens tested	Stress ratio
Al 1050	04	02	0.05
		01	0.10
		01	0.25
Al 1100	03	02	0.10
		01	0.25

Source: Prepared by the author.

The experimental crack propagation data obtained for each material related the crack propagation rate to the stress intensity factor range, using the power law as proposed by Paris and Erdogan[3]. The formulation to determine the stress intensity factor range, ΔK, for the CT geometry is included in ASTM E647-15 standard[12].

The crack growth rates, da/dN, *versus* the applied stress intensity factor range, ΔK, were satisfactorily described by the Paris law[3], individually for each stress ratio, where is influenced by these stress R-ratios.

3.3.2.4.1 Aluminium 1050

In this section, the results obtained for the Al 1050 following the standard is presented. Figure 3.15 present the fatigue crack propagation rates of the material Al 1050, for the three stress ratios tested, namely, 0.05, 0.1 and 0.25. It can be seen that the mean stress effect is verified. It is also possible to see that the slope of the fatigue crack propagation curve for R=0.05 is significantly higher when compared to the curves for stress R-ratios equal to 0.1 and 0.25, which could means that for the stress ratio R=0.05 the tests possibly started in threshold region.

Figure 3.15 - Experimental fatigue crack growth data for stress ratios, 0.05, 0.1 and 0.25, for the aluminium 1050.

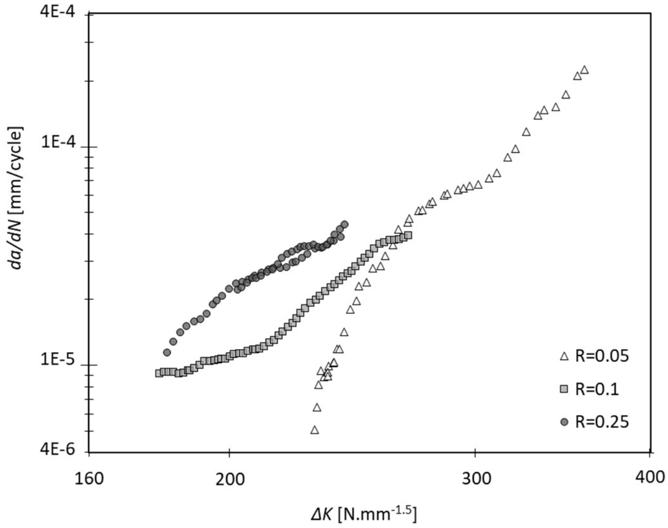

Source: Prepared by the author.

The next figures, 3.16 to 3.18, present the fatigue crack propagation rates and the Paris correlations of the material Al 1050, for three tested stress ratios, namely R=0.05, R=0.10 and R=0.25, respectively.

Figure 3.16 - Fatigue crack growth data and Paris curve for the stress R-ratio equal to 0.05 for the aluminium 1050.

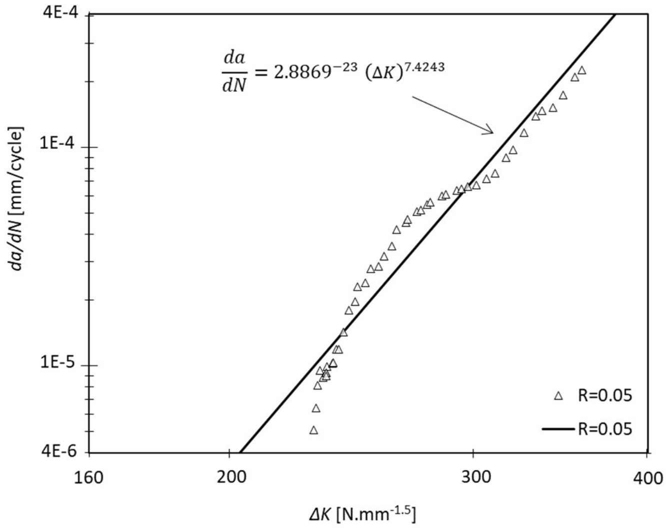

Source: Prepared by the author.

Figure 3.17 - Fatigue crack growth data and Paris curve for the stress R-ratio equal to 0.1 for the aluminium 1050.

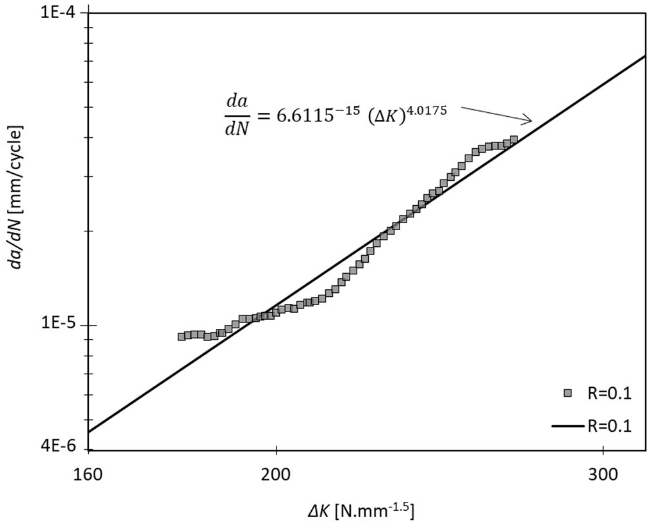

Source: Prepared by the author.

Figure 3.18 - Fatigue crack growth data and Paris curve for the stress R-ratio equal to 0.25 for the aluminium 1050.

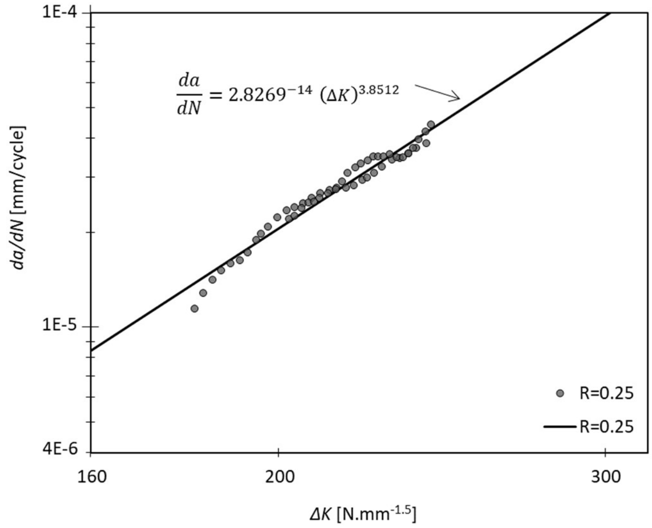

Source: Prepared by the author.

And then, finally, the Figure 3.19 compares the Paris mean regression lines for each stress ratio, where it reveals a clear stress ratio dependency of the fatigue crack propagation rate of the material. A significant increase in the fatigue crack growth rate is observed for increasing stress ratio from 0.1 to 0.25.

Figure 3.19 - Comparison between fatigue crack propagation rate trends for different stress ratios obtained for the aluminium 1050.

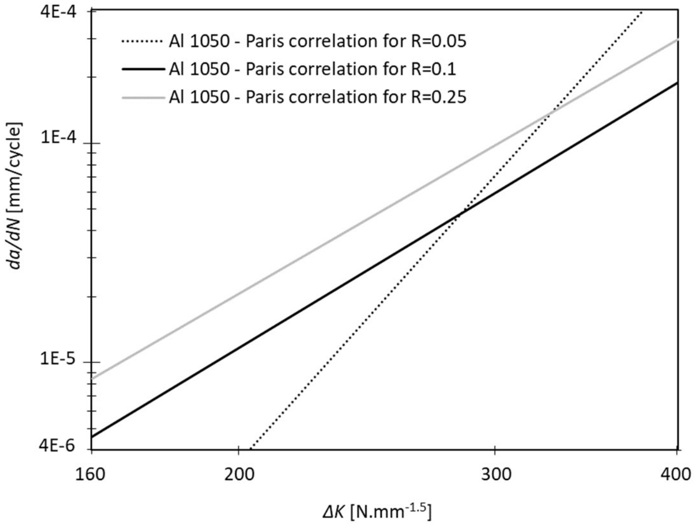

Source: Prepared by the author.

3.3.2.4.2 Aluminium 1100

Now the Al 1100 is analysed. In Figure 3.20, it is introduced the fatigue crack propagation rates of the material Al 1100, for the two stress ratios tested, namely, 0.1 and 0.25. It can be seen that the mean stress effect is also verified. It is also possible to see that the slope of the fatigue crack propagation curve for R=0.1 and R=0.25 are very close.

Figure 3.20 - Experimental fatigue crack growth data for stress ratios, 0.1 and 0.25, for the aluminium 1100.

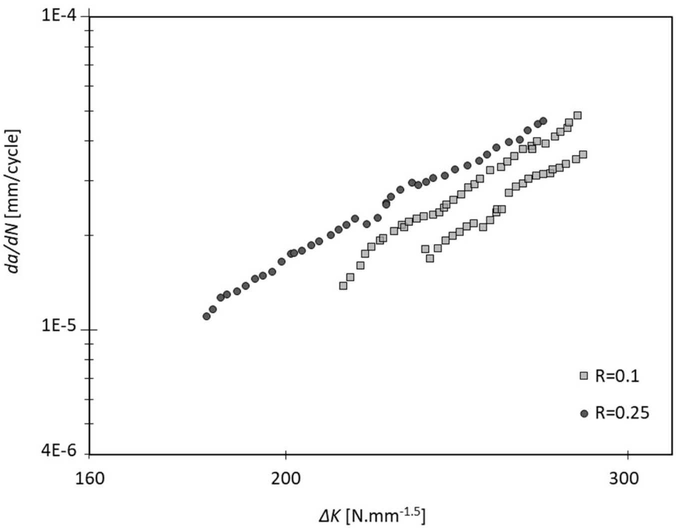

Source: Prepared by the author.

Then, the Figures 3.21 and 3.22 present the fatigue crack propagation rates and the Paris correlations of the material Al 1100, for two tested stress ratios, namely R=0.10 and R=0.25, respectively.

Figure 3.21 - Fatigue crack growth data and Paris curve for the stress R-ratio equal to 0.1 for the aluminium 1100.

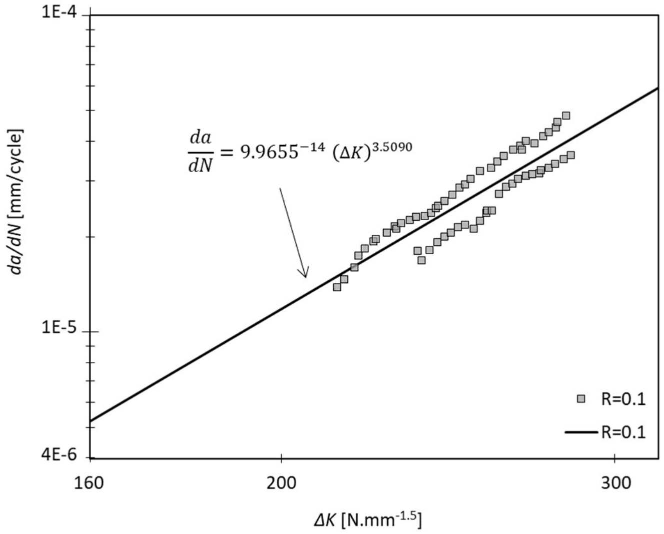

Source: Prepared by the author.

Figure 3.22 - Fatigue crack growth data and Paris curve for the stress R-ratio equal to 0.25 for the aluminium 1100.

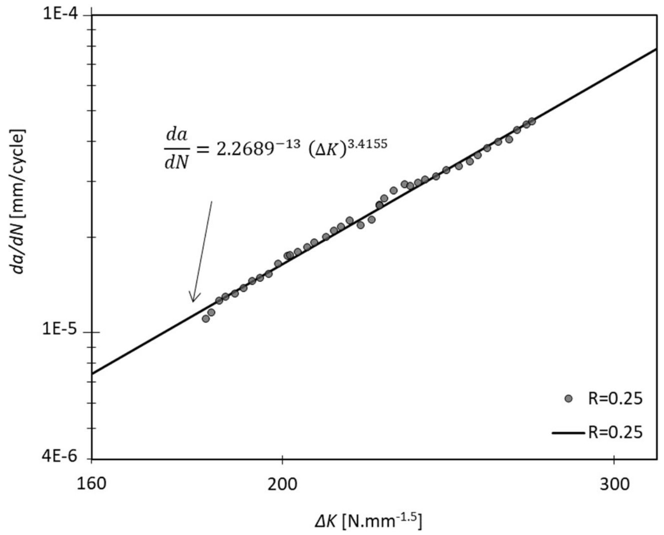

Source: Prepared by the author.

Additionally, the Figure 3.23 compares the Paris mean regression lines for each stress ratio, where the figure reveals a clear stress ratio dependency of the fatigue crack propagation rate of the material, where a significant increase in the fatigue crack growth rate is observed for the stress R-ratios equal to 0.1 and 0.25.

Figure 3.23 - Comparison between fatigue crack propagation rate trends for different stress ratios obtained for the aluminium 1100.

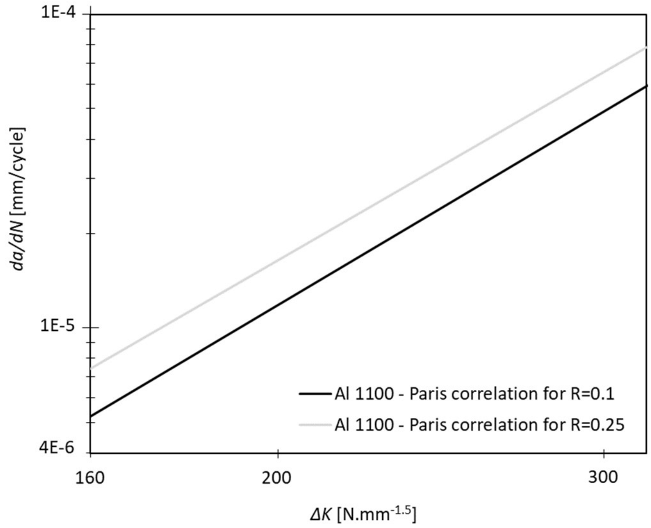

Source: Prepared by the author.

3.3.2.4.3 Comparison of suggested workbench and standard fatigue crack growth results and thickness effect

The main purpose of this section is to compare the FCG constants obtained in the suggested low-cost workbench combining an experimental-analytical analysis with the constants obtained using conventional testing machine following the ASTM standard recommendations, and assess the thickness effect.

The Figures 3.24 and 3.25 present the fatigue crack propagation rates and the Paris correlations of the materials Al 1050 and Al 1100, for two tested stress ratios, namely R=0.10 and R=0.25, respectively. For both materials under consideration, it can be concluded that for the stress ratio 0.1 there are no differences on the results observed, whereas for R=0.25, a small difference on the results is verified.

Figure 3.24 - Comparison between fatigue crack propagation rate trends for stress R-ratio equal to 0.1 obtained for the Al 1100 and Al 1050.

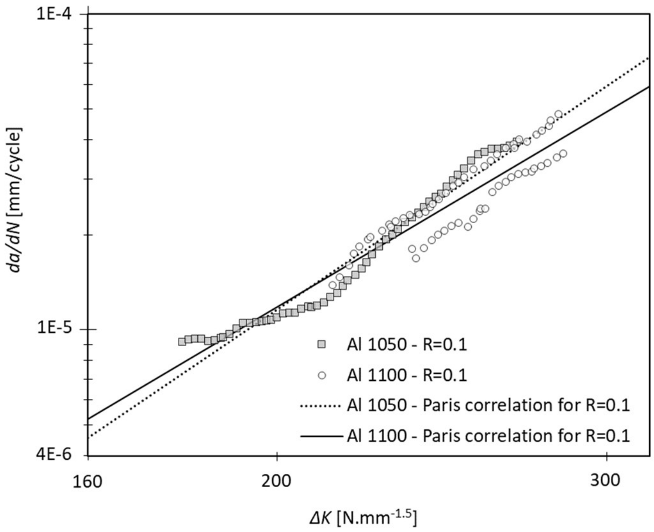

Source: Prepared by the author.

Figure 3.25 - Comparison between fatigue crack propagation rate trends for stress R-ratio equal to 0.25 obtained for the Al 1100 and Al 1050.

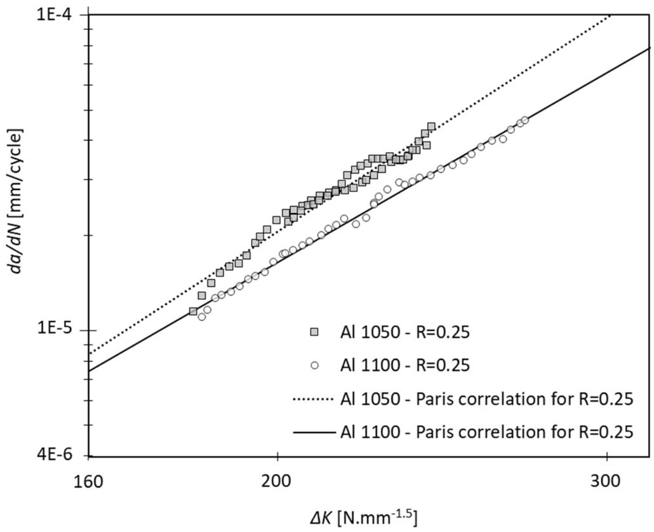

Source: Prepared by the author.

According to Figure 3.26, for the range of stress ratio 0.22-0.25, it is interesting to verify that the slope *m* obtained for the tests performed using the low-cost workbench procedure combining an experimental-analytical analysis (Section 3.3.1) is similar to those obtained based on the ASTM E647-15 standard[12]. It should be noted that the specimen geometry used in both test procedures are different, as well as the thickness, 0.3mm used in the low-cost workbench procedure (Section 3.3.1) and 3mm for the standard tests (ASTM E647). As would also be expected, in the specimen of smaller thickness (B=0.3mm), the fatigue crack growth rate is higher when compared to the FCG results obtained for the specimen CT of thickness B=3mm.

Figure 3.26 – Thickness effect for the aluminium alloys under consideration.

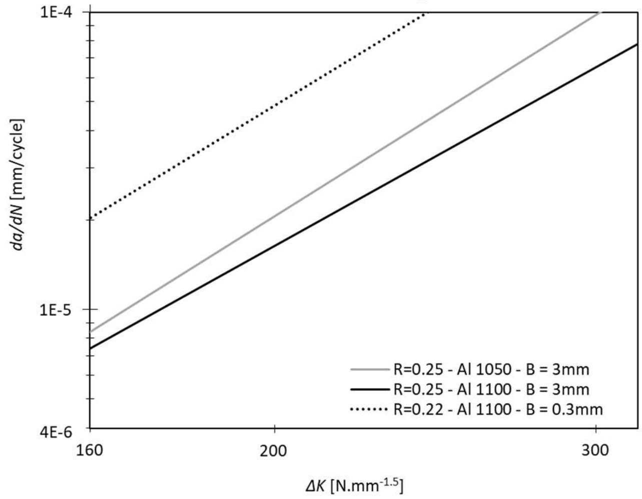

Source: Prepared by the author.

In Table 3.14, the crack growth constants obtained for both materials under consideration – Al 1050 and Al 1100 – are presented. For the materials studied, the slope *m* is similar for the stress ratios tested, with the exception of stress ratio R=0.05.

Table 3.14 - Crack growth constants obtained for both materials under consideration.

Material	Specimen Thickness (mm)	Stress ratio, R	C	m	R^2
Al 1050	3	0.05	2.8869E-23	7.4243	9.40E-01
	3	0.1	6.6115E-15	4.0175	9.55E-01
	3	0.25	2.8269E-14	3.8512	9.63E-01
Al 1100	3	0.1	9.9655E-14	3.5090	9.89E-01
	3	0.25	2.2689E-13	3.4155	9.94E-01
Al 1100 (all specimens)	0.3	0.22	1.1400E-13	3.7498	6.88E-01

In Table 3.14, *C* is the material constant for *da/dN* in *mm/cycles* and ΔK in $N.mm^{-3/2}$.

Source: Prepared by the author.

3.3.2.5 Microstructure Analysis

In Figure 3.27, the macro microscopy of the fracture surface of the specimen is investigated. For both specimens, it is possible recognize four different regions: A is the crack initiation region, B is the crack propagation region, B/C is the region of transition from propagation to huge deformation, and C is the fracture region (or huge deformation region). It could be observed in the C region, that the 1050 aluminium alloy presented a smaller thickness of the fracture surface than the 1100 aluminium alloy, which means that 1050 Al is the most ductile, or in other words, it deforms itself more until the fracture than the other alloy.

Figure 3.27 - Macro microscopy of fractured specimens.

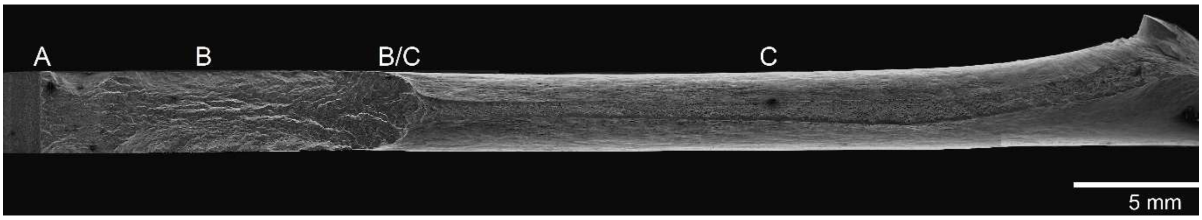

a) 1050 aluminium alloy fracture surface

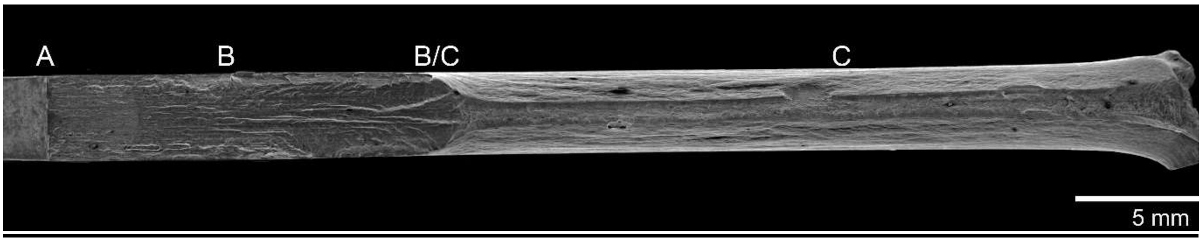

b) 1100 aluminium alloy fracture surface

Source: Prepared by the author.

In Figure 3.28, the crack initiation region (A) and propagation region (B) is analysed. According to the images shown, the surface structures are similar for the materials considered, both in crack initiation region and in the fatigue crack propagation region.

Figure 3.28 - Microscopy details of regions A and B.

AL 1050 AL1100

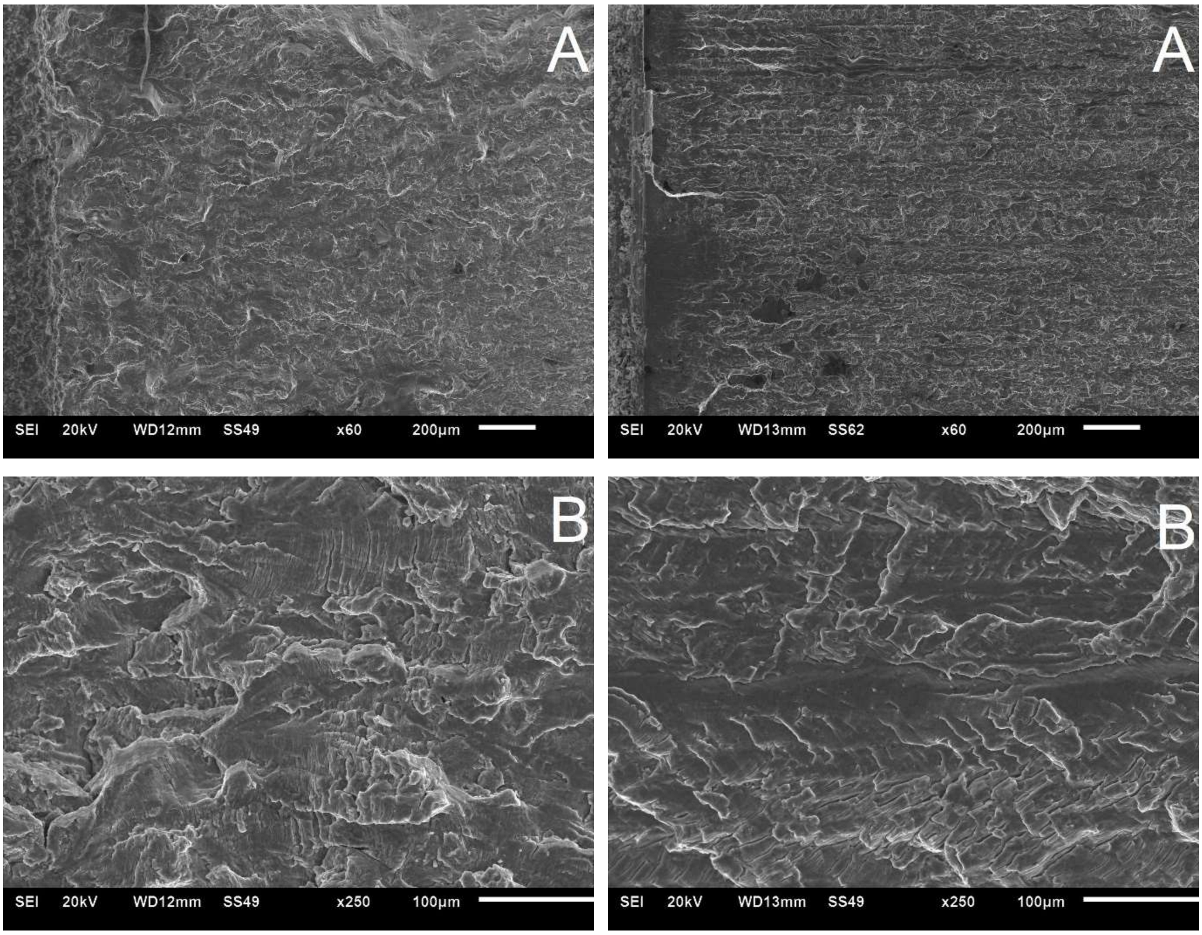

Source: Prepared by the author.

In Figure 3.29, the transition region (B/C) and fracture region (C) is studied. Analysing the B/C images for each material, and with the help of Figure 3.27 (macro microscopy), it is possible to observe that from the transition region to the fracture region, that there is difference between the fracture surface areas, being significantly smaller the area of the aluminium alloy 1050. However, comparing structures of fracture surfaces, in region C, in both materials ductile fracture could be observed.

Figure 3.29 - Microscopy details of regions B/C and C..

AL 1050 AL1100

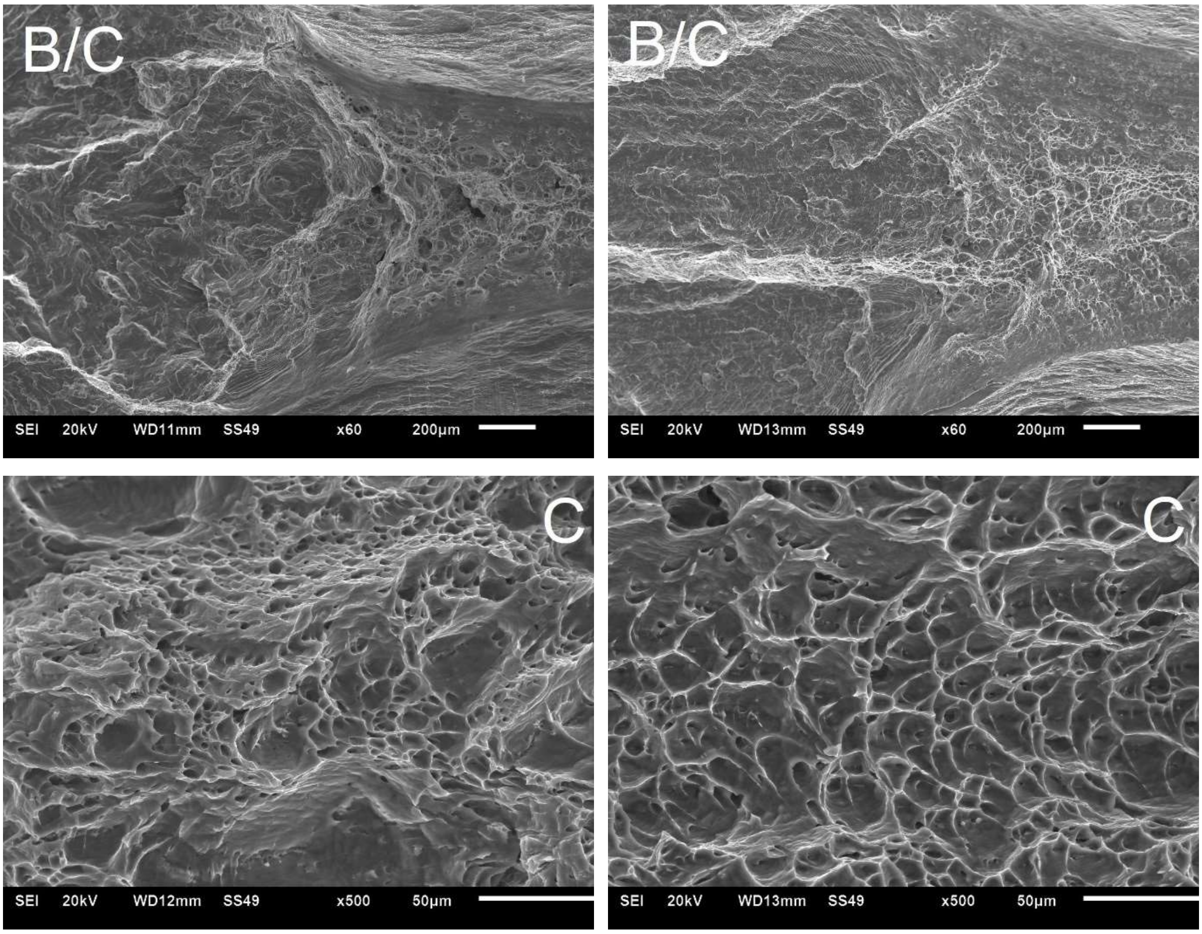

Source: Prepared by the author.

3.4 CONCLUSION

The proposed workbench/methodology presented reasonable results and seems to be promising for obtaining crack propagation data from region II, that is, from region of stable crack growth. It is notable that the costs involved for this current configuration are low and that it is possible to obtain results very quickly. However, in actual configuration it is limited to very thin specimens and for non-structural metals. Some modifications can improve the system´s power and cover a wider range of materials.

Through the literature review carried out, there was a scarcity of fatigue crack propagation results for 1100 aluminium alloy. A brief analysis of the results obtained showed a behaviour compatible with the expected when analysed together with the unique reference found, which date from the 90's, and that uses different geometries and thicknesses. Thus, further investigations using standardized CT specimens[11] are proposed for further consideration and conclusions regarding the proposed workbench methodology.

In this research work, the chemical composition, hardness measurements, tensile strength, fatigue crack propagation, and microscopy analysis for Al1100 and Al1050, were also done. The results obtained are in line with those recommended for the materials under study. A comparison between the crack growth constants obtained in the low-cost workbench combining an experimental-analytical analysis and application of the ASTM E647-15 standard[12], considering the thickness effects, was done. The results obtained for both approaches, although for different thicknesses (0.3mm and 3mm, respectively, low-cost workbench and ASTM E647-15 standard[12]), showed consistent and aligned values for the Paris law constants observing the range of the stress ratio of 0.22-0.25.

REFERENCES

1 GONCALVES, A.C.; EKWARO-OSIRE, S.; ALEMAYEHU, F.M. **Probabilistic Prognostics and Health Management of Energy Systems**, 1. ed. Cham: Springer, 2017.

2 KEBIR, T.; BENGUEDIAB, M.; AND IMAD, A. A model for fatigue crack growth in the paris regime under the variability of cyclic hardening and elastic properties. **Fatigue of Aircraft Structures**, Warsaw, v. 9, p. 117-135, 2017.

3 PARIS, P.C. A rational analytic theory of fatigue. **The trend in engineering**, Seattle, v. 13, n. 9, p. 9-14, 1961.

4 BEDEN, S.M.; ABDULLAH, S.; ARIFFIN, A.K. Review of fatigue crack propagation models for metallic components. **European Journal of Scientific Research**, Victoria, v. 28, n. 3, p. 364-397, 2009.

5 CORREIA, J.A.F.O.; DE JESUS, A.M.P.; RIBEIRO, A.S.; FERNANDES, A.A. Strain-based approach for fatigue crack propagation simulation of the 6061-T651 aluminium alloy. **International Journal of Materials and Structural Integrity**, Geneva, v. 11, n. 1-3, p. 1-15, 2017.

6 PEEKER, E.; NIEMI, E. Fatigue crack propagation model based on a local strain approach. **Journal of Constructional Steel Research**, London, v. 49, n. 2, p. 139-155,1999.

7 REBOUL, M. C.; BAROUX, B. Metallurgical aspects of corrosion resistance of aluminium alloys. **Materials and Corrosion**, Weinheim, v.62, n.3, p. 215-233, 2011.

8 DAVIS, J.R. **Aluminum and aluminum alloys**. 3. ed. Ohio: ASM International, 1993

9 SARAVANAN, S.; RAGHUKANDAN, K.; PRABHAT, K. Effect of wire mesh interlayer in explosive cladding of dissimilar grade aluminum plates. **Journal of Central South University**, Changsha, v.26, n.3, p. 604–611, 2019.

10 JOHN, R. Stress intensity factor and compliance solutions for an eccentrically loaded single edge cracked geometry. **Engineering Fracture Mechanics**, Oxford, v.58, n.1/2, p 87–96, 1997.

11 BILIR, Ŏ.G.; HARUN, M. Effect of stress ratio on the rate of growth of fatigue cracks in 1100 Al-alloy. **Engineering fracture mechanics**, Oxford, v. 37, n. 6, p. 1203-1206, 1990.

12 AMERICAN SOCIETY FOR TESTING AND MATERIALS – ASTM. **ASTM E647-15e1**: Standard test method for measurement of fatigue crack growth rates. ASTM International, West Conshohocken, 2015.

13 AMERICAN SOCIETY FOR TESTING AND MATERIALS – ASTM. **ASTM E8/E8M-21**: Standard test methods for tension testing of metallic materials. ASTM International, West Conshohocken, 2021.

14 LESIUK, G.; KUCHARSKI, P.; CORREIA, J.A.F.O.; DE JESUS, A.M.P.; REBELO, C.; SIMÕES DA SILVA, L. Mixed mode (I+II) fatigue crack growth in puddle iron. **Engineering Fracture Mechanics**, Oxford, v. 185, p. 175-192, 2017.

CHAPTER IV

4 LOW-CYCLE FATIGUE MODELLING SUPPORTED BY STRAIN ENERGY DENSITY-BASED HUFFMAN MODEL CONSIDERING THE VARIABILITY OF DISLOCATION DENSITY

4.1 INTRODUCTION

Local approaches based on fatigue damage parameters, such as stress, strain, and energy, are traditionally used to model the fatigue crack initiation, through empirical relations in the form of single- and double-power laws (e.g. stress-life and strain-life curves)[1-7]. Fracture mechanics is used for modelling the fatigue crack growth thru the Paris law[8,9] or related expressions. Traditionally, fatigue life prediction models to describe the fatigue crack initiation and propagation phases are considered unrelated phenomena[10,11]. In recent years, the scientific community has devoted more time to the development of integrated fatigue models to consider both fatigue phases[12-14], more specifically considering the fatigue crack propagation phase as successive re-initiations localized at the crack tip[15-29].

The strain-life behaviour of metallic materials can be described by the Morrow-Coffin-Manson relation that can be used to describe the low-cycle to high-cycle fatigue regimes. Several methods have been proposed to estimate the low-cycle fatigue behaviour from simple tensile data and/or hardness measurements applied in metals[30]. The strain-life fatigue predictions and their parameters have been found using statistical assessments[31].

The scientific community has also devoted much of its time to investigate the fatigue crack initiation modelling based on plasticity models supported by dislocations energy density[24,25,27,29]. In 1981, Tanaka and Mura[32] proposed a strain energy-based dislocation model where the number of cycles to initiate a crack of the grain size order is defined when the plastic strain energy of accumulated dislocations reaches a critical value. The initiation life and plastic strain range generated by the Tanaka-Mura model is in agreement with the Coffin-Manson relation. In 1989, Keller *et al.*[33] investigated the dislocations structure influence in fatigue considering the grain size effects, where the coarse grains do not develop as much constraint during deformation as fine grains.

These authors[33] also identified that the dislocation density was initially higher in the fine-grained structure.

Deshpande *et al*.[34] presented a discrete dislocation plasticity model based on the motion of edge dislocations to estimate the plastic deformation in single crystals. This model can be used to evaluate the critical crack size of the mode-pure I stress intensity factor range at the fatigue threshold.

Ye *et al*.[35] investigated the low-cycle fatigue behaviour of SUS304-HP austenitic stainless steel under strain-controlled conditions at room temperature, where the cyclic stress response exhibited variable cyclic hardening, depending on the applied cyclic strain amplitude. In the Ye *et al*. research work[35], the microstructure observations using optical and transmission electron microscopy revealed that the dislocation structure changed with the increase in the total deformation amplitudes.

An energy approach for the prediction of fatigue crack initiation, driven by the material microstructure was proposed by Sangid *et al*.[36,37]. In this approach, the failure criterion for fatigue crack initiation is given by the energy of a persistent slip band structure and uses its stability concerning dislocation motion.

In 2013, Sangid[38] has presented a review on the physics of fatigue crack initiation focused on experimental observations of strain localization and grain size measurements, as well as on the micromechanical and crystal plasticity models to be used in the fatigue crack initiation prediction.

Mugharabi[39] discussed the microstructural mechanisms of fatigue crack initiation and damage evaluation in metallic materials, in the low cycle, high cycle, and ultra-high cycle fatigue regimes, and their basic difficulties were presented.

An overview of fatigue crack initiation mechanisms in metals was discussed by Tu and Zhang[40], where the fatigue life prediction models based on the initiation of microcracks and macrocracks were reported.

Heinrich and Sundararaghavan[41] proposed a theoretical method of fatigue crack initiation prediction applied to metals based on dislocation dynamics simulations, where these authors observed that the dislocation density and energy in the dislocation networks of dislocations increases with the number of cycles.

A micromechanical model to predict fatigue crack initiation in polycrystalline materials was proposed and discussed by Boeff *et al*.[42]. This model can be used to describe the evolution of the dislocation structures observed under cyclic strain-controlled conditions and using randomly generated representative microstructures to predict fatigue crack initiation. This model allows the generation of the S-N curve for polycrystals.

Recently, Lavenstein; El-Awady[43] presented a comprehensive review on microscale fatigue mechanisms in metals taking into account the experimental observation of small-scale experiments and discrete dislocation dynamics simulations under cyclic loading. Additionally, these authors also provided an overview of the microscale fatigue mechanisms on dislocation structure evolution, fatigue life prediction, fatigue strength, and fatigue crack initiation and propagation phases.

Various techniques[44] have been proposed to directly observe dislocations as well as estimate the dislocation density, such as special metallographic procedures, X-ray diffraction applying the Berg-Barret topography, and transmission electron microscopy (TEM). Monteiro *et al*.[44] suggested a novel method for dislocation density estimation of austenitic stainless steel.

The crack propagation modelling has been done using local approaches based on strain-life[1-3], SWT-life[5], energy-life[6] relationships, but also using strain energy density approaches supported by dislocation energy density[24,32,41]. Glinka[15] was the first to propose a fatigue crack growth model using a strain-based fatigue local criterion, where the crack growth is assumed as the failure of the successive elemental blocks at the crack tip. Many other authors have also devoted their time to research on this topic, such as Peeker-Niemi[16], Noroozi[17,18], Hurley-Evans[19], Correia[20], Hafezi[21], De Jesus *et al*.[22], Huffman[24], Bang *et al*.[28], among others. Andreykiv et al.[45] described an energy approach employed for the development of the calculation model to determine of the short fatigue crack growth rate, on the specific work of plastic deformations in the pre-fracture zone, in plates. Wei et al.[46] analysed some aspects of adequate determination of the energy state of the surfaces of structural details based on the energy balance and monitoring of strains. Huffman[24] proposed an approach to model the fatigue crack initiation and propagation based on the strain energy density through critical dislocation density, which is a particularly relevant work for the study proposed in this investigation.

In this research work, a low-cycle fatigue strength modelling based on the strain energy density-based Huffman approach considering the variability of dislocation density is studied and discussed. This study is proposed to discuss Huffman's approach that uses the critical dislocation density driven by the highest strain amplitude specimen since the previously presented studies report that the dislocation structure changed with the increase in the total strain amplitudes. For this, various methodologies to evaluating low-cycle fatigue strength based on the Huffman approach by the use of dislocation density are suggested: i) critical dislocation density driven by the highest strain amplitude specimen; ii) mean value of the critical dislocation density for the available experimental fatigue data and iii) Monte Carlo (MC) stochastic prediction considering the variability of dislocations density and cyclic strain hardening coefficient. Besides, probabilistic strain-life predictions based on the Monte Carlo stochastic simulations were presented. In this study, the experimental fatigue data of 1050, 6061-T651, and AlMgSi0.8 aluminium alloys are used. A comparison between the experimental fatigue data and strain-life curves based on various suggested methodologies is made.

4.2 EXPERIMENTAL FATIGUE DATA OF VARIOUS ALUMINIUM ALLOYS

In this section, the experimental data, in terms of mechanical properties, cyclic elastoplastic and strain-life parameters, of various aluminium alloys, such as AA1050[47], AA6061-T651[26,48], and AlMgSi0.8[47], were collected and used in this investigation. This experimental data is used in the proposed methodologies (Section 4.3) for the low-cycle fatigue modelling through the strain energy density-based Huffman approach considering the variability of dislocations.

4.2.1 Cyclic elastoplastic behaviour

The cyclic elastoplastic behaviour can be given by the Ramberg and Osgood description[49]. For this, the stabilised cyclic stress-strain data from the experimental low-cycle fatigue tests are required. According to the Ramberg-Osgood description[49], the cyclic elastoplastic behaviour is given by the following equation:

$$\frac{\Delta\varepsilon}{2} = \frac{\Delta\varepsilon^E}{2} + \frac{\Delta\varepsilon^P}{2} = \frac{\Delta\sigma}{2E} + \left(\frac{\Delta\sigma}{2K'}\right)^{1/n'} \tag{4.1}$$

where:

$\Delta\varepsilon$ is the total strain range;

$\Delta\varepsilon^E$ is the elastic strain range;

$\Delta\varepsilon^P$ is the plastic strain range;

$\Delta\sigma$ is the stress range;

E is the Young modulus; and,

K' and n' are the cyclic strain hardening coefficient and exponent.

In this investigation, experimental data from aluminium alloys, Al 1050[47], AA 6061-T651[26,48], and AlMgSi0.8[47], collected in the literature[26,47,48], were used. In Table 4.1, mechanical properties and cyclic elastoplastic parameters of the aluminium alloys under consideration are presented.

Table 4.1 - Mechanical properties and cyclic elastoplastic parameters of the aluminium alloys under consideration[26,47,48].

Materials	$\boldsymbol{R_{p,0.2}}$	$\boldsymbol{R_m}$	$\boldsymbol{E}$	$\boldsymbol{\nu}$	$\boldsymbol{K'}$	$\boldsymbol{n'}$
-	[MPa]	[MPa]	[MPa]	[-]	[MPa]	[-]
Al 1050	19.0	73.5	70000	0.35	453.0	0.337
AA 6061-T651	289.9	328.5	68000	0.35	393.4	0.0567
AlMgSi0.8	157.0	260.0	66700	0.35	392.0	0.060

Source: Prepared by the author.

4.2.2 Strain-life behaviour

The strain-life behaviour is described by Morrow's suggestions[1], where the elastic strain and plastic strain are combined, using the equations proposed by Manson[2] and Coffin[3]. So, the Morrow-Coffin-Manson relationship describes the low-cycle to high-cycle fatigue regimes and is given by:

$$\frac{\Delta\varepsilon}{2} = \frac{\Delta\varepsilon^E}{2} + \frac{\Delta\varepsilon^P}{2} = \frac{\sigma_f'}{E}\left(2N_f\right)^b + \varepsilon_f'\left(2N_f\right)^c \tag{4.2}$$

where:

ε_f' is the fatigue ductility coefficient;

c is the fatigue ductility exponent;

σ_f' is the fatigue strength coefficient;

b is the fatigue strength exponent; and,

N_f is the number of cycles to failure.

The low-cycle fatigue data of the aluminium alloys – Al 1050[47], AA 6061-T651[26,48], and AlMgSi 0.8[47] – were collected and used in this investigation. These data for the Al 1050, AA 6061-T651, and AlMgSi0.8 are summarized in Tables 4.2 to 4.4, respectively. The deterministic strain-life parameters, presented in Table 4.5, were obtained through the experimental low-cycle fatigue tests of smooth specimens under strain-controlled conditions. The strain-life results, in terms of experimental data *versus* deterministic curve, of Al 1050, AA 6061-T651, and AlMgSi0.8 are shown in Figures 4.1 to 4.3, respectively.

Table 4.2 - Low-cycle fatigue data of Al 1050[47] (* run-outs).

Specimen	σ_{max} [MPa]	σ_a [MPa]	$2N_f$ [-]	N_f [-]	ε_a [%]
1050_01	39.2	39.2	21256	10628	0.134
1050_02	34.3	34.3	117928	58964	0.087
1050_03	29.4	29.4	281524	140762	0.074
1050_04	24.5	24.5	1776294	888147	0.054
1050_05*	19.6	19.6	2000000	1000000	0.034
1050_06*	17.7	17.7	2000000	1000000	0.025

Source: Prepared by the author.

Table 4.3 - Low-cycle fatigue data of AA 6061-T651[26,48].

Specimen	σ_{max} [MPa]	σ_a [MPa]	$2N_f$ [-]	N_f [-]	ε_a [%]
6061_01	313.2	313.2	170	85	1.770
6061_02	307.4	307.4	276	138	1.520
6061_03	294.4	294.4	452	226	1.260
6061_04	292.7	292.7	780	390	1.010
6061_05	283.3	283.3	1352	676	0.810
6061_06	276.0	276.0	3160	1580	0.615
6061_07	267.8	267.8	4066	2033	0.510
6061_08	266.3	266.3	6256	3128	0.470

Source: Prepared by the author.

Table 4.4 - Low-cycle fatigue data of AlMgSi0.8[47].

Specimen	σ_{max} [MPa]	σ_a [MPa]	$2N_f$ [-]	N_f [-]	ε_a [%]
AlMgSi _01	304.1	304.1	120	60	1.830
AlMgSi _02	286.5	286.5	780	390	0.970
AlMgSi _03	258.0	258.0	2400	1200	0.485
AlMgSi _04	260.0	260.0	3500	1750	0.485
AlMgSi _05	196.2	196.2	17500	8750	0.280

Source: Prepared by the author.

Table 4.5 - Strain-life parameters of the aluminium alloys under consideration[26,47,48].

Materials	σ'_f	b	ε'_f	c
-	[MPa]	[-]	[-]	[-]
Al 1050	117	-0.1089	0.0167	-0.3147
AA 6061-T651	394	-0.0453	0.8680	-0.7745
AlMgSi 0.8	481	-0.0840	1.0945	-0.8671

Source: Prepared by the author.

Figure 4.1 - Strain-life data of Al 1050 – Experimental data vs. deterministic curve.

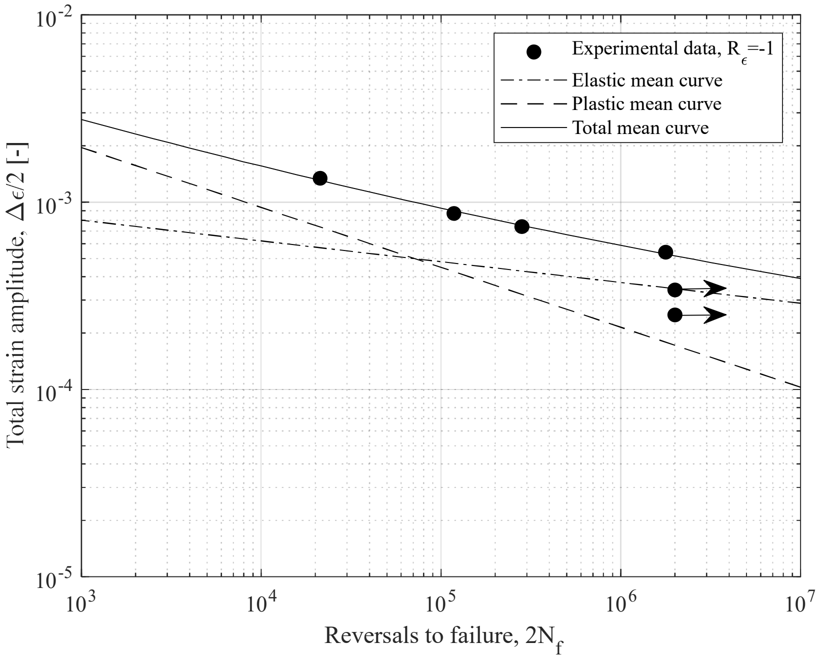

Source: Prepared by the author.

Figure 4.2 - Strain-life data of AA 6061-T651 – Experimental data vs. deterministic curve.

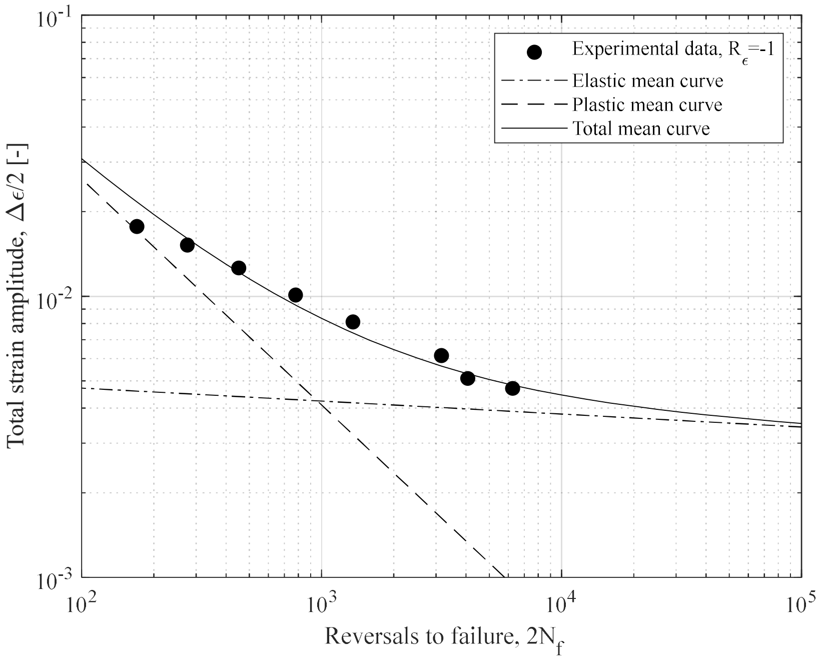

Source: Prepared by the author.

Figure 4.3 - Strain-life data of AlMgSi0.8 – Experimental data vs. deterministic curve.

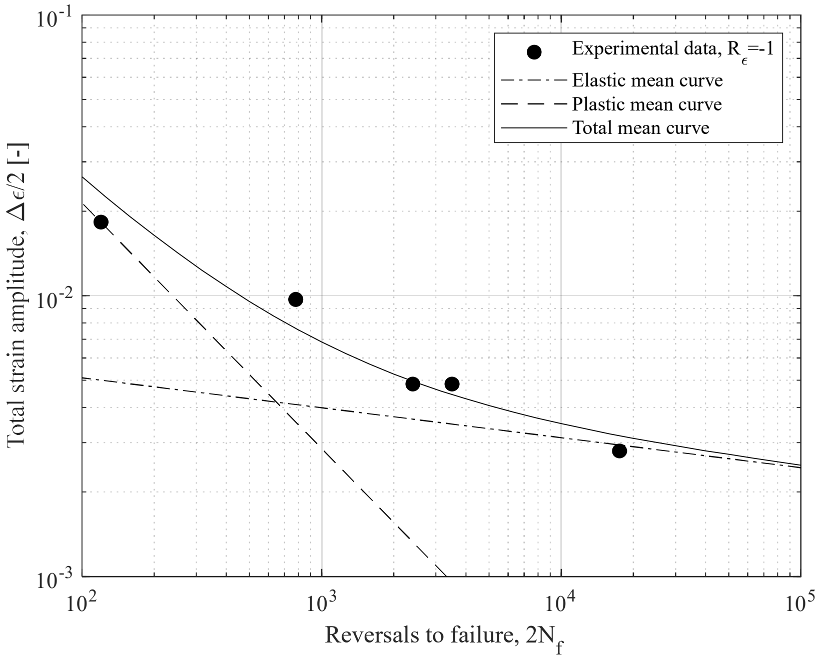

Source: Prepared by the author.

4.3 LOW-CYCLE FATIGUE MODELLING: APPLICATION AND DISCUSSION

In this section, the low-cycle fatigue modelling based on the Huffman approach[24] using the strain energy density, considering the critical dislocation density (ρ_c) driven by the highest strain amplitude specimen, is studied and discussed. Besides, two methodologies for the low-cycle fatigue modelling based on the Huffman approach are suggested – the first is through the mean value of the dislocation density (ρ_m) for the available experimental fatigue results, and the second is through a Monte Carlo (MC) stochastic prediction considering the variability of dislocation density (ρ) and cyclic strain hardening coefficient (K'). K' is normally distributed with a coefficient of variation (COV) equal to 0.1 as suggested by Jakubczak *et al.*[50]. The studied methodologies allow obtaining the strain-life parameters, namely, fatigue strength coefficient, σ_f', and fatigue ductility coefficient, ε_f'. Huffman's low-cycle fatigue modelling methodologies based on critical dislocation density and mean value of dislocation density allow obtaining the deterministic values of strain-life parameters, σ_f' and ε_f'. The methodology of MC stochastic prediction of low-cycle fatigue behaviour based on the assumptions of Huffman approach allows obtaining the probability distribution functions for the σ_f' and ε_f' parameters, as well as the probabilistic strain-life field. A comparison between the presented methodologies and the experimental low-cycle fatigue results is made. The experimental fatigue data of various aluminium alloys, such as Al 1050[47], AA 6061-T651[26,48], and AlMgSi0.8[47], are used to apply the studied methodologies.

4.3.1 Strain energy density-based Huffman model

The local fatigue damage modelling based on the strain energy density approach was proposed by Huffman[24]. This methodology is based on the cyclic stress-strain properties for predicting the low-cycle fatigue behaviour through the local fatigue damage parameters, such as stress, strain, Smith-Watson-Topper (SWT), and energy. Besides, Huffman's approach can be used to model the fatigue crack growth. The strain energy density-based Huffman's approach is given by the following fatigue damage criterion, D:

$$\left(\frac{U_e}{U_d\rho_c}\right)\left(\frac{U_p^*}{U_d\rho_c}\right) = D = \frac{2N}{2N_f} \tag{4.3}$$

where:

$\boldsymbol{U_e}$ is the elastic strain energy density;

$\boldsymbol{U_p^*}$ is the complementary plastic strain energy density;

$\boldsymbol{U_d}$ is the strain energy density from dislocations; and,

$\boldsymbol{\rho_c}$ is the critical dislocation density.

The strain energy from dislocations, $\boldsymbol{U_d}$, can be given by

$$U_d = \left(\frac{E}{2(1+\upsilon)}\right) \cdot \left|\vec{b}\right|^2 \tag{4.4}$$

where:

$\boldsymbol{\upsilon}$ is the Poisson's ratio; and,

$\vec{\boldsymbol{b}}$ is the Burger's vector.

According to Huffman[24], the $\left|\vec{b}\right|$ value for aluminium alloys or similar metals is equal to 2.86×10^{-10} m.

The strain energy density, by integrating the Ramberg-Osgood stress-strain relationship gives the damage equation in terms of materials parameters, is given by the following equation:

$$\left(\frac{2}{U_d^2 \rho_c^2 E}\right)\left(\frac{n'}{1+n'}\right)\left(\frac{1}{K'}\right)^{(1/n')} ({\sigma_{max}}^2)(\sigma_a)^{\frac{1+n'}{n'}}\left(\frac{1}{\mathrm{N}}\right) = D = \frac{1}{2N_f} \tag{4.5}$$

where, σ_{max} is the maximum stress, σ_a is the stress amplitude, E is the elastic modulus, K' and n' are the cyclic strength coefficient and cyclic strain hardening exponent, respectively.

Equation (4.3) can be used along with the elastic and plastic parts of the Ramberg-Osgood relationship separately to calculate the strain-life parameters. In this way, these parameters can be given by the following equations:

- Fatigue strength coefficient, $\boldsymbol{\sigma'_f}$

$$\sigma'_f = E\left(\frac{2}{U_d^2 \rho_c^2}\left(\frac{1}{K'}\right)^{1/n'}\left(\frac{n'}{1+n'}\right)E^{(1+2n')/n'}\right)^{\frac{-n'}{1+3n'}} \tag{4.6}$$

- Fatigue strength exponent, $\boldsymbol{b}$

$$b = \frac{-n'}{1+3n'} \tag{4.7}$$

- Fatigue ductility coefficient, $\boldsymbol{\varepsilon'_f}$

$$\varepsilon'_f = E\left(\frac{2(K')^3}{U_d^2 \rho_c^2 E}\left(\frac{n'}{1+n'}\right)\right)^{\frac{-1}{1+3n'}} \tag{4.8}$$

- Fatigue ductility exponent, $\boldsymbol{c}$

$$c = \frac{-1}{1+3n'} \tag{4.9}$$

The value of the critical dislocation density, ρ_c, can be found by fitting the resultant strain-life curve to low-cycle strain-life data, where the strain energy density approach, Equation (4.3), is used. The values of the critical dislocation density, driven by the highest strain amplitude specimen, have been found[24] between $1 \times 10^{15} \leq \rho_c \leq 3 \times 10^{16}$ m^{-2} and can be given by

$$\rho_c = \sqrt{\left(\frac{2(2N_f)}{U_d^2 EN}\right)\left(\frac{n'}{1+n'}\right)\left(\frac{1}{K'}\right)^{(1/n\prime)} \times ({\sigma_{max}}^2)(\sigma_a)^{\left(\frac{1+n\prime}{n\prime}\right)}}. \tag{4.10}$$

This model was used to evaluating the strain-life parameters of the Al 1050[47], 6061-T651[26,48], and AlMgSi0.8[47] aluminium alloys. The Huffman model was applied to the metallic alloys under consideration for predicting the Morrow constants using the strain energy density approach based on the fatigue crack initiation model. In Table 4.6, the critical dislocation density and strain-life parameters estimated based on the Huffman model for various metal alloys under consideration are presented. According to the Huffman model, the critical dislocation density, ρ_c, is estimated for the highest strain amplitude value for the experimental fatigue results available for a given material. A good agreement between the strain-life curve estimated by the strain energy density-based Huffman model and the experimental strain-life data is verified, for all materials under consideration, as shown in Figures 4.4 to 4.6. The critical dislocation density, ρ_c, driven by the highest strain amplitude specimen (Table 4.2), estimated for these materials are in line with the value recommended to a similar material[24] (Al 1100: $\rho_c = 2.81 \times 10^{15}$).

Table 4.6 - Strain-life parameters based on the Huffman model for various metal alloys under consideration.

Materials	$\boldsymbol{\rho_c}$	$\boldsymbol{U_d}$	$\boldsymbol{\sigma'_f}$	$\boldsymbol{b}$	$\boldsymbol{\varepsilon'_f}$	$\boldsymbol{c}$
-	[m/m^3]	[MPa]	[MPa]	[-]	[-]	[-]
Al 1050	1.20E+15	2.12E-15	208.20	-0.1676	0.0996	-0.4973
AA 6061-T651	5.90E+15	2.06E-15	401.69	-0.0485	1.4445	-0.8546
AlMgSi 0.8	4.51E+15	2.02E-15	387.92	-0.0508	0.8398	-0.8475

Source: Prepared by the author.

Figure 4.4 - Strain-life behaviour of Al 1050 – Experimental data vs. Huffman model.

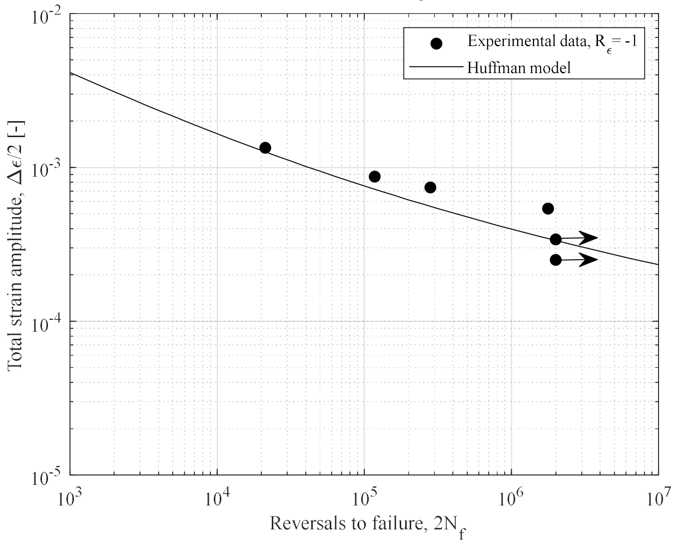

Source: Prepared by the author.

Figure 4.5 - Strain-life behaviour of Al 6061-T651 – Experimental data vs. Huffman model.

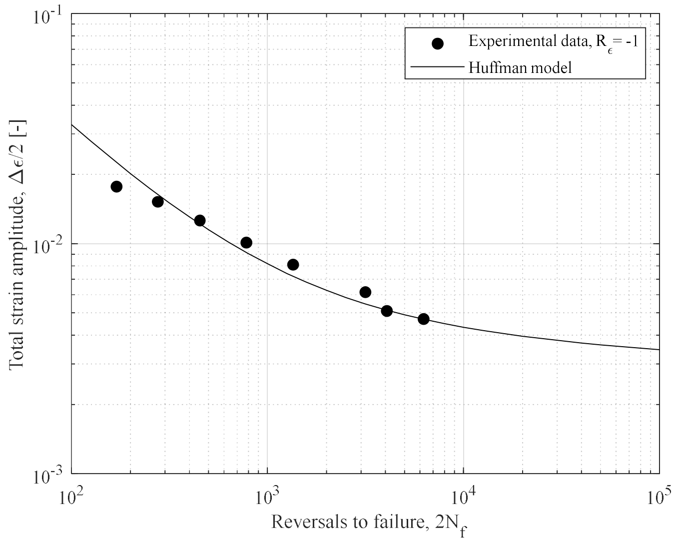

Source: Prepared by the author.

Figure 4.6 - Strain-life behaviour of AlMgSi 0.8 – Experimental data vs. Huffman model.

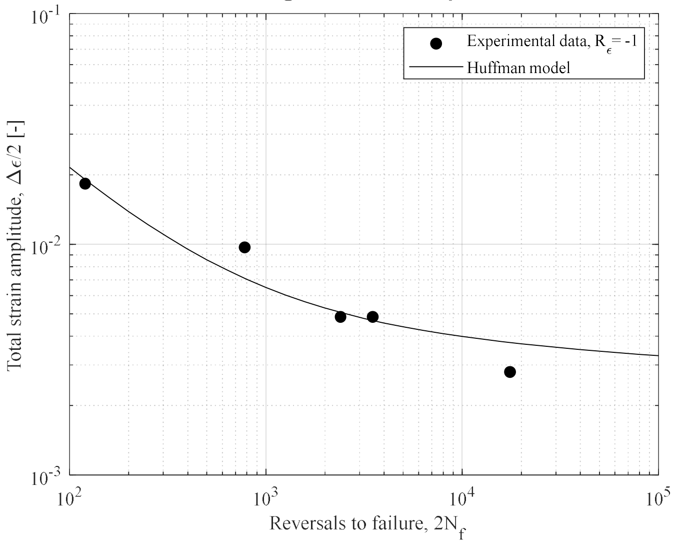

Source: Prepared by the author.

4.3.2 Strain energy density-based Huffman model considering the ρ mean value

The strain energy density-based Huffman model considers the critical dislocation density, ρ_c, that is driven by the highest strain amplitude specimen. In this section, the dislocation density, ρ, for each specimen was calculated according to Equation (4.10), for the materials under consideration. The mean value of dislocation density, $\mu(\rho)$, is given by

$$\mu(\rho) = \frac{1}{n}\sum_{i=1}^{n} \rho_i \tag{4.11}$$

where, n is the number of tested specimens, and ρ_i is the dislocation density for each tested specimen given by

$$\rho_i = \sqrt{\left(\frac{2(2N_{f,i})}{U_d^2 E N_i}\right)\left(\frac{n'}{1+n'}\right)\left(\frac{1}{K'}\right)^{(1/n\prime)} \times \left(\sigma_{max,i}{}^2\right)\left(\sigma_{a,i}\right)^{\left(\frac{1+n\prime}{n\prime}\right)}}. \tag{4.12}$$

where, N_i is the number of cycles for the tested specimen i, $2N_{f,i}$ is the number of reversals to failure for the tested specimen i, $\sigma_{max,i}$ is the maximum stress obtained during the low-cycle fatigue tests for the tested specimen i, and $\sigma_{a,i}$ is the stress amplitude obtained during the low-cycle fatigue tests for the tested specimen i. The uncertainty in dislocation density (ρ) due to low-cycle fatigue loading is normally considered.

In Tables 4.7 to 4.9, the critical dislocation density (ρ_c), the mean value of dislocation density ($\mu(\rho)$), the standard deviation ($\sigma(\rho)$), the coefficient of variation (COV), and the strain-life parameters are presented, for Al 1050, AA 6061-T651, and AlMgSi0.8, respectively. The strain-life parameters, considering the mean value of dislocation density ($\mu(\rho)$), were calculated using Equations (4.6) and (4.8). The coefficient of variation (COV) for Al 1050, AA 6061-T651, and AlMgSi0.8 are equal to 32.1%, 9.4%, and 51%, respectively. According to COV, it can be concluded that the dislocation density can have a significant impact in determining the strain-life properties based on Huffman's approach. In Figures 4.7 to 4.9, a good agreement between the strain-life curve estimated by the strain energy density-based Huffman model, using the mean value of dislocation density, and the experimental strain-life data is verified, for all materials under consideration.

Table 4.7 - Dislocation density evaluated for each failed LCF specimen for the Al 1050.

Specimen	σ_{max} [MPa]	σ_a [MPa]	$2N_f$ [-]	ρ [m/m^3]	$\mu(\rho)$	$\sigma(\rho)$	**COV [%]**	σ'_f [MPa]	ε'_f [-]
1050_01	39.2	39.2	21256	1.20E+15	1.911E+15	6.134E+14	32.1	243.36	0.1582
1050_02	34.3	34.3	117928	1.90E+15					
1050_03	29.4	29.4	281524	1.85E+15					
1050_04	24.5	24.5	1776294	2.70E+15					
1050_05*	19.6	19.6	2000000	---					
1050_06*	17.7	17.7	2000000	---					

Source: Prepared by the author.

Table 4.8 - Dislocation density evaluated for each failed LCF specimen for the AA 6061-T651.

Specimen	σ_{max} [MPa]	σ_a [MPa]	$2N_f$ [-]	ρ [m/m^3]	$\mu(\rho)$	$\sigma(\rho)$	**COV [%]**	σ'_f [MPa]	ε'_f [-]
6061_01	313.2	313.2	170	5.90E+15	6.088E+15	5.705E+14	9.4	402.91	1.5238
6061_02	307.4	307.4	276	6.20E+15					
6061_03	294.4	294.4	452	5.08E+15					
6061_04	292.7	292.7	780	6.28E+15					
6061_05	283.3	283.3	1352	5.92E+15					
6061_06	276.0	276.0	3160	6.89E+15					
6061_07	267.8	267.8	4066	5.73E+15					
6061_08	266.3	266.3	6256	6.70E+15					

Source: Prepared by the author.

Table 4.9 - Dislocation density evaluated for each failed LCF specimen for the AlMgSi 0.8.

Specimen	σ_{max} [MPa]	σ_a [MPa]	$2N_f$ [-]	ρ [m/m^3]	$\mu(\rho)$	$\sigma(\rho)$	**COV [%]**	σ'_f [MPa]	ε'_f [-]
AlMgSi _01	304.1	304.1	120	4.51E+15	4.167E+15	2.124E+15	51.0	384.77	0.7333
AlMgSi _02	286.5	286.5	780	6.40E+15					
AlMgSi _03	258.0	258.0	2400	4.01E+15					
AlMgSi _04	260.0	260.0	3500	5.22E+15					
AlMgSi _05	196.2	196.2	17500	7.33E+14					

Source: Prepared by the author.

Figure 4.7 - Strain-life behaviour of Al 1050 – Experimental data vs. modified Huffman model.

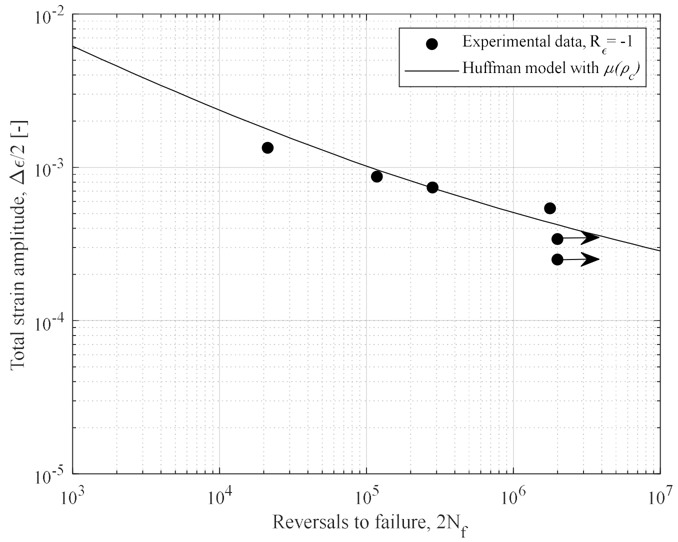

Source: Prepared by the author.

Figure 4.8 - Strain-life behaviour of AA 6061-T651 – Experimental data vs. modified Huffman model.

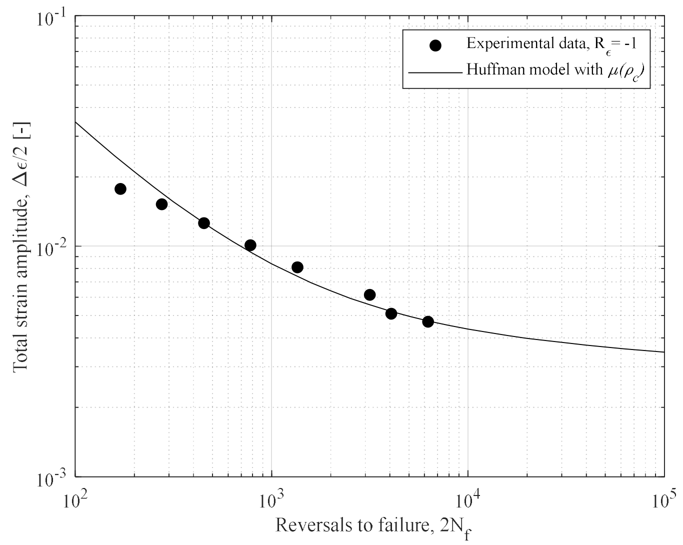

Source: Prepared by the author.

Figure 4.9 - Strain-life behaviour of AlMgSi 0.8 – Experimental data vs. modified Huffman model.

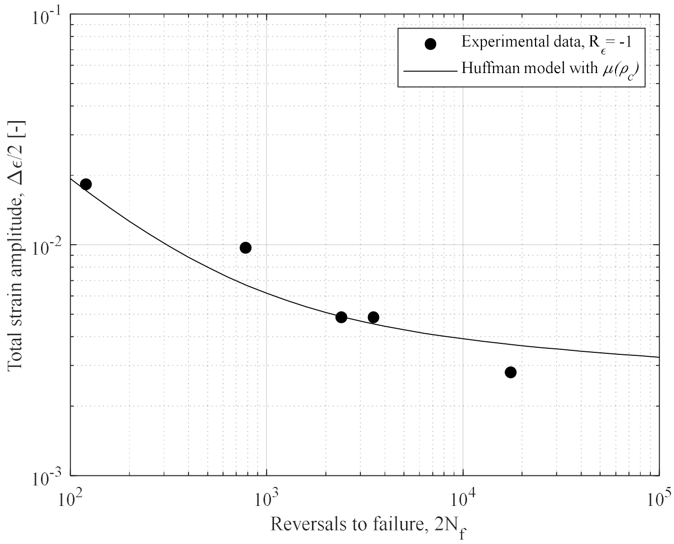

Source: Prepared by the author.

4.3.3 Monte Carlo stochastic prediction

Monte Carlo estimation method for predicting the low-cycle fatigue behaviour was used. Figure 4.10 illustrates the Monte Carlo (MC) stochastic procedure proposed to compute the fatigue ductility coefficient, ε_f', and the fatigue strength coefficient, σ_f', for the metallic materials, given the dislocation strain density, U_d, the dislocation density, ρ, the cyclic stress-strain behaviour, K' and n', and Young's modulus, E. The inputs of the model, which are defined in random variables normally distributed, are pointed out in the figure, namely: the cyclic strain hardening coefficient, K'; and, the dislocation density, ρ. K' is normally distributed with a coefficient of variation (COV) equal to 0.1 as suggested by Jakubczak *et al.*[50]. ρ is also normally distributed, where their mean and standard deviation values are evaluated for the available experimental strain-life data. In addition, the dislocation strain density, U_d, Young's modulus, E, the cyclic strain hardness exponent, n', are also used as constants. The input distributions, for the Monte Carlo (MC) simulation, were estimated using 10,000 samples. The fatigue ductility coefficient, ε_f', and fatigue strength coefficient, σ_f', are assumed as simulated outputs. For these distributed output parameters various probability functions, such as Normal, Weibull, and Logistic were fitted. A comparison between these probability distribution functions under consideration was done. The goodness-of-fit statistical tests for these probability distribution functions were evaluated by the Kolmogorov–Smirnov, Anderson–Darling, and χ-Square methods.

In Figures 4.11 to 4.13, the input distributions normally considered in the Monte Carlo stochastic prediction for Al 1050, AA 6061-T651, and AlMgSi 0.8 are presented, respectively. In these figures, the mean value, μ, and the standard deviation, σ, of each input distribution are also included.

In Figures 4.14 to 4.16, the output distributions from the Monte Carlo stochastic simulation for Al 1050, AA 6061-T651, and AlMgSi 0.8 are presented, respectively. In Table 4.10, the mean value and the standard deviation of σ_f' and ε_f' from the Monte Carlo stochastic simulation for the materials under consideration are summarized. In Figures 4.17 to 4.19, the experimental low-cycle fatigue data and mean strain-life curves based on the Monte Carlo (MC) stochastic simulation (mean values) and Huffman model to estimating σ_f' and ε_f', for Al 1050, AA 6061-T651, and AlMgSi0.8, respectively, are displayed. A good agreement between the experimental data and the strain-life curves from the Monte Carlo (MC) stochastic simulation based on the Huffman model to estimating the σ_f' and ε_f' was found.

For example, in Figures 4.20 and 4.21, the fit comparison between the probability density functions considered (Normal, Weibull and Logistic), for Al 1050 and AA 6061-T651, respectively, is displayed. In Table 4.11 and 4.12, the statistical parameters of the distribution functions under consideration for the strain-life parameters, σ_f' and ε_f', of Al 1050 and AA 6061-T651, respectively, are presented.

In Tables 4.13 and 4.14, the goodness-of-fit of several tested analytical distributions measured according to three statistical tests – Kolmogorov-Smirnov, Anderson-Darling, and the χ-Square methods – was quantified for Al 1050 and AA 6061-T651, respectively. For Al 1050, the Weibull and Logistic distributions were the ones that best fitted the fatigue strength coefficient, σ_f', and the fatigue ductility coefficient, ε_f', respectively. For AA 6061-T651, the Normal and Weibull distributions were the best fitted to the fatigue strength coefficient, σ_f', and the fatigue ductility coefficient, ε_f', respectively.

In Figures 4.22 and 4.23, the probabilistic strain-life prediction for Al 1050 and AA 6061-T651 through the Huffman approach using Monte Carlo stochastic modelling to estimating the output distributions of the strain-life parameters σ_f' and ε_f' are presented. It can be concluded that the Monte Carlo stochastic prediction allowed the generation of a probabilistic strain-life field through the ρ random variable (ρ is the dislocation density), where the experimental fatigue data are between the 5% and 95% failure probability curves.

Figure 4.10 - Monte Carlo stochastic procedure for low-cycle fatigue modelling of aluminium alloys.

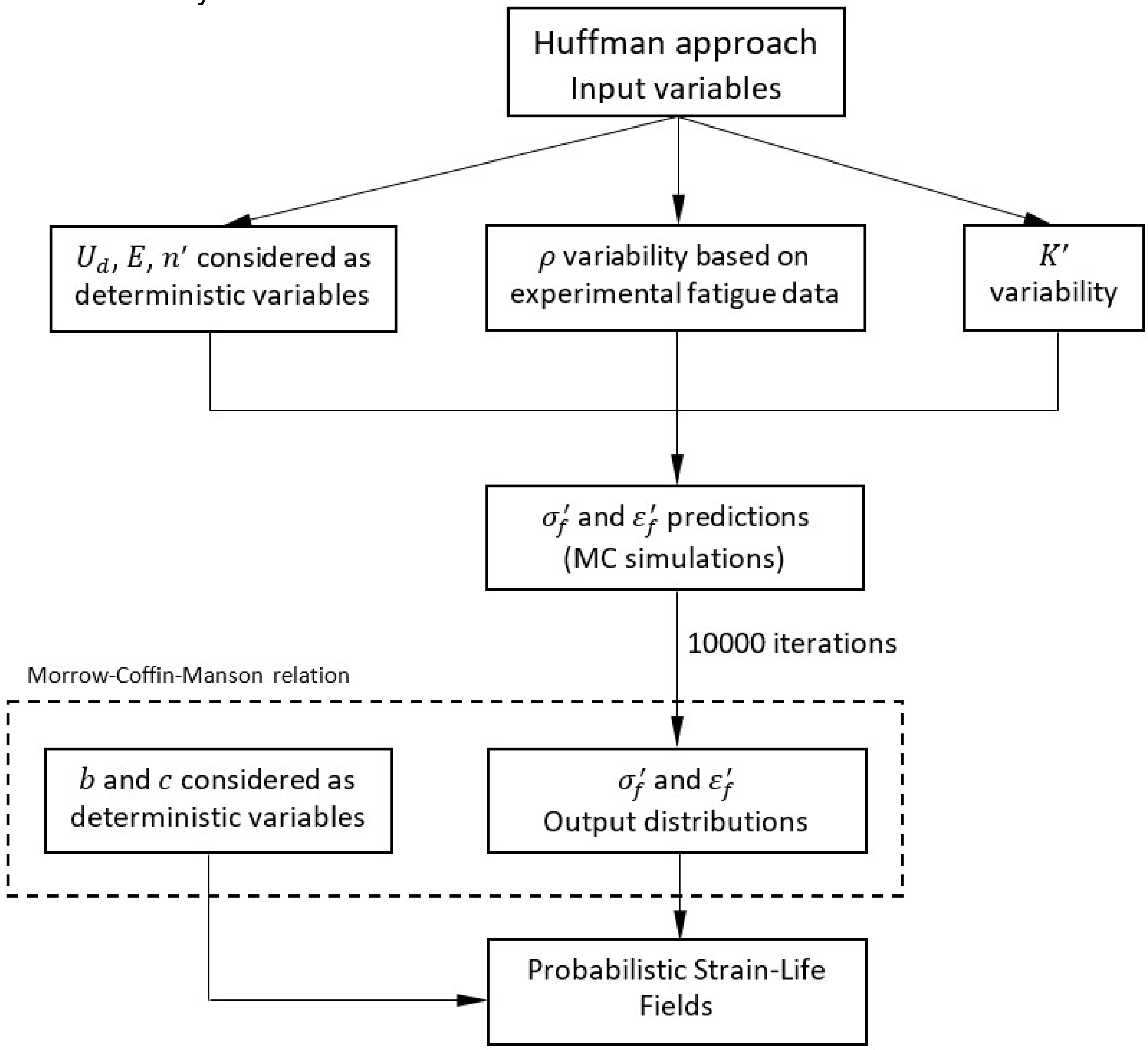

Source: Prepared by the author.

Figure 4.11 - Input distributions used in the Monte Carlo stochastic prediction for Al 1050.

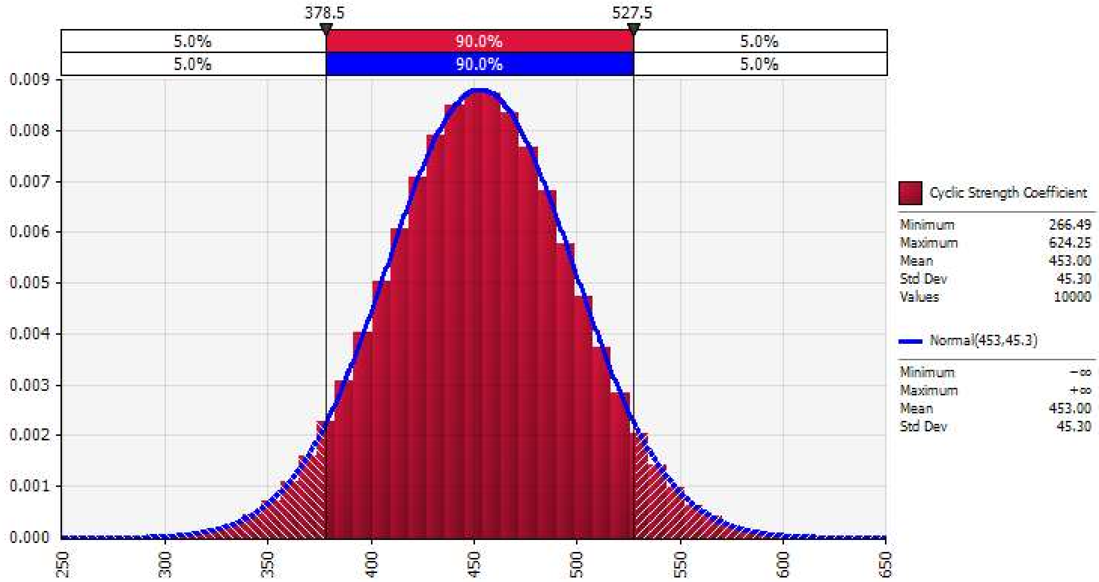

a) Cyclic strength coefficient, K' [MPa]

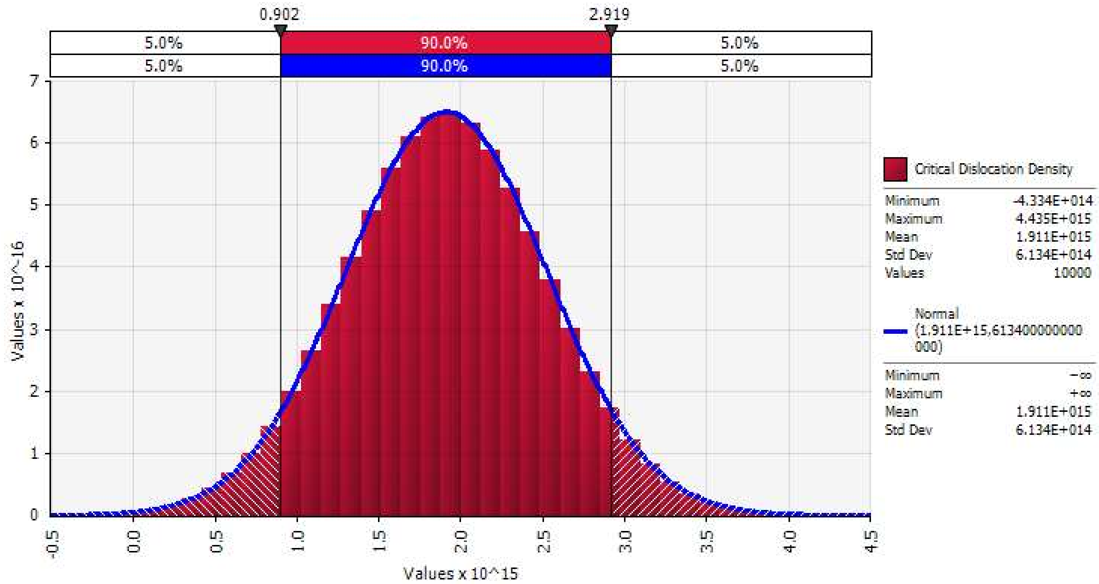

b) Critical dislocation density, ρ_c

Source: Prepared by the author.

Figure 4.12 - Input distributions used in the Monte Carlo stochastic prediction for AA 6061-T651.

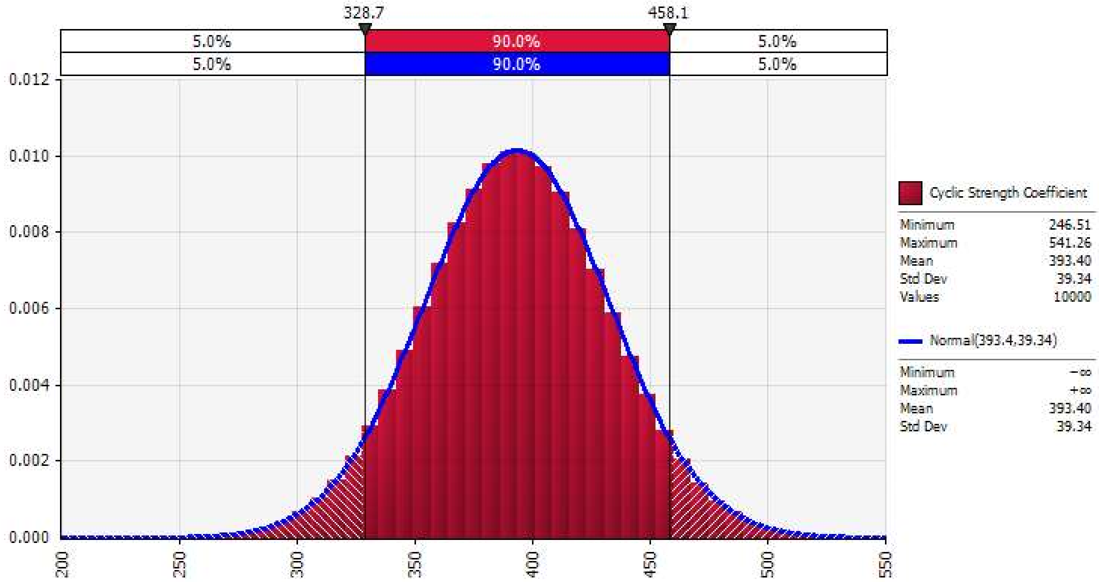

a) Cyclic strength coefficient, K' [MPa]

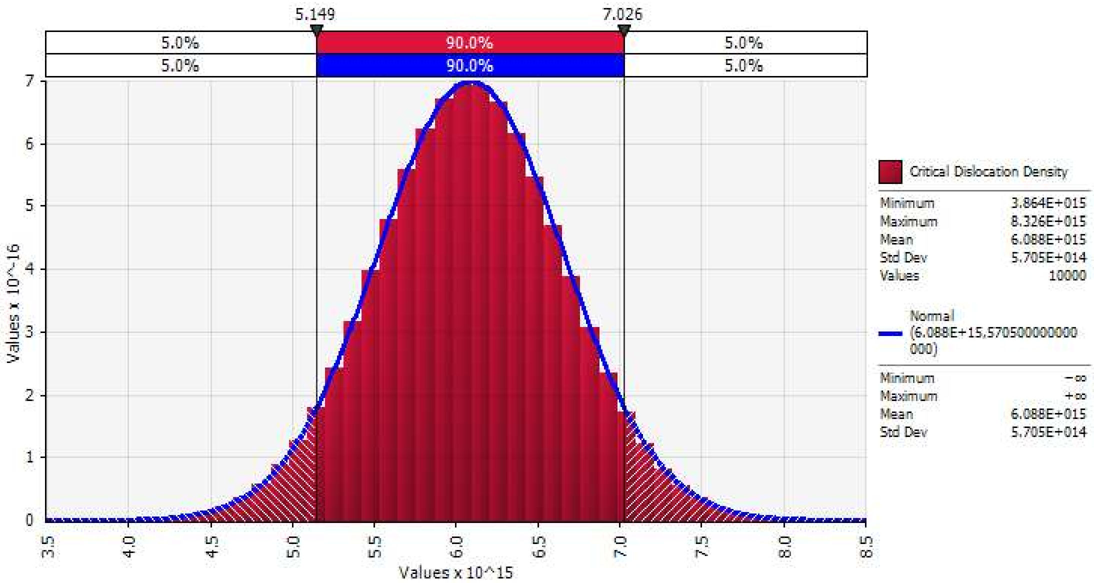

b) Critical dislocation density, ρ_c

Source: Prepared by the author.

Figure 4.13 - Input distributions used in the Monte Carlo stochastic prediction for AlMgSi 0.8.

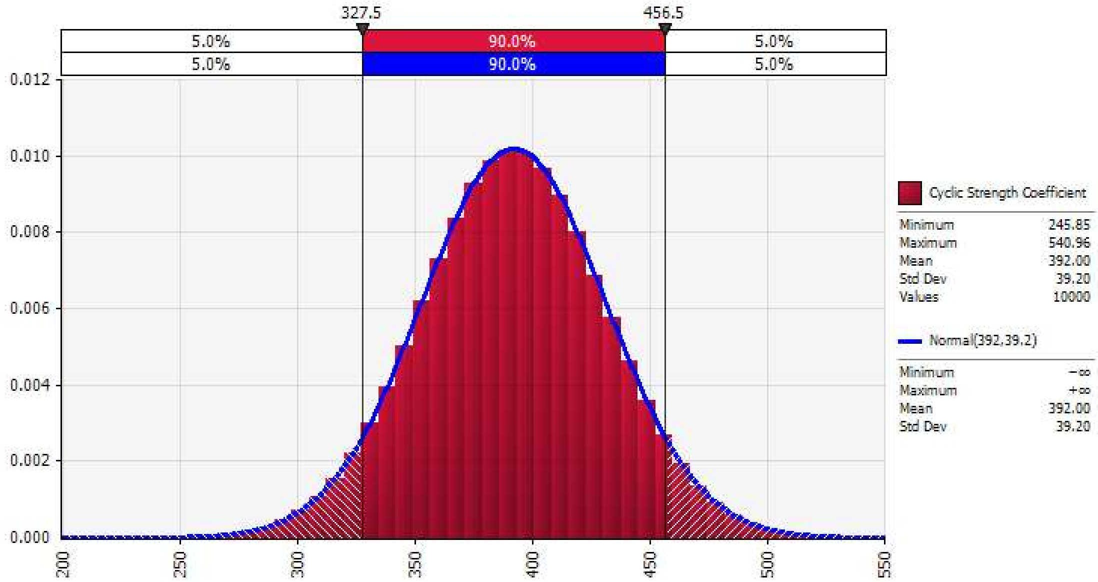

a) Cyclic strength coefficient, K' [MPa]

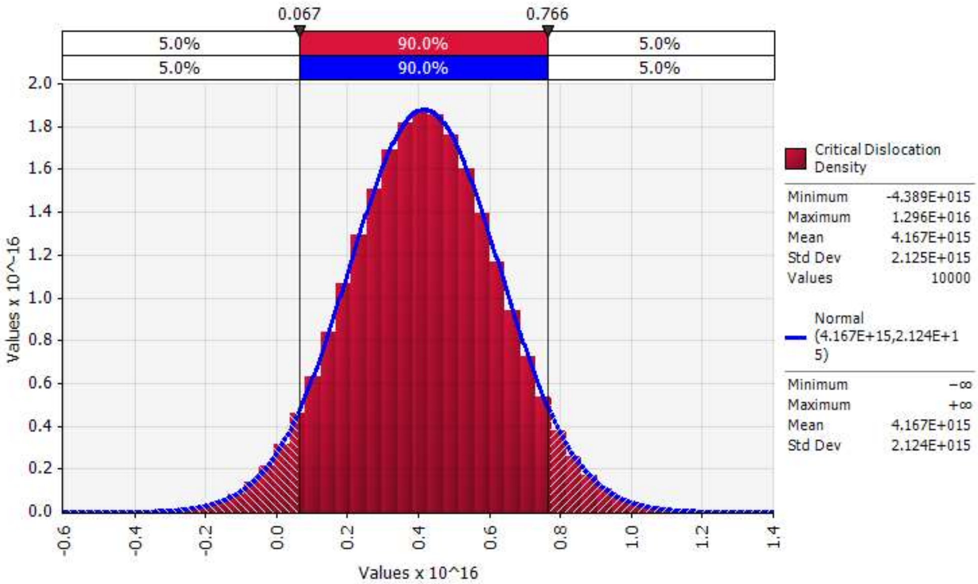

b) Critical dislocation density, ρ_c

Source: Prepared by the author.

Figure 4.14 - Output distributions from the Monte Carlo stochastic simulation for Al 1050.

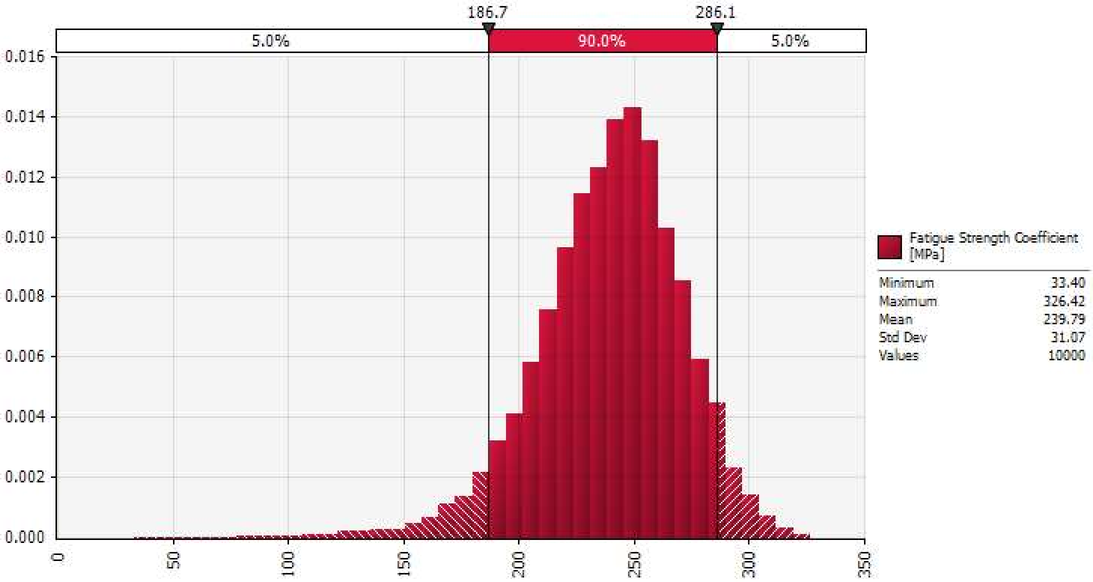

a) Fatigue strength coefficient, σ_f' [MPa]

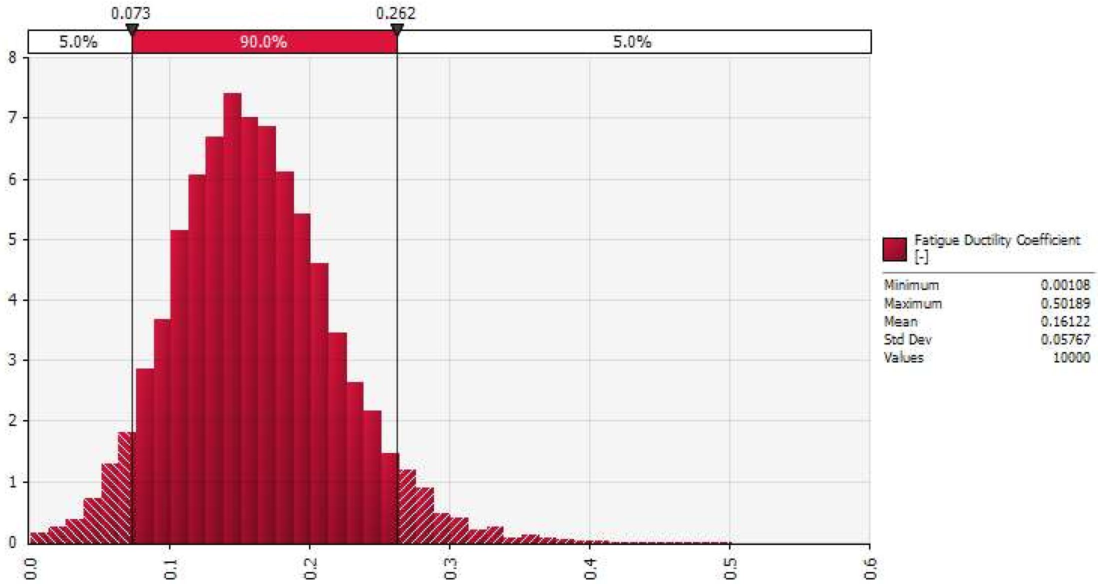

b) Fatigue ductility coefficient, ε_f'

Source: Prepared by the author.

Figure 4.15 - Output distributions from the Monte Carlo stochastic simulation for AA 6061-T651.

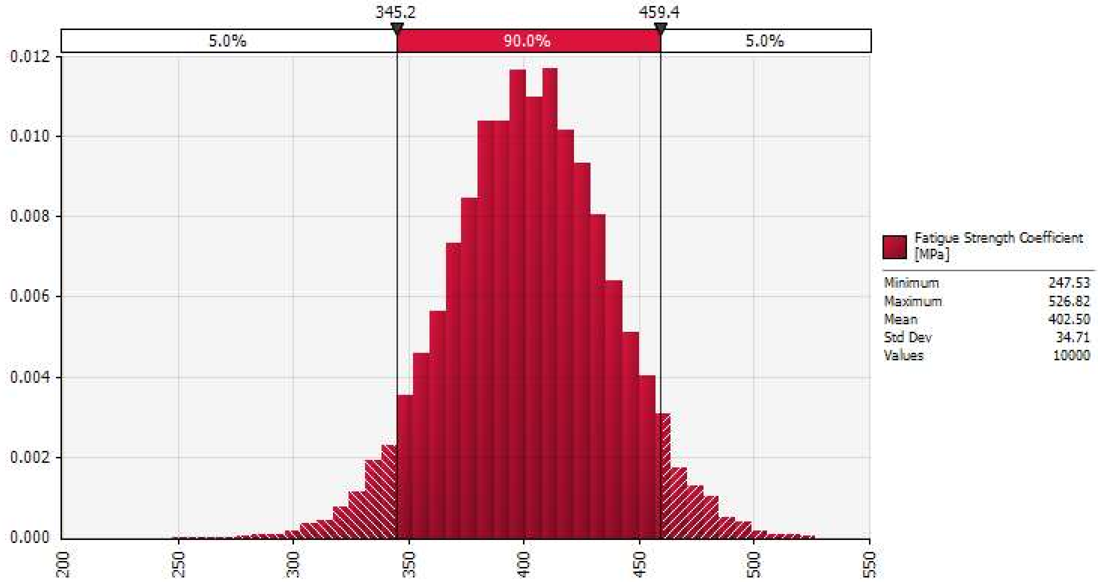

a) Fatigue strength coefficient, σ_f' [MPa]

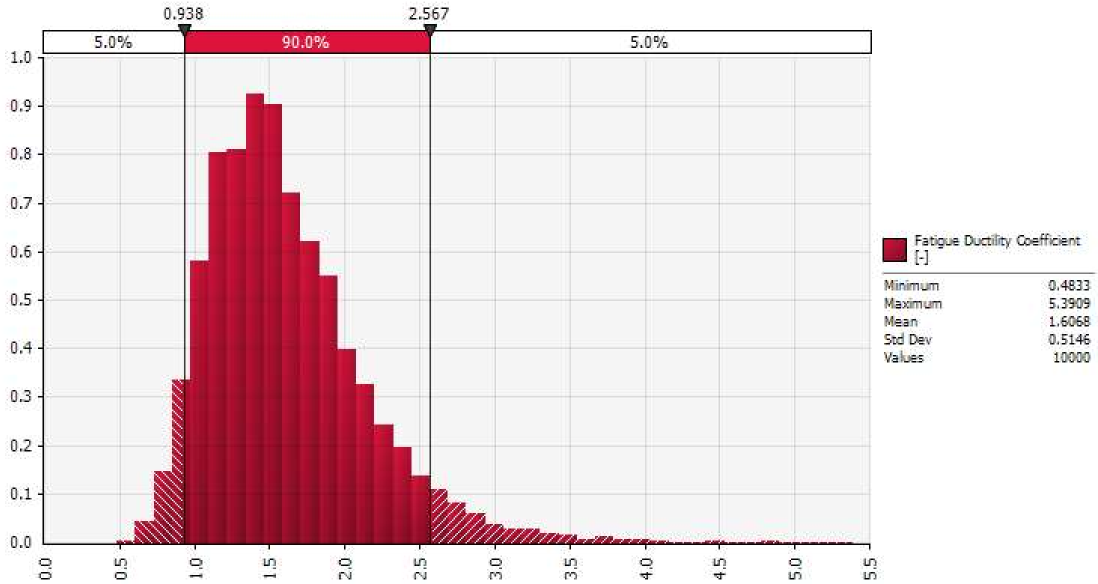

b) Fatigue ductility coefficient, ε_f'

Source: Prepared by the author.

Figure 4.16 - Output distributions from the Monte Carlo stochastic simulation for AlMgSi 0.8.

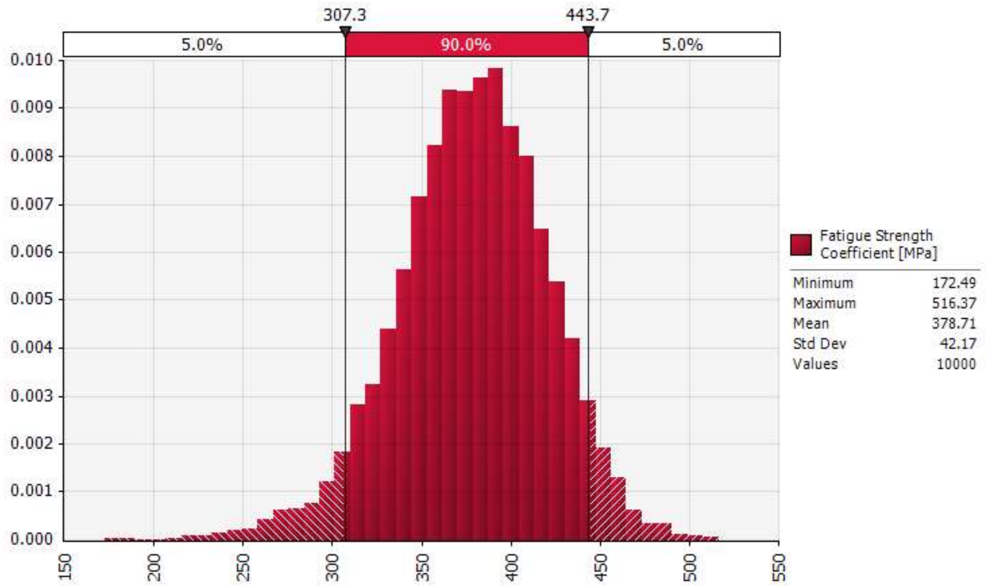

a) Fatigue strength coefficient, σ_f' [MPa]

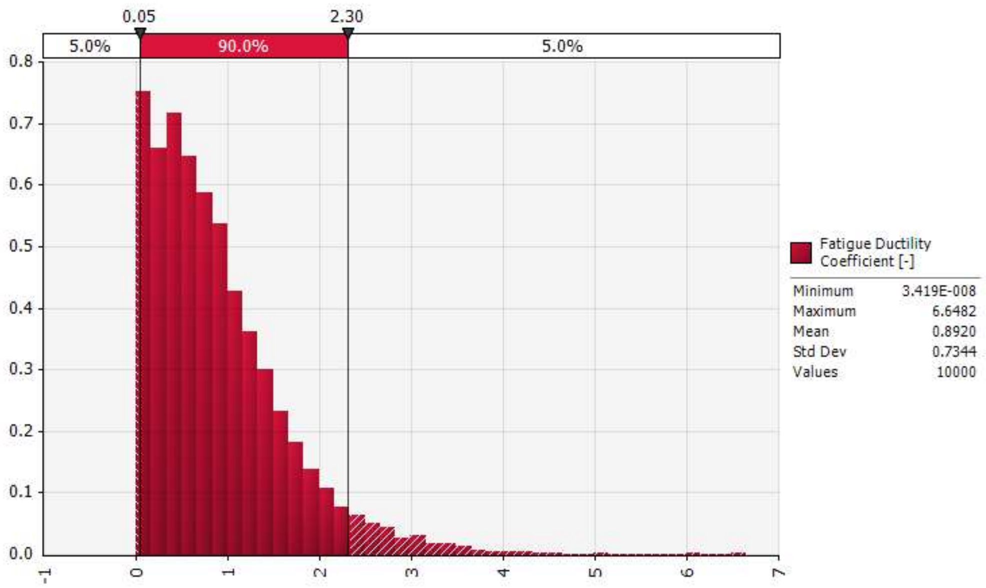

b) Fatigue ductility coefficient, ε_f'

Source: Prepared by the author.

Table 4.10 - Monte Carlo stochastic prediction of σ_f' and ε_f' for the materials under consideration.

Material	$\mu(\sigma_f')$ [MPa]	$\sigma(\sigma_f')$ [MPa]	$\mu(\varepsilon_f')$ [-]	$\sigma(\varepsilon_f')$ [-]
Al 1050	239.79	31.07	0.16122	0.05767
AA 6061-T651	402.50	34.71	1.6068	0.5146
AlMgSi 0.8	378.71	42.17	0.8920	0.7344

Source: Prepared by the author.

Figure 4.17 - Strain-life behaviour of Al 1050 – Experimental data vs. stochastic prediction (mean values) based on the Huffman model.

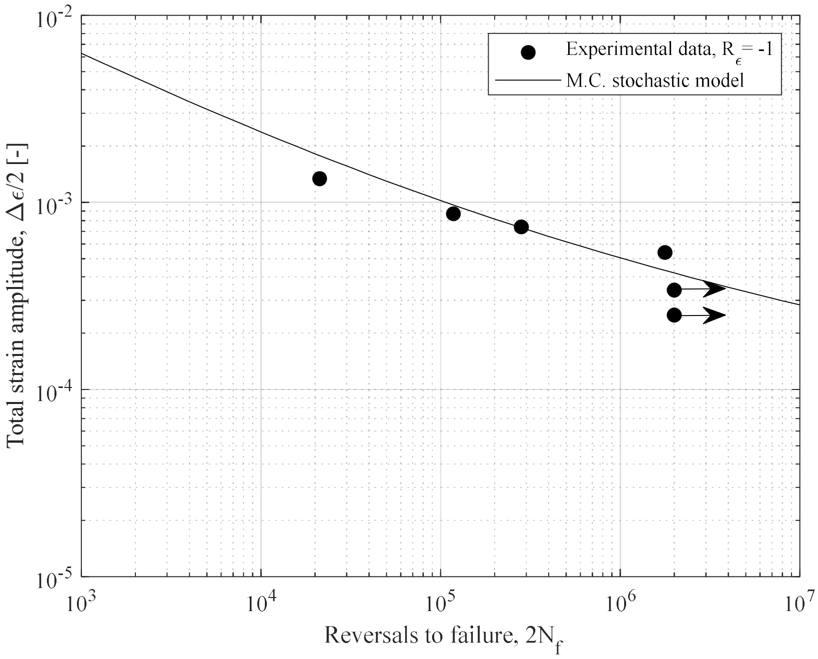

Source: Prepared by the author.

Figure 4.18 - Strain-life behaviour of AA 6061-T651 – Experimental data vs. stochastic prediction (mean values) based on the Huffman model.

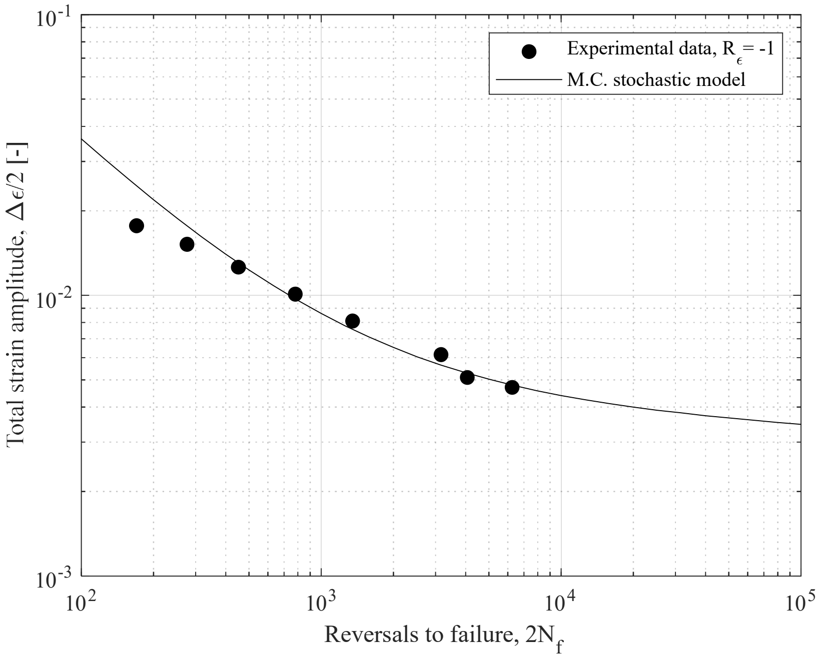

Source: Prepared by the author.

Figure 4.19 - Strain-life behaviour of AlMgSi0.8 – Experimental data vs. stochastic prediction (mean values) based on the Huffman model.

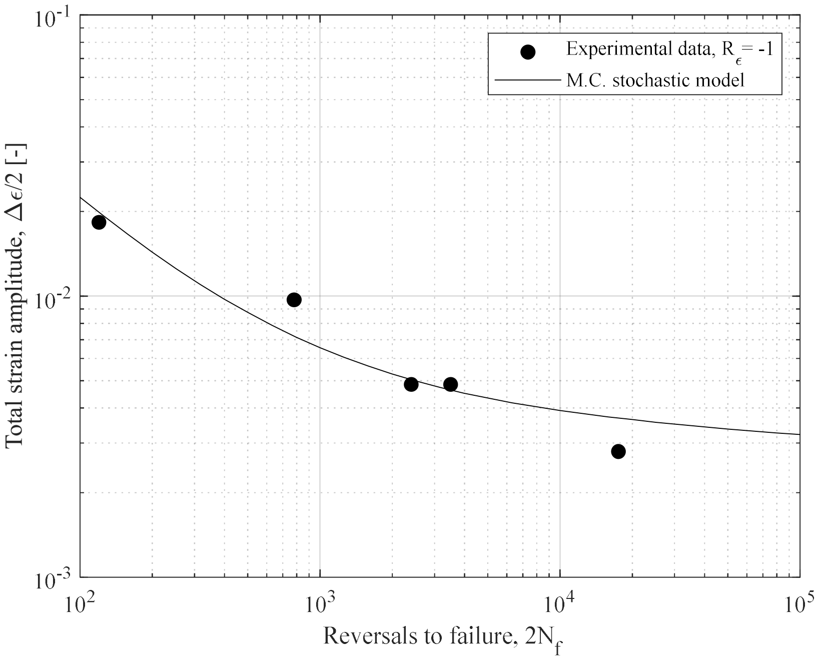

Source: Prepared by the author.

Figure 4.20 - Fit comparison between the probabilistic density functions considered for Al 1050.

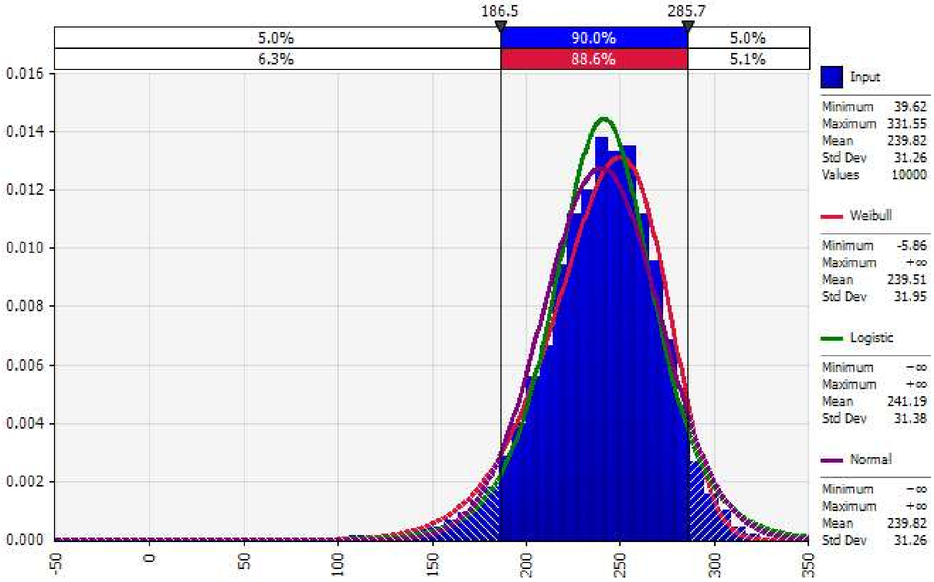

a) Fatigue strength coefficient, σ_f'

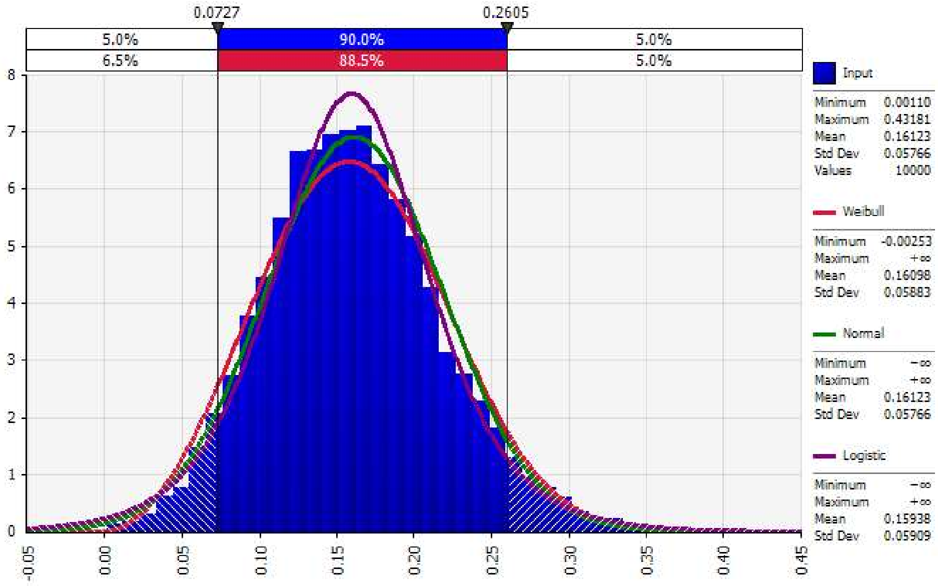

b) Fatigue ductility coefficient, ε_f'

Source: Prepared by the author.

Figure 4.21 - Fit comparison between the probabilistic density functions considered for AA 6061-T651.

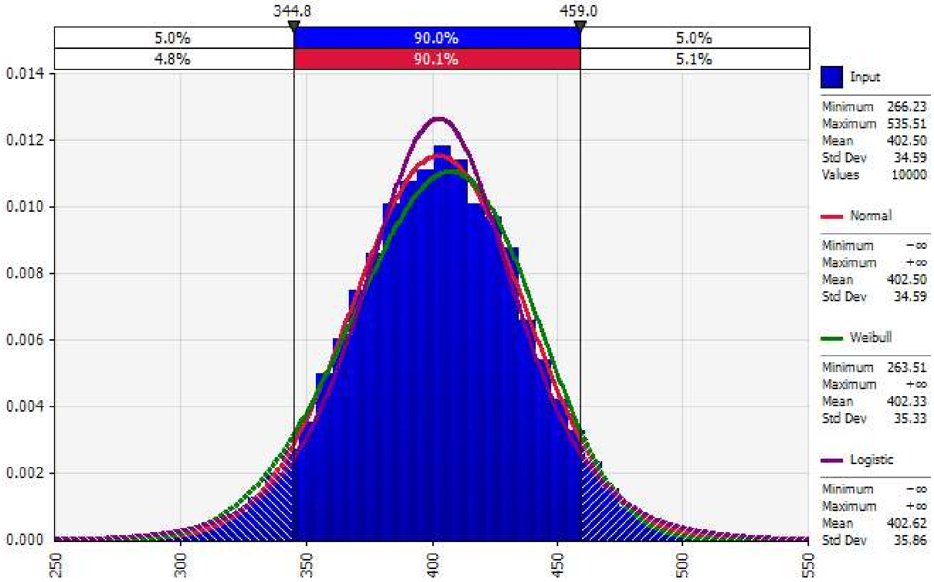

a) Fatigue strength coefficient, σ_f'

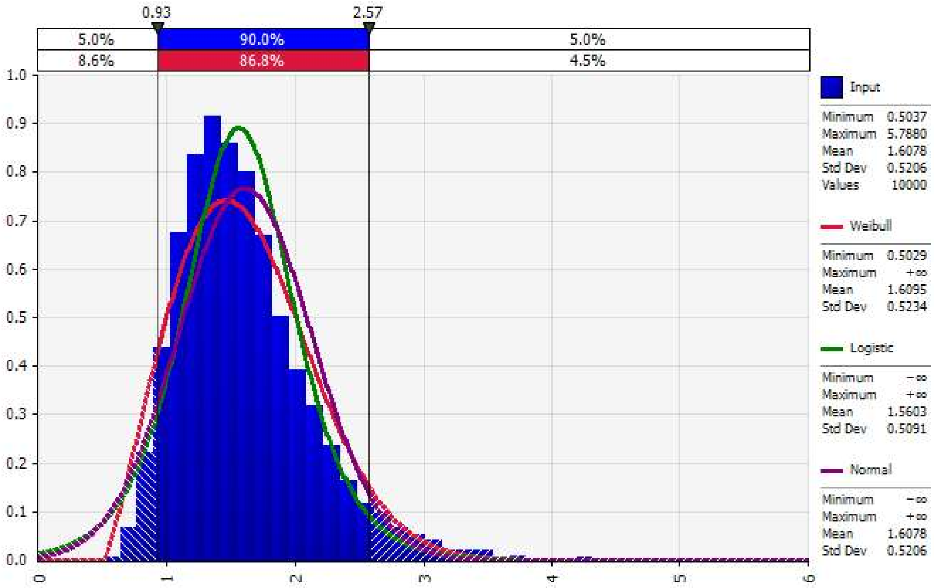

b) Fatigue ductility coefficient, ε_f'

Source: Prepared by the author.

Table 4.11 - Statistical parameters of the distribution functions under consideration for the strain-life parameters, σ_f' and ε_f', of Al 1050.

Distribution Function	Parameters	σ_f'	ε_f'
Weibull	α	9.19	3.0339
	β	258.86	0.1830
Logistic	α	241.19	0.1594
	β	17.30	0.0326
Normal	μ	239.82	0.1612
	σ	31.26	0.0577

Source: Prepared by the author.

Table 4.12 - Statistical parameters of the distribution functions under consideration for the strain-life parameters, σ_f' and ε_f', of AA 6061-T651.

Distribution Function	Parameters	σ_f'	ε_f'
Weibull	α	4.45	2.2355
	β	152.21	1.2494
Logistic	α	402.62	1.5603
	β	19.77	0.2807
Normal	μ	402.50	1.6078
	σ	34.59	0.5206

Source: Prepared by the author.

Table 4.13 - Goodness-of-fit statistical tests evaluated for several probabilistic density functions for Al 1050.

Parameter	Probabilistic density function	Kolmogorov–Smirnov	Anderson–Darling	χ-Square
σ_f'	Normal	0.0359	29.54	385.72
	Weibull	**0.0210**	**10.60**	**177.66**
	Logistic	0.0213	14.48	321.24
ε_f'	Normal	0.0245	14.29	226.27
	Weibull	0.0253	15.62	**217.43**
	Logistic	**0.0198**	**11.94**	267.31

Source: Prepared by the author.

Table 4.14 - Goodness-of-fit statistical tests evaluated for several probabilistic density functions for Al 6061.

Parameter	**Probabilistic density function**	**Kolmogorov–Smirnov**	**Anderson–Darling**	**χ-Square**
σ_f'	Normal	**0.0058**	**0.24**	**53.55**
	Weibull	0.0174	6.75	115.27
	Logistic	0.0176	7.24	190.72
ε_f'	Normal	0.0736	127.88	1357.08
	Weibull	**0.0476**	**60.88**	**614.83**
	Logistic	0.0499	70.01	1083.53

Source: Prepared by the author.

Figure 4.22 - Probabilistic strain-life prediction for Al 1050 through the Huffman model using Monte Carlo stochastic modelling.

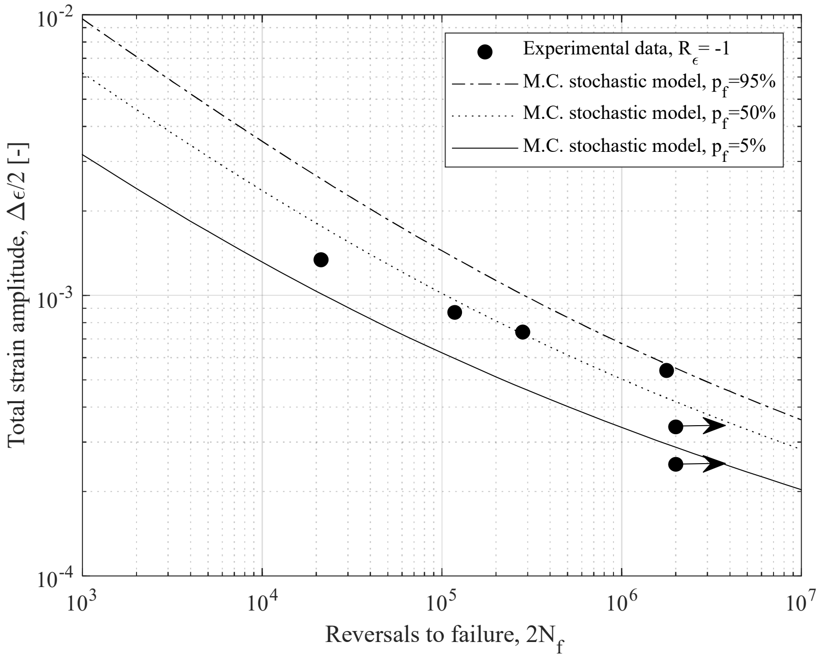

Source: Prepared by the author.

Figure 4.23 - Probabilistic strain-life prediction for Al 6061-T651 through the Huffman model using Monte Carlo stochastic modelling.

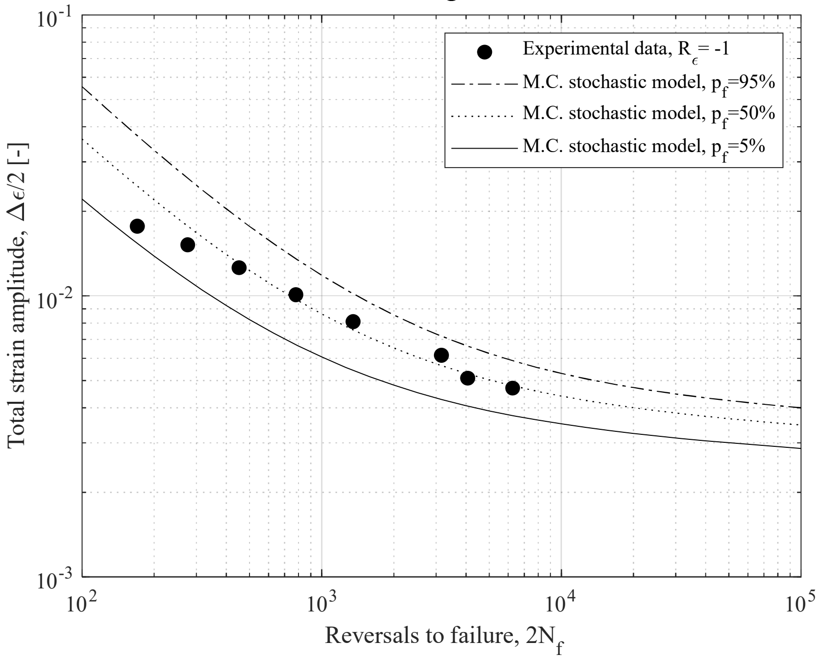

Source: Prepared by the author.

4.3.4 Comparison and discussion

In this section, comparison and discussion between the different methodologies studied are done. In Tables 4.15 to 4.17, the predicted number of cycles by the strain energy density-based Huffman model, the modified Huffman model (with $\mu(\rho)$), and the Monte Carlo stochastic modelling (mean values) applied to Huffman model considering ρ and K' as random variables are presented, respectively.

Table 4.15 - Predicted number of cycles calculated by Huffman model to estimating the strain-life parameters for the materials under consideration.

Material	Specimen	ε_a [%]	N_E [-]	N_P [-]
Al 1050	**1050_01**	0.134	10628	8966
	1050_02	0.087	58964	32145
	1050_03	0.074	140762	53818
	1050_04	0.054	888147	157614
Al 6061-T651	**6061_01**	1.770	85	122
	6061_02	1.520	138	155
	6061_03	1.260	226	212
	6061_04	1.010	390	320
	6061_05	0.810	676	510
	6061_06	0.615	1580	1060
	6061_07	0.510	2033	2099
	6061_08	0.470	3128	3094
AlMgSi 0.8	**AlMgSi _01**	1.830	60	64
	AlMgSi _02	0.970	390	72
	AlMgSi _03	0.485	1200	346
	AlMgSi _04	0.485	1750	346
	AlMgSi _05	0.280	8750	1290

Source: Prepared by the author.

Table 4.16 - Predicted number of cycles calculated by modified Huffman model (with $\mu(\rho)$) to estimating the strain-life parameters for the materials under consideration.

Material	**Specimen**	ε_a [%]	N_E [-]	N_P [-]
Al 1050	**1050_01**	0.134	10628	22746
	1050_02	0.087	58964	81554
	1050_03	0.074	140762	136541
	1050_04	0.054	888147	399890
Al 6061-T651	**6061_01**	1.770	85	130
	6061_02	1.520	138	165
	6061_03	1.260	226	226
	6061_04	1.010	390	340
	6061_05	0.810	676	543
	6061_06	0.615	1580	1129
	6061_07	0.510	2033	2235
	6061_08	0.470	3128	3294
AlMgSi 0.8	**AlMgSi _01**	1.830	60	55
	AlMgSi _02	0.970	390	164
	AlMgSi _03	0.485	1200	1241
	AlMgSi _04	0.485	1750	1241
	AlMgSi _05	0.280	8750	768215

Source: Prepared by the author.

Table 4.17 - Predicted number of cycles calculated by Huffman model and the Monte Carlo stochastic modelling (mean values) to estimating the strain-life parameters for the materials under consideration.

Material	Specimen	ε_a [%]	N_E [-]	N_P [-]
Al 1050	**1050_01**	0.134	10628	23038
	1050_02	0.087	58964	81816
	1050_03	0.074	140762	136375
	1050_04	0.054	888147	395390
Al 6061-T651	**6061_01**	1.770	85	138
	6061_02	1.520	138	175
	6061_03	1.260	226	240
	6061_04	1.010	390	361
	6061_05	0.810	676	575
	6061_06	0.615	1580	1191
	6061_07	0.510	2033	2346
	6061_08	0.470	3128	3445
AlMgSi 0.8	**AlMgSi _01**	1.830	60	68
	AlMgSi _02	0.970	390	202
	AlMgSi _03	0.485	1200	1415
	AlMgSi _04	0.485	1750	1415
	AlMgSi _05	0.280	8750	571618

Source: Prepared by the author.

In Figures 4.24 to 4.26, the experimental number of cycles obtained in each fatigue test is compared with the predicted number of cycles obtained for the methodologies under consideration, the strain energy density-based Huffman model, the modified Huffman model (with $\mu(\rho)$), and the Monte Carlo stochastic modelling applied to Huffman model considering ρ and K' as random variables, respectively. As expected, almost all points are placed between lines of multiplicity three and a great number of them are between lines of multiplicity 1.5, for Al 1050 and AA 6061-T651. The same is not true for AlMgSi0.8, where the strain energy density-based Huffman model, using the critical dislocation density for the higher strain amplitude specimen, shows results outside of these bands. When the methodologies are compared with each other, it can be seen that Huffman's approach using the mean value of the dislocation density ($\mu(\rho)$) and the Monte Carlo stochastic modelling applied to Huffman model considering ρ and K' as random variables exhibit better performances than the strain energy density-based Huffman approach using the critical dislocation density obtained from the highest strain amplitude specimen. This investigation makes it clear that the determination of the strain-life parameters through the strain energy density-based Huffman approach, using the critical dislocation density for the higher strain amplitude specimen, will have to be the object of a deeper analysis, where stochastic approaches can play an important role.

Figure 4.24 - Predicted number of cycles, N_P, versus experimental number of cycles, N_E for Al 1050: Huffman model; Huffman model with $\mu(\rho)$; MC stochastic modelling.

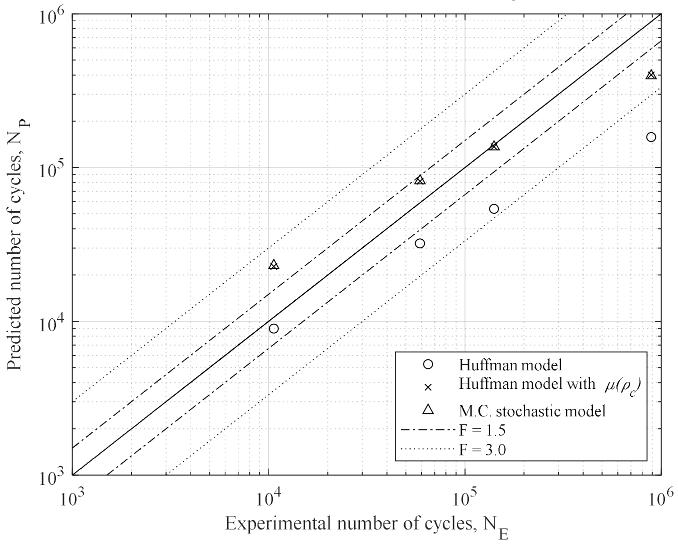

Source: Prepared by the author.

Figure 4.25 - Predicted number of cycles, N_P, versus experimental number of cycles, N_E for AA 6061-T651: Huffman model; Huffman model with $\mu(\rho)$; MC stochastic modelling.

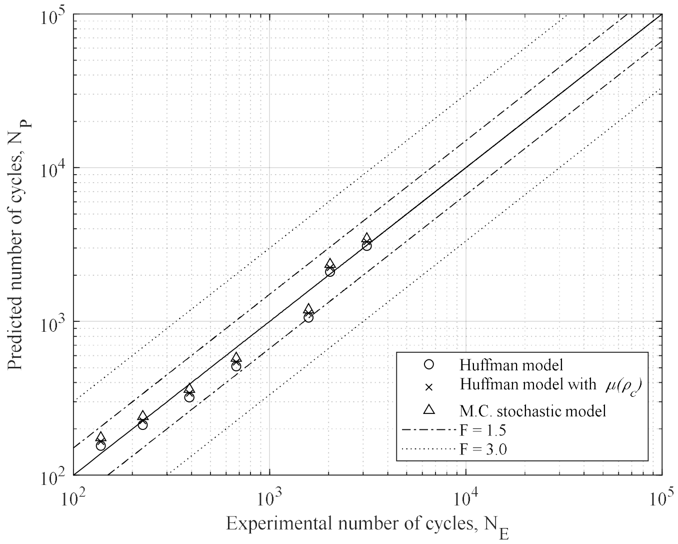

Source: Prepared by the author.

Figure 4.26 - Predicted number of cycles, N_P, versus experimental number of cycles, N_E for AlMgSi 0.8: Huffman model; Huffman model with $\mu(\rho)$; MC stochastic modelling.

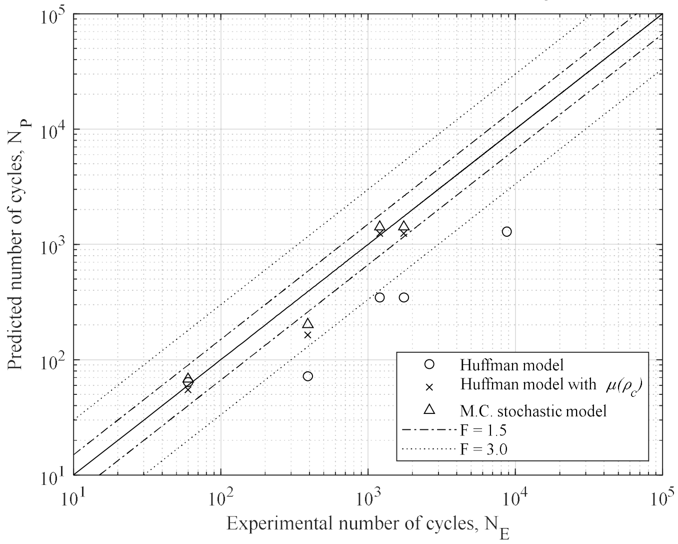

Source: Prepared by the author.

4.4 CONCLUSIONS

In this research, the low-cycle fatigue modelling supported by strain energy density-based Huffman model considering various methodologies is studied and discussed. Various methodologies for evaluating low-cycle fatigue strength based on the Huffman approach, using the critical dislocation density driven by the highest strain amplitude specimen, the mean value of the dislocation density (ρ_m) for the available experimental fatigue data, and a Monte Carlo (MC) stochastic prediction considering the variability of dislocation density (ρ) and cyclic strain hardening coefficient (K') were suggested and compared. The concluding remarks are the following:

- The various methodologies studied were able to model the low-cycle fatigue behaviour based on the strain energy density approach and a good agreement between the experimental fatigue data and the modelled curve is found;
- The strain-life parameters, σ_f' and ε_f', were estimated based on the Huffman model through the critical dislocation density (ρ_c), the mean value of the dislocation density (ρ_m), and the dislocation density (ρ) stochastically considered;
- Among the various methodologies used, the strain-life parameters, σ_f' and ε_f', estimated by strain energy density-based Huffman approach through the mean value of dislocation density (ρ_m) and the dislocation density (ρ) stochastically considered lead to better results when the comparison is made with experimental fatigue data since according to the literature, the dislocation structure changes with the total strain amplitude;
- The output discrete distributions generated by Monte Carlo (MC) stochastic simulation for the strain-life parameters, σ_f' and ε_f', shows that there is not a single probability distribution function suitable to describe each of these variables, for the metal materials under consideration;
- The Weibull and Logistic distribution functions showed the best fitting when compared with the output distributions obtained by stochastic prediction for the fatigue strength coefficient, σ_f', and the fatigue ductility coefficient, ε_f', respectively, for the 1050 aluminium. While, for the 6061-T651 aluminium alloy, the Normal and Weibull distributions exhibited the best fitting with the MC simulation-based output distributions for the fatigue strength coefficient, σ_f', and the fatigue ductility coefficient, ε_f', respectively;
- The probabilistic strain-life curves generated through the Huffman approach using the Monte Carlo stochastic simulation to estimating the output distributions of the strain-life parameters σ_f' and ε_f' are presented. It can be concluded that the Monte Carlo stochastic prediction allowed the generation of

a probabilistic strain-life field through the ρ random variable (ρ is the dislocation density), where the experimental fatigue data are between the 5% and 95% failure probability curves.

REFERENCES

1 MORROW, J.D. Cyclic plastic strain energy and fatigue of metals. **American Society for Testing and Materials Special Technical Publication**, West Conshohocken, v. 378, p. 45-87, 1965.

2 MANSON, S.S. Behaviour of materials under conditions of thermal stress. **National Advisory Committee for Aeronautics - NACA TN-2933**, Washington DC, p.1-105, 1954.

3 COFFIN, L.F. A study of the effects of the cyclic thermal stresses on a ductile metal. **Transactions of The American Society of Mechanical Engineers**, New York, v. 76, n. 6, p. 931–950, 1954.

4 DOWLING, N.E. Mean stress effects in strain-life fatigue. **Fatigue and Fracture of Engineering Materials and Structures**, Chichester v. 32, n. 12, p. 1004-1019, 2009.

5 SMITH, K.N.; WATSON, P.; TOPPER, T.H. Stress-strain function for the fatigue of metals, **Journal of Materials**, West Conshohocken, v. 5, n. 4, p. 767-778, 1970.

6 ZHU, S.; HUANG, H.; ONTIVEROS, V.; HE, L.; MODARRES, M. Probabilistic low cycle fatigue life prediction using an energy-based damage parameter and accounting for model uncertainty. **International Journal of Damage Mechanics**, London, v. 21, n. 8, p. 1128-1153, 2012.

7 CORREIA, J.; APETRE, N.; ARCARI, A.; DE JESUS, A.; MUÑIZ-CALVENTE, M.; CALÇADA, R.; BERTO, F.; FERNÁNDEZ-CANTELI, A. Generalized probabilistic model allowing for various fatigue damage variables. **International Journal of Fatigue**, London, v. 100, p. 187-194, 2017.

8 PARIS, P.C. A rational analytic theory of fatigue. **The trend in engineering**, Seattle, v. 13, n. 9, p. 9-14, 1961.

9 PARIS, P.; ERDOGAN, F. A critical analysis of crack propagation laws. **Journal of Fluids Engineering**, New York, v. 85, n. 4, p. 528-533, 1963.

10 LESIUK, G.; CORREIA, J.A.F.O.; KRECHKOVSKA, H.V.; PEKALSKI, G.; JESUS, A.M.P.; STUDENT, O. Fatigue and fracture behaviour of long term operated bridge materials and components. **Structural Integrity**, Bingley, v. 15, p. 127-205, 2021.

11 CORREIA, J.A.F.O.; DE JESUS, A.M.P.; SILVA, A.L.L.; PEDROSA, B.; REBELO, C.; CALÇADA, R.A.B. FE simulation of S-N curves for a riveted connection using

two-stage fatigue models. **Advances in Computational Design**, Daejeon, v. 2, n. 4, p. 333-348, 2017.

12 CORREIA, J.A.F.O.; DE JESUS, A.M.P.; FERNÁNDEZ-CANTELI, A. Local unified probabilistic model for fatigue crack initiation and propagation: Application to a notched geometry. **Engineering Structures**, Oxford, v. 52, p. 394-407, 2013.

13 RAPOSO, P.; CORREIA, J.A.F.O.; DE JESUS, A.M.P.; CALÇADA, R.A.B.; LESIUK, G.; HEBDON, M.; FERNÁNDEZ-CANTELI, A. Probabilistic fatigue S-N curves derivation for notched components. **Frattura ed Integrita Strutturale**, Cassino, v. 11, n. 42, p. 105-118, 2017.

14 CORREIA, J.A.F.O.; HUFFMAN, P.J.; DE JESUS, A.M.P.; CICERO, S.; FERNÁNDEZ-CANTELI, A.; BERTO, F.; GLINKA, G. Unified two-stage fatigue methodology based on a probabilistic damage model applied to structural details. **Theoretical and Applied Fracture Mechanics**, Amsterdam, v. 92, p. 252-265, 2017.

15 GLINKA, G. A notch stress-strain analysis approach to fatigue crack growth. **Engineering Fracture Mechanics**, Oxford, v. 21, n. 2, p. 245-261, 1985.

16 PEEKER, E.; NIEMI, E. Fatigue crack propagation model based on a local strain approach. **Journal of Constructional Steel Research**, London, v. 49, n. 2, p. 139-155,1999.

17 NOROOZI, A.H.; GLINKA, G.; LAMBERT, S. A two parameter driving force for fatigue crack growth analysis. **International Journal of Fatigue**, London, v. 27, n. 10-12, p. 1277-1296, 2005.

18 NOROOZI, A.H.; GLINKA, G.; LAMBERT, S. A study of the stress ratio effects on fatigue crack growth using the unified two-parameter fatigue crack growth driving force. **International Journal of Fatigue**, London, v. 29, n. 9-11, p. 1616-1633, 2007.

19 HURLEY, P.J.; EVANS, W.J. A methodology for predicting fatigue crack propagation rates in titanium based on damage accumulation, **Scripta Materialia**, Oxford, v. 56, n. 8, p. 681-684, 2007.

20 CORREIA, J.A.F.O.; JESUS, A.M.P.D.; FERNÁNDEZ-CANTELI, A. A procedure to derive probabilistic fatigue crack propagation data. **International Journal of Structural Integrity**, Bingley, v. 3, n. 2, p. 158-183, 2012.

21 HAFEZI, M.H.; ABDULLAH, N.N.; CORREIA, J.F.O.; DE JESUS, A.M.P. An assessment of a strain-life approach for fatigue crack growth. **International Journal of Structural Integrity**, Bingley, v. 3, n. 4, p. 344-376, 2012.

22 DE JESUS, A.M.P.; CORREIA, J.A.F.O. Critical assessment of a local strain-based fatigue crack growth model using experimental data available for the P355NL1 steel. **Journal of Pressure Vessel Technology**, New York, v. 135, n. 1, 2013.

23 CORREIA, J.A.F.O.; DE JESUS, A.M.P.; FERNÁNDEZ-CANTELI, A.; CALÇADA, R.A.B. Modelling probabilistic fatigue crack propagation rates for a mild structural steel. **Frattura ed Integrita Strutturale**, Cassino, v. 31, p. 80-96, 2015.

24 HUFFMAN, P.J. A strain energy based damage model for fatigue crack initiation and growth. **International Journal of Fatigue**, London, vol. 8, p. 197-204, 2016.

25 HUFFMAN, P.J.; FERREIRA, J.; CORREIA, J.A.F.O.; DE JESUS, A.M.P.; LESIUK, G.; BERTO, F.; FERNÁNDEZ-CANTELI, A.; GLINKA, G. Fatigue crack propagation prediction of a pressure vessel mild steel based on a strain energy density model. **Frattura ed Integrita Strutturale**, Cassino, v. 11, n. 42, p. 74-84, 2017.

26 CORREIA, J.A.F.O.; DE JESUS, A.M.P.; RIBEIRO, A.S.; FERNANDES, A.A. Strain-based approach for fatigue crack propagation simulation of the 6061-T651 aluminium alloy. **International Journal of Materials and Structural Integrity**, Geneva, v. 11, n. 1-3, p. 1-15, 2017.

27 CORREIA, J.A.F.O.; HUFFMAN, P.J.; DE JESUS, A.M.P.; LESIUK, G.; CASTRO, J.M.; CALCADA, R.A.B.; BERTOD, F. Probabilistic Fatigue Crack Initiation and Propagation Fields Using the Strain Energy Density. **Strength of Materials**, New York, v. 50, n. 4, p. 620-635, 2018.

28 BANG, D.J.; INCE, A.; NOBAN, M. Modeling approach for a unified crack growth model in short and long fatigue crack regimes. **International Journal of Fatigue**, London, vol. 128, 2019.

29 PEDROSA, B.; CORREIA, J.; LESIUK, G.; REBELO, C.; HUFFMAN, P.; JESUS, A. Probabilistic fields of fatigue crack growth rates of puddle iron based on huffman local approach. **Synergy of Culture and Civil Engineering - History and Challenges**, Zurich, p. 804-811, 2020

30 LEE, K.; SONG, J. Estimation methods for strain-life fatigue properties from hardness. **International Journal of Fatigue**, London, v. 28, n. 4, p. 386-400, 2006.

31 MEGGIOLARO, M.A.; CASTRO, J.T.P. Statistical evaluation of strain-life fatigue crack initiation predictions. **International Journal of Fatigue**, London, v. 26, n. 5, p. 463-476, 2004.

32 TANAKA, K.; MURA, T. A dislocation model for fatigue crack initiation. **Journal of Applied Mechanics**, New York, v. 48, n. 1, p. 97-103, 1981.

33 KELLER, R.; ZIELINSKI, W.; GERBERICH, W.W. On the onset of low-energy dislocation substructures in fatigue: Grain size effects. **Materials Science and Engineering A**, Wilmington, v. 113, n. C, p. 267-280,1989.

34 DESHPANDE, V.S.; NEEDLEMAN, A.; VAN DER GIESSEN, E. Discrete dislocation plasticity modeling of short cracks in single crystals. **Acta Materialia**, Oxford, v. 51, n. 1, p. 1-15, 2003.

35 YE, D.; MATSUOKA, S.; NAGASHIMA, N.; SUZUKI, N. The low-cycle fatigue, deformation and final fracture behaviour of an austenitic stainless steel. **Materials Science and Engineering A**, Wilmington, v. 415, n. 1-2, p. 104-117, 2006.

36 SANGID, M.D.; MAIER, H.J.; SEHITOGLU, H. An energy-based microstructure model to account for fatigue scatter in polycrystals. **Journal of the Mechanics and Physics of Solids**, Oxford, v. 59, n. 3, p. 595-609, 2011.

37 SANGID, M.D.; MAIER, H.J.; SEHITOGLU, H. The role of grain boundaries on fatigue crack initiation - An energy approach. **International Journal of Plasticity**, Oxford, v. 27, n. 5, p. 801-821, 2011.

38 SANGID, M.D. The physics of fatigue crack initiation. **International Journal of Fatigue**, London, v. 57, p. 58-72, 2013.

39 MUGHRABI, H. Microstructural mechanisms of cyclic deformation, fatigue crack initiation and early crack growth. **Philosophical Transactions of the Royal Society A: Mathematical, Physical and Engineering Sciences**, London, v. 373, n. 2038, 2015.

40 TU, S.-T.; ZHANG, X.-C. Fatigue crack initiation mechanisms. *In:* TU, S.-T.; ZHANG, X.-C. **Reference module in materials science and materials engineering**. [S.l.: s.n.], 2016. p. 1-23.

41 HEINRICH, C.; SUNDARARAGHAVAN, V. A method to predict fatigue crack initiation in metals using dislocation dynamics. **Corrosion Reviews**, Berlin, v. 35, n. 4-5, p. 325-341, 2017.

42 BOEFF, M.; HASSAN, H.U.; HARTMAIER, A. Micromechanical modeling of fatigue crack initiation in polycrystals. **Journal of Materials Research**, Heidelberg, v. 32, n. 23, p. 4375-4386, 2017.

43 LAVENSTEIN, S.; EL-AWADY, J.A. Micro-scale fatigue mechanisms in metals: Insights gained from small-scale experiments and discrete dislocation dynamics simulations. **Current Opinion in Solid State and Materials Science**, Oxford, v. 23, n. 5, 2019.

44 MONTEIRO, S.N.; BRANDÃO, L.P.; SOUSA, T.G.D.; GARCIA FILHO, F.D.C. Novel methods for dislocation density estimation in highly compacted tangles. **Journal of Materials Research and Technology**, Rio de Janeiro, v. 9, n. 2, p. 2072-2078, 2020.

45 ANDREYKIV, O.E.; SHTAYURA, N.S.; YAREMA, R.Y. Energy-Based Approach to Evaluation of Short Fatigue Crack Growth Rate in Plates. **Strength of Materials**, New York, v. 49, n. 6, p. 778-787, 2017.

46 WEI, M.; IVANYTS'KYI, Y.L.; KUN', P.S.; SHYSHKOVS'KYI, R.O. Modeling of the Elastoplastic Deformation of a Body Based on the Energy Balance and Monitoring of Strains. **Materials Science**, New York, v. 55, n. 3, p. 352-357, 2019.

47 BOLLER C.; SEEGER T. **Materials Data for Cyclic Loading**: Part D: Aluminium and Titanium Alloys. Materials Science Monographs, v. 42D, Amsterdam: Elsevier Science Publishers, 1987.

48 RIBEIRO, A.S.; JESUS, A.M.P.; FERNANDES, A.A. Fatigue crack propagation rates of the aluminium alloy 6061-T651. *In*: INTERNATIONAL CONGRESS OF MECHANICAL ENGINEERING, 18.; 2005, Ouro Preto. **Proceedings** […]. Ouro Preto: COBEM, 2005.

49 RAMBERG, W.; OSGOOD, W.R. Description of stress–strain curves by three parameters. **National Advisory Committee for Aeronautics – NACA-TN-902**, Washington DC, n. 902, 1943.

50 JAKUBCZAK, H.; SOBCZYKIEWICZ, W.; GLINKA, G. Fatigue reliability of structural components. **International Journal of Materials and Product Technology**, Geneva, v. 25, n. 1-3, p. 64-83, 2006.

CHAPTER V

5 APPLICATION AND DISCUSSION OF VARIOUS CRACK CLOSURE MODELS TO PREDICT FATIGUE CRACK GROWTH IN 6061-T651 ALUMINIUM ALLOY

5.1 INTRODUCTION

Fatigue is the main cause of failures and mechanical fracture in structural systems when subjected to cyclic loading. The study of this phenomenon began in the early nineteenth century with Albert and Wöhler[1], being still very much explored by the scientific and technical community, today. Many of the developments related to the fatigue phenomenon are used in design codes[2] for fatigue verification as well as for the residual life estimation based on fracture mechanics approaches and fatigue crack growth laws of structural components[3-8].

The scientific community has explored and developed fatigue crack propagation models to characterise different fatigue regions. The pioneer in this type of studies was Paris[9,10], in 1961, in which he developed a semi-empirical relationship between fatigue crack growth rates, da/dN, and applied stress intensity factor range, ΔK. The linear elastic fracture mechanics was used to model the fatigue crack growth behaviour. Several laws have been proposed to describe regions I+II[7,11], II[11], II+III[11], and I+II+III[7,11,12]. In 1970, Elber[13,14] proposed that the fatigue crack propagation behaviour is not driven by ΔK but by the effective stress intensity factor range, giving rise to what is now call crack closure/opening phenomenon.

In this section, the fatigue crack growth (FCG) models[7,11,12], where the relationship between the fatigue crack propagation rates, da/dN, and applied stress intensity factor ranges, ΔK, for distinct regions are presented. Besides, the crack closure/opening models[13-18] to estimate the quantitative parameter, U, as a function of the applied stress ratio, R, are also detailed.

In this research work, a comparison between various crack closure/opening models – Elber[13,14], Katcher and Kaplan[19], Clerivet and Bathias[20], Schijve[21], Zhang[22], Newman [23], Savaidis[24-26], Codrington-Kotousov[27], and Correia[28-30] – on the fatigue crack growth behaviour of 6061-T651 aluminium alloy is presented and compared with the experimental measurements collected in literature[31-34]. The relation between effective stress ratio, R_{eff}, and applied stress ratio, R, for various crack closure models under consideration are obtained and compared with the experimental results. Deterministic relations between U vs R and R_{eff} vs. R based on second-degree polynomial functions are suggested for 6061 aluminium alloys ($0 \leq R \leq 0.5$), using the experimental results collected in literature[31-34].

5.1.1 Fatigue crack growth models

Linear elastic fracture mechanics approaches are used to model the fatigue crack growth behaviour and to estimate the residual fatigue life of structural components[35,36]. The first fatigue crack growth law was suggested by Paris[9,10], in 1961. This relation allowed the relationship between the stress intensity factor range, ΔK, at a crack tip and the fatigue crack growth rates, da / dN. This law is widely used by researchers and engineers and is included in design codes (BS7910[2], EC3[37], DNVGL[38], etc.), describing the fatigue crack propagation behaviour in region II (Figure 5.1), commonly called the Paris region:

$$\frac{da}{dN} = C \cdot (\Delta K)^m \tag{5.1}$$

where: da/dN is the fatigue crack growth rate; ΔK is the stress intensity factor range; and, C and m are material constants. The stress intensity factor range, ΔK, is given by

$$\Delta K = K_{max} - K_{min} \tag{5.2}$$

Where, K_{max} and K_{min} are the maximum and minimum values of the stress intensity factor at the maximum and minimum applied stresses σ_{max} and σ_{min}, respectively, during cyclic loading. These relations can be given by Irwin relation[39]:

$$K_{max} = Y\sigma_{max}\sqrt{\pi a} \tag{5.3}$$

$$K_{min} = Y\sigma_{min}\sqrt{\pi a} \tag{5.4}$$

where: Y is a function depending on the geometries and loading conditions; and, a is the crack length.

Therefore, the fatigue crack propagation behaviour is described by three distinct regions, the region I or threshold fatigue crack growth region, region II or Paris region, and finally the near unstable crack propagation regime (region III) – see Figure 5.1.

Figure 5.1 - Fatigue crack growth curve for all regions.

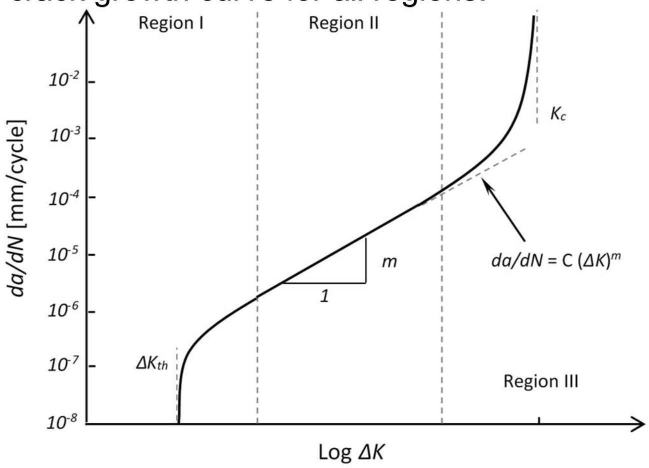

Source: Prepared by the author.

In Table 5.1, some fatigue crack propagation models, under constant amplitude loading, since Paris law (region II) to other models, including I+II, II+III, and I+II+III regions, can be found. Several FCG laws for region II were proposed by Paris[9,10], Walker[11], Frost and Pook[11], Dowling and Begley[11]. FCG laws for I+II regions were also introduced by McEvily[11], Zheng[11], and Correia *et al*.[7]. Laws to describe only regions II and II can also be found – Forman[11] and Wang *et al*.[11]. Besides, in literature can be found several FCG laws to describe the I+II+III regions such as the proposals suggested by Hartman and Schijve[11], Collipriest[11], McEvily[11], Castillo and Canteli[12], and Correia *et al*.[7].

Generally, fatigue crack growth (FCG) models should consider several factors such as geometry, loads, mechanical properties of the material, time, temperature, etc. Usually, these laws are based on theoretical and/or semi-empirical arguments. The experimental FCG measurements are normally made according to the ASTM E647 standard[40], using Compact Tensile (CT) specimens, where the mode I stress intensity factor range, ΔK_I, is given in function of applied load (P) and ratio a/w – see Figure 5.2. In this way, C and m FCG material constants of Paris law (Equation (5.1)) are determined.

Figure 5.2 - Scheme of the CT specimen with load P and function of the a_i/w ratio.

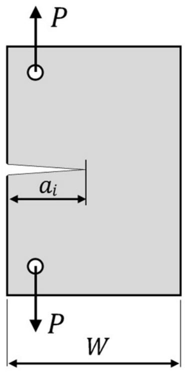

Source: Prepared by the author.

For aluminium alloys according to the BS7910 standard, the threshold stress intensity factor range, ΔK_{th}, can be assumed equal to 21 N/mm$^{3/2}$ (air or other non-aggressive environments up to 20 °C). However, ΔK_{th} can be estimated by experimental measurements according to the ASTM E647 standard[40], or by using the efficient and time-saving procedure as suggested by Murakami; Gotoh[41]. The material fracture toughness (K_C) can be evaluated from one of the following: - measured linear-elastic plane strain fracture toughness, K_{IC}; or, - correlations from the Charpy V-notch impact test data; or, - conversion from J using the Equation (5.5):

$$K_{mat}^2 = \frac{E \cdot J_{mat}}{1 - \nu^2} \tag{5.5}$$

where: K_{mat} is the material toughness measured by stress intensity factor; E is the elastic or Young modulus; J_{mat} is the material toughness measured by J-methods; ν is the Poisson's ratio. For aluminium alloys, according to the BS7910 standard[2], the recommended material constants, C and m, for the on-stage crack growth relationship are the following:

$$m = 3 \tag{5.6}$$

$$C = 5.21 \times 10^{-13} \left(\frac{E_{steel}}{E}\right)^3 \tag{5.7}$$

where, E is the elastic modulus to another material (e.g. aluminium alloys). Similarly, the threshold stress intensity factor range can be determined by

$$\Delta K_{th} = \Delta K_{th,steel} \left(\frac{E}{E_{steel}}\right) \tag{5.8}$$

Additionally, several authors[42,43] have also investigated the mixed-mode fatigue crack propagation behaviour of metallic materials.

Table 5.1 - Fatigue crack growth models.

Model	Regions	Function Form	Equation
Paris *et al*. (1961)	II	$\frac{da}{dN} = C \cdot (\Delta K)^m$	(5.9)
Walker (1970)	II	$\frac{da}{dN} = C_w \cdot \left(\frac{\Delta K}{(1-R)^{1-\gamma_w}}\right)^{m_w} = C_w \cdot (\overline{\Delta K})^{m_w}$	(5.10)
Forman (1972)	II+III	$\frac{da}{dN} = \frac{C_F(\Delta K)^{m_F}}{(1-R)K_c - \Delta K} = \frac{C_F(\Delta K)^{m_F}}{(1-R)(K_c - K_{max})}$	(5.11)
Hartman and Schijve (1970)	I+II+III	$\frac{da}{dN} = \frac{C_{HS}(\Delta K - \Delta K_{th})^{m_{HS}}}{(1-R)K_c - \Delta K}$	(5.12)
Collipriest (1972)	I+II+III	$\frac{da}{dN} = C(K_c\Delta K)^{m/2} EXP\left[\ln\left(\frac{K_c}{\Delta K_0}\right)^{m/2} \tanh^{-1}\left(\frac{\ln\left[\frac{\Delta K^2}{(1-R)K_c\Delta K_0}\right]}{\ln\left[\frac{(1-R)K_c}{\Delta K_0}\right]}\right)\right]$	(5.13)
McEvily (1974)	I+II	$\frac{da}{dN} = \frac{8}{\pi E^2}(\Delta K^2 - \Delta K_{th}^2)$	(5.14)
McEvily (1974)	I+II+III	$\frac{da}{dN} = \frac{4A}{\pi\sigma_y E}(\Delta K^2 - \Delta K_{th}^2)\left(1 + \frac{\Delta K}{K_c - K_{MAX}}\right)$ $\Delta K_{th} = \frac{1.2(\Delta K_{th,0})}{1 + 0.2\left(\frac{(1+R)}{(1-R)}\right)}$	(5.15)
Frost and Pook (1971)	II	For plane stress: $\frac{da}{dN} = \frac{9}{\pi}\left(\frac{\Delta K}{E}\right)^2$ For plane strain: $\frac{da}{dN} = \frac{7}{\pi}\left(\frac{\Delta K}{E}\right)^2$	(5.16)
Zheng (1983)	I+II	$\frac{da}{dN} = \frac{1}{2\pi E\sigma_f\varepsilon_f}(\Delta K - \Delta K_{th})^2$	(5.17)
Wang *et al*. (1994)	II+III	$\frac{da}{dN} = \alpha\frac{K_{max}^4}{\bar{\sigma}_y^2}\left[\frac{1}{1-\xi^2} - \frac{1}{1-(R\xi)^2}\right]\left[\frac{1}{\sqrt{1-\xi^2}} - \frac{1}{\sqrt{1-(R\xi)^2}}\right]^2$ $\xi^2 = \frac{K_{max}^2}{2K_{nf}^2}$; $K_{nf} = \sigma_y\sqrt{\pi a}$	(5.18)
Dowling and	II	$\frac{da}{dN} = C_{DB}\Delta J^{m_{DB}}$	(5.19)

Begley (1976)			
Castillo; Canteli (2014)	I+II+III	$\frac{da^*(N^*)}{dN^*} = exp\left[F^{-1}\left(\frac{log\ \Delta K^* - log\ \Delta K_{th}^*}{log\ \Delta K_{up}^* - log\ \Delta K_{th}^*}\right)\right]$ $a^* = \frac{a}{W}; N^* = \frac{N}{N_0}; \Delta K^* = \frac{K_{max}-K_{min}}{K_c}; \Delta K_{th}^* = \frac{\Delta K_{th}}{K_c}; \Delta K_{up}^* = \frac{\Delta K_{up}}{K_c}$	(5.20)
Correia *et al*. (2016)	I+II	$\frac{da}{dN} = C_C(\Delta J - \Delta J_{th})^{mc}$	(5.21)
Correia *et al*. (2016)	I+II+III	$\frac{da^*(N^*)}{dN^*} = exp\left[F^{-1}\left(\frac{log\ \Delta J^* - log\ \Delta J_{th}^*}{log\ \Delta J_{up}^* - log\ \Delta J_{th}^*}\right)\right]$ $a^* = \frac{a}{W}; N^* = \frac{N}{N_0}; \Delta J^* = \frac{J_{max}-J_{min}}{J_C}; \Delta J_{th}^* = \frac{\Delta J_{th}}{J_C}; \Delta J_{up}^* = \frac{\Delta J_{up}}{J_C}$	(5.22)

Source: Prepared by the author.

5.1.2 Fatigue crack closure models

The crack closure effects under cyclic loading were discovered by Elber[13,14] in 1970. In his studies, Elber[13,14] identified crack closure as a result of creating a plastic zone where the yield strength of the material is exceeded. The surrounding regions of the plastic zone remain elastic. During the crack growth process, that is, loading and unloading cycles, the crack surfaces contact each other, as shown in Figure 5.3. Therefore, Elber[13,14] suggested that the growth of fatigue cracks is not driven by the applied stress intensity factor range, ΔK, but rather by the effective stress intensity factor range, ΔK_{eff} (see Figure 5.3), as follows:

$$\Delta K_{eff} = K_{max} - K_{op} \tag{5.23}$$

where, K_{op} is the crack opening stress intensity factor. Figure 5.3 illustrates the scheme on the definition of the crack closure/opening concept and effective stress intensity factor. In Figure 5.4, a scheme for various crack closure mechanisms presented by Pippan; Hohenwarter[17,44] – oxide induced, roughness induced, and plasticity induced – is shown. The oxide-induced crack closure mechanism is used for the explanation of different phenomena near threshold regime as presented by Pippan; Hohenwarter[17,44]. The concept of the roughness-induced crack closure mechanism is used to explain the microstructural sensitive, load ratio and environmental conditions on near-threshold fatigue crack propagation[45]. The plasticity-induced crack closure mechanism is associated with the development of the plastic zone around the fatigue crack tip of under plane stress and plain strain conditions described by degree of plasticity at the crack tip through the level of material constrain[17,44].

Figure 5.3 - Scheme on the definition of the crack closure/opening concept and effective stress intensity factor.

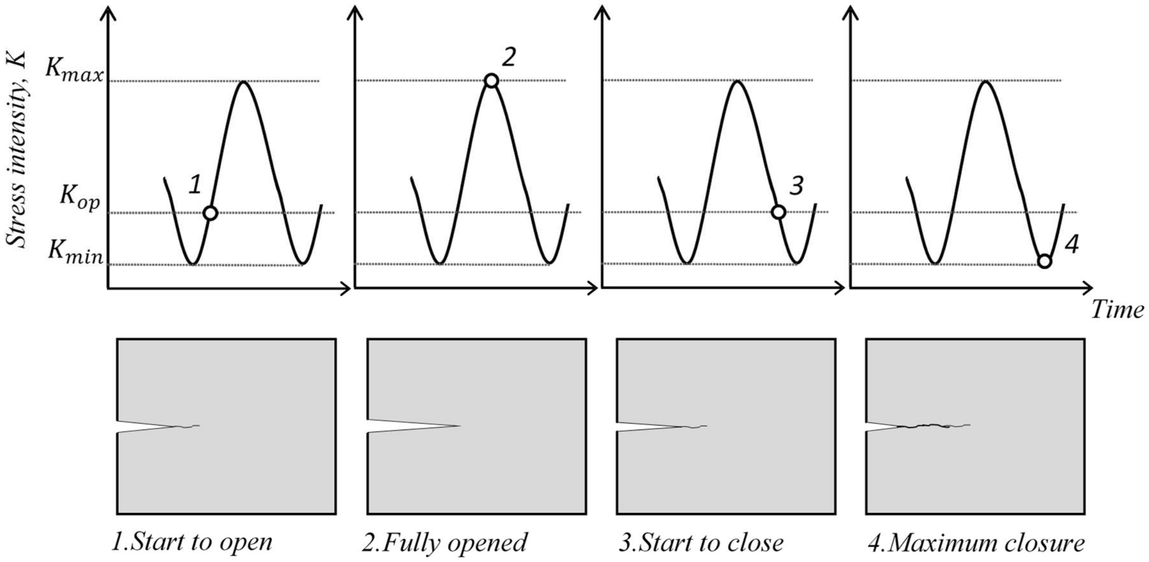

Source: Prepared by the author.

Figure 5.4 - Scheme for various crack closure mechanisms.

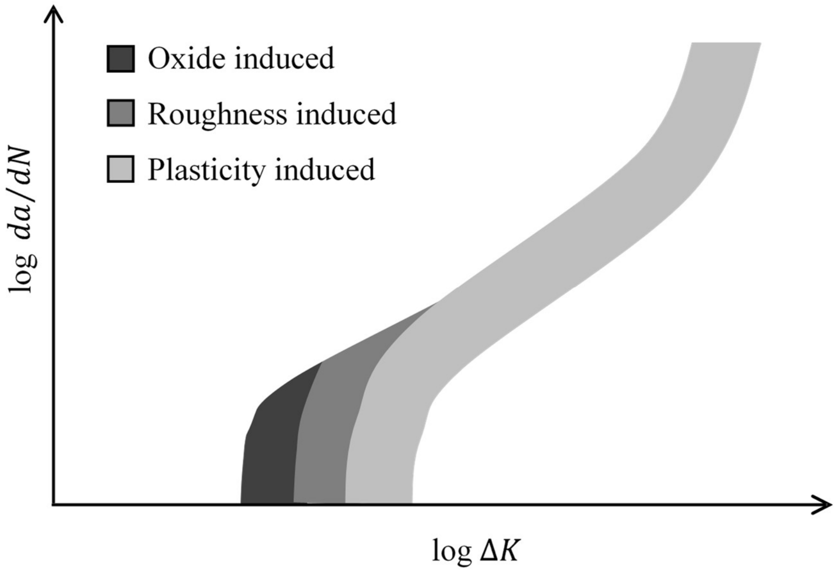

Source: Prepared by the author.

Therefore, a relationship between ΔK_{eff} and ΔK is established to quantify the crack/closure effects and given by the following expression:

$$\mathrm{U} = \frac{\Delta K_{eff}}{\Delta K} = \frac{K_{max} - K_{op}}{K_{max} - K_{min}} \tag{5.24}$$

where U is the quantitative parameter of the crack closure/opening effects. The fatigue crack propagation law can be rewritten as

$$\frac{da}{dN} = f(\Delta K_{eff}) = f(U\Delta K) \quad (5.25)$$

Thus, the crack closure quantitative parameter, U, can be described as a function of the applied stress ratio, R:

$$U = \mathrm{f}(R)$$
$$0 < U \leq 1 \quad (5.26)$$

Several authors have studied the crack closure phenomenon and have suggested several relationships based on linear relations, second- and thirst-degree polynomial functions, non-linear regressions analysis, etc.; using monotonic and cycle properties, microstructures, and localised plasticity, through experimental and analytical studies[46-50] – see Table 5.2.

Elber[13,14] in his studies on the fatigue crack propagation behaviour of the aluminium 2024-T3 proposed a relationship to the crack closure quantitative parameter given by Equation (5.27), where a good agreement with the experimental data under constant amplitude loading was verified. The validation of the relation proposed by Elber[13,14] is for the applied stress ratio range $-0.1 < R < 0.7$ with the stress intensity ranged between $13MPa.m^{1/2}$ and $40MPa.m^{1/2}$.

Linear relations between quantitative parameter, U, and applied stress ratio, R, were also proposed by Katcher and Kaplan[19], Equation (5.28), and Clerivet and Bathias[20], Equation (5.30). These crack closure relations on fatigue crack growth behaviour were also suggested for aluminium alloys. Bachmann and Munz[51] suggested a crack closure model applied to a titanium alloy where the U parameter is a function of stress ratio, R, and maximum stress intensity factor, K_{max} (see Equation (5.29)).

A second-degree polynomial function to describe the crack closure quantitative parameter, U, for 2024-T3 sheet material was proposed by Schijve[21] for the applied stress ratio range $-1 \leq R \leq 1$, given by Equation (5.31).

Srivastava and Garg[52] studied the crack closure effects and crack growth behaviour on 6063-T6 aluminium alloy. In their research work, a relation between U parameter and stress ratio, R, and applied stress intensity factor range, ΔK, was found (see Equation (5.32)).

In 1987, Zhang *et al.*[22] suggested a similar relation to proposed by Schijve[21], Equation (5.33), in his studies on crack propagation of Al 7475 under constant- and variable-amplitude loading. Equation (5.33) is validated for the applied stress ratio $R \geq$

0. Another crack closure model to quantify the parameter U was also proposed by ASTM[40,53] and given by Equations (5.34)-(5.37).

An alternative approach to modelling the crack closure effects was introduced by Newman[23] and later explored by Vormwald[24] and Savaidis[25,26]. The model proposed by Newman (Equations (5.38)-(5.44)) is based on Dugdale's concept or strip-yield model[54]. The fatigue crack growth behaviour of 2024-T3 aluminium alloy specimens for various applied stress ratios under constant amplitude loading was used to validate the model proposed. In his studies, Newman suggested that the flow stress σ_0 to be the average between the monotonic uniaxial yield stress, $\mathrm{R}_{p,0.2}$, and uniaxial ultimate tensile strength, R_m.

Vormwald and Seeger[24] based on Newman's assumptions proposed a fatigue crack closure model using the cyclic yield stress to estimate the flow stress. In the same way, Savaidis[25,26] proposed a model considering the cyclic elastoplastic properties such as the cyclic hardening exponent, n', and the cyclic hardening coefficient, K' (see Equations (5.45)-(5.50)).

Codrington and Kotousov[27] proposed a crack closure model for small-scale yielding conditions where the quantitative parameter U should be calculated using material properties, applied or maximum load, and also the effects of plate thickness, which provides an alternative to empirical correction factors or finite element models describing the stress state effects. A non-linear relation was proposed by Codrington and Kotousov[27], Equations (5.51)-(5.55), where the non-dimensional parameter η is a function of K_{max} (maximum stress intensity) or ΔK (applied stress intensity range), σ_f (flow stress) and plate thickness $(2h)$.

Hudak and Davidson[28] presented a study on the crack closure effects in aluminium alloy 7091 and 304 stainless steel based on both optical and electron microscopy measurements where the crack-tip opening loads were quantified. Thus, Hudak and Davidson's model is given by Equations (5.56)-(5.58). According to the studies of these authors[28], the models based on Newman's proposal need to be reformulated by underestimating the crack closure effects and they suggested that other closure mechanisms are operative in addition to plasticity-induced closure.

Ellyin[29] presented an approach based on Hudak and Davidson's studies to calculate the effective stress intensity range, ΔK_{eff}, as a function of the applied stress ratio, R, and the threshold value of the stress intensity factor range, ΔK_{th}, for constant amplitude loading. Important assumptions were suggested by Ellyin[29], where $\Delta K_{op} < \Delta K_{th}$ and $\Delta K_{cl} < \Delta K_{op} < \Delta K_{th}$. Ellyin[29] proposed the Equations (5.59) and (5.60) to estimate the effective stress intensity factor range, ΔK_{eff}, respectively, $R \approx 0$ and $R \neq 0$.

More recently, Correia[30] proposed a crack closure/opening model based on the assumptions of the Hudak and Davidson's model[28] and Ellyin approach[29], using Walker's propagation law[55] to take into account the effects of the applied stress ratio, R, and the Klesnil and Lukáš model[56] to describe the relationship between the threshold stress intensity factor range, ΔK_{th}, and applied stress R-ratio, R. Also Dowling in his studies[57] on the effect of applied stress R-ratio on the threshold stress intensity factor range (ΔK_{th}) suggested the model proposed by Klesnil and Lukáš model[56] to be incorporated into Walker's propagation law[55]. The Correia's crack closure model is given by Equations (5.61) and (5.62), where the crack closure quantitative parameter is a function of the threshold stress intensity range for $R = 0$ ($\Delta K_{th,0}$), material parameter γ, maximum stress intensity factor K_{max} (or ΔK), applied stress ratio, R, and a limit stress intensity factor (no crack closure).

Recently, a physics-based energy method connects physical opening stress to ΔK_{eff} agreeing well with existing closure corrections was suggested by van Kuijk et al.[58] (see Equations (5.63) and (5.64)). These authors demonstrated, by observation from the finite element analysis (FEA), the R dependency of the effective stress intensity factor ratio as follows:

$$U_{SIF} = \frac{\Delta K_{eff}}{\Delta K} \tag{5.65}$$

More detailed work on U_{SIF}, for steel and aluminum, was compiled by Maljaars et al.[59], where $U_{SIF} = 1$ near $R = 1$ is correctly predicted by FEA[58], showing R values for which the crack is permanently open. In Equations (5.63) and (5.64), $S_{op_{phen}}$ is the opening stress used in ΔK_{eff}, and S_{max} is the maximum stress.

Several works have been published where various phenomena have been studied, such as the corrosion-fatigue mechanism [60,61,62], the quantitative dependence of the oxide-induced crack closure [63], among others. Wu et al. [64] presented a study on the residual life assessment of steel railway axles through an integrated stress rebuilding strategy of unit pressure and proportional integral approach. An overview on safe life and damage tolerance methods applied to railway axles was discussed by

Zerbst et al.[65]. Hu et al. [66] proposed a study on the fatigue resistance and remaining life assessment of induction-hardened S38C railway axles to serve as a basic reference for the optimization and extension of the inspection intervals for these railway axles. Forman; Mettu[67] studied the behaviour of surface and corner cracks to failure under monotonic and fatigue loading, where this work was conducted experimentally and analytically. These authors compared those results with numerical predictions using the NASA/FLAGRO computer program. Wu et al.[68] suggested a fatigue crack growth model based on the uniaxial tensile behaviour by correlating the uniaxial tensile properties with cyclic plastic parameters and developing a unified fatigue crack closure factor suitable for broad stress ratios. These authors[68] formulated a novel FCG model of improved LAPS (iLAPS) in terms of linear damage accumulation and Rice-Kujawski-Ellyin field. In addition, Wu et al.[69] proposed an improved long and physically short (LAPS) crack model, formulated from low cycle fatigue properties and the Rice-Kujawski-Ellyin asymptotic field, with proper crack opening functions for closure effects.

So, this paper presents a comparative study of several crack closure models on the fatigue crack propagation behaviour of aluminium alloy 6061-T651[31-34], where the relationship between crack closure quantitative parameter, U, and applied stress ratio, R, as well as effective stress ratio, R_{eff}, and applied stress ratio, R, for various crack closure models under consideration are generated. A comparison between these crack closure models and the experimental/deterministic results is made. The error index modulus obtained for each crack closure model under consideration was compared with the experimental/deterministic crack closure data.

Table 5.2 - Crack closure/opening models.

Model	Function Form	Validity	Eq.
Elber[13,14]	$U = 0.5 + 0.4\mathrm{R}$	$-0.1 < R < 0.7$	(5.27)
Katcher and Kaplan[19]	$U = 0.68 + 0.91R$	$0.08 \leq R \leq 0.32$	(5.28)
Bachmann and Munz[51]	$U = \frac{1}{1-R}\left(1 - \frac{6.67R - 4.27}{K_{max}}\right)$	$0.05 \leq R \leq 0.2$	(5.29)
Clerivet and Bathias[20]	$U = 0.4 + 0.4R$	-	(5.30)
Schijve[21]	$U = 0.55 + 0.33R + 0.12R^2$	$-1 \leq R \leq 1$	(5.31)
Srivastava and Garg[52]	$U = \left(\frac{13.5R + 5.925}{1000}\right)\Delta K + 1.35R + 0.223$	$0 \leq R \leq 0.3$	(5.32)
Zhang *et al.*[22]	$U = 0.618 + 0.365R + 0.139R^2$	$R \geq 0$	(5.33)

ASTM[40;49]	$\Delta K = K_{max}$	$R < 0$	(5.34)
	$\Delta K = K_{max} - K_{min}$	$R \geq 0$	(5.35)
	$U = 0.576 + 0.015R + 0.409R^2$		(5.36)
	$\frac{K_{op}}{K_{max}} = 0.424 + 0.561R - 0.394R^2 + 0.409R^3$		(5.37)
Newman[23]	$\frac{\sigma_{op}}{\sigma_{max}} = A_0 + A_1R + A_2R^2 + A_3R^3$	$R \geq 0$	(5.38)
	$\frac{\sigma_{op}}{\sigma_{max}} = A_0 + A_1R$	$-1 \leq \mathrm{R} < 0$	(5.39)
	when $\sigma_{op} \geq \sigma_{max}$, the four non dimensional constants A_0, A_1, A_2, A_3 are as follows:		
	$A_0 = (0.825 - 0.34\alpha + 0.05\alpha^2)\left[\cos\left(\frac{\pi\sigma_{max}}{2\sigma_0}\right)\right]^{1/\alpha}$		(5.40)
	$A_1 = (0.415 - 0.071\alpha)\frac{\sigma_{max}}{\sigma_0}$		(5.41)
	$A_2 = 1 - A_0 - A_1 - A_3$		(5.42)
	$A_3 = 2A_0 + A_1 - 1$		(5.43)
	and $\sigma_o = \frac{\mathrm{R}_{p,0.2} + R_m}{2}$		(5.44)
	$\alpha = 1$ for plane stress		
	$\alpha = 3$ for plane strain		
Savaidis *et al.*[24-26]	$\frac{\sigma_{op}}{\sigma_{max}} = A_0 + A_1R + A_2R^2 + A_3R^3$	$R \geq 0$	(5.45)
	$\frac{\sigma_{op}}{\sigma_{max}} = A_0 + A_1R$	$-1 \leq \mathrm{R} < 0$	(5.46)
	With $A_0 = 0.535.\cos\left[\frac{\pi}{2}.\frac{\sigma_{\max(x)}}{0.002^{n'}.K'}\right]$		(5.47)
	$A_1 = 0.344.\frac{\sigma_{\max(x)}}{0.002^{n'}.K'}$		(5.48)
	$A_2 = 1 - A_0 - A_1 - A_3$		(5.49)
	$A_3 = 2A_0 + A_1 - 1$		(5.50)
Codrington and Kotousov[27]	$U(R,\eta) = A(\eta) + B(\eta)R + C(\eta)R^2$	-	(5.51)
	with $A(\eta) = 0.446 + 0.266.e^{-0.41\eta}$		(5.52)
	$B(\eta) = 0.373 + 0.354.e^{-0.235\eta}$		(5.53)
	$C(\eta) = 0.2 - 0.667.e^{-0.515\eta}$		(5.54)
	where the non-dimensional parameter η $\eta = \frac{K_{max}}{\sigma_f\sqrt{h}} = \frac{\Delta K}{(1-R)\sigma_f\sqrt{h}}$		(5.55)
Hudak and Davidson[28]	$U = \gamma\left(1 - \frac{K_o}{K_{max}}\right)$	$K_{max} \leq K_L$	(5.56)
		$K_{max} \geq K_L$	(5.57)

	$U = 1$ Where $\gamma = \left(1 - \frac{K_o}{K_L}\right)$		(5.58)
Ellyin[29]	$\Delta K_{eff,0} = (\Delta K^2 - \Delta K_{th}^2)^{1/2}$ $\Delta K_{eff,0} \approx \Delta K \left[1 - \frac{1}{2}\left(\frac{\Delta K_{th}}{\Delta K}\right)^2\right] > \Delta K - \Delta K_{th}$	$R \approx 0$	(5.59)
	$\Delta K_{eff,0} \approx \Delta K \left[1 - \frac{1}{2}\left(\frac{\Delta K_{th}}{\Delta K}\right)^2\right] > \Delta K - \Delta K_{th}$	$R \neq 0$	(5.60)
Correia[30]	$U = \left(1 - \frac{\Delta K_{th,0}}{K_{max}}\right)(1 - R)^{\gamma - 1}$	$K_{max} \leq K_L$	(5.61)
	$U = 1$	$K_{max} \geq K_L$	(5.62)
van Kuijk et al.[58]	$\left.\frac{S_{op_{phen}}}{S_{max}}\right\|_{elastic} = \frac{1}{2} + \frac{1}{2}R^2$	$R \geq 0$	(5.63)
	$\left.\frac{S_{op_{phen}}}{S_{max}}\right\|_{elastic} = \frac{1}{2}$	$R < 0$	(5.64)

Source: Prepared by the author.

5.2 EXPERIMENTAL FATIGUE DATA OF AA 6061-T651

The 6061 T651 aluminium alloy is often used in automotive and marine frames due to its high strength coupled with corrosion resistance and weldability (spot welding process is commonly used for joining sheets of this aluminium alloy). The mechanical properties of the aluminium alloy under consideration were collected from literature[34]. The fatigue behaviour of the AA 6061 T651 was evaluated by Ribeiro[70] and collected by Correia *et al.*[31]. The experimental tests to characterising the cyclic elastoplastic behaviour were performed according to the ASTM E606[26]. The fatigue crack growth (FCG) data using CT and SENB specimens were determined by applying the ASTM E647 standard procedures[40]. The FCG results were collected from Correia *et al.*[31] and Henkel[32].

5.2.1 Cyclic elastoplastic behaviour

The fatigue tests of smooth and polished cylindrical specimens, with 8 mm of diameter, were carried out under strain-controlled conditions (strain ratio, R_ε, equal to –1) according to the ASTM E606 standard[71].

The Ramberg and Osgood description[72] was used by Ribeiro[31,70] to determine the cyclic elastoplastic behaviour to the stabilised cyclic stress-strain data from the experimental low-cycle fatigue tests. The cyclic elastoplastic behaviour is the following:

$$\frac{\Delta\varepsilon}{2} = \frac{\Delta\varepsilon^E}{2} + \frac{\Delta\varepsilon^P}{2} = \frac{\Delta\sigma}{2E} + \left(\frac{\Delta\sigma}{2K'}\right)^{1/n\prime} \tag{5.66}$$

where, $\Delta\varepsilon$ is the total strain range, $\Delta\varepsilon^E$ is the elastic strain range, $\Delta\varepsilon^P$ is the plastic strain range, $\Delta\sigma$ is the stress range, E is the Young modulus, K' and n' are the cyclic strain hardening coefficient and exponent.

The strain-life curve proposed by Morrow[73], combining the equations suggested by Manson[74] and Coffin[75], can be used to describe the low- and high-cycle fatigue regimes. This equation is given by:

$$\frac{\Delta\varepsilon}{2} = \frac{\Delta\varepsilon^E}{2} + \frac{\Delta\varepsilon^P}{2} = \frac{\sigma_f'}{E}\left(2N_f\right)^b + \varepsilon_f'\left(2N_f\right)^c \tag{5.67}$$

where, ε_f' is the fatigue ductility coefficient, c is the fatigue ductility exponent, σ_f' is the fatigue strength coefficient, *b* is the fatigue strength exponent, N_f is the number of cycles to failure.

The mechanical properties[34], cyclic elastoplastic and strain-life parameters of the 6061-T651 aluminium alloy[31] are summarized in Table 5.3.

Table 5.3 - Mechanical properties, cyclic elastoplastic and strain-life parameters of the 6061-T651 aluminum alloy[31,34].

$R_{p,0.2}$ [MPa]	R_m [MPa]	E [GPa]	K' [MPa]	n' [-]	σ'_f [MPa]	b [-]	ε'_f [-]	c [-]
289.90	328.50	68.0	393.4	0.0567	394.0	-0.0453	0.8680	-0.7745

Source: Prepared by the author.

5.2.2 Fatigue crack growth behaviour

The fatigue crack growth (FCG) tests were performed by Ribeiro[31,70] using CT specimens, with nominal thickness, $B = 10$mm, and width, $W = 40$mm, according to the specifications of the ASTM E647 standard[40]. The FCG tests were conducted under load-controlled conditions, for the stress ratios, R, equal to 0.1 and 0.5. Correia in his work[31] commented that the fatigue crack growth behaviour is influenced by the stress ratio, R, as shown in Figure 5.5. The same was identified by Henkel[32] in fatigue crack propagation tests for the same aluminium alloy, using SENB specimens with the geometry of 10 x 20 x 100 mm^3. The FCG tests were performed for several stress ratios, R, of 0.1, 0.3, and 0.5, under constant amplitude loading. The FCG tests were also conducted according to the ASTM E647 standard. The crack length was measured by the elastic compliance method as referred by Henkel[32]. In Figures 5.5 and 5.6 are presented the FCG data and da/dN vs. ΔK curves based on Paris law for the AA 6061-T651. The fatigue crack propagation curves were fitted to the experimental data by relation proposed by Paris and given by

$$\frac{da}{dN} = C \cdot \Delta K^m \tag{5.68}$$

where, da/dN is the fatigue crack propagation rate, ΔK is the applied stress intensity factor range, C and m are the material constants. The material constants were obtained for the FCG data collected from Correia *et al.*[31] and Henkel *et al.*[32] for each stress ratio, R, are summarized in Table 5.4. The threshold value of the stress intensity factor range, $\Delta K_{th,0}$, was assumed to be equal to 128.96 N.mm$^{-1.5}$, according to Correia *et al.*[31].

Table 5.4 - Material constants concerning the Paris law of the 6061-T651 aluminum alloy.

R	f Hz	a_0 mm	F_{max} N	F_{min} N	C^*	m	ΔK_{max} N.mm$^{-1.5}$	R^2
0.1[(a)]	15	10	3676.8	367.6	8.282E-16	4.334	779.18	0.981
0.3[(b)]	65-77	4	3346.2	1003.9	2.674E-15	4.276	477.50	0.972
0.5[(a)]	15	10	8372.7	4186.3	2.050E-14	3.957	571.89	0.991

* da/dN in mm/cycle and ΔK in N.mm$^{-1.5}$; a – CT specimen; b – SENB specimen.

Source: Prepared by the author.

Figure 5.5 - FCG data of AA 6061-T651 collected from Correia et al.[31] and Henkel et al.[32]

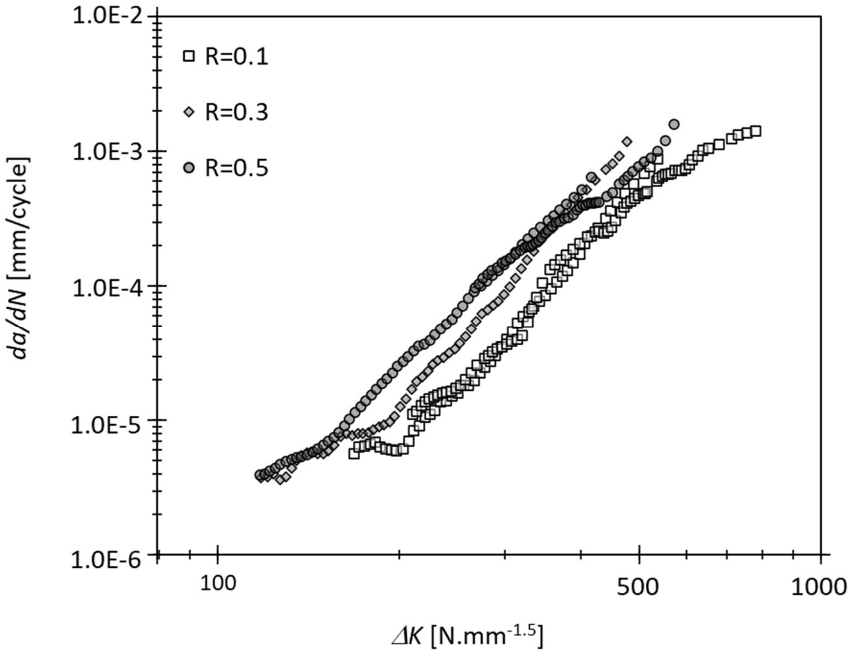

Source: Prepared by the author.

Figure 5.6 - da/dN vs. ΔK curves based on Paris law for the AA 6061-T651[31,32].

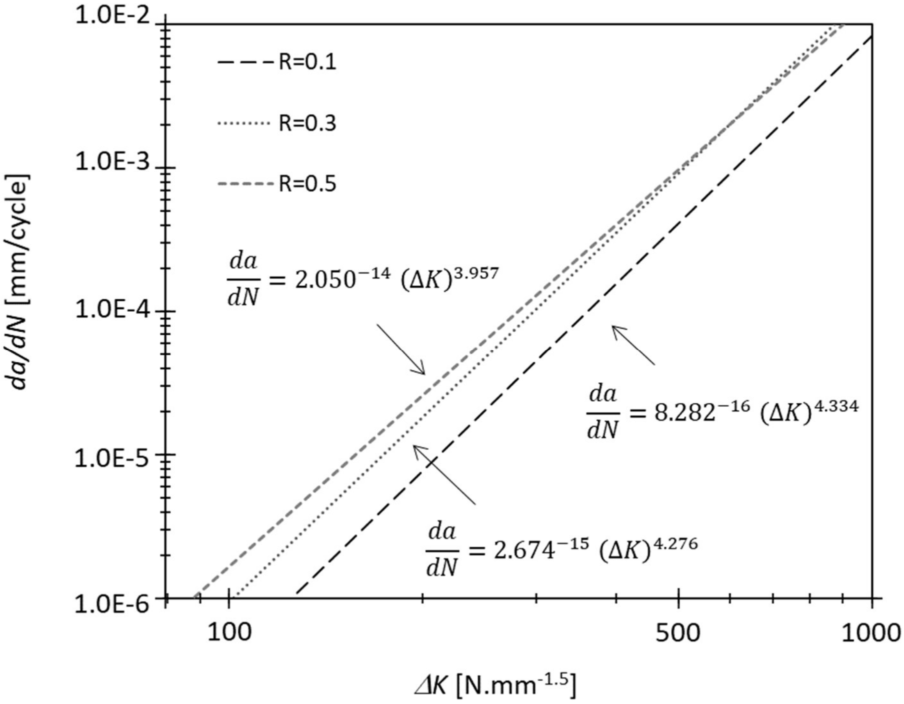

Source: Prepared by the author.

5.3 APPLICATION AND DISCUSSION

In this section, the fatigue crack propagation rates (da/dN) versus effective stress factor range (ΔK_{eff}) data based on various crack closure models were estimated. In this study, the crack closure models – Elber[13,14], Katcher and Kaplan[19], Clerivet and Bathias[20], Schijve[21], Zhang[22], Newman[23], Savaidis[25,26], Codrington-Kotousov[27], and Correia[30] – were applied. Additionally, da/dN vs. ΔK_{eff} curves based on Paris law were evaluated. The relation between effective stress ratio, R_{eff}, and applied stress ratio, R, for several crack closure models under consideration was also presented and a comparison with the experimental results collected in literature[31-34] was done. Therefore, a comparative study on the evaluation of the crack opening/closure effects on fatigue crack propagation of the 6061-T651 aluminium alloy is presented.

5.3.1 da/dN vs. ΔK_{eff} curves based on various crack closure models

In this section, da/dN vs. ΔK_{eff} curves for AA 6061 T651 based on various crack closure models such as Elber[13,14], Katcher and Kaplan[19], Clerivet and Bathias[20], Schijve[21], Zhang[22], Newman[23], Savaidis[25,26], Codrington-Kotousov[27], and Correia[30] were estimated. In this study, the fatigue crack growth data for the stress R-ratios, of 0.1, 0.3, and 0.5, were collected from Correia *et al.*[31] and Henkel *et al.*[32]. The experimental results of the quantitative parameter, U, for each stress ratio, R, of 0, 0.2, and 0.5, were estimated by Lal *et al.*[33]. In Lal's experimental work, the crack opening/closure observations were conducted by an eddy current probe in close proximity to the crack tip. These estimations were done for the 6061 T6 aluminium alloy (Table 5.5). For the estimation of U parameters for each stress R-ratio, 0.1, 0.3, and 0.5, second-degree polynomial functions were adjusted to the experimental data available for the 1st cycle (U_1) and stabilised (U_s) measurements, and, respectively, given by

$$U_{d,1} = 0.566667 \cdot R^2 + 0.336667 \cdot R + 0.69$$
$$0 \leq R \leq 0.5 \tag{5.69}$$
$$R^2 = 1$$
$$U_{d,s} = -0.933333 \cdot R^2 + 0.786667 \cdot R + 0.84 \tag{5.70}$$
$$0 \leq R \leq 0.5$$
$$R^2 = 1$$

Table 5.5 - Experimental results of R *versus* U for the 1st cycle and stabilised measurements[33].

$\boldsymbol{R}$	$\boldsymbol{U}$	
-	1st cycle	Stabilised
0.0	0.69	0.84
0.2	0.78	0.96
0.5	~1	~1

Source: Prepared by the author.

A comparison between the experimental and deterministic data of the relationship U versus R for the 1st cycle and stabilised measurements can be seen in Figures 5.8, respectively. Based on Figures 5.7 and 5.8, a good agreement can be verified between the experimental and deterministic data for the 1st cycle (U_1) and stabilised (U_s) measurements, respectively.

Figure 5.7 - Relationship between quantitative parameter, U, and applied stress ratio, R: experimental data (U_1) and deterministic curve ($U_{d,1}$) for the 1st cycle measurements.

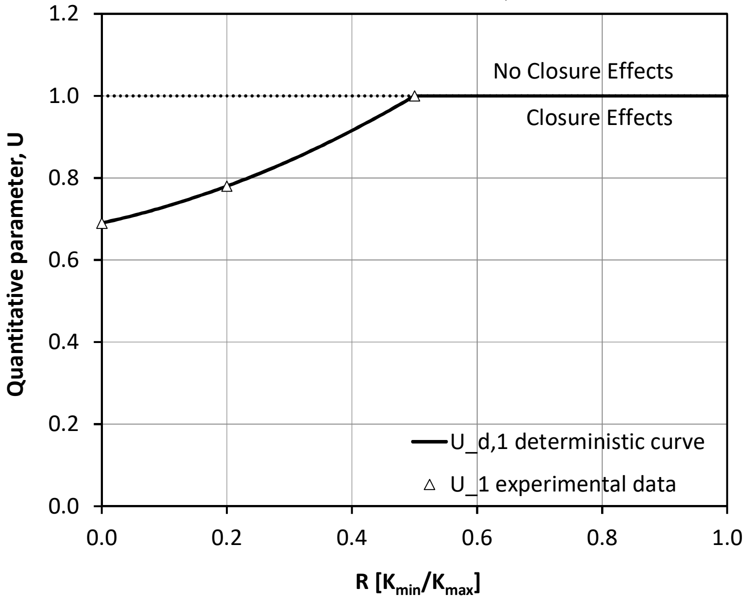

Source: Prepared by the author.

Figure 5.8 - Relationship between quantitative parameter, U, and applied stress ratio, R : experimental data (U_s) and deterministic curve ($U_{d,s}$) for the stabilised measurements.

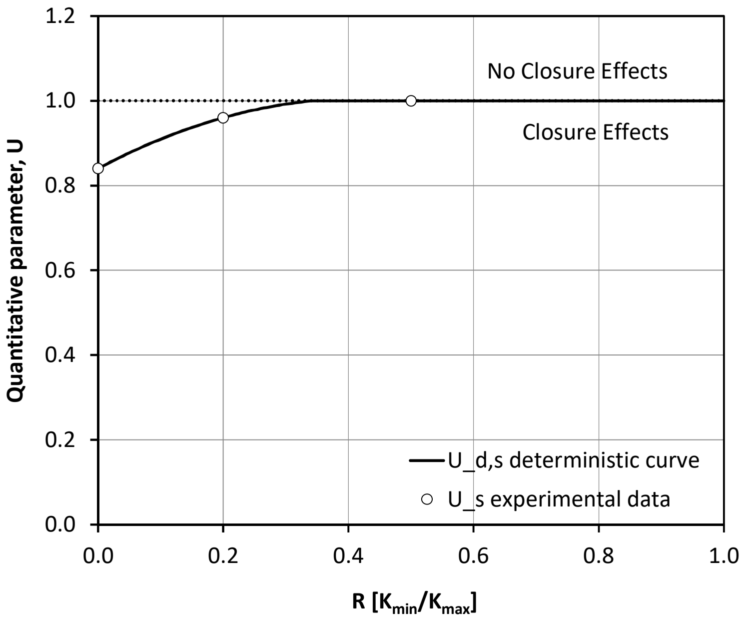

Source: Prepared by the author.

In Figure 5.9, da/dN vs. ΔK_{eff} data based on experimental measurements, estimated by Lal *et al.*[33], are shown. According to Figure 5.9, the experimental measurements of crack closure effects may have been made with some inaccuracy, since the experimental da/dN vs. ΔK_{eff} data present a reasonable performance. The fatigue crack propagation curve considering the crack closure effects was estimated based on the second-degree polynomial function ($U_{d,s}$), Equation (5.70), adjusted to the experimental data available for the stabilised (U_s) measurements. The material constants, C and m, concerning the Paris law are included in the figure. The determination coefficient, R^2, for the experimental da/dN vs. ΔK_{eff} data is presented in Table 5.6.

Figure 5.9 - da/dN vs. ΔK_{eff} data based on experimental measurements.

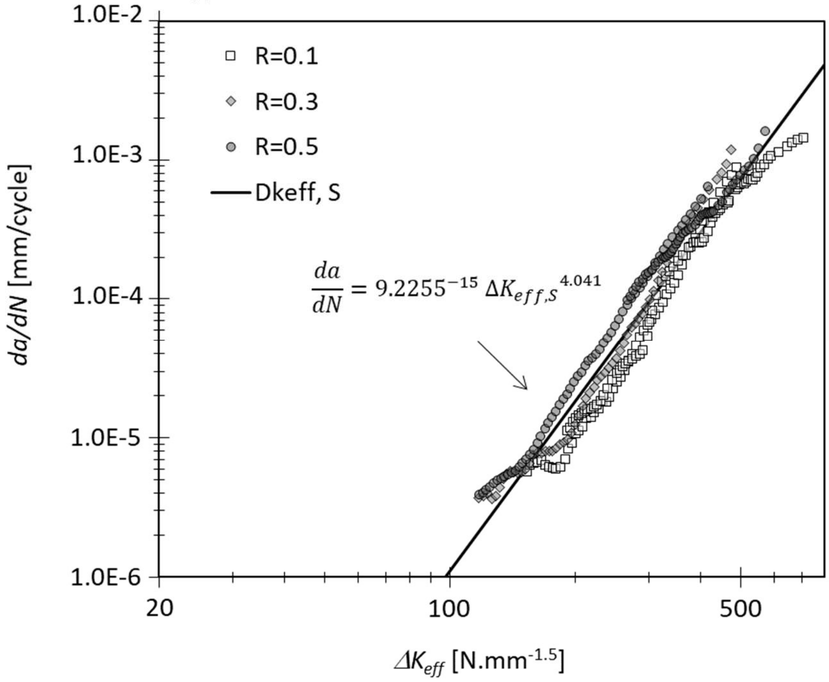

Source: Prepared by the author.

In Figures 5.10 to 5.18, da/dN vs. ΔK_{eff} data generated based on various crack closure models such as Elber[13,14], Katcher and Kaplan[19], Clerivet and Bathias[20], Schijve[21], Zhang[22], Newman[23], Savaidis[25,26], Codrington-Kotousov[27], and Correia[30] are presented, respectively. The fatigue crack closure models proposed by Elber[13,14], Katcher and Kaplan[19], Clerivet and Bathias[20], Schijve[21], Zhang[22] are given by polynomial functions between quantitative parameter, U, and applied stress ratio, R, and can be found in Section 5.1.2 (Table 5.2). The models proposed by Newman[23], and Savaidis[25,26] are based on polynomial functions where the non-dimensional constants are estimated using monotonic and cyclic properties, respectively, where the variables and non-dimensional constants are presented in Tables 5.7 and 5.8. In the same way, Codrington-Kotousov's model[27] is based on the non-dimensional parameter η that is a function of K_{max} (maximum stress intensity) or ΔK (applied stress intensity range), with σ_f (flow stress) and plate thickness $(2h)$. The variables in the last model are presented in Table 5.9. To apply Correia's model30, Equations (5.61) and (5.62), the variables γ and $\Delta K_{th,0}$ presented in Table 5.10, obtained experimentally for AA 6061, were used. In this last model, the quantitative parameters U for various stress R-ratios are estimated using the maximum values of K_{max} or ΔK of the Paris region for which the parameters U are stabilised. Equations (5.71) and (5.72) were obtained by the application of Correia's model.

$$R = \{0.1;\ 0.3\} \qquad U = \left(1 - \frac{128.96}{K_{max}}\right)(1-R)^{-0.4333} \qquad for\ K_{max} \leq K_L \tag{5.71}$$

$$R = 0.5 \qquad U = 1 \qquad for\ K_{max} > K_L \tag{5.72}$$

Table 5.6 - Material constants concerning the Paris law of the 6061-T651 aluminum alloy.

Model	$\boldsymbol{C^*}$	$\boldsymbol{m}$	$\Delta\boldsymbol{K_{eff,min}}$ N.mm$^{-1.5}$	$\Delta\boldsymbol{K_{eff,max}}$ N.mm$^{-1.5}$	$\boldsymbol{R^2}$
Elber	4.029E-14	4.108	73.13	420.76	9.79E-01
Katcher and Kaplan	5.557E-15	4.189	112.41	600.75	9.82E-01
Clerivet and Bathias	8.998E-14	4.095	61.34	343.13	9.76E-01
Schijve	3.213E-14	4.097	77.83	455.20	9.78E-01
Zhang	2.011E-14	4.096	87.29	511.06	9.78E-01
Newman	8.234E-15	4.113	108.0	634.05	9.76E-01
Savaidis	2.689E-14	4.107	80.76	465.94	9.79E-01
Codrington-Kotousov	8.503E-15	4.133	104.66	604.30	9.78E-01
Correia	1.119E-14	4.021	111.51	693.85	9.58E-01
Experimental data	9.226E-15	4.041	117.01	708.54	9.54E-01

* $\boldsymbol{da/dN}$ in mm/cycle and $\Delta\boldsymbol{K}$ in N.mm$^{-1.5}$

Source: Prepared by the author.

Table 5.7 - Variables and non-dimensional constants of Newman's model.

α [-]	f_y [MPa]	f_u [MPa]	σ_0 [MPa]	σ_{max} [MPa]	σ_{max}/σ_0 [-]	A_0 [-]	A_1 [-]	A_2 [-]	A_3 [-]
3.00	289.90	328.50	309.20	103.07	0.33	0.25018	0.06733	1.11479	-0.43230

Source: Prepared by the author.

Table 5.8 - Variables and non-dimensional constants of Savaidis's model.

f_y [MPa]	f_u [MPa]	σ_0 [MPa]	σ_{max} [MPa]	K' [MPa]	n' [-]	A_0 [-]	A_1 [-]	A_2 [-]	A_3 [-]
289.90	328.50	309.20	103.07	393.4	0.0567	0.44592	0.12820	0.40583	0.02005

Source: Prepared by the author.

Table 5.9 - Variables and non-dimensional constants of Codrington-Kotousov's model.

$2h$ [mm]	f_y [MPa]	f_u [MPa]	σ_f [MPa]
10	289.90	328.50	309.20

Source: Prepared by the author.

Table 5.10 - Variables of Correia's model.

γ	$\Delta K_{th,0}$ [N.mm$^{-1.5}$]	$(K_{max})_{max,R=0.1}$ [N.mm$^{-1.5}$]	$(K_{max})_{max,R=0.3}$ [N.mm$^{-1.5}$]	$(K_{max})_{max,R=0.5}$ [N.mm$^{-1.5}$]	$(K_L)_{R=0.1}$ [N.mm$^{-1.5}$]	$(K_L)_{R=0.3}$ [N.mm$^{-1.5}$]	$(K_L)_{R=0.5}$ [N.mm$^{-1.5}$]
0.5667	128.96	865.76	682.15	1143.78	2914.22	906.75	500.38

Source: Prepared by the author.

In Figures 5.10-18 and Table 5.6, the material constants concerning the Paris law of the 6061-T651 aluminium alloy based on the deterministic data and crack closure models under consideration are also summarised. The estimated determination coefficients, R^2, for the $da/dN - \Delta K_{eff}$ data obtained from the application of the crack closure models under consideration are also shown in Table 5.6. All of them present good results in terms of determination coefficient, R^2.

Figure 5.10 - da/dN vs. ΔK_{eff} data using Elber's crack closure model.

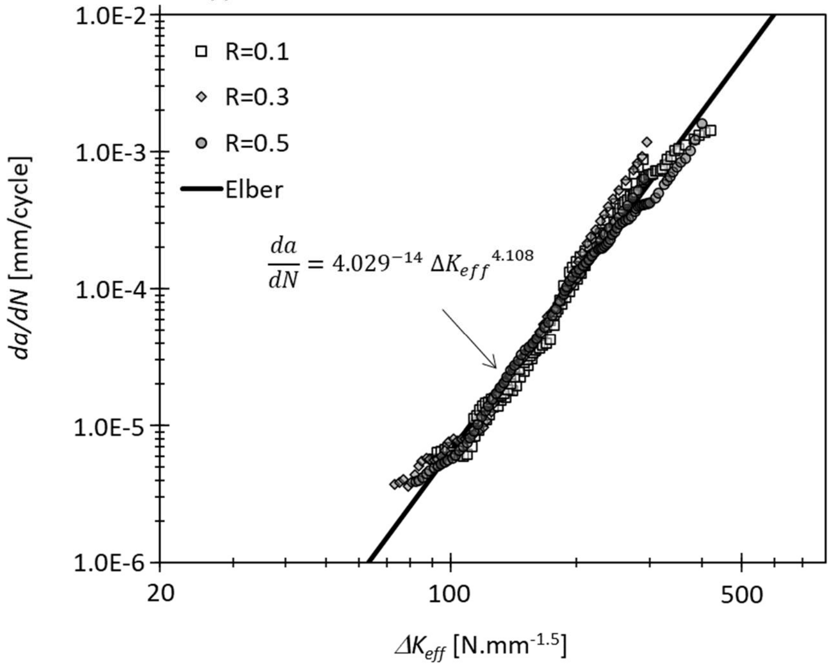

Source: Prepared by the author.

Figure 5.11 - da/dN vs. ΔK_{eff} data using Katcher and Kaplan's crack closure model.

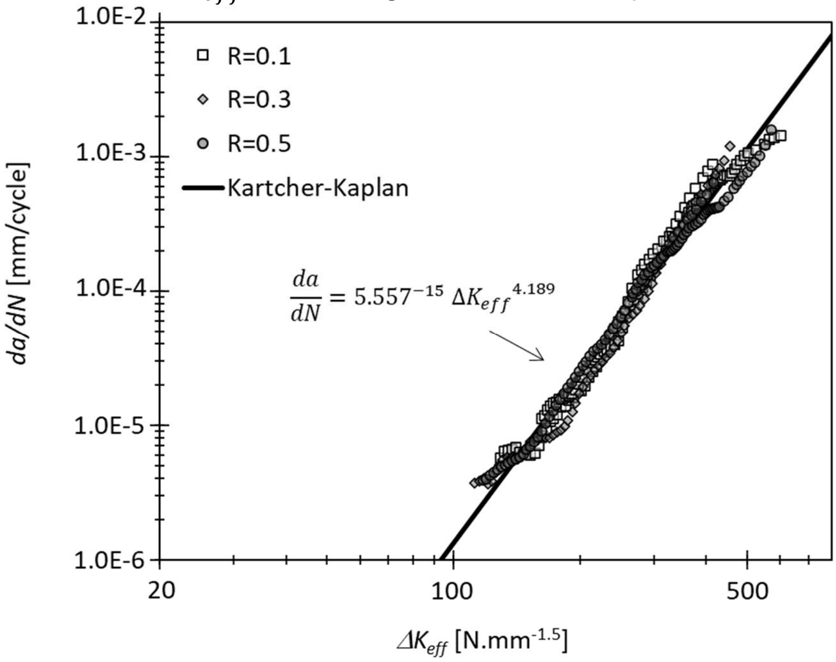

Source: Prepared by the author.

Figure 5.12 - da/dN vs. ΔK_{eff} data using Clerivet and Bathias's crack closure model.

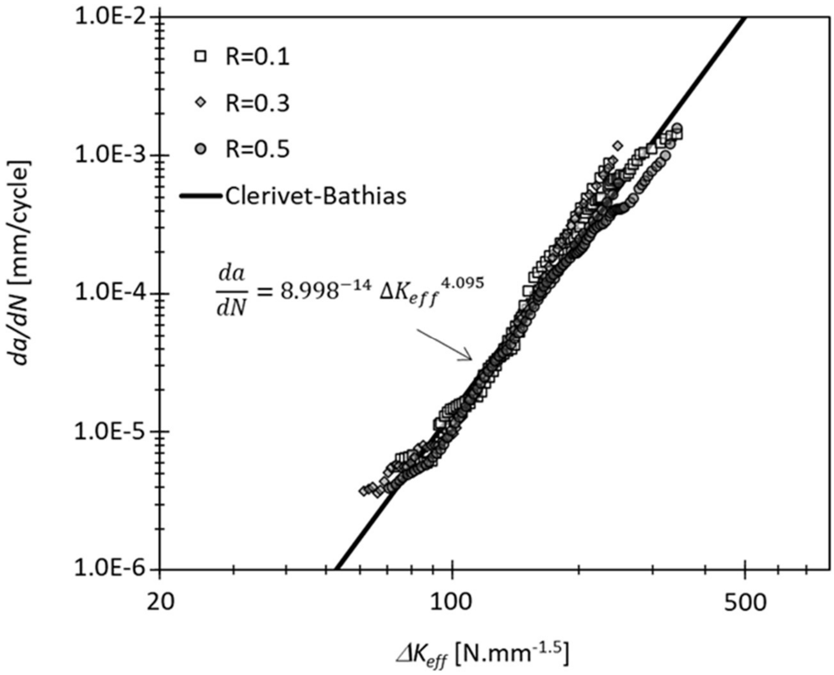

Source: Prepared by the author.

Figure 5.13 - da/dN vs. ΔK_{eff} data using Schijve's crack closure model.

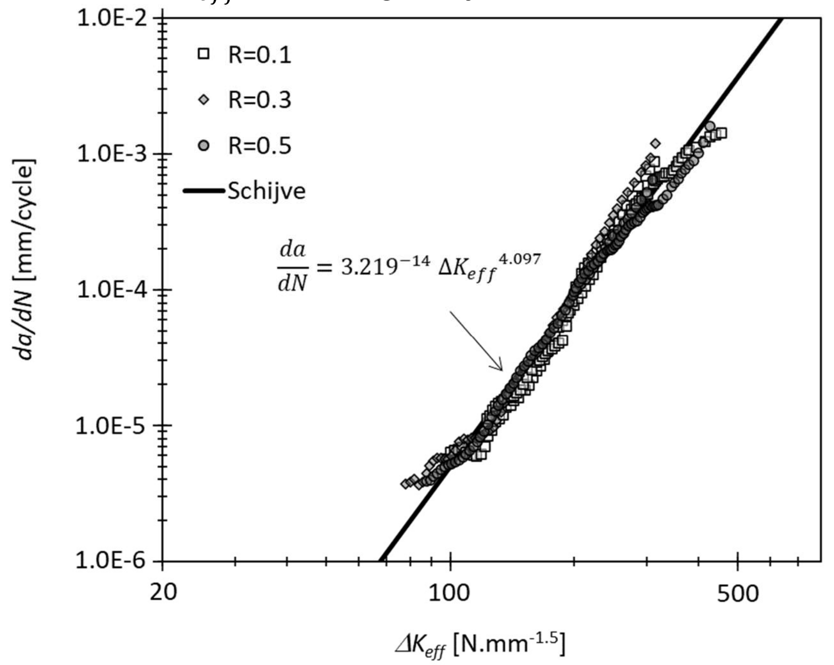

Source: Prepared by the author.

Figure 5.14 - da/dN vs. ΔK_{eff} data using Zhang's crack closure model.

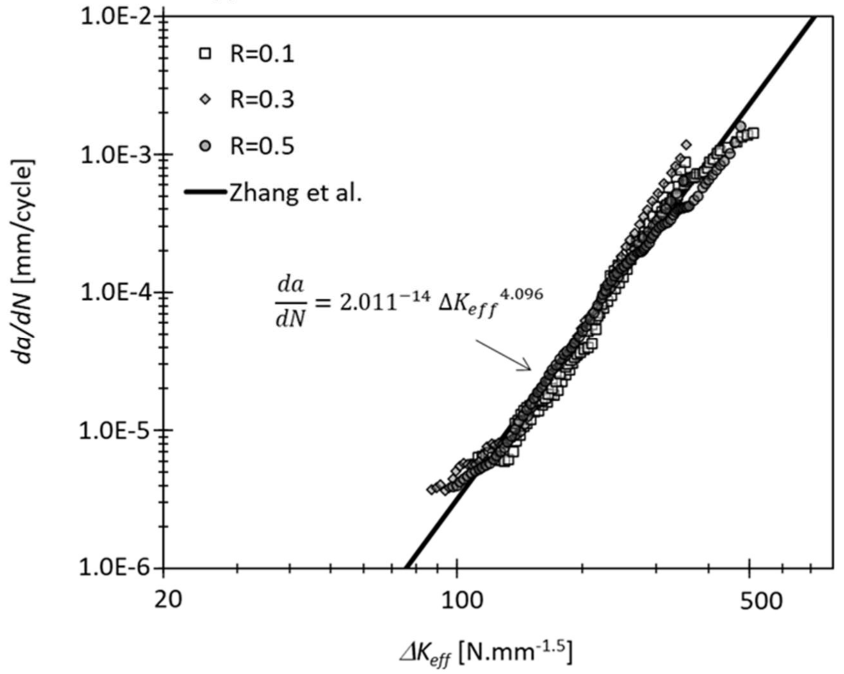

Source: Prepared by the author.

Figure 5.15 - da/dN vs. ΔK_{eff} data using Newman´s crack closure model.

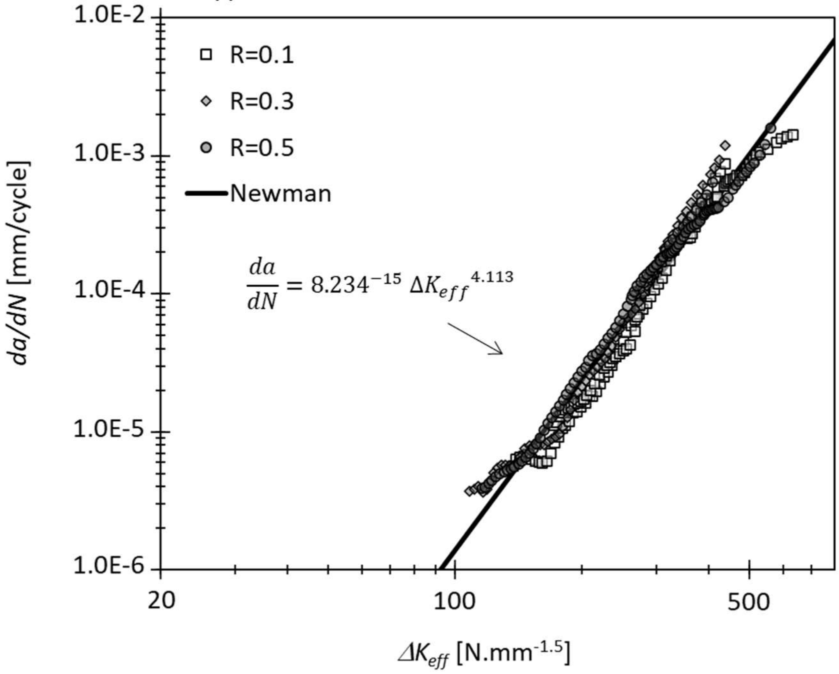

Source: Prepared by the author.

Figure 5.16 - da/dN vs. ΔK_{eff} data using Savaidis´s crack closure model.

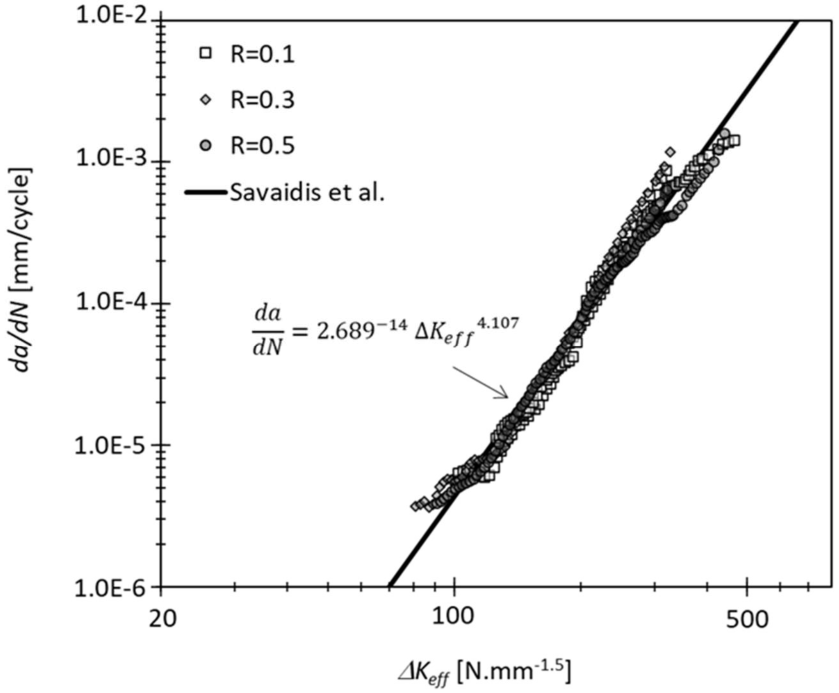

Source: Prepared by the author.

Figure 5.17 - da/dN vs. ΔK_{eff} data using Codrington-Kotousov´s crack closure model.

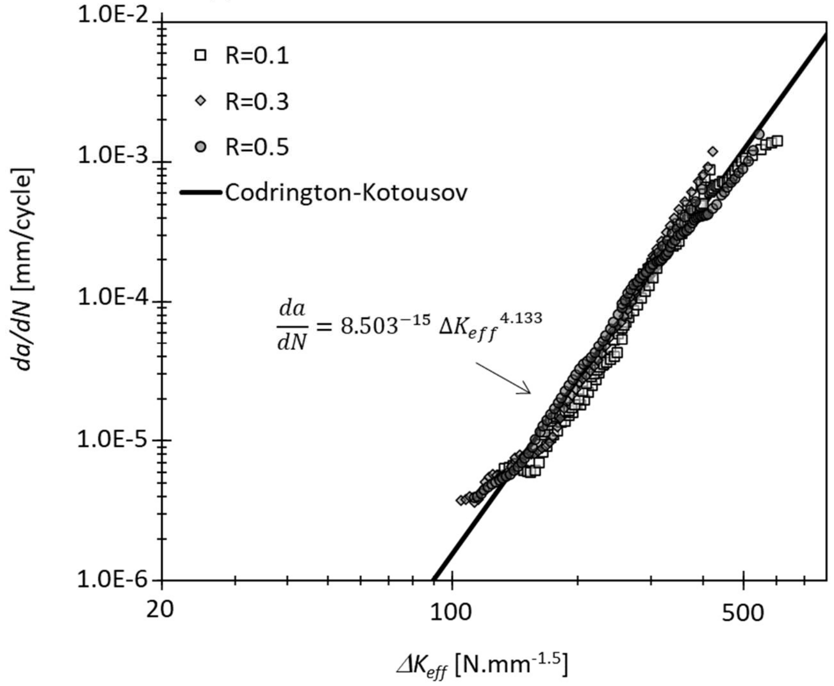

Source: Prepared by the author.

Figure 5.18 - da/dN vs. ΔK_{eff} data using Correia´s crack closure model.

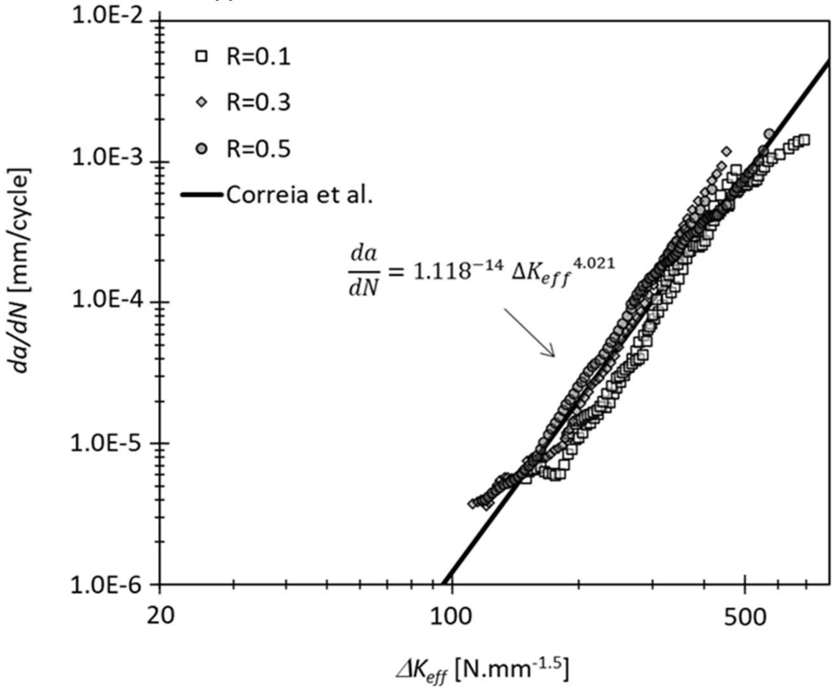

Source: Prepared by the author.

5.3.2 A comparison between all da/dN vs. ΔK_{eff} curves

In this section, the $da/dN - \Delta K_{eff}$ curves obtained for each crack closure model are compared with the experimental $da/dN - \Delta K_{eff}$ data. In Figure 5.19 it can be observed that the crack closure models proposed by Newman[23], Correia[30], Codrington-Kotousov[27], and Katcher[19] are more close to the $da/dN - \Delta K_{eff}$ curve based on experimental measurements[31-34]. These models are the most suitable to describe the crack closure effects for the 6061 T651 aluminium alloy. The other models studied overestimate these effects as can be observed in Figure 5.19.

Figure 5.19 - da/dN vs. ΔK_{eff} curves obtained for the crack closure models under consideration.

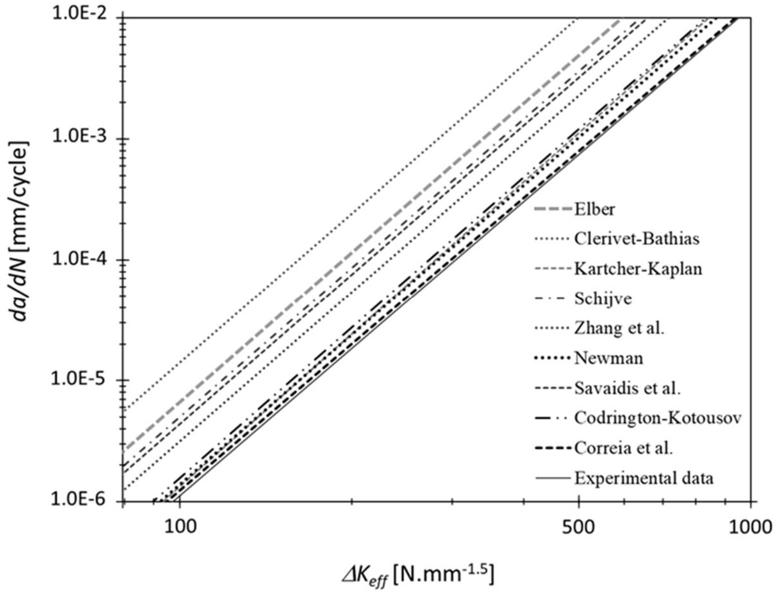

Source: Prepared by the author.

Alternatively, it is recommended to compare the quantitative parameter, U, obtained experimentally with the data calculated from the application of each crack closure model, as performed in this study and summarized in Tables 5.11 and 5.12.

In these Tables, the quantitative parameter, U, evaluated for each model under consideration and the deterministic curves based on the 1st cycle and stabilised measurements, respectively, are presented.

The error index module, e, between the calculated quantitative parameter, U, for each crack closure model and the deterministic parameter based on the 1st cycle or stabilised measurements, $U_{d,1}$ and $U_{d,s}$, respectively, is given by

$$e(\%) = \left|\frac{U_d - U}{U_d}\right| \cdot 100\% \tag{5.73}$$

Additionally, the mean value of the error index module, $\bar{e}$, was also calculated for each crack closure model.

In Table 5.11, it can be seen that the Newman, Katcher-Kaplan, and Codrington-Kotousov model present a better agreement with the deterministic data $U_{d,1}$ obtained based on the 1st cycle measurements, where $\bar{e}$ is equal to 7.34%, 6.3% and 5.41%, respectively. The crack closure models proposed by Zhang[22] and Correia[30], when compared with $U_{d,1}$, present mean values of the module of error index, $\bar{e}$, of 12.89%, and 11.96%, respectively. These models can be considered suitable to describe the crack closure effects, taking into account the mean values of the error index module $\bar{e}$ obtained. Concerning the other models also studied and presented in Table 5.11, the mean values of the error index module are practically greater than 20%.

When the same analysis is performed concerning the deterministic data based on the stabilised measurements, $U_{d,s}$, see Table 5.12, it can be verified that Newman[23], Katcher; Kaplan[19], and Correia model[30] present the lowest mean values of the error index module, 6.63%, 6.38% and 2.46%. The model proposed by Codrington-Kotousov[27] can be considered adequate to describe the crack closure effects since the mean value of the error index module, $\bar{e}$, are of 5.41%. The other models also studied have mean values of the error index module, $\bar{e}$, greater than 20%, and are not considered adequate to describe the crack closure effects, when compared with the models – Newman[23], Correia[30], Codrington-Kotousov[27], and Katcher and Kaplan[19] – with the mean values of the error index module, $\bar{e}$, below 6.5%.

Table 5.11 - Quantitative parameter, U, evaluated for each model under consideration and the deterministic curve, $U_{d,1}$.

Model	R	U	$U_{d,1}$	Error index, e	$\bar{e}$
	-	-	-	(%)	(%)
Elber	0.1	0.540000	0.729337	25.96	27.44
	0.3	0.620000	0.842013	26.37	
	0.5	0.700000	1	30	
Katcher and Kaplan	0.1	0.771000	0.729337	5.71	6.3
	0.3	0.953000	0.842013	13.18	
	0.5	1	1	0	
Clerivet and Bathias	0.1	0.440000	0.729337	39.67	39.3
	0.3	0.520000	0.842013	38.24	
	0.5	0.600000	1	40	
Schijve	0.1	0.584200	0.729337	19.90	22.35
	0.3	0.659800	0.842013	21.64	
	0.5	0.745000	1	25.50	
Zhang	0.1	0.655890	0.729337	10.07	12.89
	0.3	0.740010	0.842013	12.11	
	0.5	0.835250	1	16.48	
Newman	0.1	0.813744	0.729337	11.57	7.34
	0.3	0.915657	0.842013	8.75	
	0.5	0.982985	1.000000	1.70	
Savaidis	0.1	0.596864	0.729337	18.16	19.92
	0.3	0.683643	0.842013	18.81	
	0.5	0.772026	1	22.8	
Codrington-Kotousov	0.1	0.778035	0.729337	6.68	5.41
	0.3	0.886442	0.842013	5.28	
	0.5	0.957088	1	4.29	
Correia	0.1	0.889375	0.729337	21.94	11.96
	0.3	0.950745	0.842013	12.91	
	0.5	0.989675	1	1.03	

Source: Prepared by the author.

Table 5.12 - Quantitative parameter, U, evaluated for each model under consideration and the deterministic curve, $U_{d,s}$.

Model	R	U	$U_{d,s}$	Error index, e	$\bar{e}$
	-	-	-	(%)	(%)
Elber	0.1	0.540000	0.909337	40.62	36.04
	0.3	0.620000	0.992013	37.5	
	0.5	0.700000	1	30	
Katcher and Kaplan	0.1	0.771000	0.909337	15.21	6.38
	0.3	0.953000	0.992013	3.93	
	0.5	1	1	0	
Clerivet and Bathias	0.1	0.440000	0.909337	51.61	46.40
	0.3	0.520000	0.992013	47.58	
	0.5	0.600000	1	40	
Schijve	0.1	0.584200	0.909337	35.76	31.58
	0.3	0.659800	0.992013	33.49	
	0.5	0.745000	1	25.5	
Zhang	0.1	0.655890	0.909337	27.87	23.25
	0.3	0.740010	0.992013	25.4	
	0.5	0.835250	1	16.48	
Newman	0.1	0.813744	0.909337	10.51	6.64
	0.3	0.915657	0.992013	7.70	
	0.5	0.982985	1.000000	1.70	
Savaidis	0.1	0.596864	0.909337	34.36	29.42
	0.3	0.683643	0.992013	31.09	
	0.5	0.772026	1	22.8	
Codrington-Kotousov	0.1	0.778035	0.909337	14.44	9.79
	0.3	0.886442	0.992013	10.64	
	0.5	0.957088	1	4.29	
Correia	0.1	0.889375	0.909337	2.2	2.46
	0.3	0.950745	0.992013	4.16	
	0.5	0.989675	1	1.03	

Source: Prepared by the author.

5.3.3 R_{eff} *versus* R: experimental results and analytical models

In this section, a discussion on the relationship between effective stress ratio, R_{eff}, and applied stress ratio, R, based on experimental data and crack closure models under consideration are also made, respectively.

The relationships between R_{ef} and R estimated through the various crack closure models – Elber[13,14], Katcher and Kaplan[19], Clerivet and Bathias[20], Schijve[21], Zhang[22], Newman[23], Savaidis[25,26], Codrington-Kotousov[27], and Correia[30] – are presented in Figure 20. Additionally, the experimental results of the 6061 aluminium alloy for the R_{eff} and R relation is also shown in Figure 5.20, where this relationship is presented for the 1st cycle and stabilised measurements (Table 5.13), collected from Lal *et al.*[33].

Table 5.13 - Experimental results of R *versus* R_{eff} for the 1st cycle and stabilised measurements[33].

R	R_{eff}	
-	1st cycle	Stabilised
0.0	0.31	0.16
0.2	0.376	0.232
0.5	~0.5	~0.5

Source: Prepared by the author.

From Figure 5.20, the crack closure models proposed by Newman[23], Codrington-Kotousov[27] and Correia[30] exhibit a good agreement with the experimental results. Newman's and Codrington-Kotousov's crack closure models describe a good agreement when compared with the 1st cycle measurements while Correia's model shows a good agreement with the stabilised measurements. In addition to the Newman, Codrington-Kotousov and Correia models, the ones that present a better approximation to the experimental results are the crack closure models proposed by Zhang[22], and Katcher and Kaplan[19]. The Katcher and Kaplan's model presents an agreement that can be considered reasonable for stress ratios, R, between 0.1 and 0.3, as proposed by these authors[19]. The other models applied in this comparative study overestimate the crack closure effects. Among the models applied in this study, Clerivet and Bathias's model is the one with the highest overestimation of the crack closure effects when compared with the experimental results. The Savaidis model[25,26] overestimate the crack closure effects. The crack closure models proposed by Elber[13,14], Schijve[21], and Savaidis[25,26] exhibit results close to each other.

Therefore, Figure 5.20 also shows that there is a huge scatter using different models. This clearly indicates that R is not the only parameter affecting crack closure. It can be explained by the influence of material, since different materials were considered to generate the different models used in this analysis, by variability of experimental measurements or by a thickness effect. Besides, the scatter may also be attributed to the influence of K_{max}, which adds to the influence of stress ratio, R. So, to improve the discussion about the crack closure effects and improve the models that have been proposed in the literature, the simultaneous monitoring of CTOD-based experimental measurements of the crack closure effects and getting the crack tip stress-strain field based on digital image correlation (DIC) measurements, supported by analytical/numerical solutions, seems to be a good way to describe the fatigue crack growth correctly, as suggested in the scientific work developed by Ferreira-Castro-Meggiolaro[76,77].

Figure 5.20 - Relation between R_{eff} and R for the various crack closure models.

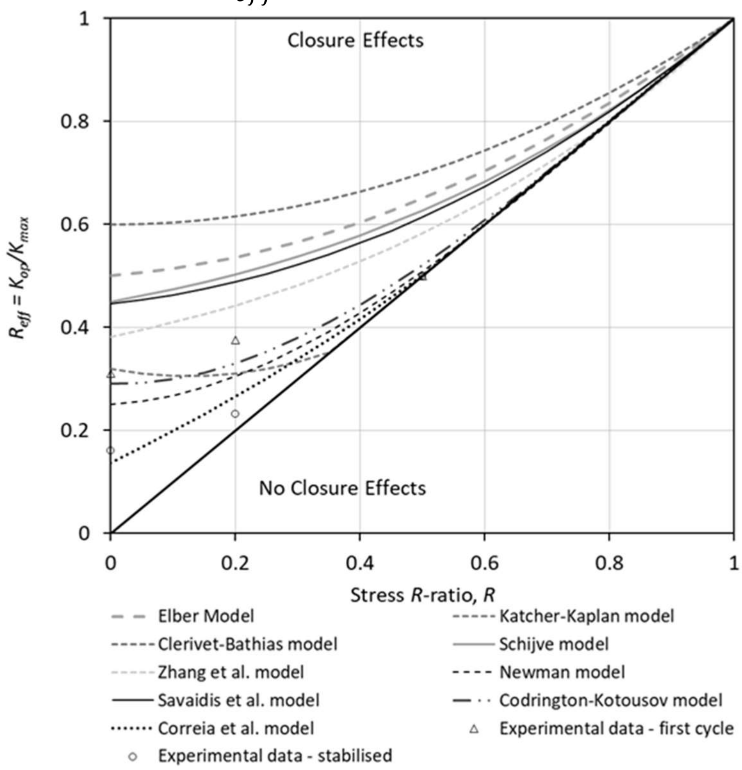

Source: Prepared by the author.

The experimental results of the effective stress ratio, R_{eff}, for each stress ratio, R, of 0, 0.2, and 0.5, were collected from Lal *et al.*[33]. These estimations were done for the 6061 T6 aluminium alloy by Lal *et al.*[33] and presented in Table 5.13. Second-degree polynomial functions were adjusted to the experimental data $R_{eff,1}$ and $R_{eff,s}$ available for the 1st cycle and stabilised measurements, respectively, for the estimation of R_{eff} values for each stress R-ratio, 0.1, 0.3 and 0.5. These polynomial functions to describe the relationship between R_{eff} and R for the 1st cycle and stabilised measurements are given by

$$R_{eff,1} = 0.166667 \cdot R^2 + 0.296667 \cdot R + 0.31$$
$$0 \leq R \leq 0.5 \tag{5.74}$$
$$R^2 = 1$$

$$R_{eff,s} = 1.066667 \cdot R^2 + 0.146667 \cdot R + 0.16 \tag{5.75}$$
$$0 \leq R \leq 0.5$$
$$R^2 = 1$$

A comparison between the experimental and deterministic data of the relationship R_{eff} versus R for the 1st cycle and stabilised measurements can be seen in Figures 5.21 and 5.22, respectively. In these figures, a good agreement can be verified between the experimental data and deterministic data for the 1st cycle and stabilised measurements.

Figure 5.21 - Relationship between effective stress ratio, R_{eff}, and applied stress ratio, R: experimental data and deterministic curve for the 1st cycle measurements.

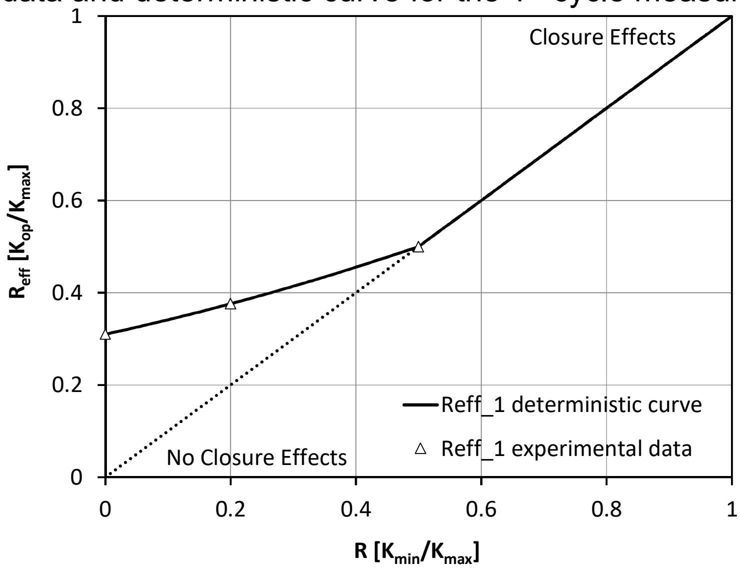

Source: Prepared by the author.

Figure 5.22 - Relationship between effective stress ratio, R_{eff}, and applied stress ratio, R: experimental data and deterministic curve for the stabilised measurements.

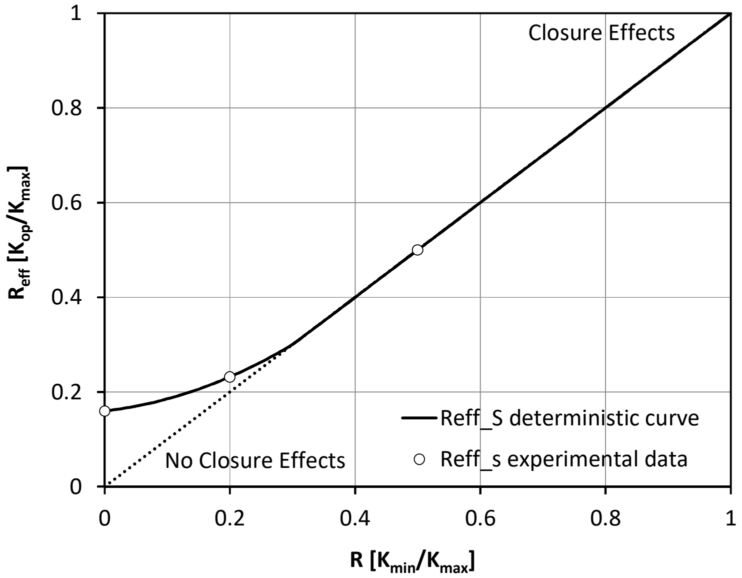

Source: Prepared by the author.

The same procedure used in Section 5.3.2, to estimating the error index module, e, between the calculated quantitative parameter, U, for each crack closure model and the deterministic parameter based on the 1st cycle or stabilised measurements, is now used to estimating the error index module between the calculated effective stress ratio, R_{eff}, for each crack closure model and the deterministic values based on the 1st cycle or stabilised measurements.

In Table 5.14, it can be seen that the Newman[23], Codrington-Kotousov[27] and Katcher and Kaplan's[19] models present a better agreement with the deterministic data $R_{eff,1}$ obtained based on the 1st cycle measurements, where mean values of error index module are equal to 12.19%, 8.27% and 9.97%, respectively. The other models also studied based on the 1st cycle measurements, $R_{eff,1}$, have mean values of the error index module, $\bar{e}$, greater than 15%. For the Zhang[22] and Correia's[30] models, the mean values of the error index module, $\bar{e}$, are of 17.64% and 20.59%, respectively. However, it is important to note that in this analysis the deterministic data of $R_{eff,1}$ used to compare with the R_{eff} values obtained for each model under consideration are based on the 1st cycle measurements.

When the same analysis is performed concerning the deterministic data of the effective stress ratio based on the stabilised measurements, $R_{eff,s}$, see Table 5.15, it can be verified that Newman's and Correia's models present the lowest mean values of the error index module, 21.93% and 6.73%. The other models also studied based on the stabilised measurements, $R_{eff,s}$, have mean values of the error index module, $\bar{e}$, greater than 25%, and are not considered adequate to describe the crack closure effects.

Table 5.14 - Effective stress ratio, R_{eff}, evaluated for each model under consideration and the deterministic value, $R_{eff,1}$.

Model	R	R_{eff}	$R_{eff,1}$	Error index, e	$\bar{e}$
	-	-	-	(%)	(%)
Elber	0.1	0.514000	0.341337	50.58	39.1
	0.3	0.566000	0.414013	36.71	
	0.5	0.650000	0.500025	29.99	
Katcher and Kaplan	0.1	0.306100	0.341337	10.32	9.97
	0.3	0.332900	0.414013	19.59	
	0.5	0.500000	0.500025	0	
Clerivet and Bathias	0.1	0.604000	0.341337	76.95	56.85
	0.3	0.636000	0.414013	53.62	
	0.5	0.700000	0.500025	39.99	
Schijve	0.1	0.474220	0.341337	38.93	31.47
	0.3	0.538140	0.414013	29.98	
	0.5	0.627500	0.500025	25.49	
Zhang	0.1	0.409699	0.341337	20.03	17.64
	0.3	0.481993	0.414013	16.42	
	0.5	0.582375	0.500025	16.47	
Newman	0.1	0.267630	0.341337	21.59	12.19
	0.3	0.359040	0.414013	13.28	
	0.5	0.508507	0.500025	1.70	
Savaidis	0.1	0.462823	0.341337	35.59	28.11
	0.3	0.521450	0.414013	25.95	
	0.5	0.613987	0.500025	22.79	
Codrington-Kotousov	0.1	0.299768	0.341337	12.18	8.27
	0.3	0.379491	0.414013	8.34	
	0.5	0.521456	0.500025	4.29	
Correia	0.1	0.199562	0.341337	41.54	20.59
	0.3	0.334479	0.414013	19.21	
	0.5	0.505163	0.500025	1.03	

Source: Prepared by the author.

Table 5.15 - Effective stress ratio, R_{eff}, evaluated for each model under consideration and the deterministic value, $R_{eff,s}$.

Model	R	R_{eff}	$R_{eff,s}$	Error index, e	$\bar{e}$
	-	-	-	(%)	(%)
Elber	0.1	0.514000	0.185337	177.33	98.66
	0.3	0.566000	0.300013	88.66	
	0.5	0.650000	0.500000	30	
Katcher and Kaplan	0.1	0.306100	0.185337	65.16	25.37
	0.3	0.332900	0.300013	10.96	
	0.5	0.500000	0.500000	0	
Clerivet and Bathias	0.1	0.604000	0.185337	225.89	125.96
	0.3	0.636000	0.300013	111.99	
	0.5	0.700000	0.500000	40	
Schijve	0.1	0.474220	0.185337	155.87	86.91
	0.3	0.538140	0.300013	79.37	
	0.5	0.627500	0.500000	25.5	
Zhang	0.1	0.409699	0.185337	121.06	66.06
	0.3	0.481993	0.300013	60.66	
	0.5	0.582375	0.500000	16.47	
Newman	0.1	0.267630	0.185337	44.40	21.93
	0.3	0.359040	0.300013	19.67	
	0.5	0.508507	0.500000	1.70	
Savaidis	0.1	0.462823	0.185337	149.72	82.11
	0.3	0.52145	0.300013	73.81	
	0.5	0.613987	0.500000	22.8	
Codrington-Kotousov	0.1	0.299768	0.185337	61.74	30.84
	0.3	0.379491	0.300013	26.49	
	0.5	0.521456	0.500000	4.29	
Correia	0.1	0.199562	0.185337	7.68	6.73
	0.3	0.334479	0.300013	11.49	
	0.5	0.505163	0.500000	1.03	

Source: Prepared by the author.

5.4 CONCLUDING REMARKS

In this research, a comparative study of the fatigue crack propagation rates (da/dN) versus effective stress factor range (ΔK_{eff}) data calculated through the various crack closure models under consideration was done, where Correia's and Newman's models present a good agreement when compared with the experimental $da/dN - \Delta K_{eff}$ data, and in terms of comparing U and R_{eff} obtained through the Correia's model when compared with the deterministic data based on experimental measurements. It is important to note that experimental measurements of crack closure effects may have been made with some inaccuracy since the experimental $da/dN - \Delta K_{eff}$ data present a reasonable performance.

In this analysis, the deterministic values of the quantitative parameter, U, and the effective stress ratio, R_{eff}, based on the first cycle and stabilised measurements were obtained. Also, the values of U and R_{eff} were calculated for each crack closure model under consideration.

Correia's model presents good results for U and R_{eff} when compared to the deterministic data based on stabilised measurements, where the mean values of the error index module are of 2.46% and 6.73%, respectively. Newman's model also shows good results in terms of U and R_{eff}, presenting error index modules of 6.64% and 21.93%, respectively, when the comparison is made with deterministic data based on stabilised measurements. When the same comparison of U and R_{eff} are made with the deterministic values based on the 1st cycle measurements, the Newman's, Codrington-Kotousov's and Katcher and Kaplan's models present a good agreement, where the mean values of the error index module of 7.34%, 5.41% and 6.30%, and 12.19%, 8.27% and 9.97%, respectively. The other models also studied based on the 1st cycle and stabilised measurements have mean values of the error index module, $\bar{e}$, greater than 20%, and are not considered adequate to describe the crack closure effects.

The assumptions suggested in the Hudak and Davidson's investigations and later also recommended by Ellyin[20] were confirmed by the use of the Correia's model, where the crack closure quantitative parameter is a function of applied stress R-ratio, maximum stress intensity factor (or ΔK), and driven by threshold stress intensity factor range, ΔK_{th}. Also, Correia's crack closure model based on experimental data suggest the limit stress intensity factor (K_L) in estimating the quantitative parameter (U) to describe the crack closure effects. In this study, the quantitative parameter (U) was estimated by using the maximum stress intensity factor (K_{max}) for stabilised cycles.

Therefore, it can be concluded that the simultaneous monitoring of CTOD-based experimental measurements of the crack closure effects and getting the crack tip stress-strain field based on digital image correlation (DIC) measurements, supported by analytical/numerical solutions, seems to be a good way to describe the fatigue crack growth correctly, as suggested by Ferreira-Castro-Meggiolaro[76,77].

REFERENCES

1 SCHÜTZ, W. A history of fatigue. **Engineering Fracture Mechanics**, Oxford, v. 54, n. 2, p. 263-300, 1996.

2 BRITISH STANDARDS INSTITUTION. **BS7910:2005**: Guidance on Methods for Assessing the Acceptability of Flaws in Metallic Structures. London: BSI, 2005.

3 SURESH, S. **Fatigue of materials**. 2. ed. Cambridge: Cambridge university press, 1998.

4 AYATOLLAHI, M.R.; RASHIDI MOGHADDAM, M.; RAZAVI, S.M.J.; BERTO, F. Geometry effects on fracture trajectory of PMMA samples under pure mode-I loading. **Engineering Fracture Mechanics**, Oxford, v. 163, p. 449-461, 2016.

5 BERTO, F.; LAZZARIN, P. Multiparametric full-field representations of the in-plane stress fields ahead of cracked components under mixed mode loading. **International Journal of Fatigue**, London, v. 46, p. 16-26, 2013.

6 SILVA, A.L.L.; DE JESUS, A.M.P.; XAVIER, J.; CORREIA, J.A.F.O.; FERNANDES, A.A. Combined analytical-numerical methodologies for the evaluation of mixed-mode (I + II) fatigue crack growth rates in structural steels. **Engineering Fracture Mechanics**, Oxford, v. 185, p. 124-138, 2017.

7 CORREIA, J.A.F.O.; BLASÓN, S.; DE JESUS, A.M.P.; CANTELI, A.F.; MOREIRA, P.M.G.P.; TAVARES, P.J. Fatigue life prediction based on an equivalent initial flaw size approach and a new normalized fatigue crack growth model. **Engineering Failure Analysis**, Oxford, vol. 69, pp. 15-28, 2016.

8 CORREIA, J.A.F.O.; HUFFMAN, P.J.; DE JESUS, A.M.P.; CICERO, S.; FERNÁNDEZ-CANTELI, A.; BERTO, F.; GLINKA, G. Unified two-stage fatigue methodology based on a probabilistic damage model applied to structural details. **Theoretical and Applied Fracture Mechanics**, Amsterdam, v. 92, p. 252-265, 2017.

9 PARIS, P.C. A rational analytic theory of fatigue. **The trend in engineering**, Seattle, v. 13, n. 9, p. 9-14, 1961.

10 PARIS, P.; ERDOGAN, F. A critical analysis of crack propagation laws. **Journal of Fluids Engineering**, New York, v. 85, n. 4, p. 528-533, 1963.

11 BEDEN, S.M.; ABDULLAH, S.; ARIFFIN, A.K. Review of fatigue crack propagation models for metallic components. **European Journal of Scientific Research**, Victoria, v. 28, n. 3, p. 364-397, 2009.

12 CASTILLO, E.; FERNÁNDEZ-CANTELI, A.; SIEGELE, D. Obtaining S-N curves from crack growth curves: An alternative to self-similarity. **International Journal of Fracture**, Dordrecht, v. 187, n. 1, p. 159-172, 2014.

13 ELBER, W. Fatigue crack closure under cyclic tension. **Engineering Fracture Mechanics**, Oxford, v. 2, n. 1, p. 37-44, 1970.

14 ELBER, W. The significance of fatigue crack closure. **American Society for Testing and Materials Special Technical Publication**, Philadelphia, v. 486, p. 230–242, 1971.

15 KUMAR, R. Review on crack closure for constant amplitude loading in fatigue, **Engineering Fracture Mechanics**, Oxford, v. 42, n. 2, p. 389-400, 1992.

16 SCHIJVE, J. Fatigue of structures and materials in the 20th century and the state of the art. **International Journal of Fatigue**, London, v. 25, n. 8, p. 679-702, 2003.

17 PIPPAN, R.; HOHENWARTER, A. Fatigue crack closure: a review of the physical phenomena. **Fatigue and Fracture of Engineering Materials and Structures**, Chichester, v. 40, n. 4, p. 471-495, 2017.

18 CORREIA, J.A.F.O.; BLASÓN, S.; ARCARI, A.; CALVENTE, M.; APETRE, N.; MOREIRA, P.M.G.P.; DE JESUS, A.M.P.; CANTELI, A.F. Modified CCS fatigue crack growth model for the AA2019-T851 based on plasticity-induced crack-closure. **Theoretical and Applied Fracture Mechanics**, Amsterdam, v. 85, p. 26-36, 2016.

19 KATCHER, M.; KAPLAN, M. Effect of r factor and crack closure on fatigue crack growth for aluminium and titanium alloys. **American Society for Testing and Materials Special Technical Publication**, West Conshohocken, v. 559, p. 264-282, 1974.

20 CLERIVET, A.; BATHIAS, C. Study of crack tip opening under cyclic loading taking into account the environment and R ratio. **Engineering Fracture Mechanics**, Oxford, v. 12, n. 4, p. 599-611, 1979.

21 SCHIJVE, J. Some formulas for the crack opening stress level. **Engineering Fracture Mechanics**, Oxford, v. 14, n. 3, p. 461-465, 1981.

22 ZHANG, S.; MARISSEN, R.; SCHULTE, K.; TRAUTMANN, K.K.; NOWACK, H.; SCHIJVE, J. Crack propagation studies on Al 7475 on the basis of constant amplitude and selective variable amplitude loading histories. **Fatigue; Fracture of Engineering Materials; Structures**, Chichester, v. 10, n. 4, p. 315-332, 1987.

23 NEWMAN, JR.; J.C. A crack opening stress equation for fatigue crack growth. **International Journal of Fracture**, Dordrecht, v. 24, n. 4, p. R131-R135, 1984.

24 VORMWALD, M.; SEEGER, T. The consequences of short crack closure on fatigue crack growth under variable amplitude loading. **Fatigue; Fracture of Engineering Materials; Structures**, Chichester, v. 14, n. 2-3, p. 205-225, 1991.

25 SAVAIDIS, G.; DANKERT, M.; SEEGER, T. An analytical procedure for predicting opening loads of cracks at notches. **Fatigue; Fracture of Engineering Materials; Structures**, Chichester, v. 18, n. 4, p. 425-442, 1995.

26 SAVAIDIS, G.; SAVAIDIS, A.; ZERRES, P.; VORMWALD, M. Mode I fatigue crack growth at notches considering crack closure. **International Journal of Fatigue**, London, v. 32, n. 10, p. 1543-1558, 2010.

27 CODRINGTON, J.; KOTOUSOV, A. A crack closure model of fatigue crack growth in plates of finite thickness under small-scale yielding conditions. **Mechanics of Materials**, Amsterdam, v. 41, n. 2, p. 165-173, 2009.

28 HUDAK, S. J.; DAVIDSON, D. L. The dependence of crack closure on fatigue loading variables. **American Society for Testing and Materials Special Technical Publication**, Philadelphia, v. 982, p. 121-138, 1988.

29 ELLYIN, F. **Fatigue Damage, Crack Growth and Life Prediction**. 1. ed. London: Chapman; Hall, 1997

30 CORREIA, J.A.F.O.; DE JESUS, A.M.P.; MOREIRA, P.M.G.P.; TAVARES, P.J.S. Crack Closure Effects on Fatigue Crack Propagation Rates: Application of a Proposed Theoretical Model. **Advances in Materials Science and Engineering**, Oxford, v. 2016, 2016.

31 CORREIA, J.A.F.O.; DE JESUS, A.M.P.; RIBEIRO, A.S.; FERNANDES, A.A. Strain-based approach for fatigue crack propagation simulation of the 6061-T651 aluminium alloy. **International Journal of Materials and Structural Integrity**, Geneva, v. 11, n. 1-3, p. 1-15, 2017.

32 HENKEL, S.; LIEBELT, E.; BIERMANN, H.; ACKERMANN, S.; ZYBELL, L. Crack growth behavior of aluminum alloy 6061 T651 under uniaxial and biaxial planar testing condition. **Frattura ed Integrita Strutturale**, Cassino, v. 9, n. 34, p. 466-475, 2015.

33 LAL, K.M.; GARG, S.B.L.; LE MAY, I. On effective stress range factor in fatigue, **Journal of Engineering Materials and Technology**, New York, v. 102, n. 1, p. 147-152, 1980.

34 JOGI, B.F.; BRAHMANKAR, P.K.; NANDA, V.S.; PRASAD, R.C. Some studies on fatigue crack growth rate of aluminum alloy 6061. **Journal of Materials Processing Technology**, Amsterdam, v. 201, n. 1-3, p. 380-384, 2008.

35 KAFIE MARTINEZ, J.; KEATING, P.B.; MONTENEGRO, P.; CORREIA, J.A.F.O.

Fracture mechanics analysis of the effect of clamping stress on the fatigue life of riveted built-up railroad girders under variable amplitude loading. **Engineering Failure Analysis**, Oxford, v. 118, 2020.

36 LU, T.; ZHAO, P.; XUAN, F. Fatigue life prediction for component with local structural discontinuity based on stress field intensity. **Structural Integrity**, Cham v. 7, p. 245-251, 2019.

37 EUROPEAN COMMITTEE FOR STANDARDIZATION **CEN-TC 250. EN 1993-1-9: Eurocode 3**: Design of steel structures – Part 1-9: Fatigue.; Brussels: European Committee for Standardization, 2003.

38 DET NORSKE VERITAS AND GERMANISCHER LLOYD GROUP - DNV GL Group. **DNVGL-RP-C203:** fatigue design of offshore steel structures. Oslo: DNV GL AS, 2016.

39 IRWIN, G. Analysis of stresses and strains near the end of a crack traversing a plate. **Journal of Applied Mechanics**, Tehran, v. 24, p. 361-364, 1957.

40 AMERICAN SOCIETY FOR TESTING AND MATERIALS – ASTM. **ASTM E647-15e1**: Standard test method for measurement of fatigue crack growth rates. ASTM International, West Conshohocken, 2015.

41 MURAKAMI, K.; GOTOH, K. Practical determination method of the threshold stress intensity factor range Δkth, Yosetsu Gakkai Ronbunshu. **Quarterly Journal of the Japan Welding Society**, Tokyo, v. 35, n. 4, p. 149-153, 2017.

42 XIN, H.; CORREIA, J.A.F.O.; VELJKOVIC, M. Three-dimensional fatigue crack propagation simulation using extended finite element methods for steel grades S355 and S690 considering mean stress effects. **Engineering Structures**, Oxford vol. 227, 2021.

43 LEBLOND, J.; KARMA, A.; PONSON, L.; VASUDEVAN, A. Configurational Stability of a Crack Propagating in Mixed-Mode I + II + III. **Structural Integrity**, Cham, v. 8, p. 101-105, 2019.

44 ISHIHARA, S.; SUGAI, Y.; MCEVILY, A. J. On the distinction between plasticity- and roughness-induced fatigue crack closure. **Metallurgical and Materials Transactions A: Physical Metallurgy and Materials Science**, New York, v. 43, n. 9, p. 3086-3096, 2012.

45 GRAY, G.T.; WILLIAMS, J.C.; THOMPSON, A.W. Roughness-Induced Crack Closure: An Explanation for Microstructurally Sensitive Fatigue Crack Growth. **Metallurgical and Materials Transactions A**, New York, v. 14, p. 421-433, 1983.

46 LESIUK, G.; SZATA, M.; CORREIA, J.A.F.O.; DE JESUS, A.M.P.; BERTO, F. Kinetics of fatigue crack growth and crack closure effect in long term operating steel manufactured at the turn of the 19th and 20th centuries. **Engineering Fracture Mechanics**, Oxford, v. 185, p. 160-174, 2017.

47 ANTUNES, F.V.; PAIVA, L.; BRANCO, R.; BORREGO, L.P. Effect of underloads on plasticity-induced crack closure: A numerical analysis. **Journal of Engineering Materials and Technology**, New York, v. 141, n. 3, 2019.

48 CAMAS, D.; GARCIA-MANRIQUE, J.; ANTUNES, F.V.; GONZALEZ-HERRERA, A. Numerical analysis of the influence of crack growth scheme on plasticity induced crack closure results. **Structural Integrity**, Cham, v. 7, p. 155-160, 2019.

49 ANTUNES, F.V.; CHEGINI, A.G.; BRANCO, R.; CAMAS, D. A numerical study of plasticity induced crack closure under plane strain conditions. **International Journal of Fatigue**, London, v. 71, p. 75-86, 2015.

50 MCCLUNG, R.C. Finite element analysis of specimen geometry effects on fatigue crack closure. **Fatigue; Fracture of Engineering Materials; Structures**, Chichester, v. 17, n. 8, p. 861-872, 1994.

51 BACHMANN, V.; MUNZ D. Crack closure in fatigue of titanium alloy. **International Journal of Fracture**, Dordrecht, v. 11, p. 713-716, 1975.

52 SRIVASTAVA, Y.P.; GARG, S.B.L. Influence of R on effective stress range ratio and crack growth. **Engineering Fracture Mechanics**, Oxford, v. 22, n. 6, p. 915-926, 1985.

53 GEERLOFS, N.; ZUIDEMA, J.; SIETSMA, J. On the Paris exponent and crack closure effects of alporas aluminum foam. *In*: EUROPEAN CONFERENCE OF FRACTURE, ECF15, ADVANCED FRACTURE MECHANICS FOR LIFE AND SAFETY ASSESSMENTS, 15, 2004, Stockholm. **Proceedings of the** […]. Stockholm: [s.n.], 2004.

54 DUGDALE, D.S. Yielding of steel sheets containing slits. **Journal of the Mechanics and Physics of Solids**, Oxford, v. 8, n. 2, p. 100-104,1960.

55 WALKER, K. The Effect of Stress Ratio During Crack Propagation and Fatigue for 2024-T3 and 7075-T6 Aluminum. **American Society for Testing and Materials Special Technical Publication**, Philadelphia, v. 462, p. 1–14, 1970.

56 KLESNIL, M.; LUKÁŠ, P. **Fatigue of Metallic Materials**, 2. ed.; Amsterdam: Elsevier Science Publisher, 1992.

57 DOWLING, N.E. **Mechanical Behaviour of Materials**. Engineering Methods for Deformation, Fracture and Fatigue. 3 ed. London: Pearson Prentice Hall, 2007.

58 VAN KUIJK, J.J.A.; ALDERLIESTEN, R.C.; BENEDICTUS, R. Unraveling the myth of closure corrections: Sharpening the definition of opening and closure stresses with an energy approach. **International Journal of Fatigue**, London, v. 143, 2021.

59 MALJAARS, J.; PIJPERS, R.; SLOT, H. Load sequence effects in fatigue crack growth of thick-walled welded C-Mn steel members. **International Journal of Fatigue**, London, v. 79, p. 10-24, 2015.

60 LARROSA, N.O.; AKID, R.; AINSWORTH, R.A. Corrosion-fatigue: a review of damage tolerance models. **International Materials Reviews**, Abingdon, v. 63, n. 5, p. 283-308, 2010.

61 BERETTA, S.; CARBONI, M.; FIORE, G.; LO CONTE, A. Corrosion-fatigue of A1N railway axle steel exposed to rainwater. **International Journal of Fatigue**, London, v. 32, n. 6, p. 952-961, 2010.

62 HU, Y.; WU, S.; WITHERS, P.J.; CAO, H.; CHEN, P.; ZHANG, Y.; SHEN, Z.; VOJTEK, T.; HUTAŘ, P. Corrosion fatigue lifetime assessment of high-speed railway axle EA4T steel with artificial scratch. **Engineering Fracture Mechanics**, Oxford, v. 245, 2021.

63 VOJTEK, T.; POKORNÝ, P.; KUBĚNA, I.; NÁHLÍK, L.; FAJKOŠ, R.; HUTAŘ, P. Quantitative dependence of oxide-induced crack closure on air humidity for railway axle steel. **International Journal of Fatigue**, London, v. 123, p. 213-224, 2019.

64 WU, S.C.; XU, Z.W.; LIU, Y.X.; KANG, G.Z.; ZHANG, Z.X.; On the residual life assessment of high-speed railway axles due to induction hardening. **International Journal of Rail Transportation**, Abingdon, v. 6, n. 4, p. 218-232, 2018.

65 ZERBST, U.; BERETTA, S.; KÖHLER, G.; LAWTON, A.; VORMWALD, M.; BEIER, H.T.; KLINGER, C.; ČERNÝ, I.; RUDLIN, J.; HECKEL, T.; KLINGBEIL, D. Safe life and damage tolerance aspects of railway axles - A review. **Engineering Fracture Mechanics**, Oxford, v. 98, n. 1, p. 214-271, 2013.

66 HU, Y.; QIN, Q.; WU, S.; ZHAO, X.; WANG, W. Fatigue resistance and remaining life assessment of induction-hardened S38C steel railway axles. **International Journal of Fatigue**, London, v. 144, 2021.

67 FORMAN, R.; METTU, S. Behavior of surface and corner cracks subjected to tensile and bending loads in a Ti-6Al-4V alloy. **NASA Technical Memorandum**, Houston, n. 102165, 64 pages, 1992.

68 WU, S.C.; LI, C.H.; LUO, Y.; ZHANG, H.O.; KANG, G.Z. A uniaxial tensile behavior based fatigue crack growth model. **International Journal of Fatigue**, London, v. 131, 2020.

69 WU, S.C.; XU, Z.W.; YU, C.; KAFKA, O.L.; LIU, W.K. A physically short fatigue crack growth approach based on low cycle fatigue properties. **International Journal of Fatigue**, London, v. 103, p. 185-195, 2017.

70 RIBEIRO, A.S.; JESUS, A.M.P.; FERNANDES, A.A. Fatigue crack propagation rates of the aluminium alloy 6061-T651. *In*: INTERNATIONAL CONGRESS OF MECHANICAL ENGINEERING, 18.; 2005, Ouro Preto. **Proceedings** […]. Ouro Preto: COBEM, 2005.

71 AMERICAN SOCIETY FOR TESTING AND MATERIALS – ASTM. **ASTM E606M-19e1**: Standard Test Method for Strain-Controlled Fatigue Testing, ASTM International, West Conshohocken, 2019

72 RAMBERG, W.; OSGOOD, W.R. Description of stress–strain curves by three parameters. **National Advisory Committee for Aeronautics – NACA-TN-902**, Washington DC, n. 902, 1943.

73 MORROW, J.D. Cyclic plastic strain energy and fatigue of metals. **American Society for Testing and Materials Special Technical Publication**, West Conshohocken, v. 378, p. 45-87, 1965.

74 MANSON, S.S. Behaviour of materials under conditions of thermal stress, **National Advisory Committee for Aeronautics - NACA TN-2933**, Washington DC, p.1-105, 1954.

75 COFFIN, L.F. A study of the effects of the cyclic thermal stresses on a ductile metal. **Transactions of The American Society of Mechanical Engineers**, New York, v. 76, n. 6, p. 931–950, 1954.

76 FERREIRA, S.E.; DE CASTRO, J.T.P.; MEGGIOLARO, M.A. A model to quantify fatigue crack growth by cyclic damage accumulation calculated by strip-yield procedures. **Frattura ed Integrita Strutturale**, Cassino, v. 11, n. 41, p. 129-138, 2017.

77 FERREIRA, S.E.; CASTRO, J.T.P.D.; MEGGIOLARO, M.A.; OLIVEIRA MIRANDA, A.C.D. Crack closure effects on fatigue damage ahead of crack tips. **International Journal of Fatigue**, London, vol. 125, pp. 187-198, 2019.

CHAPTER VI

6 FATIGUE CRACK GROWTH MODELLING SUPPORTED BY STRAIN ENERGY DENSITY-BASED HUFFMAN MODEL CONSIDERING THE RESIDUAL STRESS EFFECTS

6.1 INTRODUCTION

The fatigue crack growth (FCG) behaviour is essentially obtained through experimental tests. Various fatigue crack propagation models based on experimental measurements have emerged for the purpose of describing the three crack growth regions – near-threshold (region I), stable crack growth (region II), and unstable crack growth (region III). In 1961, Paris et al.[1] proposed the first crack growth law based on experimental FCG measurements of materials, where the FCG of materials can be described for the stable crack growth region (region II), also called the Paris region. The Paris law is given by the relationship between the fatigue crack growth rates, da/dN, and the applied stress intensity factor range, ΔK. In 1970, Walker[2] suggested an alternative FCG law for the Paris region to take into account the stress R-ratio effects. In 1972, an improved Walker FCG law to include the unstable crack growth region (region III) and the stress R-ratio effects was presented by Forman[3]. In this line of investigation by Forman[3], Hartman and Schijve[4] suggested a new expression including the stress R-ratio effects, fracture toughness K_c (region III), and near-threshold stress intensity factor range, ΔK_{th}. Collispriest[5] and Miller; Gallagher[5], respectively, in 1972 and 1977, also proposed FCG laws that are capable to describe the three fatigue crack propagation regimes, where the stress R-ratio effects, ΔK_{th}, and K_c where also included. Miller; Gallagher[5] have also tried to incorporate the concept of crack closure effects into their formulations. Some authors, McEvily[5] and Alves et al.[6], presented expressions to describe the near-threshold and stable crack growth regions (I and II). In the literature, several formulations can also be found to represent the stable crack growth region (Paris region) – Frost; Pook (1971), Lal; Weiss (1978), Zheng (1983), Wang (1994), Miller; Gallagher (1981)[5]. In 2014, a new formulation, proposed by Castillo-Canteli-Siegele (CCS)[7], was developed to describe the fatigue crack propagation behaviour based on the Gumbel cumulative distribution function.

In the fatigue crack growth laws previously reported, the stress intensity factor range (ΔK) is given in the field of linear-elastic Fracture Mechanics (LEFM). Dowling; Begley[8] proposed the J-Integral parameter (ΔJ) under elastoplastic conditions, where is applicable the Elastoplastic Fracture Mechanics (EPFM) to describe the fatigue crack growth behaviour. Alves; Correia[6,9] suggested an expression for the fatigue crack growth law using the J-integral parameter to cover the near-threshold and stable crack growth regions (regions I and II). In 2016, Correia et al.[10] proposed an extension of CCS model, where the intensity factor range (ΔK) is replaced by the cyclic J-integral range (ΔJ) and not including the stress R-ratio effects, to consider the case-study under elastoplastic conditions.

In 1970 and 1971, Elber[11,12] was the first to suggest the concept of crack closure effects on the fatigue crack propagation data, where the fatigue crack growth rate (da/dN) is a function of the effective stress intensity factor range ($\Delta K_{eff} = U\Delta K$, U is the quantitative closure parameter). Other expressions to describe the crack closure effects based on experimental measurements from fatigue crack propagation tests and theoretical assumptions were proposed by Hudak et al.[13], Ellyin[14] and Correia et al.[15,16]. Newman[17], Vormwald et al.[18] and Savaidis et al.[19] suggested the fatigue crack closure and opening effects based on the plasticity-induced effects applied to the applied stress intensity factor range (ΔK). In 2016, a modified CCS fatigue crack growth model was proposed by Correia et al. [20], taking into account the crack opening/closure effects based on plasticity-induced crack-closure model of the material under consideration, where the applied stress intensity factor range (ΔK) is replaced by the effective stress intensity factor range (ΔK_{eff}) in the original CCS law[7].

The modelling of the fatigue crack growth behaviour can be given using the cyclic stress-strain properties and local fatigue damage criteria, where the actual elastoplastic stress and strain distributions ahead of the crack tip are computed by analytical or numerical solutions, as a process of continuous crack re-initializations, as suggested by Glinka[21], Peeker and Niemi[22], Noroozi et al.[23,24,25], Hurley and Evans[26]. In 1985, Glinka[21] proposed a fatigue crack growth model based on a strain-based fatigue local criterion, where crack increments are considered notches on all successive crack advances. In their studies to model fatigue crack growth behaviour, it is assumed that a process of successive restarts leads to the failure of consecutive material elements.

This topic has also been explored by other authors such as Correia[27-32], Hafezi[33], De Jesus et al.[34], Huffman[35,36], Bang et al.[37-39], Pedrosa et al.[40], among others. In 2016, Huffman[35] proposed an approach based on the strain energy density to model the fatigue crack initiation and propagation.

In this research, the modelling of the fatigue crack growth behaviour for the 6061-T651 aluminium alloy through the Huffman fatigue crack growth (FCG) approach based on the strain energy density from dislocations considering the residual stress effects is studied and discussed. The calculations of the elastoplastic stresses and strains ahead of the crack tip needed for the FCG modelling are done using Neuber's or Glinka's approach. Two residual stress approaches supported by the Noroozi and Huffman's suggestions were considered in this investigation. Besides, the influence of the strain energy density calculated for different values of dislocations on the fatigue crack growth behaviour was also analysed.

6.2 EXPERIMENTAL LCF AND FCG DATA

In this research work, the experimental low-cycle fatigue (LCF) and fatigue crack growth (FCG) data of the 6061-T651 aluminium alloy[16,30] were used. These experimental data are used in the fatigue crack growth modelling (Section 6.3) based on the strain energy density approach proposed by Huffman[35] through the application of a local damage criteria, considering the residual stress effects as suggested by Huffman[35] or Noroozi et al.[23-25]. Additionally, the critical dislocation density (ρ_c) driven by the highest strain amplitude specimen and the mean value of the dislocation density (ρ_m) for the available experimental fatigue results, estimated by Ribeiro et al.[42] for the LCF data of the 6061-T651 aluminium alloy, are used in the fatigue crack growth modelling to assess their influence.

6.2.1 Cyclic elastoplastic data

The cyclic elastoplastic behaviour is estimated for the stabilised cyclic stress-strain data from the experimental low-cycle fatigue tests and given by the Ramberg and Osgood description[43]:

$$\frac{\Delta\varepsilon}{2} = \frac{\Delta\varepsilon^E}{2} + \frac{\Delta\varepsilon^P}{2} = \frac{\Delta\sigma}{2E} + \left(\frac{\Delta\sigma}{2K'}\right)^{1/n'} \quad (6.1)$$

where: $\Delta\varepsilon$ is the total strain range; $\Delta\varepsilon^E$ is the elastic strain range; $\Delta\varepsilon^P$ is the plastic strain range; $\Delta\sigma$ is the stress range; E is the Young modulus; and, K' and n' are the cyclic strain hardening coefficient and exponent. In Table 6.1, the experimental data of the AA 6061-T65[16,30], mechanical properties and cyclic elastoplastic parameters, are presented.

Table 6.1 - Mechanical properties and cyclic elastoplastic parameters[16,30].

Materials	$\boldsymbol{R_{p,0.2}}$	$\boldsymbol{R_m}$	$\boldsymbol{E}$	$\boldsymbol{K'}$	$\boldsymbol{n'}$
-	[MPa]	[MPa]	[MPa]	[MPa]	[-]
AA 6061-T651	289.9	328.5	68000	393.4	0.0567

Source: Prepared by the author.

6.2.2 Strain-life data

The Morrow's suggestion[44] is used to describe the strain-life behaviour of metals, where the elastic strain and plastic strain equations proposed by Manson[45] and Coffin[46] are combined, respectively. From this combination, the so-called Morrow-Coffin-Manson relationship is given by:

$$\frac{\Delta\varepsilon}{2} = \frac{\Delta\varepsilon^E}{2} + \frac{\Delta\varepsilon^P}{2} = \frac{\sigma_f'}{E}\left(2N_f\right)^b + \varepsilon_f'\left(2N_f\right)^c \tag{6.2}$$

where: ε_f' is the fatigue ductility coefficient; c is the fatigue ductility exponent; σ_f' is the fatigue strength coefficient; b is the fatigue strength exponent; and, N_f is the number of cycles to failure. In Table 6.2 and Figure 6.1, the deterministic strain-life parameters and strain-life results (experimental data *versus* deterministic curve) obtained through the experimental low-cycle fatigue tests of smooth specimens under strain-controlled conditions, are shown, respectively.

Table 6.2 - Strain-life parameters of the AA 6061-T651 under consideration[16,30].

Materials	$\boldsymbol{\sigma'_f}$	$\boldsymbol{b}$	$\boldsymbol{\varepsilon'_f}$	$\boldsymbol{c}$
-	[MPa]	[-]	[-]	[-]
AA 6061-T651	394	-0.0453	0.8680	-0.7745

Source: Prepared by the author.

Figure 6.1 - Strain-life data of AA 6061-T651 – Experimental data vs. deterministic curve.

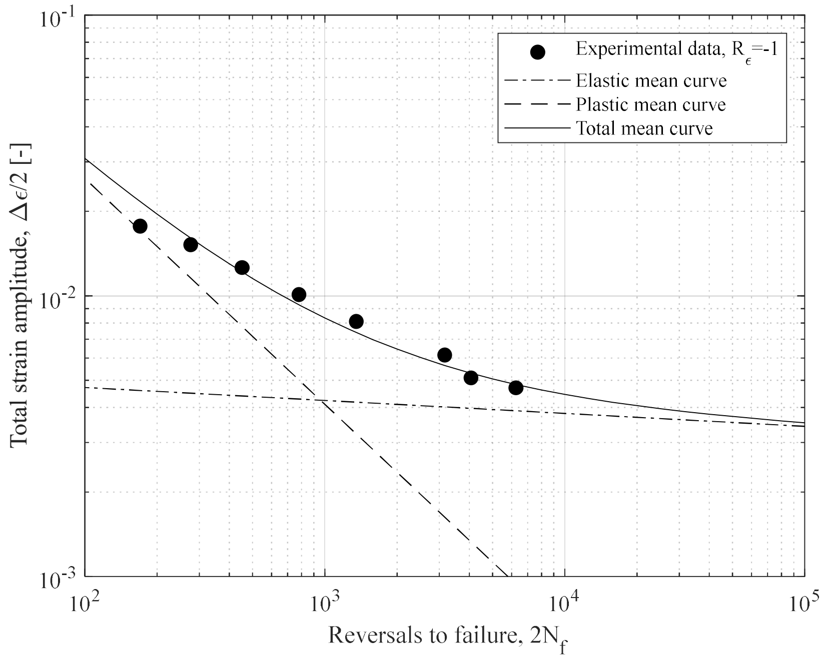

Source: Prepared by the author.

6.2.3 Fatigue crack growth data

The fatigue crack propagation curves for the 6061-T651 aluminium alloy were collected from the literature[16,30]. According to Ribeiro[47], the Compact Tension (CT) specimens with a thickness B=10 mm and nominal width W=50 mm were used. The specimen dimensions and the fatigue crack propagation tests were performed according to the ASTM E647 standard[48]. The deterministic curves for the fatigue crack propagation, da/dN versus ΔK, were fitted to the experimental data through the Paris law[1]:

$$\frac{da}{dN} = C \cdot \Delta K^m \tag{6.3}$$

where, da/dN is the fatigue crack growth rate, ΔK is the applied stress intensity factor range, C and m are the Paris constants (material parameters).

In Figure 6.2, the experimental data and deterministic curves describing the fatigue crack propagation behaviour for the 6061-T651 aluminium alloy, for two stress R-ratios equal to 0.1 and 0.5, are presented. The crack growth rates, da/dN, *versus* the applied stress intensity factor range, ΔK, can be satisfactorily described by the Paris law[1], individually for each stress ratio, where is influenced by these stress R-ratios.

Figure 6.2 - Fatigue crack propagation behaviour of AA 6061-T651 – Experimental data vs. deterministic curve.

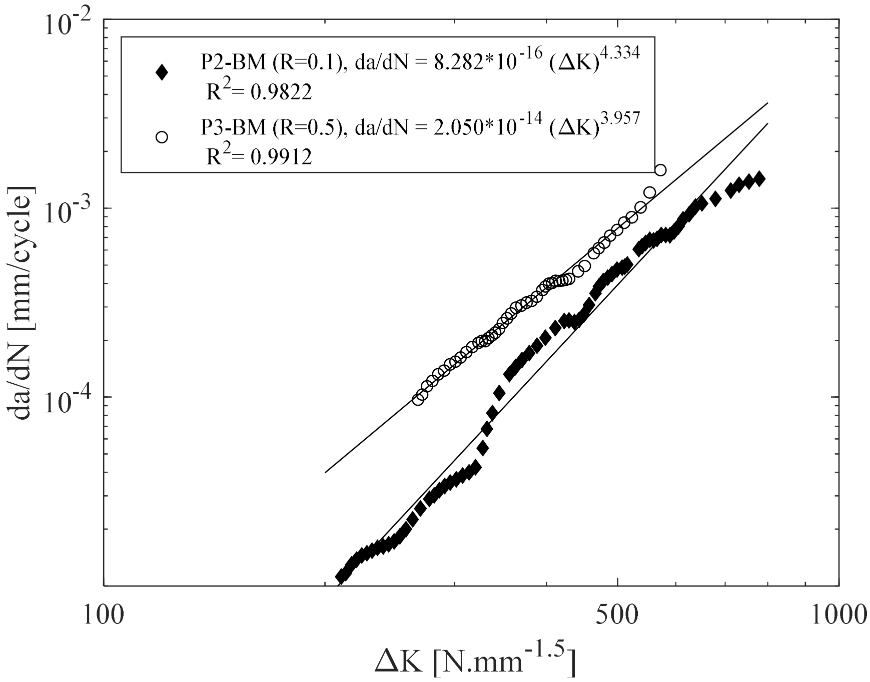

Source: Prepared by the author.

6.3 FATIGUE CRACK GROWTH MODELLING: APPLICATION AND DISCUSSION

In this section, the fatigue crack growth (FCG) modelling based on the strain energy density approach proposed by Huffman[35] for the AA 6061-T651 is done. For the FCG modelling, the critical dislocation density (ρ_c) driven by the highest strain amplitude specimen and the mean value of the dislocation density (ρ_m) for the available experimental fatigue results, including the residual stress effects as suggested by Huffman[35] and Noroozi et al.[23-25], are applied and discussed.

The Huffman fatigue crack growth modelling is based on the cyclic stress-strain properties and fatigue local damage criteria (e.g. strain-life, SWT-life, etc.), where the actual elastoplastic stresses and strains, ahead of the crack tip, are computed using the Neuber's or Glinka's approach[41,49]. The Huffman's fatigue damage model is given by

$$\left(\frac{U_e}{U_d\rho_c}\right)\left(\frac{U_p^*}{U_d\rho_c}\right) = D = \frac{2N}{2N_f} \quad (6.4)$$

where:

U_e is the elastic strain energy density;

U_p^* is the complementary plastic strain energy density;

U_d is the strain energy density from dislocations; and,

ρ_c is the critical dislocation density.

The strain energy from dislocations, U_d, can be given by

$$U_d = \left(\frac{E}{2(1+\upsilon)}\right) \cdot \left|\vec{b}\right|^2 \tag{6.5}$$

where:

υ is the Poisson's ratio; and,

$\vec{b}$ is the Burger's vector.

The $\left|\vec{b}\right|$ value for aluminium alloys or similar metals is equal to 2.86×10^{-10} m, as recommended by ref.[35].

The strain energy density, by integrating the stress-strain relation proposed by Ramberg-Osgood[43] gives the damage criterion equation in terms of materials parameters, can be described by the following equation:

$$\left(\frac{2}{U_d^2 \rho_c^2 E}\right)\left(\frac{n'}{1+n'}\right)\left(\frac{1}{K'}\right)^{(1/n\prime)} ({\sigma_{max}}^2)(\sigma_a)^{\frac{1+n\prime}{n\prime}}\left(\frac{1}{\mathrm{N}}\right) = D = \frac{1}{2N_f} \tag{6.6}$$

where, σ_{max} is the maximum stress, σ_a is the stress amplitude, E is the elastic modulus, K' and n' are the cyclic strength coefficient and cyclic strain hardening exponent, respectively.

The value of the critical dislocation density, driven by the highest strain amplitude specimen as proposed by Huffman[35], for the AA 6061-T651 was found equal to $\rho_c = 5.9 \times 10^{15}$ m^{-2} [42], according to Ribeiro et al.[42,47]. The critical dislocation density was determined by

$$\rho_c = \sqrt{\left(\frac{2(2N_f)}{U_d^2 E N}\right)\left(\frac{n'}{1+n'}\right)\left(\frac{1}{K'}\right)^{(1/n\prime)} \times ({\sigma_{max}}^2)(\sigma_a)^{\left(\frac{1+n\prime}{n\prime}\right)}}. \tag{6.7}$$

Alternatively, the dislocation density, ρ, for each tested specimen can be calculated according to Equation (6.7). The mean value of dislocation density, $\mu(\rho)$, is given by

$$\mu(\rho) = \frac{1}{n}\sum_{i=1}^{n} \rho_i \tag{6.8}$$

where, n is the number of tested specimens, and ρ_i is the dislocation density for each tested specimen given by

$$\rho_i = \sqrt{\left(\frac{2(2N_{f,i})}{U_d^2 E N_i}\right)\left(\frac{n'}{1+n'}\right)\left(\frac{1}{K'}\right)^{(1/n\prime)} \times \left({\sigma_{max,i}}^2\right)\left(\sigma_{a,i}\right)^{\left(\frac{1+n\prime}{n\prime}\right)}}. \tag{6.9}$$

where, N_i is the number of cycles for the tested specimen i, $2N_{f,i}$ is the number of reversals for the tested specimen i, $\sigma_{max,i}$ is the maximum stress obtained during the low-cycle fatigue tests for the tested specimen i, and $\sigma_{a,i}$ is the stress amplitude obtained during the low-cycle fatigue tests for the tested specimen i. Ribeiro et al.[42] estimated the mean value of the critical dislocation density, for the experimental low-cycle fatigue data available, as being equal to $\rho_c = 6.088 \times 10^{15}$ m^{-2}.

The Huffman fatigue crack growth rates using the Δa as a calibrator parameter can be given by

$$\left(\frac{\Delta a}{U_d^2 \rho_c^2}\right)\left(\frac{n'}{1+n'}\right)\left(\frac{1}{K'}\right)(\sigma_{max}{}^2)(\sigma_a)^{\left(\frac{1+n\prime}{n\prime}\right)} = \frac{\Delta a}{N_f - 0} \approx \frac{da}{dN} \tag{6.10}$$

In Equation (6.10), the stresses, σ_a and σ_{max}, are the local stress amplitude and maximum stress over each material block ahead of the crack tip that can be related to the load, geometry, and fatigue crack growth parameters. These local stresses can be calculated by Neuber[41] or Glinka[49] rules and Ramberg-Osgood description[43] combined with Creager-Paris solutions[50] as proposed by Noroozi et al.[23-25]. The fatigue crack growth rate considering the driving force is given by Equation (6.11).

$$\frac{da}{dN} = C(\Delta\kappa)^{\gamma} \tag{6.11}$$

In Equation (6.11), γ is the fatigue crack growth rate exponent, $\Delta\kappa$ is the fatigue crack growth driving force, and C is the fatigue crack growth rate coefficient that can be calculated by Equation (6.12).

$$C = \left(\frac{\Delta a}{U_d^2 \rho_c^2}\right)\left(\frac{n'}{1+n'}\right)(K')^{\frac{2}{1+n\prime}}(E)^{-\left(\frac{4n'+2}{n'+1}\right)}\left(\frac{1}{2}\right)^{\frac{1}{n\prime}}\left(\frac{1}{2\pi x}\right)^{\frac{1+3n\prime}{1+n\prime}} \tag{6.12}$$

The fatigue crack growth driving force, $\Delta\kappa$, can be calculated by

$$\Delta\kappa = K_{max}^{p}(\Delta K)^{1-p} \tag{6.13}$$

$$K_{max} = K_{max,applied} + K_r \tag{6.14}$$

$$\Delta K_{tot} = \Delta K_{applied} + K_r \tag{6.15}$$

$$p = \frac{2n'}{1+3n'} \tag{6.16}$$

$$\gamma = \frac{2+6n'}{1+n'} = \frac{-2}{b+c} \tag{6.17}$$

where, ΔK_{tot} is the total stress intensity factor range, ΔK is the total minimum stress intensity factor, $\Delta K_{applied}$ is the applied stress intensity factor range, $K_{max,applied}$ is the maximum applied stress intensity factor, and K_r is the residual stress intensity factor. The adjustment of the Huffman fatigue crack growth model to the experimental results is made using the values of Δa and x as calibration parameters. The residual stress intensity factor, K_r , can be estimated by integrating the residual stress distribution, $\sigma_r(x)$, estimated for unloading reversals, by using the weight function method[51], $m(x,a)$, as given by Equation (6.18).

$$K_r = \int_0^a \sigma_r(x) \cdot m(x,a)\, dx \tag{6.18}$$

The relationship between the total stress intensity factor range, ΔK_{tot}, and the applied stress intensity factor range, $\Delta K_{applied}$, instead of crack size, where are included the residual stress effects, can be estimated analytical as recommended by Huffman[35] and Noroozi et al.[23-25], or numerically as suggested by Correia et al.[27-32].

In section 6.3.1, an elastoplastic stresses analysis ahead of the crack tip through analytical solutions based on Neuber[41] or Glinka's[49] approaches combined with Creager-Paris solutions[50], according to Noroozi et al.[23-25], and numerical solutions using the finite element modelling (FEM) under loading and unloading reversals, as suggested by Correia et al.[27-32], is presented and discussed.

In Section 6.3.2, the fatigue crack growth modelling through the Huffman strain energy density approach considering the Neuber rule-based residual stress effects (suggested by Noroozi et al.[23-25]) was applied and discussed.

In Section 6.3.3, the fatigue crack growth behaviour for the AA 6061-T651 based on strain energy density approach proposed by Huffman[35], where the residual stress effects are given by Huffman recommendations[35], was also obtained. In both sections, the critical dislocation density, ρ_c, driven by the highest strain amplitude specimen and the mean value of the dislocation density (ρ_m) for the available experimental fatigue results, were also considered in the analysis.

6.3.1 Stresses and strains near the crack tip

The analysis of elastoplastic strains and stresses at the crack tip for the CT geometry can be done using the analytical solutions based on Neuber[41] or Glinka's[49] approaches combined with Creager-Paris solutions[50], according to Noroozi et al.[23-25].

Alternatively, numerical solutions using the finite element modelling (FEM) under loading and unloading reversals, as suggested by Correia et al.[27-32], where a comparison between the numerical and analytical solutions of the elastoplastic stress distribution from the crack tip was presented. For these analyses, input data such as the material properties, loads, dimensions of the CT specimen, the initial and final crack size, are needed.

The residual stress distribution ahead of the crack front was estimated, where the stresses were computed at points equally spaced[30]. The discretization thorough small elements (material block size of 2E-5 m suggested by Correia et al.[30]) on the residual stress distribution, given by weight function methods, is needed to compute the residual stress intensity factor.

The simplified elastoplastic analysis through a bi-dimensional finite element model of the CT specimen, as suggested by Correia et al.[30], was also done. Figure 6.3 illustrates the finite element mesh of the CT geometry, including the boundary conditions. In the numerical simulation, only ½ of the CT geometry is modelled, where was taken into account the existing symmetry plane under plane stress conditions. The load was applied at a node located in the geometrical centre of the pin, using the rigid-to-flexible contact with a friction coefficient equal to 0.3. The cyclic elastoplastic behaviour was considered using the Ramberg-Osgood description whose constants are given in Table 6.1. Six node quadratic plane elements were adopted in the finite-element analyses. More details about the numerical simulation can be found in refs.[27-32]. The two stress R-ratios, 0.1 and 0.5, with a sequence of two load steps – loading and unloading reversals (maximum load of 3309.2 N) – were considered.

In Figure 6.4, a comparison of numerical and analytical elastoplastic stress distributions (σ_{xx}, σ_{yy}) for the CT geometry with a crack size of 10mm and R=0.1 is done. The analytical elastoplastic distributions were estimated based on Neuber and Glinka's approaches. A good agreement between numerical results and analytical results is found.

In Figure 6.5, the same comparison is made for stress R-ratio equal to 0.5. The numerical elastoplastic stress distribution results agree satisfactorily with the analytical results based on Neuber and Glinka's approaches.

In Figure 6.6, a comparison of numerical and analytical residual stress distributions (y direction) for the CT geometry with a crack size of 10mm under two distinct stress ratios, 0.1 and 0.5, is presented.

The numerical model predicts a narrower compressive stress distribution when compared with the analytical results based on Neuber and Glinka's approaches. Therefore, the compressive stress distribution is sensitive to the stress R-ratio and more localized when it increases (R=0.5), which makes the residual stress intensity factor tend to 0. These results are aligned with the conclusions obtained by Noroozi et al. [23-25] and Correia et al.[27-32].

Figure 6.3 - Finite element mesh of the CT specimen: a) global mesh and boundary conditions; b) zoom of the mesh around the crack tip.

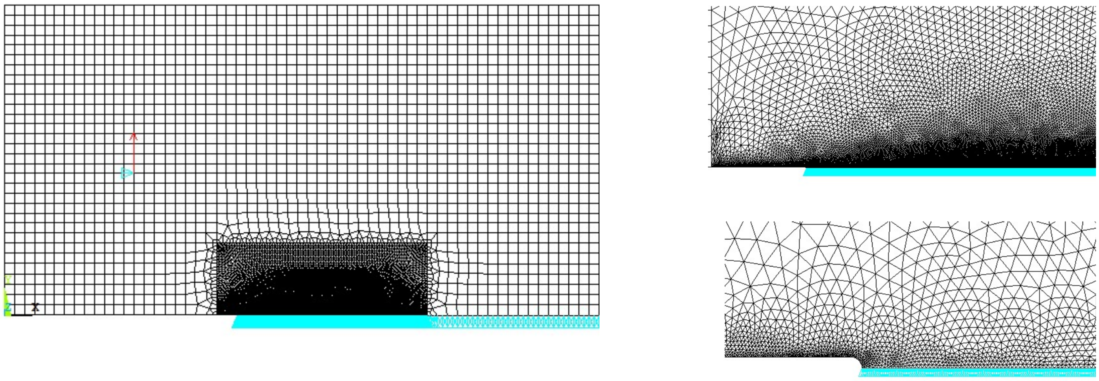

a) b)

Source: Prepared by the author.

Figure 6.4 - Comparison of numerical and analytical elastoplastic stress distributions for the CT geometry with $a = 10$mm and $R = 0.1$: a) σ_{yy}; b) σ_{xx}.

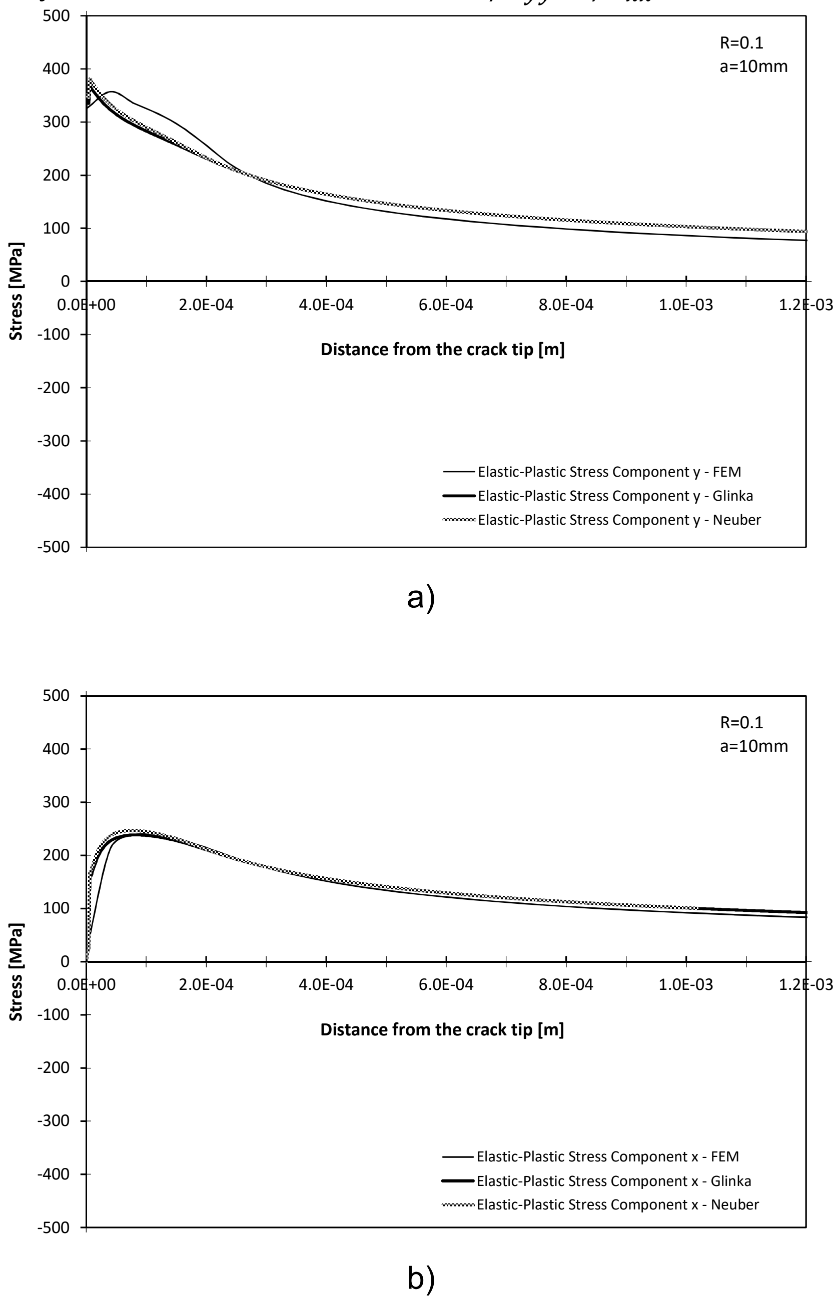

Source: Prepared by the author.

Figure 6.5 - Comparison of numerical and analytical elastoplastic stress distributions for the CT geometry with $a = 10$mm and $R = 0.5$: a) σ_{yy}; b) σ_{xx}.

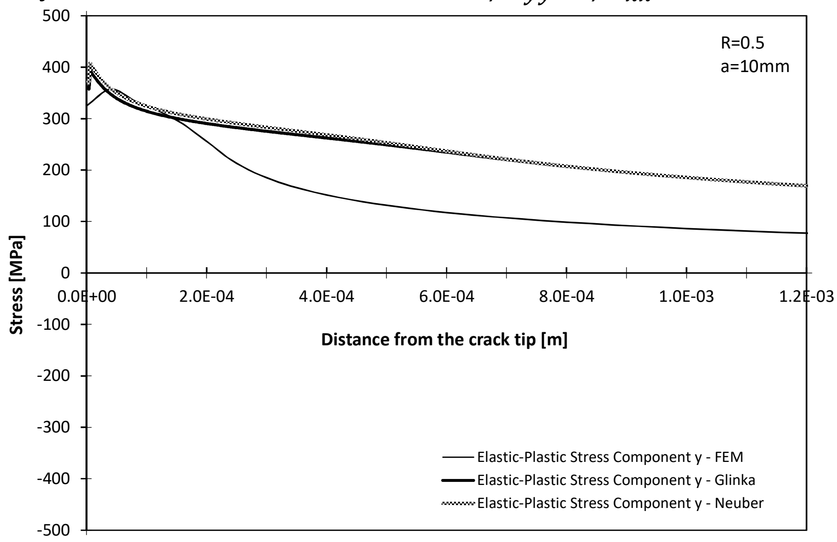

a)

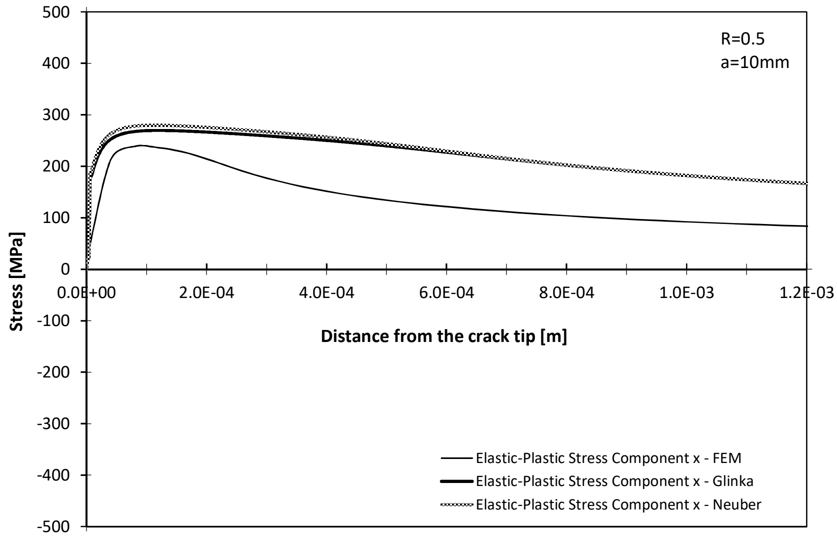

b)

Source: Prepared by the author.

Figure 6.6 - Comparison of numerical and analytical residual stress distributions for the CT geometry under two distinct stress ratios: a) $R = 0.1$; b) $R = 0.5$.

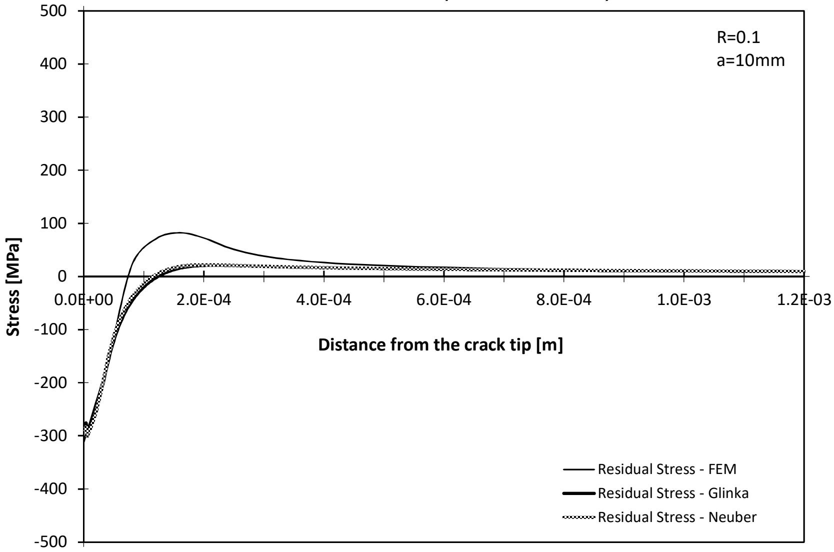

a)

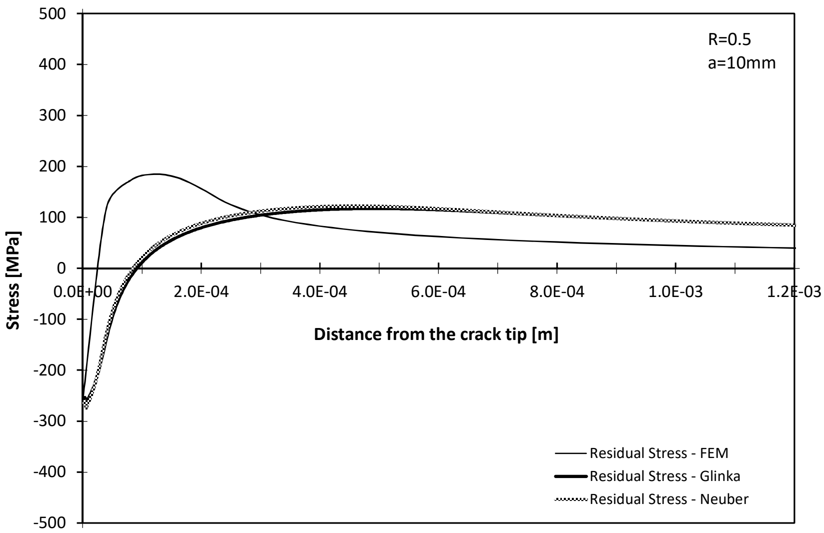

b)

Source: Prepared by the author.

6.3.2 **Strain energy density model considering the Neuber rule-based residual stress** effects

In this section, the modelling of the fatigue crack growth behaviour through the strain energy density approach proposed by Huffman[35] (Equations (6.4)-(6.18)) considering the Neuber rule-based residual stress effects (suggested by Noroozi et al.[23-25]) was done. In this research work, the values of the critical dislocation density (ρ_c) estimated by Ribeiro et al.[42], driven by the highest strain amplitude specimen

(Equation (6.7)) and the mean value of the dislocation density (ρ_m) for the available experimental fatigue results (Equations (6.8)-(6.9)), to be used in the Huffman strain energy density approach to generate the fatigue crack propagation behaviour, were also considered in this investigation.

In Figure 6.7, the relationship between ΔK_{tot} and $\Delta K_{applied}$ for the CT geometry made of Al 6061-T651 using Neuber rule-based residual stress effects (Equation (6.18)), to be used in the modelling of the fatigue crack growth behaviour based on Huffman strain energy density approach, is presented.

Thus, the fatigue crack propagation modelling for both stress R-ratios is generated based on the strain energy density approach proposed by Huffman[35] and considering the relation obtained between the total stress intensity range, ΔK_{tot}, and the applied stress intensity range, $\Delta K_{applied}$ (Figure 6.7), estimated by the Neuber rule, and still using the values of the critical dislocation density (ρ_c), driven by the highest strain amplitude specimen and the mean value of the dislocation density (ρ_m) for the available experimental fatigue results, respectively, Figures 6.8 and 6.9. In Table 6.3, the fatigue crack growth constants determined by the strain energy density model application (Equations (6.4)-(6.17)) considering the Neuber rule-based residual stress effects are shown. Thus, in the modelling of the fatigue crack propagation behaviour, it is concluded that the use of critical dislocation density values of $5.90E + 15$ and $6.088E + 15$ does not have an influence that can be said to be significant.

Table 6.3 - Fatigue crack growth constants - Strain energy density model considering the Neuber rule-based residual stress effects.

$\boldsymbol{\rho_c}$ [m/m^3]	$\boldsymbol{U_d}$ [MPa]	$\Delta\boldsymbol{a}$ [m]	$\boldsymbol{x}$ [m]	$\boldsymbol{C}$ [$\boldsymbol{MPa^{\gamma} m^{\gamma/2-1}}$]	$\boldsymbol{\gamma}$ [-]	$\boldsymbol{p}$ [-]
5.90E+15	2.06E-15	1.25E-04	1.63E-05	5.39E-13	2.2146	0.0969
6.088E+15	2.06E-15	1.35E-04	1.63E-05	5.47E-13	2.2146	0.0969

Source: Prepared by the author.

Figure 6.7 - ΔK_{tot} vs. $\Delta K_{applied}$ for the CT geometry made of Al 6061-T651 using Neuber rule, as suggested by Noroozi et al.[23-25].

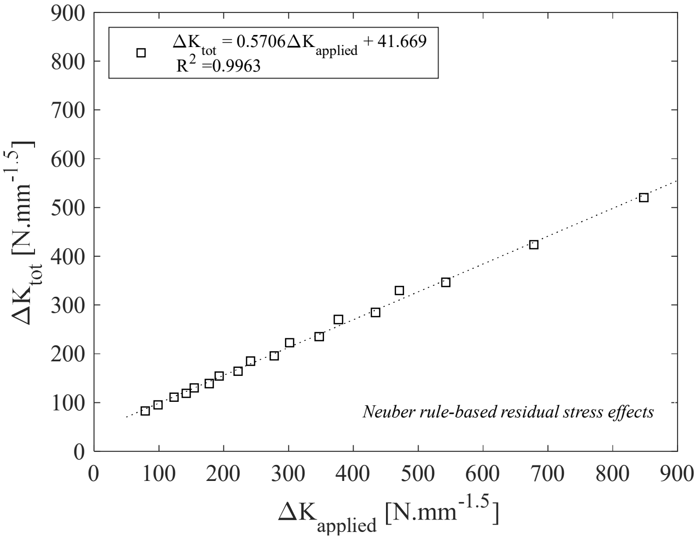

Source: Prepared by the author.

Figure 6.8 - Fatigue propagation behaviour of Al 6061-T651 – Experimental data vs. Strain energy density model considering the Neuber rule-based residual stress effects ($\rho_c = 5.90E + 15$ m/m³).

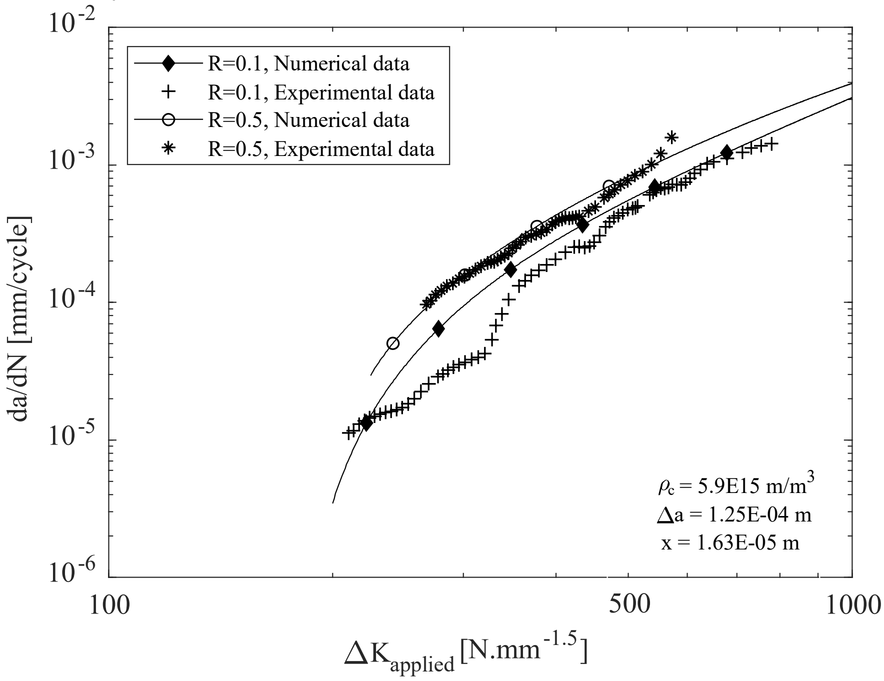

Source: Prepared by the author.

Figure 6.9 - Fatigue propagation behaviour of Al 6061-T651 – Experimental data vs. Strain energy density model considering the Neuber rule-based residual stress effects ($\rho_c = 6.088E + 15$ m/m^3).

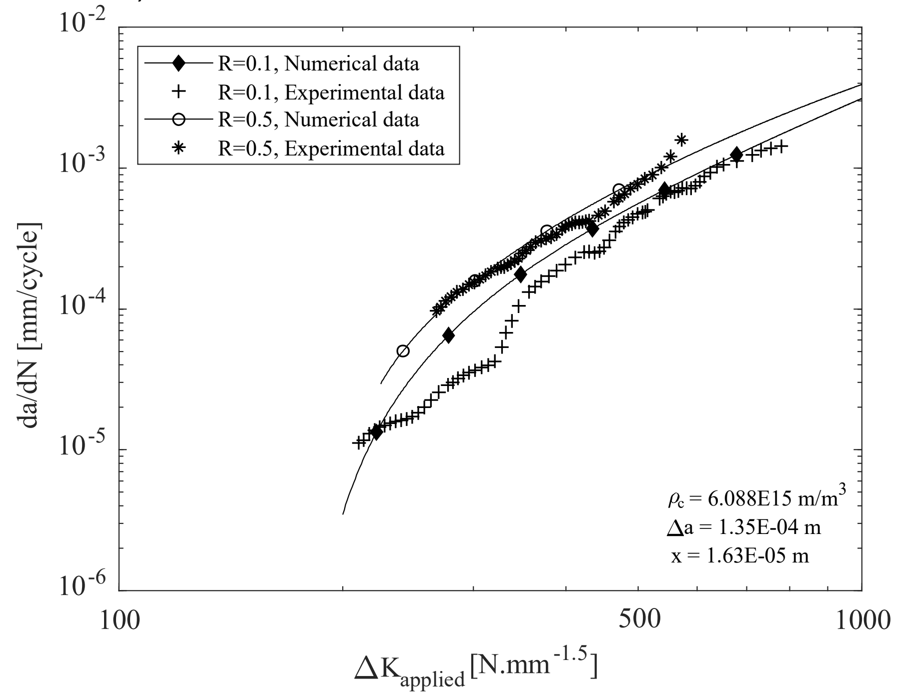

Source: Prepared by the author.

6.3.3 Strain energy density model considering the Huffman residual stress effects

In this section, the modelling of the fatigue crack growth behaviour through the strain energy density approach (Equations (6.4)-(6.17)) considering the Huffman residual stress effects (Equation (6.19)) was done. In this research work, the values of the critical dislocation density (ρ_c), driven by the highest strain amplitude specimen (Equation (6.7)) and the mean value of the dislocation density (ρ_m) for the available experimental fatigue results (Equations (6.8)-(6.9)), to be used in the Huffman strain energy density approach to generate the fatigue crack propagation behaviour, were also considered for discussion. These values of critical dislocation density were estimated by Ribeiro et al.[42].

The residual stress effects from the plastic strains ahead of the crack tip, for positive stress ratios, as suggested by Huffman[35], can be given by

$$K_{tot} \approx K_{applied}\left(1 - \left(\frac{\sigma_{\varepsilon_p=0.05} - \sigma_{\varepsilon_p=0.001}}{\sigma_{\varepsilon_p=0.05}}\right)(1-R)\right) \tag{6.19}$$

where, K_{tot} is the total stress intensity factor, $K_{applied}$ is the applied stress intensity factor, $\sigma_{\varepsilon_p=0.05}$ is the stress at 0.05 plastic strain, $\sigma_{\varepsilon_p=0.001}$ is the stress at 0.001 plastic strain, and R is the stress ratio. According to Huffman[35], K_{max} and ΔK use K_{tot}, with which they incorporate the residual stress estimation.

In Figure 6.10, the relationship between ΔK_{tot} and $\Delta K_{applied}$ for the CT geometry made of Al 6061-T651 using the residual stress effects suggested by Huffman[35], Equation (6.19), to be used in the modelling of the fatigue crack growth behaviour based on Huffman strain energy density approach (Equations (6.4)-(6.17)), is presented.

Thus, the fatigue crack propagation modelling for both stress R-ratios is generated based on the strain energy density approach proposed by Huffman[35] and considering the residual stress effects as suggested by Huffman[35] and given by Equation (6.19). In this evaluation, the values of the critical dislocation density (ρ_c), driven by the highest strain amplitude specimen (Equation (6.7)) and the mean value of the dislocation density (ρ_m) for the available experimental fatigue results (Equations (6.8)-(6.9)), were cons, In Figures 6.11 and 6.12, the fatigue propagation behaviour of the 6061-T651 aluminium alloy for ρ_c equal to $5.90E + 15$ and $6.088E + 15$, respectively, are presented. In these Figures, the experimental FCG data are compared with the fatigue crack growth behaviour based on the strain energy density model considering the Huffman residual stress effects. In Table 6.4, the fatigue crack growth constants determined from the strain energy density model application considering the residual stress effects, as suggested by Huffman[35], are presented. It is verified that the fatigue crack propagation behaviour doesn't exhibit an influence significantly to the critical dislocation density values of $5.90E + 15$ and $6.088E + 15$ m^{-2}.

Figure 6.10 - ΔK_{tot} vs. $\Delta K_{applied}$ for the CT geometry made of Al 6061-T651 using Huffman residual stress effects.

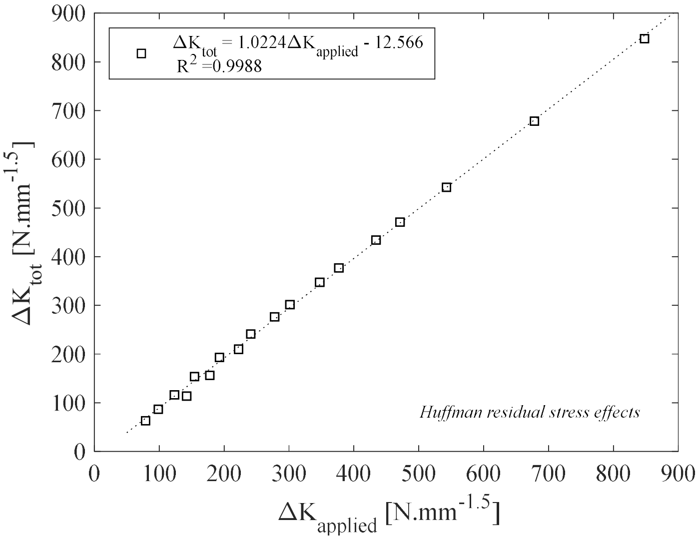

Source: Prepared by the author.

Table 6.4 - Fatigue crack growth constants - Strain energy density model considering the Huffman residual stress effects.

ρ_c [m/m³]	U_d [MPa]	Δa [m]	x [m]	C [$MPa^{\gamma}m^{\gamma/2-1}$]	γ [-]	p [-]
5.90E+15	2.06E-15	3.25E-05	1.75E-05	1.52E-13	2.2146	0.0969
6.088E+15	2.06E-15	3.50E-05	1.75E-05	1.53E-13	2.2146	0.0969

Source: Prepared by the author.

Figure 6.11 - Fatigue propagation behaviour of Al 6061-T651 – Experimental data vs. Strain energy density model considering the Huffman residual stress effects ($\rho_c = 5.90E + 15$ m/m³).

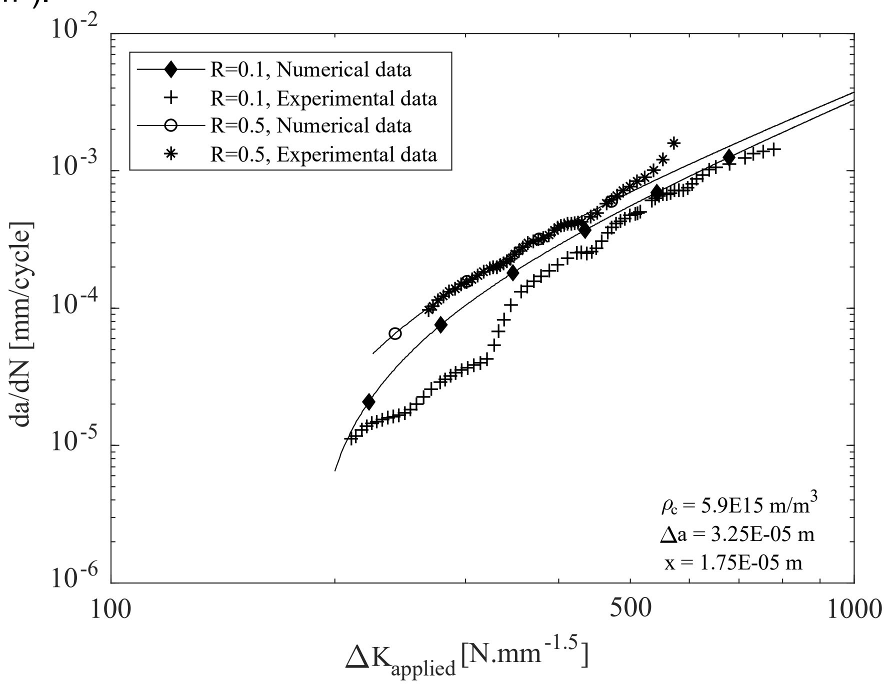

Source: Prepared by the author.

Figure 6.12 - Fatigue propagation behaviour of Al 6061-T651 – Experimental data vs. Strain energy density model considering the Huffman residual stress effects ($\rho_c = 6.088E + 15$ m/m^3).

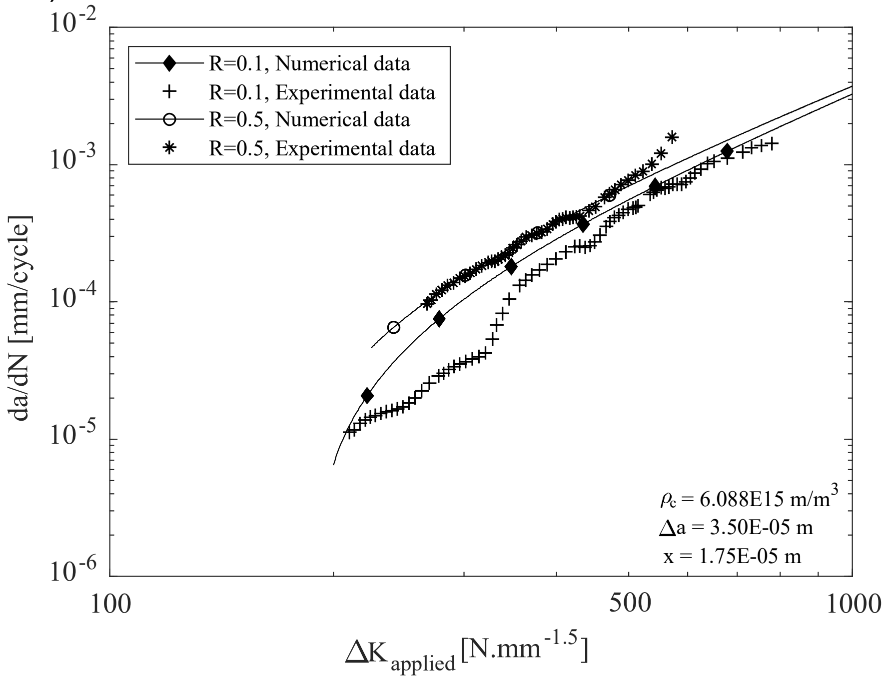

Source: Prepared by the author.

6.4 CONCLUSIONS

In this research, the fatigue crack growth modelling for the 6061-T651 aluminium alloy supported by the strain energy density-based Huffman approach considering the residual stress effects ahead of the crack tip is generated and discussed. The residual stress effects as suggested by Noroozi et al.[23-25] and Correia et al.[27-32], respectively, estimated by analytical and numerical solutions, were implemented in this study. The analytical procedure to estimate the residual stresses is based on the Neuber rule combined with Creager-Paris solutions. Another approach suggested by Huffman[35] were also studied. In this study, the fatigue crack propagation behaviour of the 6061-T651 aluminium alloy, for values of critical dislocation density driven by the highest strain amplitude specimen and the mean value of the dislocation density for the available experimental fatigue results, was also explored.

An elastoplastic stress/strain analytical analysis at the crack tip region based on the multiaxial Neuber and Glinka's rules was assumed, where the both approaches revelled similar elastoplastic stress distributions. Additionally, a comparison on the elastoplastic stress distributions between the numerical results from the finite element modelling of the CT specimen and the analytical results based on Neuber and Glinka's rules was done. A good agreement for the maximum elastoplastic stresses was found.

The comparison on the residual stress distributions between numerical and analytical solutions showed deviations that increase for a stress ratio equal 0.5, revelling that the analytical solutions overestimate the residual stresses.

For values of critical dislocation density of 5.90E+15 and 6.088E+15 m^{-2}, both modelling analyses of the fatigue crack propagation behaviour based on the strain energy density approach, considering the residual stress effects estimated by Neuber rule or Huffman suggestion, exhibited very similar results. The critical dislocation density, driven by the highest strain amplitude specimen or by mean value of the dislocation density for the available experimental fatigue results, does not influence significantly the fatigue crack propagation behaviour modelled by the strain energy density approach.

For both procedures to consider the residual stress effects, Neuber rule and Huffman suggestion, the fatigue crack growth constants obtained from the modelling based on the strain energy density approach are very similar with the exception of the Δa calibration parameter. It is concluded that the procedure for considering the residual stress effects influences the Δa calibrator. Therefore, it is not possible to conclude which is the most recommended method to describe the residual stress effects, since there is no measured data to support such analysis.

The used approach allows to model the fatigue crack propagation behaviour for the near-threshold and Paris regions.

In future studies, the residual stress effects need to be determined experimentally by digital image correlation, where the stresses and strains ahead of the crack tip for some crack sizes and different stress ratios can be estimated. This analysis will be used to understand what residual stress approaches (Noroozi or Huffman suggestions) are more suitable to model the fatigue crack propagation behaviour. Therefore, the fatigue crack propagation calibration parameters (Δa, x) to be estimated by applying the approach based on the Huffman strain energy density may be seen to be representative of the metals under study. Another aspect to be explored is perhaps the probabilistic fatigue crack propagation modelling using the strain energy density approach through a stochastic analysis, where the parameters of the cyclic stress-strain curve, mainly the cyclic strain hardening coefficient (K'), are described by probability density functions.

REFERENCES

1 PARIS, P.; ERDOGAN, F. A critical analysis of crack propagation laws. **Journal of Fluids Engineering**, New York, v. 85, n. 4, p. 528-533, 1963.

2 DOWLING, N.E. **Mechanical Behaviour of Materials**. Engineering Methods for Deformation, Fracture and Fatigue. 3 ed. London: Pearson Prentice Hall, 2007.

3 FORMAN, R.G. Study of fatigue crack initiation from flaws using fracture mechanics theory. **Engineering Fracture Mechanics**, Oxford, v. 4, n. 2, p. 333-345, 1972.

4 HARTMAN, A.; SCHIJVE, J. The effects of environment and load frequency on the crack propagation law for macro fatigue crack growth in aluminium alloys. **Engineering Fracture Mechanics**, Oxford, v. 1, n. 4, p. 615-631, 1970.

5 BEDEN, S.M.; ABDULLAH, S.; ARIFFIN, A.K. Review of fatigue crack propagation models for metallic components. **European Journal of Scientific Research**, Victoria, v. 28, n. 3, p. 364-397, 2009.

6 ALVES, A.S.F.; SAMPAYO, L.M.C.M.V.; CORREIA, J.A.F.O.; DE JESUS, A.M.P.; MOREIRA, P.M.G.P.; TAVARES, P.J.S. Fatigue Life Prediction Based on Crack Growth Analysis Using an Equivalent Initial Flaw Size Model: Application to a Notched Geometry. **Procedia Engineering**, Amsterdam p. 730, 2015.

7 CASTILLO, E.; FERNÁNDEZ-CANTELI, A.; SIEGELE, D. Obtaining S-N curves from crack growth curves: An alternative to self-similarity. **International Journal of Fracture**, Dordrecht, v. 187, n. 1, p. 159-172, 2014.

8 DOWLING, N.E.; BEGLEY, J.A. Fatigue crack growth during gross plasticity and the Jintegral, Mechanics of Crack Growth. **American Society for Testing and Materials Special Technical Publication,** Philadelphia, v. 590, p. 82–105, 1976.

9 CORREIA, J.A.F.O.; DE JESUS, A.M.P.; FERNÁNDEZ-CANTELI, A.; BRIGHENTI, R.; MOREIRA, P.M.G.P.; CALÇADA, R.A.B. A procedure to obtain the probabilistic kitagawa-takahashi diagram. **UPB Scientific Bulletin, Series D: Mechanical Engineering**, Bucharest, v. 78, n. 1, p. 3-12, 2016.

10 CORREIA, J.A.F.O.; BLASÓN, S.; DE JESUS, A.M.P.; CANTELI, A.F.; MOREIRA, P.M.G.P.; TAVARES, P.J. Fatigue life prediction based on an equivalent initial flaw size approach and a new normalized fatigue crack growth model. **Engineering Failure Analysis**, Oxford, v. 69, p. 15-28, 2016.

11 ELBER, W. Fatigue crack closure under cyclic tension. **Engineering Fracture Mechanics**, Oxford, v. 2, n. 1, p. 37-44, 1970.

12 ELBER, W. The significance of fatigue crack closure. **American Society for Testing and Materials Special Technical Publication**, Philadelphia, v. 486, p. 230–242, 1971.

13 HUDAK, S.J.; DAVIDSON, D.L. The dependence of crack closure on fatigue loading variables. **American Society for Testing and Materials Special Technical Publication**, Philadelphia, v. 982, p. 121-138, 1988.

14 ELLYIN, F. **Fatigue damage, crack growth and life prediction**. 1. ed. London: Chapman; Hall, 1997

15 CORREIA, J.A.F.O.; DE JESUS, A.M.P.; MOREIRA, P.M.G.P.; TAVARES, P.J.S. Crack closure effects on fatigue crack propagation rates: application of a proposed theoretical model. **Advances in Materials Science and Engineering**, Oxford, v. 2016, 2016.

16 RIBEIRO, V.; CORREIA, J.; LESIUK, G.; GONÇALVES, A.; DE JESUS, A.; BERTO, F. Application and discussion of various crack closure models to predict fatigue crack growth in 6061-T651 aluminium alloy. **International Journal of Fatigue**, London, v. 153, 2021.

17 NEWMAN JR, J.C.; A crack opening stress equation for fatigue crack growth. **International Journal of Fracture**, Dordrecht, v. 24, n. 4, p. R131-R135, 1984.

18 VORMWALD, M.; SEEGER, T. The consequences of short crack closure on fatigue crack growth under variable amplitude loading. **Fatigue; Fracture of Engineering Materials; Structures**, Chichester, v. 14, n. 2-3, p. 205-225, 1991.

19 SAVAIDIS, G.; DANKERT, M.; SEEGER, T. An analytical procedure for predicting opening loads of cracks at notches. **Fatigue; Fracture of Engineering Materials; Structures**, Chichester, v. 18, n. 4, p. 425-442, 1995.

20 CORREIA, J.A.F.O.; BLASÓN, S.; ARCARI, A.; CALVENTE, M.; APETRE, N.; MOREIRA, P.M.G.P.; DE JESUS, A.M.P.; CANTELI, A.F. Modified CCS fatigue crack growth model for the AA2019-T851 based on plasticity-induced crack-closure. **Theoretical and Applied Fracture Mechanics**, Amsterdam, v. 85, p. 26-36, 2016.

21 GLINKA, G. A notch stress-strain analysis approach to fatigue crack growth. **Engineering Fracture Mechanics**, Oxford, v. 21, n. 2, p. 245-261, 1985.

22 PEEKER, E.; NIEMI, E. Fatigue crack propagation model based on a local strain approach. **Journal of Constructional Steel Research**, London, v. 49, n. 2, p. 139-155,1999.

23 NOROOZI, A.H.; GLINKA, G.; LAMBERT, S. A two parameter driving force for fatigue crack growth analysis. **International Journal of Fatigue**, London, v. 27, n. 10-12, p. 1277-1296, 2005.

24 NOROOZI, A.H.; GLINKA, G.; LAMBERT, S. A study of the stress ratio effects on fatigue crack growth using the unified two-parameter fatigue crack growth driving force. **International Journal of Fatigue**, London, v. 29, n. 9-11, p. 1616-1633, 2007.

25 NOROOZI, A.H.; GLINKA, G.; LAMBERT, S. Prediction of fatigue crack growth under constant amplitude loading and a single overload based on elasto-plastic crack

tip stresses and strains. **Engineering Fracture Mechanics**, Oxford, v. 75, n. 2, p. 188-206, 2008.

26 HURLEY, P.J.; EVANS, W.J. A methodology for predicting fatigue crack propagation rates in titanium based on damage accumulation. **Scripta Materialia**, Oxford, v. 56, n. 8, p. 681-684, 2007.

27 CORREIA, J.A.F.O.; JESUS, A.M.P.D.; FERNÁNDEZ-CANTELI, A. A procedure to derive probabilistic fatigue crack propagation data. **International Journal of Structural Integrity**, Bingley, v. 3, n. 2, p. 158-183, 2012.

28 CORREIA, J.A.F.O.; DE JESUS, A.M.P.; FERNÁNDEZ-CANTELI, A. Local unified probabilistic model for fatigue crack initiation and propagation: Application to a notched geometry. **Engineering Structures**, Oxford, v. 52, p. 394-407, 2013.

29 CORREIA, J.A.F.O.; DE JESUS, A.M.P.; FERNÁNDEZ-CANTELI, A.; CALÇADA, R.A.B. Modelling probabilistic fatigue crack propagation rates for a mild structural steel. **Frattura ed Integrita Strutturale**, Cassino, v. 31, p. 80-96, 2015.

30 CORREIA, J.A.F.O.; DE JESUS, A.M.P.; RIBEIRO, A.S.; FERNANDES, A.A. Strain-based approach for fatigue crack propagation simulation of the 6061-T651 aluminium alloy. **International Journal of Materials and Structural Integrity**, Geneva, v. 11, n. 1-3, p. 1-15, 2017.

31 CORREIA, J.A.F.O.; HUFFMAN, P.J.; DE JESUS, A.M.P.; CICERO, S.; FERNÁNDEZ-CANTELI, A.; BERTO, F.; GLINKA, G. Unified two-stage fatigue methodology based on a probabilistic damage model applied to structural details. **Theoretical and Applied Fracture Mechanics**, Amsterdam, v. 92, p. 252-265, 2017.

32 CORREIA, J.A.F.O.; HUFFMAN, P.J.; DE JESUS, A.M.P.; LESIUK, G.; CASTRO, J.M.; CALCADA, R.A.B.; BERTOD, F. Probabilistic Fatigue Crack Initiation and Propagation Fields Using the Strain Energy Density. **Strength of Materials**, New York, v. 50, n. 4, p. 620-635, 2018.

33 HAFEZI, M.H.; ABDULLAH, N.N.; CORREIA, J.F.O.; DE JESUS, A.M.P. An assessment of a strain-life approach for fatigue crack growth. **International Journal of Structural Integrity**, Bingley, v. 3, n. 4, p. 344-376, 2012.

34 DE JESUS, A.M.P.; CORREIA, J.A.F.O. Critical assessment of a local strain-based fatigue crack growth model using experimental data available for the P355NL1 steel. **Journal of Pressure Vessel Technology**, New York, v. 135, n. 1, 2013.

35 HUFFMAN, P.J. A strain energy based damage model for fatigue crack initiation and growth. **International Journal of Fatigue**, London, v. 88, p. 197-204, 2016.

36 HUFFMAN, P.J.; FERREIRA, J.; CORREIA, J.A.F.O.; DE JESUS, A.M.P.; LESIUK, G.; BERTO, F.; FERNÁNDEZ-CANTELI, A.; GLINKA, G. Fatigue crack propagation prediction of a pressure vessel mild steel based on a strain energy density model. **Frattura ed Integrita Strutturale, Cassino**, Cassino, v. 11, n. 42, p. 74-84, 2017.

37 BANG, D.J.; INCE, A.; TANG, L.Q. A modification of UniGrow 2-parameter driving force model for short fatigue crack growth. **Fatigue and Fracture of Engineering Materials and Structures**, Chichester, v. 42, n. 1, p. 45-60, 2019.

38 BANG, D.J.; INCE, A.; NOBAN, M. Modeling approach for a unified crack growth model in short and long fatigue crack regimes. **International Journal of Fatigue**, London, vol. 128, 2019.

39 BANG, D.J.; INCE, A. A short and long crack growth model based on 2-parameter driving force and crack growth thresholds. **International Journal of Fatigue**, London, v. 141, 2020.

40 PEDROSA, B.; CORREIA, J.; LESIUK, G.; REBELO, C.; HUFFMAN, P.; JESUS, A. Probabilistic fields of fatigue crack growth rates of puddle iron based on Huffman local approach. **Synergy of Culture and Civil Engineering - History and Challenges**, Zurich, p. 804-811, 2020

41 NEUBER H. Theory of stress concentration for shear-strained prismatical bodies with arbitrary nonlinear stress–strain law. **Journal of Applied Mechanics**, New York; v. 28, n. 4, p. 544–551, 1961.

42 RIBEIRO, V.; CORREIA, J.; MOURÃO, A.; LESIUK, G.; GONÇALVES, A.; DE JESUS, A.; BERTO, F. Low-cycle fatigue modelling supported by strain energy density-based Huffman model considering the variability of dislocation density. **Engineering Failure Analysis**, Oxford, v. 128, 2021.

43 RAMBERG, W.; OSGOOD, W.R. Description of stress–strain curves by three parameters. **National Advisory Committee for Aeronautics – NACA-TN-902**, Washington DC, n. 902, 1943.

44 MORROW, J.D. Cyclic plastic strain energy and fatigue of metals. **American Society for Testing and Materials Special Technical Publication**, West Conshohocken, v. 378, p. 45-87, 1965.

45 MANSON, S.S. Behaviour of materials under conditions of thermal stress. **National Advisory Committee for Aeronautics - NACA TN-2933**, Washington DC, n. 2933, p.1-105, 1954.

46 COFFIN, L.F. A study of the effects of the cyclic thermal stresses on a ductile metal. **Transactions of The American Society of Mechanical Engineers**, New York, v. 76, n. 6, p. 931–950, 1954.

47 RIBEIRO, A.S.; JESUS, A.M.P.; FERNANDES, A.A. Fatigue crack propagation rates of the aluminium alloy 6061-T651. *In*: INTERNATIONAL CONGRESS OF MECHANICAL ENGINEERING, 18.; 2005, Ouro Preto. **Proceedings** […]. Ouro Preto: COBEM, 2005.

48 AMERICAN SOCIETY FOR TESTING AND MATERIALS – ASTM. **ASTM E647-15e1**: Standard test method for measurement of fatigue crack growth rates. West Conshohocken: ASTM International, 2015.

49 GLINKA, G. Energy density approach to calculation of inelastic strain-stress near notches and cracks. **Engineering Fracture Mechanics**, Oxford, v. 22, n. 3, p. 485-508, 1985.

50 CREAGER, M.; PARIS, P.C. Elastic field equations for blunt cracks with reference to stress corrosion cracking. **International Journal of Fracture Mechanics**, Dordrecht, v. 3, n. 4, p. 247-252,1967.

51 GLINKA, G. Development of weight functions and computer integration procedures for calculating stress intensity factors around cracks subjected to complex stress fields. **Stress and Fatigue-Fracture Design,** Petersburg, v. 1, n. 1, p. 1, 1996.

CHAPTER VII

7 CONCLUSIONS

7.1 CONCLUDING REMARKS

This thesis was dedicated to contributing to: - development of a low-cost workbench (methodology) combining an experimental-analytical analysis to characterize the fatigue crack growth behaviour for the ESE(T) specimens of small thickness (0.3mm) made of 1100 aluminium alloy and constant amplitude tests up to 100N. A comparison between the crack growth constants obtained in the low-cost workbench combining an experimental-analytical analysis and application of the ASTM E647 standard was done.; low-cycle fatigue modelling supported by strain energy density-based Huffman model considering the variability of dislocation density applied to the experimental fatigue data of 1050, 6061-T651, and AlMgSi0.8 aluminium alloys; - application and discussion of various crack closure models to predict fatigue crack growth in 6061-T651 aluminium alloy; and, - fatigue crack growth modelling supported by strain energy density-based Huffman model considering the residual stress effects for the 6061-T651 aluminium alloy.

An experimental programme to characterize the fatigue crack growth of 1100 aluminium alloy

Understanding the current political and scientific scenario in which future researchers are inserted in and knowing the difficulty in obtaining financial support, studies involving less-time-consuming experiments and low-cost workbenches are always welcome. Therefore, this investigation also aims to assess FCG data from the proposed workbench combining an experimental-analytical analysis for the 1100 aluminium alloy specimens, where results seem to be promising for fatigue crack propagation from the stable crack growth (Paris region II). However, in the actual configuration, it is limited to very thin specimens and for non-structural metals. Additionally, the chemical composition, hardness measurements, tensile strength, fatigue crack propagation, and microscopy analysis for Al1100 and Al1050, were also assessed. The results obtained are in line with those recommended for the materials under study. A comparison between the crack growth constants obtained in the low-cost workbench combining an experimental-analytical analysis and application of the

ASTM E647 standard, considering the thickness effects, was done. The results obtained for both approaches, although for different thicknesses (0.3mm and 3mm, respectively, low-cost workbench and ASTM E647 standard), showed consistent and aligned values for the Paris law constants.

Low-cycle fatigue modelling supported by strain energy density-based Huffman model considering the variability of dislocation density

The main conclusions on the low-cycle fatigue modelling supported by strain energy density-based Huffman model considering various addressed methodologies, applied to the experimental fatigue data of 1050, 6061-T651, and AlMgSi0.8 aluminium alloys[1] are given by

- The various methodologies studied were able to model the low-cycle fatigue behaviour based on the strain energy density approach and a good agreement between the experimental fatigue data and the modelled curve is found.
- The strain-life parameters, σ_f' and ε_f', were estimated based on the Huffman model through the critical dislocation density (ρ_c), the mean value of the dislocation density (ρ_m), and the dislocation density (ρ) stochastically considered.
- Among the various methodologies used, the strain-life parameters, σ_f' and ε_f', estimated by strain energy density-based Huffman approach through the mean value of dislocation density (ρ_m) and the dislocation density (ρ) stochastically considered lead to better results when the comparison is made with experimental fatigue data since according to the literature, the dislocation structure changes with the total strain amplitude.
- The output discrete distributions generated by Monte Carlo (MC) stochastic simulation for the strain-life parameters, σ_f' and ε_f', shows that there is not a single probability distribution function suitable to describe each of these variables, for the metal materials under consideration.
- The Weibull and Logistic distribution functions showed the best fitting when compared with the output distributions obtained by stochastic prediction for the fatigue strength coefficient, σ_f', and the fatigue ductility coefficient, ε_f', respectively, for the 1050 aluminium. While, for the 6061-T651 aluminium alloy, the Normal and Weibull distributions exhibited the best fitting with the MC

simulation-based output distributions for the fatigue strength coefficient, σ_f', and the fatigue ductility coefficient, ε_f', respectively.

- The probabilistic strain-life curves generated through the Huffman approach using the Monte Carlo stochastic simulation to estimating the output distributions of the strain-life parameters σ_f' and ε_f' are presented. It can be concluded that the Monte Carlo stochastic prediction allowed the generation of a probabilistic strain-life field through the ρ random variable (ρ is the dislocation density), where the experimental fatigue data are between the 5% and 95% failure probability curves.

Application and discussion of various crack closure models to predict fatigue crack growth in 6061-T651 aluminium alloy

The main conclusions on a comparative study of the fatigue crack propagation rates (da/dN) versus effective stress factor range (ΔK_{eff}) data, in 6061-T651 aluminium alloy, calculated through the various crack closure models under consideration can be summarized as follows[2]:

- The deterministic values of the quantitative parameter, U, and the effective stress ratio, R_{eff}, based on the first cycle and stabilised measurements were obtained. Also, the values of U and R_{eff} were calculated for each crack closure model under consideration.
- Correia's model[3] presents good results for U and R_{eff} when compared to the deterministic data based on stabilised measurements, where the mean values of the error index module are of 2.46% and 6.73%, respectively. Newman's model also shows good results in terms of U and R_{eff}, presenting error index modules of 6.64% and 21.93%, respectively, when the comparison is made with deterministic data based on stabilised measurements. When the same comparison is made with the deterministic values based on the 1st cycle measurements, the Newman's[4], Codrington-Kotousov's[5] and Katcher and Kaplan's[6] models present a good agreement, where the mean values of the error index module of 7.34%, 5.41% and 6.30%, and 12.19%, 8.27% and 9.97%, respectively. The other models also studied based on the 1st cycle and stabilised measurements have mean values of the error index module, $\bar{e}$, greater than 20%, and are not considered adequate to describe the crack closure effects.

- The assumptions suggested in the Hudak and Davidson's[7] investigations and later also recommended by Ellyin[8] were confirmed by the use of the Correia's model[3], where the crack closure quantitative parameter is a function of applied stress R-ratio, maximum stress intensity factor (or ΔK), and driven by threshold stress intensity factor range, ΔK_{th}. Also, Correia's crack closure model based on experimental data suggest the limit stress intensity factor (K_L) in estimating the quantitative parameter (U) to describe the crack closure effects. In this study, the quantitative parameter (U) was estimated by using the maximum stress intensity factor (K_{max}) for stabilised cycles.

Fatigue crack growth modelling supported by strain energy density-based Huffman model considering the residual stress effects

The main conclusions on the fatigue crack growth modelling for the 6061-T651 aluminium alloy supported by the strain energy density-based Huffman approach considering the residual stress effects ahead of the crack tip are the following[9]:

- An elastoplastic stress/strain analytical analysis at the crack tip region based on the multiaxial Neuber[10] and Glinka's[11] rules was assumed, where the both approaches revelled similar elastoplastic stress distributions.
- A comparison on the elastoplastic stress distributions between the numerical results from the finite element modelling of the CT specimen and the analytical results based on Neuber and Glinka's rules was done. A good agreement for the maximum elastoplastic stresses was found.
- The comparison on the residual stress distributions between numerical and analytical solutions showed deviations that increase for a stress ratio equal 0.5, revelling that the analytical solutions overestimate the residual stresses.
- For values of critical dislocation density of 5.90E+15 and 6.088E+15 m^{-2}, both modelling analyses of the fatigue crack propagation behaviour based on the strain energy density approach, considering the residual stress effects estimated by Noroozi et al.[23-25] or Huffman suggestions[10,12], exhibited very similar results.
- The critical dislocation density, driven by the highest strain amplitude specimen or by mean value of the dislocation density for the available experimental fatigue results, does not influence significantly the fatigue crack propagation behaviour modelled by the strain energy density approach.

- For both procedures to consider the residual stress effects, Noroozi and Huffman suggestions, the fatigue crack growth constants obtained from the modelling based on the strain energy density approach are very similar with the exception of the Δa calibration parameter. It is concluded that the procedure for considering the residual stress effects influences the Δa calibrator. Therefore, it is not possible to conclude which is the most recommended method to describe the residual stress effects, since there is no measured data to support such analysis.
- The used approach allows to model the fatigue crack propagation behaviour for the near-threshold and Paris regions.

7.2 FUTURE WORKS

This study tries to cover the most relevant aspects of fatigue crack initiation and propagation modelling based on the strain energy density of aluminium alloys, as well as to discuss the residual stress effects ahead of the crack tip, i.e.; the concept of virtual crack closure effects, where various issues and challenges still need to be investigated in next steps. Future works can be considered as the following:

<u>*An experimental programme to characterize the fatigue crack growth of 1100 aluminium alloy*</u>

The low-cost workbench approach combining an experimental-analytical analysis to characterize the fatigue crack growth behaviour needs to be able to perform tests in accordance with ASTM E647 standard, test thicker specimens, measure the crack closure, and implement an automatic measurement system of fatigue crack propagation rates, applied stress intensity factor ranges, and virtual crack closure effects.

<u>*Low-cycle fatigue modelling supported by strain energy density-based Huffman model considering the variability of dislocation density*</u>

A comparison between the dislocation densities obtained based on the strain energy density approach and experimental techniques, such as special metallographic procedures, X-ray diffraction, and transmission electron microscopy (TEM), must be performed. In addition, a study on the evolution of the dislocation density as a function of the level of strain amplitude and number of cycles to failure must be carried out. Adequate relationships between the dislocation density (ρ) and the cyclic stress-strain parameters, considering that this parameter may vary throughout the low-cycle fatigue test for each strain amplitude, supported eventually by stochastic analysis, must be found. Further studies should be done on the use of approaches based on the strain energy density to model the fatigue crack initiation and propagation phases.

Application and discussion of various crack closure models to predict fatigue crack growth in 6061-T651 aluminium alloy

It can be stated that the simultaneous monitoring of CTOD-based experimental measurements of the crack closure effects and getting the crack tip stress–strain field based on digital image correlation (DIC) measurements, supported by analytical/numerical solutions, seems to be a good way to describe the fatigue crack growth correctly, as suggested by Ferreira-Castro-Meggiolaro[13,14]. This analysis may be relevant to evaluate the residual stress effects and find a relationship with the concept of virtual crack closure, since the phenomena may be related.

Fatigue crack growth modelling supported by strain energy density-based Huffman model considering the residual stress effects

The residual stress effects need to be determined experimentally by digital image correlation, where the stresses and strains ahead of the crack tip for some crack sizes and different stress ratios can be estimated. This analysis will be used to understand what residual stress approaches (Noroozi[15] or Huffman[12] suggestions) are more suitable to model the fatigue crack propagation behaviour. Therefore, the fatigue crack propagation calibration parameters (Δa, x) to be estimated by applying the approach based on the Huffman strain energy density may be seen to be representative of the metals under study. Another aspect to be explored is perhaps the probabilistic fatigue crack propagation modelling using the strain energy density approach through a stochastic analysis, where the parameters of the cyclic stress-strain curve, mainly the cyclic strain hardening coefficient (K'), are described by probability density functions.

REFERENCES

1 RIBEIRO, V.; CORREIA, J.; LESIUK, G.; GONÇALVES, A.; DE JESUS, A.; BERTO, F. Application and discussion of various crack closure models to predict fatigue crack growth in 6061-T651 aluminium alloy. **International Journal of Fatigue**, London, v. 153, 2021.

2 RIBEIRO, V.; CORREIA, J.; MOURÃO, A.; LESIUK, G.; GONÇALVES, A.; DE JESUS, A.; BERTO, F. Low-cycle fatigue modelling supported by strain energy density-based Huffman model considering the variability of dislocation density. **Engineering Failure Analysis**, Oxford, v. 128, 2021.

3 CORREIA, J.A.F.O.; DE JESUS, A.M.P.; MOREIRA, P.M.G.P.; TAVARES, P.J.S. Crack Closure Effects on Fatigue Crack Propagation Rates: Application of a Proposed Theoretical Model. **Advances in Materials Science and Engineering**, London, v. 2016, 2016.

4 NEWMAN JR.; J.C. A crack opening stress equation for fatigue crack growth. **International Journal of Fracture**, Dordrecht, v. 24, n. 4, p. R131-R135,1984.

5 CODRINGTON, J.; KOTOUSOV, A. A crack closure model of fatigue crack growth in plates of finite thickness under small-scale yielding conditions. **Mechanics of Materials**, Amsterdam, v. 41, n. 2, p. 165-173, 2009.

6 KATCHER, M.; KAPLAN, M. Effect of r factor and crack closure on fatigue crack growth for aluminium and titanium alloys. **American Society for Testing and Materials Special Technical Publication**, West Conshohocken, v. 559, p. 264-282, 1974.

7 HUDAK, S. J.; DAVIDSON, D. L. The dependence of crack closure on fatigue loading variables. **American Society for Testing and Materials Special Technical Publication**, Philadelphia, v. 982, p. 121-138, 1988.

8 ELLYIN, F.; **Fatigue Damage, Crack Growth and Life Prediction**. 1. ed. London: Chapman; Hall, 1997

9 RIBEIRO, V.; CORREIA, J.; MOURÃO, A.; LESIUK, G.; GONÇALVES, A.; DE JESUS, A.; BERTO, F. Fatigue crack growth modelling supported by strain energy density-based Huffman model considering the residual stress effects. **Engineering Failure Analysis**, Oxford, v. 140, 2022.

10 NEUBER, H. Theory of stress concentration for shear-strained prismatical bodies with arbitrary nonlinear stress–strain law. **Journal of Applied Mechanics**, New York; v. 28, n. 4, p. 544–551, 1961.

11 GLINKA, G. Energy density approach to calculation of inelastic strain-stress near notches and cracks. **Engineering Fracture Mechanics**, v. 22, n. 3, p. 485-508, 1985.

12 HUFFMAN, P.J. A strain energy based damage model for fatigue crack initiation and growth. **International Journal of Fatigue**, London, v. 88, p. 197-204, 2016.

13 FERREIRA, S.E.; DE CASTRO, J.T.P.; MEGGIOLARO, M.A. A model to quantify fatigue crack growth by cyclic damage accumulation calculated by strip-yield procedures. **Frattura ed Integrita Strutturale, Cassino**, Cassino, v. 11, n. 41, p. 129-138, 2017.

14 FERREIRA, S.E.; CASTRO, J.T.P.D.; MEGGIOLARO, M.A.; OLIVEIRA MIRANDA, A.C.D. Crack closure effects on fatigue damage ahead of crack tips. **International Journal of Fatigue**, London, v. 125, p. 187-198, 2019.

15 NOROOZI, A.H.; GLINKA, G.; LAMBERT, S. A two parameter driving force for fatigue crack growth analysis. **International Journal of Fatigue**, London, v. 27, n. 10-12, p. 1277-1296, 2005.

APPENDIX

PUBLICATIONS

This section contains papers published by author in scientific journals and conferences:

Scientific journals

1. RIBEIRO, V.; CORREIA, J.; LESIUK, G.; GONÇALVES, A.; DE JESUS, A.; BERTO, F. Application and discussion of various crack closure models to predict fatigue crack growth in 6061-T651 aluminium alloy. **International Journal of Fatigue**, London, v. 153, 2021.

2. RIBEIRO, V.; CORREIA, J.; MOURÃO, A.; LESIUK, G.; GONÇALVES, A.; DE JESUS, A.; BERTO, F. Low-cycle fatigue modelling supported by strain energy density-based Huffman model considering the variability of dislocation density. **Engineering Failure Analysis**, Oxford, v. 128, 2021.

3. RIBEIRO, V.; CORREIA, J.; MOURÃO, A.; LESIUK, G.; GONÇALVES, A.; DE JESUS, A.; BERTO, F. Fatigue crack growth modelling supported by strain energy density-based Huffman model considering the residual stress effects. **Engineering Failure Analysis**, Oxford, v. 140, 2022.

Scientific conferences

1. **RIBEIRO, V. H.** *et al*. Combined Experimental-Numerical Methodology to Evaluating the Fatigue Crack Growth Rates for the 1100 Aluminum. *In:* First international symposium on risk analysis and safety of complex structures and components, IRAS 2019, 1., 2019, Porto.

2. **RIBEIRO, V. H.** *et al*. Crack closure effects on fatigue crack propagation under constant amplitude loading for the 6061-T651 aluminium. 2020. *In:* The first Virtual Conference on Mechanical Fatigue, VCMF 2020, 1., 2020, Virtual Conference.

3. **RIBEIRO, V. H.** *et al*. Estimation of strain-life properties through the strain energy density-based Huffman model for various aluminium alloys. 2021. *In:* The International Congress on Structural Integrity and Maintenance, SIM 2021, 1., 2021, Virtual Conference.